Olfactory system pathology in Alzheimer's Disease

Olfactory system pathology in Alzheimer's Disease:

evidences from rodent and human studies

Gowoon Son

This research was conducted at Maastricht University and Daegu Gyeongbuk Institute of Science and Technology.

Cover	Gowoon Son (Created with BioRender.com)
Printing	Gildeprint - www.gildeprint.nl

Olfactory system pathology in Alzheimer's Disease:

evidences from rodent and human studies

DISSERTATION

To obtain the degree of Doctor at Maastricht University,

on the authority of the Rector Magnificus, Prof. Dr. Rianne M. Letschert,

in accordance with the decision of the Board of Deans,

to be defended in public

on Wednesday 26th of May 2021 at 10.00 am.

by

Gowoon Son

Supervisors:

Prof. Dr. H.W.M. Steinbusch

Prof. Dr. C. Moon (Daegu Gyeongbuk Institute of Science and Technology, South Korea)

Co-supervisor:

Dr. A. Jahanshahi

Assessment Committee:

Prof. Dr. D.E.J. Linden (Chair)

Prof. Dr. E.C.M. Mariman

Prof. Dr. L. Moroni

Dr. L.T. Grinberg, M.D. (University of California San Francisco, USA)

Dr. H.K. Choe (Daegu Gyeongbuk Institute of Science and Technology, South Korea)

To all patients with Alzheimer's disease,
olfactory dysfunction,
and their caregivers.

Table of Contents

Chapter 1

General Introduction

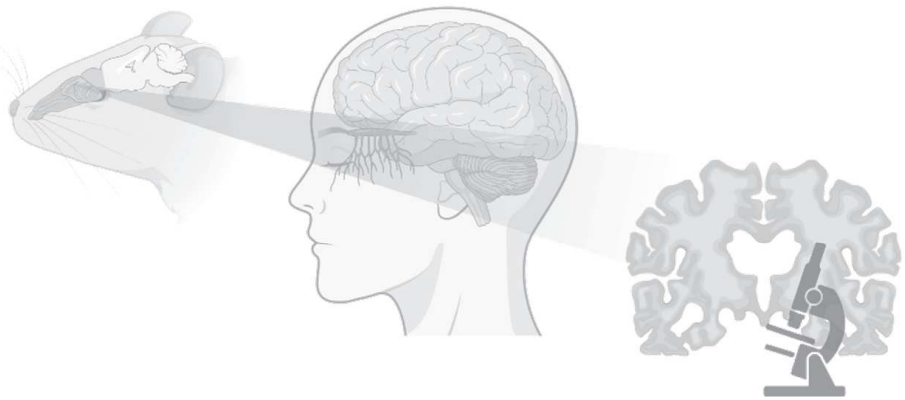

1. Alzheimer's disease

Alzheimer's disease (AD) accounts for 60-80% of those with neurodegenerative dementias (1). Typically, symptoms of AD lead to progressive memory loss and cognitive decline for 10 to 20 years, albeit many cases run a somewhat shorter course (2). AD is recognized as an irreversible neurodegenerative disease because once neurons are damaged and lose their function, they rarely recover. Several drugs for treatment of AD have been approved by the US Food and Drug Administration (FDA) (3, 4) and some current medications are thought to delay the disease progression when the drug treatment is applied in a timely appropriate manner (*5*). Nonetheless, ultimately, recovery is not achieved.

Patients with AD have four recognized stages in the progression of their disease, namely, mild cognitive impairment (MCI) prior to the diagnosis of AD and followed by mild, moderate, and severe AD (*6*). Understanding early symptoms of the disease is essential to approach identifying mechanisms in the initiation of AD. According to previous research, depression (*7*), sleep disturbance (*8*), and olfactory dysfunction (*9*) are commonly occurred in the MCI stage, together with memory and cognitive loss.

2. Olfactory dysfunction in Alzheimer's disease

Olfactory dysfunction usually occurs as a reduction in the sense of smell, identified as hyposmia in AD patients (*10*). It is gradually progressive and there is no effective therapy. Numerous previous studies over the past few decades have reported that abnormal olfaction is one of the earliest clinical manifestations of AD

(*11*). Thus, it coexists in the prodromal stage that presages the onset of neurological symptoms in AD (*12, 13*). Specifically, decreased olfactory sensation has been shown with MCI, and it is proportional to cognitive impairment in MCI (*14-16*). Thus, hyposmia has been suggested as a behavioral marker predictive for AD (*17, 18*).

Because olfaction involves episodic memory consolidation and retrieval (*19*), impaired olfaction has been considered an indicator of brain damage (*20*). Cortical neurodegeneration has been thought to account for or underly olfactory deficits in AD (*21, 22*). Nevertheless, little is known about the role and cause of AD-pathology identified in the olfactory system, including the olfactory epithelium and bulb (*23, 24*).

Interestingly, AD patients who have difficulty in olfaction are not typically hyposmic and cannot smell all odors equally (*11, 25*). Clinical research has showed that patients with olfactory dysfunction had difficulty identifying a specific subset of odorants presented (*26, 27*). In particular, the peanut butter test was suggested as a measurement that can distinguish patients with AD (*28*). Other literature reported that performance on a 10-item smell identification scale is related to risk for Alzheimer's disease (*29*). In fact, previous reports highlight that olfactory dysfunction may have undefined characteristics and, therefore, the study of pathological alterations in the olfactory system might identify specific types of olfactory dysfunction in AD.

3. The pathology of Alzheimer's disease

The brains of AD patients brain exhibit cerebral cortical atrophy and lesions that are seen at autopsy, such as accumulated neurofibrillary tangle and senile plaques (*30*). The lesions are distributed in transentorhinal, limbic, and neocortical regions of the brain (*31*). In the clinic, association of amyloid deposition (A), hyperphosphorylated tau inclusion (T), and neurodegeneration (N) is used to provide a biological definition of AD called the ATN category (*32*). Interestingly, these misfolded pathogenic proteins and brain atrophy appear to initiate in specific brain areas and spread spatiotemporally (*33*). Braak staging, a cardinal method to classify the degree of neuropathology in AD, describes the progression of senile plaque and neurofibrillary tangle (*34*).

Aβ proteins appeared in the early phase of AD (*35*). According to the ATN categorization, the National Institute on Aging in the US considers in the definition of AD that the positive amyloid groups are AD, but that ATN-negative groups are to be categorized to non-AD pathologic change groups (*36*). Thus, it emphasizes that considering Aβ pathogenesis in AD is essential to elucidate the mechanisms of early symptoms and develop advances in detection tools.

4. β-amyloid protein: structure and physiology

β-amyloid (Aβ) is a peptide of 36 ~ 43 amino acids catalyzed from the amyloid precursor protein (APP). APP is a transmembrane protein with which and the first cleavage is determined by two cleavage enzymes, α-secretase and β-secretase (*37*). The Aβ is the final proteolytic product of β-secretase and γ-secretase cleavage, which is referred to as amyloidogenic APP processing (*38*). The single peptide, *i. e.,* Aβ monomer, generates several types of assemblies (*39*). The species of Aβ comprises n-*mer* structures, including dimer, trimer, and fibrils. Significantly, the 12-*mer* (Aβ *56; 56 kDa) Aβ is a soluble oligomer that appears to be related to memory deficits (*40*). Accumulation of Aβ proteins is relevant to neurotoxicity where, especially, oligomerized Aβ confers impairments of synaptic transmission and neural networks (*41*). Soluble Aβ oligomers reduce excitatory neurotransmitter release (*42, 43*) and also induce postsynaptic deficits by suppressing long-term potentiation or lead to long-term synaptic depression (*44*). In addition to primary toxicity, neural damage by Aβ accumulation provides a secondary genesis of misfolded proteins (*45*). Eventually, this process accelerates a vicious cycle that could cause further damage (*46*).

In the past, the failure of drug development to target brain Aβ plaques resulted in controversies with respect to the amyloid hypothesis as being the primary cause of AD, albeit that it cannot be denied that Aβ genesis contributes to the neurogenerative cascade. In other words, Aβ aggregation can seed pathogenic reservoirs, or substrates, such as neuroinflammation (*47*). Microglia drive neuronal

damage by pro-inflammatory processes that might accelerate causes of amyloidopathy (*48*). Although activated microglia cause phagocytosis to eliminate Aβ aggregates, excessive Aβ burden impairs the clearance (*49*). Another adverse effect is that the Aβ proteins dysregulate the cellular Ca^{2+} homeostasis and membrane Ca^{2+} permeable channels or receptors (*50, 51*), critical to maintaining vital neural balance and stable synaptic transmission (*52*).

5. Transgenic mouse model for study of β-amyloid pathology

Scientific interest regarding pathogenesis mechanisms of AD fostered the development of a genetically modified transgenic mouse with mutation of the APP protein (*53*). Among various transgenic models, this thesis covered two types of mouse lines. To substantiate the olfactory dysfunction as a feature in typical AD progression, the Tg2576 model was used because it is the widely used conventional transgenic line. It overexpresses a mutant form with the Swedish mutation (KM670/671NL) on humanized APP gene controlled by the hamster prion protein (PrP) promoter. The Tg2576 model was confirmed to develop excessive Aβ pathology and age-associated cognitive deficits (*54*). As well, a double transgenic mouse designed for the earlier deposition of Aβ by human APP and γ-secretase mutation was studied. Therefore, the 5xFAD model which overexpresses three-APP (Swedish, Florida; I716V, and London; V717I) and two-PS1 (γ-secretase; M146L and L286V) transgenes. In this model amyloid deposition begins around the age of two-

months-old (*55*), and serves to identify a possible role of Aβ etiology in AD development and progression rather than age-related alteration.

6. Human subject validation for the study of β-amyloid pathology

The current standard paradigm to diagnose AD comprises three approaches: clinical examination, neuroimaging, and molecular markers in body fluids. The Aβ proteins are utilized as biomarkers (*56, 57*). In addition, the level of Aβ in the brain is analyzed to evaluate and validate the novel marker and symptoms because it is considered to mirror the AD progression (*58*).

The most common criteria in the clinic are the National Institute of Neurologic, Communicative Disorders and Stroke and the Alzheimer's Disease and Related Diseases Association (NINCDS-ADRDA) (*59*), and the Diagnostic and Statistical Manual (DSM) (*60*). Combining these criteria, the Consortium to Establish a Registry for Alzheimer's Disease (CERAD) (*61*) and the Thal Aβ phase (TAP) (*31*) represent standardized protocols assessing AD neuropathology that have been used. Additionally, cognitive decline is evaluated by the scores of the Mini-Mental Status Examination (MMSE) (*62*), the Global Deteriorating Scale (GDS) (*63*), and the Clinical Dementia Rating (CDR) (*64*), in association with Aβ deposit indicating AD-related cerebral dysfunction (*65*). Brain imaging has also been used over the past four decades. Imaging measures structural alterations using computed tomography (CT) and magnetic resonance imaging (MRI), with functional deficits shown by functional

MRI. Pathologic molecular substrates can be imaged by using positron emission tomography (PET) (*66*). Aβ proteins are useful tracers in brain imaging, enabling identification of AD with high disease specificity (*67*). Detecting Aβ species in cerebrospinal fluid (CSF) and plasma facilitate early AD screening in body fluid without brain autopsy (*68*).

In summary, the scientific premise of studying Aβ mechanisms is that it takes a priority to identify AD neuropathology. The research contributes to find ideal biomarkers and elucidate the pathogenesis mechanism related to disease initiation.

7. Overview of this thesis

The current thesis investigates the olfactory system and its pathology in AD and elucidates how any such pathology contributes to the onset of smell dysfunction in AD. This thesis begins with an overview of the neuropathological features and mechanisms in the olfactory system in AD progression **(Chapter 2)**. Using transgenic mouse models, I identified that olfactory dysfunction of partial hyposmia was evident in early pathogenesis of AD. The abnormality was determined by region-specific Aβ accumulation in the olfactory sensory neurons **(Chapter 3-4)**. Next, using postmortem tissue from AD patients, I demonstrated multimodal damage, including morphological alteration with Aβ accumulation concomitant to microglial reactivation and neurotransmitter deficits in the human olfactory glomerulus **(Chapter 5)**. By applying evidence from the results of previous chapters, I identified AD biomarkers in nasal discharge, thereby predicting AD patients' cognitive decline **(Chapter 6)**. Lastly, I summarized and discussed the current thesis findings that olfactory pathology is involved in ongoing neurodegeneration, and outlined the implications of this as applied to the pathophysiology **(Chapter 7)**.

References

1. 2020 Alzheimer's disease facts and figures. *Alzheimers Dement*, (2020).
2. R. Tarawneh, D. M. Holtzman, The clinical problem of symptomatic Alzheimer disease and mild cognitive impairment. *Cold Spring Harb Perspect Med* **2**, a006148 (2012).
3. S. J. Thomas, G. T. Grossberg, Memantine: a review of studies into its safety and efficacy in treating Alzheimer's disease and other dementias. *Clin Interv Aging* **4**, 367-377 (2009).
4. R. Cacabelos, Donepezil in Alzheimer's disease: From conventional trials to pharmacogenetics. *Neuropsychiatr Dis Treat* **3**, 303-333 (2007).
5. J. H. Barnett, L. Lewis, A. D. Blackwell, M. Taylor, Early intervention in Alzheimer's disease: a health economic study of the effects of diagnostic timing. *BMC Neurol* **14**, 101 (2014).
6. R. A. Sperling *et al.*, Toward defining the preclinical stages of Alzheimer's disease: recommendations from the National Institute on Aging-Alzheimer's Association workgroups on diagnostic guidelines for Alzheimer's disease. *Alzheimers Dement* **7**, 280-292 (2011).
7. E. Chemerinski, G. Petracca, L. Sabe, J. Kremer, S. E. Starkstein, The specificity of depressive symptoms in patients with Alzheimer's disease. *Am J Psychiatry* **158**, 68-72 (2001).
8. K. Palmer, M. Mitolo, F. Burgio, F. Meneghello, A. Venneri, Sleep Disturbance in Mild Cognitive Impairment and Association With Cognitive Functioning. A Case-Control Study. *Front Aging Neurosci* **10**, 360 (2018).
9. C. Murphy, Olfactory and other sensory impairments in Alzheimer disease. *Nat Rev Neurol* **15**, 11-24 (2019).
10. M. M. E. Silva, P. B. S. Mercer, M. C. Z. Witt, R. R. Pessoa, Olfactory dysfunction in Alzheimer's disease Systematic review and meta-analysis. *Dement Neuropsychol* **12**, 123-132 (2018).
11. D. P. Devanand *et al.*, Olfactory deficits in patients with mild cognitive impairment predict Alzheimer's disease at follow-up. *Am J Psychiatry* **157**, 1399-1405 (2000).
12. D. P. Devanand *et al.*, Combining early markers strongly predicts conversion from mild cognitive impairment to Alzheimer's disease. *Biol Psychiatry* **64**, 871-879 (2008).
13. R. S. Wilson *et al.*, Olfactory impairment in presymptomatic Alzheimer's disease. *Ann N Y Acad Sci* **1170**, 730-735 (2009).
14. J. H. Yoon, M. Kim, S. Y. Moon, S. W. Yong, J. M. Hong, Olfactory function and neuropsychological profile to differentiate dementia with Lewy bodies from Alzheimer's disease in patients with mild cognitive impairment: A 5-year follow-up study. *J Neurol Sci* **355**, 174-179 (2015).
15. R. O. Roberts *et al.*, Association Between Olfactory Dysfunction and Amnestic Mild Cognitive Impairment and Alzheimer Disease Dementia. *JAMA Neurol* **73**, 93-101 (2016).
16. M. Vyhnalek *et al.*, Olfactory identification in amnestic and non-amnestic mild cognitive impairment and its neuropsychological correlates. *J Neurol Sci* **349**, 179-184 (2015).
17. D. P. Devanand *et al.*, Olfactory deficits predict cognitive decline and Alzheimer dementia in an urban community. *Neurology* **84**, 182-189 (2015).
18. M. E. Growdon *et al.*, Odor identification and Alzheimer disease biomarkers in clinically normal elderly. *Neurology* **84**, 2153-2160 (2015).

19. S. Chu, J. J. Downes, Odour-evoked autobiographical memories: psychological investigations of proustian phenomena. *Chem Senses* **25**, 111-116 (2000).
20. T. Kovacs, Mechanisms of olfactory dysfunction in aging and neurodegenerative disorders. *Ageing Res Rev* **3**, 215-232 (2004).
21. C. S. Dintica *et al.*, Impaired olfaction is associated with cognitive decline and neurodegeneration in the brain. *Neurology* **92**, e700-e709 (2019).
22. M. Serby, P. Larson, D. Kalkstein, The nature and course of olfactory deficits in Alzheimer's disease. *Am J Psychiatry* **148**, 357-360 (1991).
23. S. E. Arnold *et al.*, Olfactory epithelium amyloid-beta and paired helical filament-tau pathology in Alzheimer disease. *Ann Neurol* **67**, 462-469 (2010).
24. I. Ubeda-Banon *et al.*, The human olfactory system in two proteinopathies: Alzheimer's and Parkinson's diseases. *Transl Neurodegener* **9**, 22 (2020).
25. Y. M. Zou, D. Lu, L. P. Liu, H. H. Zhang, Y. Y. Zhou, Olfactory dysfunction in Alzheimer's disease. *Neuropsychiatr Dis Treat* **12**, 869-875 (2016).
26. D. Jimbo, M. Inoue, M. Taniguchi, K. Urakami, Specific feature of olfactory dysfunction with Alzheimer's disease inspected by the Odor Stick Identification Test. *Psychogeriatrics* **11**, 196-204 (2011).
27. S. Parola, P. Liberini, Assessing olfaction in the Italian population: methodology and clinical application. *Ital J Neurol Sci* **20**, 287-296 (1999).
28. J. J. Stamps, L. M. Bartoshuk, K. M. Heilman, A brief olfactory test for Alzheimer's disease. *J Neurol Sci* **333**, 19-24 (2013).
29. M. H. Tabert *et al.*, A 10-item smell identification scale related to risk for Alzheimer's disease. *Ann Neurol* **58**, 155-160 (2005).
30. P. T. Nelson, H. Braak, W. R. Markesbery, Neuropathology and cognitive impairment in Alzheimer disease: a complex but coherent relationship. *J Neuropathol Exp Neurol* **68**, 1-14 (2009).
31. D. R. Thal, U. Rub, M. Orantes, H. Braak, Phases of A beta-deposition in the human brain and its relevance for the development of AD. *Neurology* **58**, 1791-1800 (2002).
32. C. R. Jack, Jr. *et al.*, Associations of Amyloid, Tau, and Neurodegeneration Biomarker Profiles With Rates of Memory Decline Among Individuals Without Dementia. *JAMA* **321**, 2316-2325 (2019).
33. M. P. Mattson, Pathways towards and away from Alzheimer's disease. *Nature* **430**, 631-639 (2004).
34. H. Braak, E. Braak, Neuropathological stageing of Alzheimer-related changes. *Acta Neuropathol* **82**, 239-259 (1991).
35. C. R. Jack, Jr. *et al.*, Hypothetical model of dynamic biomarkers of the Alzheimer's pathological cascade. *Lancet Neurol* **9**, 119-128 (2010).
36. C. R. Jack, Jr. *et al.*, NIA-AA Research Framework: Toward a biological definition of Alzheimer's disease. *Alzheimers Dement* **14**, 535-562 (2018).
37. J. Nunan, D. H. Small, Regulation of APP cleavage by alpha-, beta- and gamma-secretases. *FEBS Lett* **483**, 6-10 (2000).
38. T. E. Golde, S. Estus, L. H. Younkin, D. J. Selkoe, S. G. Younkin, Processing of the amyloid protein precursor to potentially amyloidogenic derivatives. *Science* **255**, 728-730 (1992).
39. M. P. Lambert *et al.*, Diffusible, nonfibrillar ligands derived from Abeta1-42 are potent central nervous system neurotoxins. *Proc Natl Acad Sci U S A* **95**, 6448-6453 (1998).
40. S. Lesne *et al.*, A specific amyloid-beta protein assembly in the brain impairs memory. *Nature* **440**, 352-357 (2006).
41. J. J. Palop, L. Mucke, Amyloid-beta-induced neuronal dysfunction in Alzheimer's

disease: from synapses toward neural networks. *Nat Neurosci* **13**, 812-818 (2010).
42. Y. He *et al.*, Amyloid beta oligomers suppress excitatory transmitter release via presynaptic depletion of phosphatidylinositol-4,5-bisphosphate. *Nat Commun* **10**, 1193 (2019).
43. F. Kamenetz *et al.*, APP processing and synaptic function. *Neuron* **37**, 925-937 (2003).
44. H. Hsieh *et al.*, AMPAR removal underlies Abeta-induced synaptic depression and dendritic spine loss. *Neuron* **52**, 831-843 (2006).
45. I. Benilova, E. Karran, B. De Strooper, The toxic Abeta oligomer and Alzheimer's disease: an emperor in need of clothes. *Nat Neurosci* **15**, 349-357 (2012).
46. C. Haass, D. J. Selkoe, Soluble protein oligomers in neurodegeneration: lessons from the Alzheimer's amyloid beta-peptide. *Nat Rev Mol Cell Biol* **8**, 101-112 (2007).
47. H. Sarlus, M. T. Heneka, Microglia in Alzheimer's disease. *J Clin Invest* **127**, 3240-3249 (2017).
48. T. Wyss-Coray, L. Mucke, Inflammation in neurodegenerative disease--a double-edged sword. *Neuron* **35**, 419-432 (2002).
49. S. E. Hickman, E. K. Allison, J. El Khoury, Microglial dysfunction and defective beta-amyloid clearance pathways in aging Alzheimer's disease mice. *J Neurosci* **28**, 8354-8360 (2008).
50. A. Demuro, I. Parker, G. E. Stutzmann, Calcium signaling and amyloid toxicity in Alzheimer disease. *J Biol Chem* **285**, 12463-12468 (2010).
51. A. Demuro *et al.*, Calcium dysregulation and membrane disruption as a ubiquitous neurotoxic mechanism of soluble amyloid oligomers. *J Biol Chem* **280**, 17294-17300 (2005).
52. M. J. Berridge, Neuronal calcium signaling. *Neuron* **21**, 13-26 (1998).
53. C. Balducci, G. Forloni, APP transgenic mice: their use and limitations. *Neuromolecular Med* **13**, 117-137 (2011).
54. K. Hsiao *et al.*, Correlative memory deficits, Abeta elevation, and amyloid plaques in transgenic mice. *Science* **274**, 99-102 (1996).
55. H. Oakley *et al.*, Intraneuronal beta-amyloid aggregates, neurodegeneration, and neuron loss in transgenic mice with five familial Alzheimer's disease mutations: potential factors in amyloid plaque formation. *J Neurosci* **26**, 10129-10140 (2006).
56. A. Nakamura *et al.*, High performance plasma amyloid-beta biomarkers for Alzheimer's disease. *Nature* **554**, 249-254 (2018).
57. S. Palmqvist, N. Mattsson, O. Hansson, I. Alzheimer's Disease Neuroimaging, Cerebrospinal fluid analysis detects cerebral amyloid-beta accumulation earlier than positron emission tomography. *Brain* **139**, 1226-1236 (2016).
58. S. Boluda *et al.*, A comparison of Abeta amyloid pathology staging systems and correlation with clinical diagnosis. *Acta Neuropathol* **128**, 543-550 (2014).
59. G. McKhann *et al.*, Clinical diagnosis of Alzheimer's disease: report of the NINCDS-ADRDA Work Group under the auspices of Department of Health and Human Services Task Force on Alzheimer's Disease. *Neurology* **34**, 939-944 (1984).
60. American Psychiatric Association., American Psychiatric Association. DSM-5 Task Force., *Diagnostic and statistical manual of mental disorders : DSM-5*. (American Psychiatric Association, Washington, D.C., ed. 5th, 2013), pp. xliv, 947 p.
61. S. S. Mirra *et al.*, The Consortium to Establish a Registry for Alzheimer's Disease (CERAD). Part II. Standardization of the neuropathologic assessment of Alzheimer's disease. *Neurology* **41**, 479-486 (1991).
62. M. F. Folstein, S. E. Folstein, P. R. McHugh, "Mini-mental state". A practical method for grading the cognitive state of patients for the clinician. *J Psychiatr Res* **12**, 189-198

(1975).
63. B. Reisberg, S. H. Ferris, M. J. de Leon, T. Crook, The Global Deterioration Scale for assessment of primary degenerative dementia. *Am J Psychiatry* **139**, 1136-1139 (1982).
64. J. C. Morris, The Clinical Dementia Rating (CDR): current version and scoring rules. *Neurology* **43**, 2412-2414 (1993).
65. W. Huijbers *et al.*, Amyloid-beta deposition in mild cognitive impairment is associated with increased hippocampal activity, atrophy and clinical progression. *Brain* **138**, 1023-1035 (2015).
66. K. A. Johnson, N. C. Fox, R. A. Sperling, W. E. Klunk, Brain imaging in Alzheimer disease. *Cold Spring Harb Perspect Med* **2**, a006213 (2012).
67. A. G. Vlassenko, T. L. Benzinger, J. C. Morris, PET amyloid-beta imaging in preclinical Alzheimer's disease. *Biochim Biophys Acta* **1822**, 370-379 (2012).
68. K. Blennow, H. Hampel, M. Weiner, H. Zetterberg, Cerebrospinal fluid and plasma biomarkers in Alzheimer disease. *Nat Rev Neurol* **6**, 131-144 (2010).

Chapter 2

Olfactory neuropathology in Alzheimer's disease: a sign of ongoing neurodegeneration

Gowoon Son [1,2,3], Ali Jahanshahi [2,3], Seung-Jun Yoo [4,5], Jackson T. Boonstra [2,3], David A. Hopkins [6], Harry W. M. Steinbusch [1,3,*], and Cheil Moon [1,4,*]

[BMB Reports, 2021, doi: 10.5483/BMBRep.2021.54.6.055]

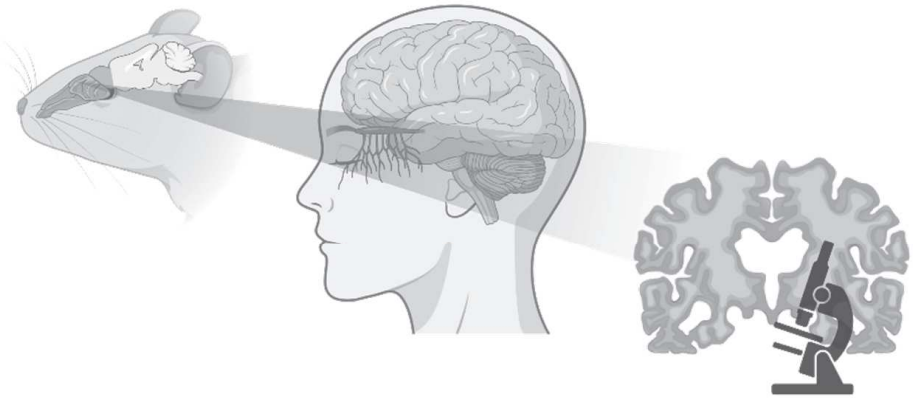

Abstract

Olfactory neuropathology is a cause of olfactory loss in Alzheimer's disease (AD). Olfactory dysfunction is also associated with memory and cognitive dysfunction and is an incidental finding of AD dementia. Here we review neuropathological research on the olfactory system in AD, considering both structural and functional evidence. Experimental and clinical findings identify olfactory dysfunction as an early indicator of AD. In keeping with this, amyloid-β production and neuroinflammation are related to underlying causes of impaired olfaction. Notably, physiological features of the spatial map in the olfactory system suggest the evidence of ongoing neurodegeneration. Our aim in this review is to examine olfactory pathology findings essential to identifying mechanisms of olfactory dysfunction in the development of AD in hopes of supporting investigations leading towards revealing potential diagnostic methods and causes of early pathogenesis in the olfactory system.

List of abbreviations

AD, Alzheimer's disease; MCI, mild cognitive impairment; OSN, olfactory sensory neuron; OB, olfactory bulb; OE, olfactory epithelium; Aβ, β-amyloid; aMCI, amnestic MCI; APP/PS1, humanized amyloid precursor protein/presenilin 1 mutated; hAPP, humanized amyloid precursor protein; BACE1, β-secretase protein 1

1. Introduction

Alzheimer's disease (AD) is a progressive neurodegenerative disorder and one of the most prevalent forms of dementia (*1*). Major symptoms include memory loss and cognitive dysfunction. Several comorbidities in AD often coexist or are prominent, such as depression, circadian rhythm or sleep disturbances, and sensory-perceptual problems (*2-4*). Among other AD symptoms, olfactory dysfunction is not only a highly prevalent symptom in AD (*5*) but also an early diagnostic biomarker (*6*). That is, olfactory dysfunction is present in the early stages of AD and in probable AD patients who have mild cognitive impairment (MCI) (*7*). Therefore, olfactory deficits in AD have received increasing attention over the past few years in fundamental to clinical research. Because the representative pathologic hallmarks of AD are amyloid plaques and neurofibrillary tangles as well as brain atrophy (*8*), characterization of such pathological alterations in the olfactory system have been explored in an attempt to identify early stages of AD.

The olfactory system transmits chemical signals from the sensory epithelium and bulb to the olfactory cortex, following a serial synaptic interface (*9-11*). The olfactory bulb is the convergence of the peripheral olfactory system and the central subcortical systems that interconnect the olfactory sensory neuronal axons and the mitral cell dendrites. When studying olfactory dysfunction in AD, recent research efforts have implicated cortical olfactory regions (*12, 13*). However, several studies have reported clear pathogenesis in the olfactory sensory neurons (OSN) as well as

olfactory bulbs (OB) in both rodent and human subjects (*14, 15*), little is known about the roles of the olfactory epithelium (OE) and the OB in AD progression.

Herein, we review literature on olfactory dysfunction in AD in order to examine how anatomical and physiological characteristics are disrupted in OSNs and OB and how that contributes to olfactory dysfunction in AD. In agreement with a recent review (*16*), we suggest a mechanism of olfactory impairment involving OE and OB neurodegeneration. Pathophysiologic findings are mainly from human studies, whereas cellular, molecular, and mechanistic evidences come mostly from rodent research. We then discuss the significance of the peripheral olfactory (including the OE and a part of OB) degeneration in smell dysfunction in AD.

2. Methods

We conducted a systematic search using PubMed for pathophysiologic findings underlying olfactory dysfunction in AD as described in rodent and human studies. We conducted the search within English literature published up to March 2021 using the following search terms: "Alzheimer's disease", "olfactory dysfunction", "Alzheimer's pathology", "olfactory system". We used keywords independently and in various combinations. Research articles and reviews obtained were mainly published within the previous five years. We added additional articles following a cross-reference search within review and original articles.

3. The neuropathology of Alzheimer's disease

AD is progressive and incurable neurodegenerative disease that can be characterized neuropathologically by protein accumulation including amyloid plaques and neurofibrillary tangles (*17*). Amyloid plaques are composed of misfolded amyloid-β (Aβ) proteins and are first found in the basal temporal cortex and orbitofrontal cortex, then progress to the neocortex, basal ganglia, hippocampal formation and the amygdala as AD progresses (*17*). Neurofibrillary tangles made of tau inclusions appear in the locus coeruleus and entorhinal cortex, then spread to the neocortex and hippocampal formation throughout the brain (*18*). Because of the increasing distribution of the protein aggregates, AD patients show brain atrophy as a pathological feature with severe memory and cognitive impairment as clinical symptoms (*19*).

Current clinical trials are assessing the ability of various interventions to reduce cognitive deficits and progressive neural impairment of patients with AD (*20*). Because neuronal injury is currently irreversible, identifying appropriate diagnostics, interventions, and treatment methods for AD is essential. Epidemiological studies indicate that olfactory dysfunction can predict cognitive decline (*21*) and Murphy (2019) reported that olfactory impairment might serve as an early indicator of AD (*2*).

4. Olfactory dysfunction in Alzheimer's disease

Anatomical and physiological alterations of the olfactory system in AD have been studied using various approaches (Tables 1 and 2). In AD patients, olfactory dysfunction usually appears as a reduced smelling ability known as hyposmia (*22*). Unlike congenital anosmia, olfactory deficits in AD patients appear during preclinical stages of the disease before the manifestation of cardinal AD symptoms. Specifically, decreased olfactory abilities have been shown in MCI and are proportional to cognitive impairment in amnestic MCI (aMCI) (*6*). Dysfunction of odor discrimination has therefore been suggested as a predictive behavioral measure for AD (*22*). For this reason, a particular "Odorant Item Specific Olfactory Identification" test has been proposed where certain odors can differentiate AD from general aging (*23*).

Because deficits in olfactory performance are associated with impaired memory and cognitive function, deficits in olfaction in AD can be interpreted a consequence of a decline in perceptual processing and episodic memory (*24*). However, olfactory impairment also predicted cognitive deficits in the non-demented adult population (*25*). Nonetheless, the AD pathogenesis in the olfactory system (see details "Neuropathology of the olfactory system in AD") supports the premise that olfactory deficits occur and progress prior to severe cognitive and memory decline in AD progression. Thus, attempts to characterize the early stages of AD have highlighted the interest in the olfactory system as revealing olfactory dysfunction pathophysiology in AD.

Table 1 Pathological alterations in the olfactory system of patients with Alzheimer's disease (AD).

Findings	**Methods**	**Clinical stage**	**Measured [5] AD pathology**	**Refs.**
- Reduced [1] OB volume and white matter of the olfactory tract	[2] MRI, [3] DTI 3T-MRI	[4] aMCI	[6] n/a	(*26*)
- $A\beta_{1\text{-}42}$, p-tau, and astrogliosis in the glomerular layer, anterior olfactory nucleus, olfactory tubercle	[7] IHC	MCI, moderate-AD, severe-AD	$\beta_{1\text{-}42}$, p-tau, astrogliosis	(*13*)
- β-amyloid aggregates, PHF-tau, and α-synuclein in the anterior olfactory nucleus	IHC	n/a	β-amyloid, [12] PHF-tau, α-synuclein	(*12*)
- β-amyloid, tau in the piriform cortex	IHC	AD	β-amyloid, tau	(*27*)
- Deficit in olfactory identification	Olfactory identification test, DTI 3T-MRI	aMCI, AD, MCI-[8] DLB, MCI-AD	Lewy body	(*6, 26, 28, 29*)
- Deficit in olfactory identification differentiated AD from aging	Olfactory identification test	aMCI, AD, healthy aging	n/a	(*23*)
- Reduced ability to identify a specific subset of smell	Olfactory identification test	AD	n/a	(*30, 31*)
- Impaired olfactory identification (proportional to cognitive impairment in aMCI)	Olfactory identification test	aMCI, non-aMCI	n/a	(*22*)
- Implication: damaged [9] OSNs and olfactory malfunction following exposure to air-pollutants	Statistics, Epidemiology	n/a	n/a	(*32*)
- One-fifth of allergic and chronic rhinitis patients develop AD	Medical examination, IgE assay	allergic diseases with AD	Inflammation	(*33*)

- β-amyloid aggregates, PHF-tau, and α-synuclein in the [10] OE	IHC	AD, [11] OND	β-amyloid, [12] PHF-tau, α-synuclein	(*14*)
- β-amyloid in nasal secretions	WB, IME biosensor	AD, OND	β-amyloid	(*34*)
- β-amyloid in nasal discharge (correlated with cognitive decline)	LC/MS, WB, IME biosensor	probable AD (mild, moderate AD)	β-amyloid (Aβ*56, AβO)	(*35*)
- apoE4 correlated with odor identification deficits	Odor threshold test, Olfactory identification test	n/a	apoE4	(*36*)

[1] OB: olfactory bulb, [2] MRI: magnetic resonance imaging, [3] DTI-3T: 3.0 Tesla diffusion tensor imaging, [4] aMCI: amnestic mild cognitive impairment, [5] AD: Alzheimer's disease, [6] n/a: non-applicable, [7] IHC: immunohistochemistry, [8] DLB: dementia with Lewy body, [9] OSN: olfactory sensory neuron, [10] OE: olfactory epithelium, [10] OND: other neurodegenerative disease, [11] PHF: paired helical filament.

Table 2 Pathological alterations in the olfactory system in mouse models of Alzheimer's disease (AD).

Findings	**Methods**	**Strain (age)**	**Refs.**
- Decreased [1] OE thickness - Increased populations of [2] TUNEL (+) cell - Decreased in number and length of dendritic spines - Deficit in olfactory behavior and β-amyloid deposition - Increased latency in finding buried food, reduced peanut butter preference	[3] IHC, TUNEL assay, [4] EM	[5] Tg2576 (6, 12[6] M) APP/PS1 (9M)	(*37, 38*)
- Distorted ultrastructure and subcellular components in the OE - Decreased mature [7] OSNs	[8] ELISA, IHC, [9] PCR, EM, [10] BrdU assay	[11] hAPP (3[12] w)	(*39, 40*)
- Earlier β-amyloid deposition in the olfactory system than the brain region	IHC, Thio-S staining	Tg2576 (3, 6, 16, 21M)	(*41*)
- Region specific APP processing - Restricted expression of β-secretase only in the olfactory glomerulus in the [13] OB	[14] WB, IHC, [15] ISH	Tg2576 (10M), [16] BACE null	(*38, 42*)
- Reduced response to odorants (only specific odorant) - Region-specific calcium inactivation of OSN correlated with Region specific β-amyloid deposition - Deficits of turnover ratio of OE	Odor detection test, Calcium imaging, IHC, TUNEL assay	Tg6799 (3M)	(*43*)
- Damaged OSNs and olfactory malfunction following exposure to air-pollutant nanoparticles	IHC, PCR, WB, nitrite assay	C57BL6 (3M), Fischer 344 rats (12w)	(*44*)
- Aberrant OSNs projection to the glomeruli	IHC, ISH, [17]AAV modulation,	Tg2576 (13, 24M)	(*15*)

- Higher expressions levels and activity of γ-secretase in the OE - β-amyloid (Aβ*56) accumulates more quickly in the OE	IHC, TUNEL assay, EM	Tg2576 (10M),	(*45*)
- Correlation between deficit of olfactory habituation and spatial-temporal β-amyloid deposition - Deficit in odor investigation and habituation	odor cross-habituation test	Tg2576 (3, 6, 16, 21M)	(*41*)
- Altered the OSN connectivity by inducing human β-amyloid - Decreased response to aversive odor in induced human β-amyloid condition	IHC, [18] TMT assay, hidden food assay	[19] CORMAP mouse, Tg2576 (13, 24M)	(*15*)
- Injected β-amyloid in the OB transferring to other brain region	β-amyloid injection, IHC, TUNEL, WB	C57BL6 (7-8w)	(*46*)

[1] OE: olfactory epithelium, [2] TUNEL (+): terminal deoxynucleotidyl transferase dUTP nick end labeling-positive. [3] IHC: immunohistochemistry, [4] EM: electric microscopy, [5] Tg: transgenic mouse, [6] M: months, [7] OSN: olfactory sensory neuron [8] ELISA: enzyme-linked immunosorbent assay [9] PCR: polymerase chain reaction, [10] BrdU: 5-bromodeo-2-deoxyuridine, [11] hAPP: human amyloid precursor protein, [12] w: weeks, [13] OB: olfactory bulb, [14] WB: western blot, [15] ISH: in situ hybridization, [16] BACE: β-site amyloid cleavage enzyme, [17] AAV: Adeno-associated virus, [18] TMT: 2,3,5-Trimethyl-3-thiazoline, [19] CORMAP: Conditional, Olfactory Sensory Neuron-Restricted Mosaic expression of APPsw and PLAP.

5. Organization of the olfactory system

5.1. Peripheral olfactory system

The processing of odor signals in mammals is initiated in the OE with OSNs being the primary neuron in the OE (Fig. 1). The somata of OSNs are organized in orderly layers based on maturity, ranging from basal cells to matured neurons (*47*) (Fig. 2). Once an odorant, *i.e.,* a gaseous molecule, or any airborne substances reaches the OE and binds to the odorant receptors located in the OSNs, the OSNs transduce the odor information into electrical signals that trigger neurotransmitter release in the OBs (*10*) (Fig. 1). Subsequently, those neuronal signals are transmitted to the olfactory cortex through the olfactory tract and tubercles (*10*). Mucus secreted by Bowman's glands and sustentacular cells protect the OE's structure and maintain its homeostasis (*48*).

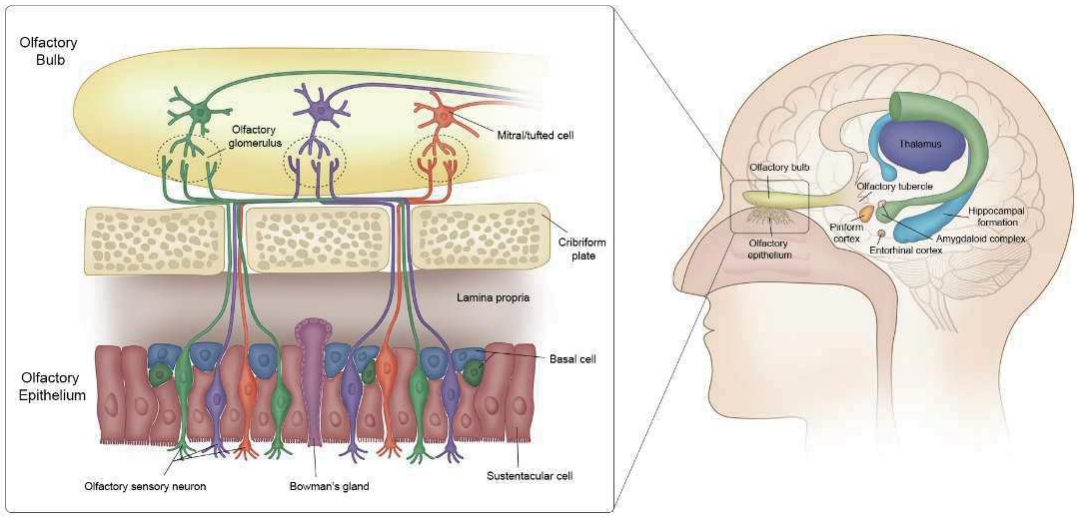

Figure 1. Scheme of the olfactory system. (Left) Scheme of olfactory sensory neuron projections. Olfactory sensory neurons transduce odor information via electrical signals that trigger neurotransmitter release in the olfactory bulb. Mucus secreted by Bowman's glands and sustentacular cells protect the olfactory epithelium's structure and maintains homeostasis. (Right) Scheme of the olfactory system according to the process of olfaction.

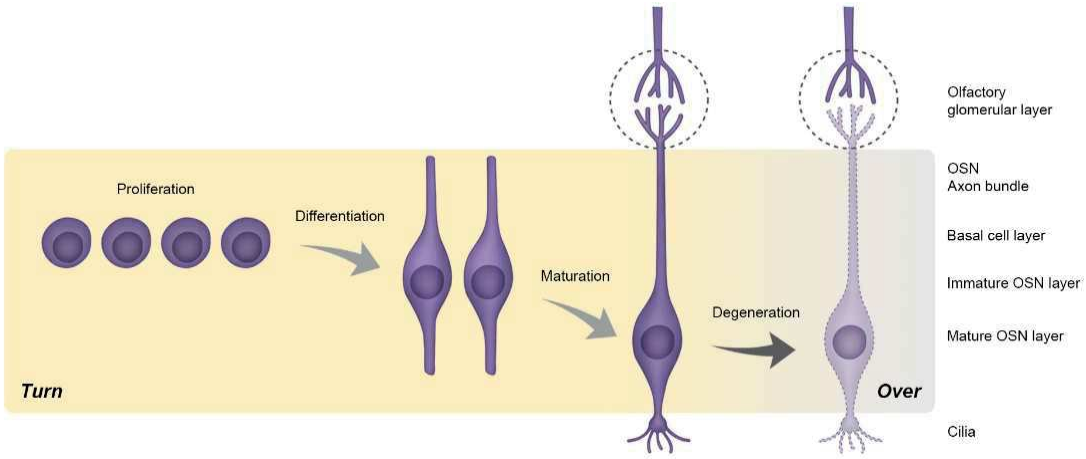

Figure 2. Scheme of the turnover of olfactory sensory neurons. Once the olfactory sensory neurons (OSNs) degenerate in the lifetime, new OSNs originate from progenitor cells located in the basal layer that proliferate and send their axons to the olfactory bulb.

5.2. Synaptic interface between peripheral and central components

Synaptic connectivity between the OSNs and central olfactory neurons in the OB glomeruli is essential for the initial detection, identification, and discrimination of the odors (*49*). Thus, early synaptic dysfunction in the OSNs could lead to greater impairment of olfactory information processing, thereby causing olfactory deficits. The structure of the OB shows a conserved laminar organization across species (*50*), Basically, the glomerulus, a neuropil structure of intertwining axons of OSNs, dendrites of periglomerular cells, and dendrites of mitral/tufted cells is the focus of initial processing of olfactory information (*51*) (Fig. 3). The glomeruli are considered the first recipient of sensory inputs, because they host the first synapse in the olfactory system. In the glomerular network, which is well described in rodents, axons from OSNs expressing the same odorant receptor converge into approximately two of the 1,800 glomeruli in each OB (*52, 53*). The periglomerular

cells are dopaminergic/GABAergic neurons that form an inhibitory feedback loop with the OSNs (*54*).

5.3. Central olfactory system

The olfactory system is anatomically distinctive and the projections are highly organized. The primary olfactory cortex includes the anterior olfactory nucleus, the olfactory tubercle, the piriform cortex, the entorhinal cortex, and the amygdala, including the orbitofrontal regions and the neural signals projecting to the secondary olfactory cortex in the orbitofrontal cortex (*55*) (Fig. 1). The afferent input from the OB is transmitted to the primary olfactory cortex through the olfactory tubercles composed of axons of mitral/tuft cells and GABAergic interneurons (*56*). These cells are differentiated from progenitor cells that have migrated from the subventricular zone (*56*). This track forms the first cranial nerve in the central nervous system (*57*).

6. Neuropathology of the olfactory system in AD

Olfaction can be compromised not only by a severe memory and cognitive disruption, but also by olfactory pathways damaged by injury or chronic exposure to toxic substances triggering AD pathogenesis. In this context, the olfactory system can be seen as a distinctly damaged site independent of the limbic system in terms of both AD pathologies and diagnostic opportunities. Clinical studies have reported forms of proteinopathy in the peripheral olfactory system in AD patients. For instance, Aβ and p-tau immunoreactivity have been found in the OE of AD patients (*14*). Interestingly, the degree of immunoreactivity in the OE correlated with

semiquantitative ratings of cortical amyloid and tau-lesion ratings (*14*). Large amounts of Aβ detected in nasal secretions may indicate that such proteins originate from the epithelium and peripheral olfactory neurons (*34*). In the glomeruli of the OB, Aβ and hyperphosphorylated tau have been detected, exhibiting progressive expression as *Braak* stages of AD pathology increased (*17*), but no significant changes were observed within the olfactory tract (*13*). Given these findings, the peripheral olfactory system could be behind the generation of the toxic misfolded proteins that affect OSNs.

Moreover, both Aβ and tau have been observed in the cortical olfactory areas in AD patients, including the olfactory peduncle, the anterior olfactory nucleus (*12, 13*), and the piriform cortex (*27*). A more recent study suggests that the olfactory system can be a hub to spread misfolded proteins to interconnected cortical areas and could seed the misfoldings of native proteins (*12*). In line with proteinopathy, patients with the apolipoprotein E4 (apoE4) allele, a well-known genetic factor linked with AD onset and an Aβ accumulation-triggering factor, are highly associated with olfactory deficits (*36*).

7. Mechanisms of the olfactory pathophysiology in AD

7.1. Amyloid precursor protein (APP) processing

In a transgenic mouse model for AD, the enzyme expression involved in AD pathogenesis indicates a mechanism that may underly olfactory pathology. Positive Aβ immunoreactivity was found within the glomerular layer in young mice (*38*) and

increased across the inner OB cell layers as the disease progressed (*41*). Expression of β-secretase, a major enzyme involved in amyloidosis, was only observed only in the glomerular layer of the OB even in C57BL/6 mouse, a common inbred strain of laboratory mice, showing that the glomerular layer is likely the main region in Aβ production among OB layers (*42*).

A correlation between olfactory dysfunction and amyloid deposition was reported in APP/PS1 mice (*37*). Transgenic mice with selective overexpressing humanized APP (hAPP) in either mature or immature OSNs exhibited widespread cell-autonomous apoptosis in OSNs, exhibiting that Aβ pathology is involved in olfactory neurodegeneration (*39*). Electron microscopy showed a decreased glomerular connectivity along with subcellular structural deficits (*39*). Furthermore, OSNs may play a role in independent APP processing. In one of the most well-characterized and widely used transgenic mouse models, the Tg2576 mouse model that conventionally overexpresses hAPP, the OE exhibits a higher expression level and activity of γ-secretase than that of other brain regions (*45*). Increased β-secretase levels in the olfactory glomerular layer have also been observed in Tg2576 (*38*).

7.2. Neuroinflammation

Apart from direct AD pathology, several environmental toxic factors can affect olfaction by damaging the OE, indicating that local toxicity is sufficient to impair smell. For instance, air dust and nanoparticles damage OSNs directly, causing oxidative stress and neuroinflammation similar to amyloid deposition (*44*). A variety of air

pollutants trigger oxidative stress in the OE, resulting in protein misfolding, mitochondrial dysfunction, and neuronal apoptosis. Furthermore, such factors recruit reactive microglia that can exacerbate inflammation by releasing pro-inflammatory cytokines such as TNF-a, IL-β, IFNγ (*58*). Interestingly, clinical studies have shown that one fifth of diagnosed patients with AD have a history of allergies and chronic rhinitis that had required some sort of treatment (*33*).

Such toxic factors not only cause neuronal damage directly but could also exacerbate ongoing pathological process such as neuroinflammation (*59*) leading to further olfactory disturbances.

7.3. Spreading pathology along the neural circuit

The OB receives serotonergic projections from brainstem raphe nuclei which could form a reciprocal pathway that receives down-top signals through the olfactory cortex and modulates OSNs' synaptic activity (*60*). Given theories that emphasize the brainstem's role in AD pathology, raphe-OB connections could play a key function in AD pathology (*61*) because raphe pathology happens at early AD stages (*62*), implying that the OB is also involved in an early stage from both anterograde and retrograde influences. According to several other studies, the OB could deliver misfolded proteins into the brain. As evidence, Aβ that was injected into the OB of C57BL/6 mice was also found in other brain regions, such as frontal cortex (*46*). A prion-like spreading of toxic molecules that could cause olfactory abnormalities might occur in the non-cortical olfactory structures (*63*).

7.4. Physiology of spatially conserved map

Physiological functions are closely related to progressive pathological alterations in the olfactory system and can induce smell dysfunction in the onset of AD. The spatially conserved map in the olfactory system may play a critical role in the manifestation and progression of olfactory impairment in AD.

According to rodent studies, a physiologically conserved axis between the OE and OB can affect decreasing or increasing AD pathogenesis and olfactory dysfunction. Naturally, the mammalian main olfactory system has a spatially-organized neuroregeneration and projection of OSNs, which originate from progenitor cells located in the basal layer that proliferate (*64*) and mature by sending their axons to reach the OB. After development, OSNs can degenerate because of physical injury, cellular stress, aging, and AD-related pathology. To maintain the structure of the OE, basal cells proliferate and differentiate into immature OSNs, then to mature OSNs, by rendering a synaptic interface with the mitral cellular dendrite in the OB (Fig. 2). This process occurs throughout life and is called the replacement or turnover of OSNs (*65*) (Fig. 2). Odorant receptor genes in the OSNs determine axonal projections to dorsal and ventral (ectoturbinates and endoturbinates in the OE's coronal plain) glomeruli in the OB (*66*) that show the topographic projection and subzonal organization (*67, 68*) (Fig. 3). OSN replacement is also regulated by a variety of physiological factors such as retinoic acid, a well-known cell differentiation promoter (*69, 70*). The two domains (endoturbinate-dorsal and ectoturbinate-ventral) summarize the zonal organization in the olfactory system and have different

physiologies (Fig. 3). For example, when progenitor cells harvested from the dorsal OE were transplanted into the ventral region in mice, the transplant-derived neurons expressed a selective immunoreactive ventral marker OCAM (olfactory cell adhesion molecule) and lost a dorsal marker NQO1 (NADPH dehydrogenase) to match their new location (*70*). Additionally, Liberia et al (*47*) and Son et al (*43*) showed that OSNs in the ventral OE have a faster ratio of turnover (regeneration and degeneration) than do those in the dorsal part, suggesting that repetitive OSN turnover triggers neuronal death of mature OSNs by driving excessive apoptosis, metabolic wastes, and neuroinflammation. Together, these events could cause more olfactory neuropathology to promote pathological processes, such as APP expression and neuroinflammation.

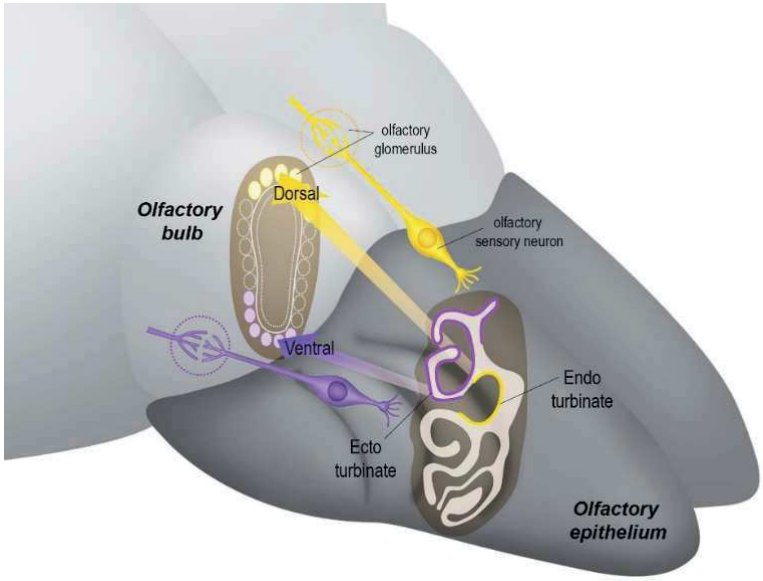

Figure 3. Scheme of the spatially conserved map in the mouse olfactory system. The zonal organization, endoturbinates-dorsal glomerulus axis (yellow), and ectoturbinates-ventral glomerulus axis (purple). The two drawings in yellow and purple are representations of two olfactory sensroy neurons, with the colors emphasizing the regional topography of sensory inputs to the olfactory bulb.

Overexpression of β-secretase could impair olfactory function by causing cell death in ventrally projecting OSNs (*38*). In line with this, mRNA of β-secretase protein 1 (BACE1) was expressed in the ectoturbinate of OE in C57BL/6 (*42*). In addition, oligomeric Aβs and β-secretase proteins were robustly expressed in the ventral parts of the glomeruli in Tg2576 (*38*). Calcium activity was decreased in the OSNs in the ventral regions where oligomeric Aβ is highly overexpressed and significantly damaged OSN turnover in the ectoturbinate OE more than in the endoturbinate OE in 5xFAD with mutated human APP and presenilin 1 gene, a transgenic mouse model that can recapitulate AD-related early and aggressive phenotypes (*43*). Regarding neuroinflammation, Hasegawa-Ishii et al (*71*) reported intranasal administration of lipopolysaccharide induced an inflammatory response and synaptic loss in OSNs by triggering both microglia and astrocyte activation in the OB. Intriguingly, inflammatory monocyte immunoreactivity (Ly-6) was highly indicated in the ectoturbinate of the OE.

Extrinsic stimulation can affect different physiologies of the spatially conserved map of the olfactory system. OSNs are exposed to inhaled air and are therefore vulnerable to environmental factors such as air pollutants that cause DNA damage and cellular stress (*72*) whereas the ectoturbinates in the OE have a curved structure that increases contact with inhaled air (*73*). OSNs are also sensitive to changes in air pressure and air flow (*47, 74*). Structural and functional changes of the spatially conserved map can affect neuronal stability in the olfactory system and initiate a vicious cycle that could cause further damage. Further studies are required to define

neuronal damage and excessive immune responses involved in the ectoturbinates and the endoturbinates.

The conserved map is strongly preserved across species (*75, 76*). Intriguingly, in a human postmortem study, the volume of ventral glomeruli was reduced in Parkinson's disease patients' OBs (*77*). However, many aspects remain to be explored in AD patients.

8. Clinical implications of olfactory pathophysiology in AD

The olfactory system has received much interest in recent years as a novel tool for drug delivery and diagnosis in AD. Despite the advances in AD biomarker research, knowledge about the applicability and accuracy of markers remains incomplete. An olfactory test for AD was developed by Richard L. Doty in 1984 (*78*), and has been applied in clinical research and diagnosis over the last 30 years. Olfactory dysfunction in AD exhibits specific features, with clinical studies showing patients have difficulties identifying a specific subset of odorants (*30*). In particular, the peanut butter smell has been suggested as a reference test for AD patients, must be closer in order of AD patients to detect the smell than is needed for healthy controls (*31*). Partial hyposmia or specific anosmia is when one has an otherwise normal sense of smell but cannot perceive one or more specific odors. A recent study using 5xFAD suggested the features and mechanism of the partial olfactory dysfunction demonstrating regionally specific Aβ accumulation influences partial

olfactory dysfunction during early AD pathogenesis (*43*). These results suggest continued research on mechanisms within olfactory-system pathophysiology can provide new light in early AD diagnoses.

Olfactory neuropathology allows us to speculate that the impaired OE includes altered cellular and molecular components. Hence nasal fluid from the OE may feasibly contain high-throughput biological material information which mirrors AD pathological changes in the olfactory system (*34*) that could be linked to the OE. The composition of oligomerized Aβ proteins in nasal discharge is also closely correlated with cognitive function during AD progression (*35*). Thus, nasal-fluid biomarkers could prove to be a candidate sourcing tool in AD similar to cerebrospinal fluid and plasma biomarkers. Correspondingly, the olfactory system may provide a new platform for conducting preclinical and clinical studies to improve diagnostics in AD and better understand the mechanisms behind neurodegeneration in AD.

9. Conclusion

This review highlights the significance of olfactory pathophysiology and olfactory dysfunction in AD progression. The olfactory function can be impaired by the AD pathologies derived by amyloidogenic APP processing and neuroinflammation in the olfactory system. In particular, the physiological features of the spatially conserved map in the OE and OB play a complex role in ongoing olfactory neurodegeneration that induces abnormal olfaction within AD. This review suggests olfactory neuropathology and neurodegeneration itself can be seen as the main underlying cause of olfactory dysfunction rather than it being derived from higher cortical area deficits seen throughout AD. Taken together, AD is an incurable and irreversible disease, but AD-related olfactory dysfunction provides clues towards diagnostic methods and gives insight into onset mechanisms in AD pathogenesis.

Acknowledgments

This work was supported by the Korea Health Industry Development Institute (HI18C0154) and Basic Science Research Program through the National Research Foundation of Korea (NRF) funded by the Ministry of Education (2020R1A6A1A03040516). The funding sources had no such involvement in study design; in the collection, analysis and interpretation of data; in the writing of the report; and in the decision to submit the article for publication.

References

1. Alzheimer's-Association, 2021 Alzheimer's disease facts and figures. *Alzheimers Dement*, (2021).
2. C. Murphy, Olfactory and other sensory impairments in Alzheimer disease. *Nat Rev Neurol* **15**, 11-24 (2019).
3. R. L. Ownby, E. Crocco, A. Acevedo, V. John, D. Loewenstein, Depression and risk for Alzheimer disease: systematic review, meta-analysis, and metaregression analysis. *Arch Gen Psychiatry* **63**, 530-538 (2006).
4. A. Brzecka *et al.*, Sleep Disorders Associated With Alzheimer's Disease: A Perspective. *Front Neurosci* **12**, 330 (2018).
5. C. R. Schubert *et al.*, Olfaction and the 5-year incidence of cognitive impairment in an epidemiological study of older adults. *J Am Geriatr Soc* **56**, 1517-1521 (2008).
6. R. O. Roberts *et al.*, Association Between Olfactory Dysfunction and Amnestic Mild Cognitive Impairment and Alzheimer Disease Dementia. *JAMA Neurol* **73**, 93-101 (2016).
7. M. M. Vasavada *et al.*, Central Olfactory Dysfunction in Alzheimer's Disease and Mild Cognitive Impairment: A Functional MRI Study. *J Alzheimers Dis* **59**, 359-368 (2017).
8. C. R. Jack, Jr. *et al.*, Associations of Amyloid, Tau, and Neurodegeneration Biomarker Profiles With Rates of Memory Decline Among Individuals Without Dementia. *JAMA* **321**, 2316-2325 (2019).
9. A. S. Barwich. (Harvard University Press,, Cambridge, Massachusetts, 2020), pp. 1 online resource.
10. S. Firestein, How the olfactory system makes sense of scents. *Nature* **413**, 211-218 (2001).
11. J. A. Gottfried, Central mechanisms of odour object perception. *Nat Rev Neurosci* **11**, 628-641 (2010).
12. I. Ubeda-Banon *et al.*, The human olfactory system in two proteinopathies: Alzheimer's and Parkinson's diseases. *Transl Neurodegener* **9**, 22 (2020).
13. P. Bathini, A. Mottas, M. Jaquet, E. Brai, L. Alberi, Progressive signaling changes in the olfactory nerve of patients with Alzheimer's disease. *Neurobiol Aging* **76**, 80-95 (2019).
14. S. E. Arnold *et al.*, Olfactory epithelium amyloid-beta and paired helical filament-tau pathology in Alzheimer disease. *Ann Neurol* **67**, 462-469 (2010).
15. L. Cao *et al.*, Abeta alters the connectivity of olfactory neurons in the absence of amyloid plaques in vivo. *Nat Commun* **3**, 1009 (2012).
16. M. Dibattista, S. Pifferi, A. Menini, J. Reisert, Alzheimer's Disease: What Can We Learn From the Peripheral Olfactory System? *Front Neurosci* **14**, 440 (2020).
17. D. R. Thal, U. Rub, M. Orantes, H. Braak, Phases of A beta-deposition in the human brain and its relevance for the development of AD. *Neurology* **58**, 1791-1800 (2002).
18. H. Braak, E. Braak, Neuropathological stageing of Alzheimer-related changes. *Acta Neuropathol* **82**, 239-259 (1991).
19. M. A. DeTure, D. W. Dickson, The neuropathological diagnosis of Alzheimer's disease. *Mol Neurodegener* **14**, 32 (2019).
20. J. Cummings, G. Lee, A. Ritter, M. Sabbagh, K. Zhong, Alzheimer's disease drug development pipeline: 2020. *Alzheimers Dement (NY)* **6**, e12050 (2020).
21. V. S. Pankratz *et al.*, Predicting the risk of mild cognitive impairment in the Mayo Clinic Study of Aging. *Neurology* **84**, 1433-1442 (2015).
22. M. Vyhnalek *et al.*, Olfactory identification in amnestic and non-amnestic mild cognitive

impairment and its neuropsychological correlates. *J Neurol Sci* **349**, 179-184 (2015).
23. M. R. Woodward *et al.*, Odorant Item Specific Olfactory Identification Deficit May Differentiate Alzheimer Disease From Aging. *Am J Geriatr Psychiatry* **26**, 835-846 (2018).
24. R. S. Wilson, S. E. Arnold, Y. Tang, D. A. Bennett, Odor identification and decline in different cognitive domains in old age. *Neuroepidemiology* **26**, 61-67 (2006).
25. G. E. Swan, D. Carmelli, Impaired olfaction predicts cognitive decline in nondemented older adults. *Neuroepidemiology* **21**, 58-67 (2002).
26. P. A. Thomann *et al.*, Reduced olfactory bulb and tract volume in early Alzheimer's disease--a MRI study. *Neurobiol Aging* **30**, 838-841 (2009).
27. D. Saiz-Sanchez, C. De la Rosa-Prieto, I. Ubeda-Banon, A. Martinez-Marcos, Interneurons, tau and amyloid-beta in the piriform cortex in Alzheimer's disease. *Brain Struct Funct* **220**, 2011-2025 (2015).
28. D. P. Devanand *et al.*, Combining early markers strongly predicts conversion from mild cognitive impairment to Alzheimer's disease. *Biol Psychiatry* **64**, 871-879 (2008).
29. M. R. Woodward *et al.*, Olfactory identification deficit predicts white matter tract impairment in Alzheimer's disease. *Psychiatry Res Neuroimaging* **266**, 90-95 (2017).
30. M. H. Tabert *et al.*, A 10-item smell identification scale related to risk for Alzheimer's disease. *Ann Neurol* **58**, 155-160 (2005).
31. J. J. Stamps, L. M. Bartoshuk, K. M. Heilman, A brief olfactory test for Alzheimer's disease. *J Neurol Sci* **333**, 19-24 (2013).
32. A. Khan *et al.*, Environmental pollution is associated with increased risk of psychiatric disorders in the US and Denmark. *PLoS Biol* **17**, e3000353 (2019).
33. A. Bozek, P. Bednarski, J. Jarzab, Allergic rhinitis, bronchial asthma and other allergies in patients with Alzheimer's disease: unnoticed issue. *Postepy Dermatol Alergol* **33**, 353-358 (2016).
34. Y. H. Kim *et al.*, Amyloid beta in nasal secretions may be a potential biomarker of Alzheimer's disease. *Sci Rep* **9**, 4966 (2019).
35. S. J. Yoo *et al.*, Longitudinal profiling of oligomeric Aβ in human nasal discharge reflecting cognitive decline in probable Alzheimer's disease. *Sci Rep*, (2020).
36. C. Murphy, A. W. Bacon, M. W. Bondi, D. P. Salmon, Apolipoprotein E status is associated with odor identification deficits in nondemented older persons. *Ann N Y Acad Sci* **855**, 744-750 (1998).
37. Z. G. Yao, F. Hua, H. Z. Zhang, Y. Y. Li, Y. J. Qin, Olfactory dysfunction in the APP/PS1 transgenic mouse model of Alzheimer's disease: Morphological evaluations from the nose to the brain. *Neuropathology* **37**, 485-494 (2017).
38. S. J. Yoo *et al.*, Differential spatial expression of peripheral olfactory neuron-derived BACE1 induces olfactory impairment by region-specific accumulation of beta-amyloid oligomer. *Cell Death Dis* **8**, e2977 (2017).
39. N. Cheng, H. Cai, L. Belluscio, In vivo olfactory model of APP-induced neurodegeneration reveals a reversible cell-autonomous function. *J Neurosci* **31**, 13699-13704 (2011).
40. N. Cheng, S. Jiao, A. Gumaste, L. Bai, L. Belluscio, APP Overexpression Causes Abeta-Independent Neuronal Death through Intrinsic Apoptosis Pathway. *eNeuro* **3**, (2016).
41. D. W. Wesson, E. Levy, R. A. Nixon, D. A. Wilson, Olfactory dysfunction correlates with amyloid-beta burden in an Alzheimer's disease mouse model. *J Neurosci* **30**, 505-514 (2010).
42. L. Cao, G. T. Rickenbacher, S. Rodriguez, T. W. Moulia, M. W. Albers, The precision of axon targeting of mouse olfactory sensory neurons requires the BACE1 protease. *Sci Rep* **2**, 231 (2012).

43. G. Son *et al.*, Region-specific amyloid-beta accumulation in the olfactory system influences olfactory sensory neuronal dysfunction in 5xFAD mice. *Alzheimers Res Ther* **13**, 4 (2021).
44. H. Cheng *et al.*, Nanoscale Particulate Matter from Urban Traffic Rapidly Induces Oxidative Stress and Inflammation in Olfactory Epithelium with Concomitant Effects on Brain. *Environ Health Perspect* **124**, 1537-1546 (2016).
45. J. Y. Kim *et al.*, Distinct amyloid precursor protein processing machineries of the olfactory system. *Biochem Biophys Res Commun* **495**, 533-538 (2018).
46. B. He *et al.*, Injected Amyloid Beta in the Olfactory Bulb Transfers to Other Brain Regions via Neural Connections in Mice. *Mol Neurobiol* **55**, 1703-1713 (2018).
47. T. Liberia, E. Martin-Lopez, S. J. Meller, C. A. Greer, Sequential Maturation of Olfactory Sensory Neurons in the Mature Olfactory Epithelium. *eNeuro* **6**, (2019).
48. T. T. Solbu, T. Holen, Aquaporin pathways and mucin secretion of Bowman's glands might protect the olfactory mucosa. *Chem Senses* **37**, 35-46 (2012).
49. D. A. Storace, L. B. Cohen, Measuring the olfactory bulb input-output transformation reveals a contribution to the perception of odorant concentration invariance. *Nat Commun* **8**, 81 (2017).
50. H. P. Burmeister *et al.*, Imaging of lamination patterns of the adult human olfactory bulb and tract: in vitro comparison of standard- and high-resolution 3T MRI, and MR microscopy at 9.4 T. *Neuroimage* **60**, 1662-1670 (2012).
51. E. E. Morrison, R. M. Costanzo, Morphology of the human olfactory epithelium. *J Comp Neurol* **297**, 1-13 (1990).
52. M. Wachowiak, L. B. Cohen, Representation of odorants by receptor neuron input to the mouse olfactory bulb. *Neuron* **32**, 723-735 (2001).
53. A. Maresh, D. Rodriguez Gil, M. C. Whitman, C. A. Greer, Principles of glomerular organization in the human olfactory bulb--implications for odor processing. *PLoS One* **3**, e2640 (2008).
54. S. Bonzano, S. Bovetti, C. Gendusa, P. Peretto, S. De Marchis, Adult Born Olfactory Bulb Dopaminergic Interneurons: Molecular Determinants and Experience-Dependent Plasticity. *Front Neurosci* **10**, 189 (2016).
55. V. S. Ramachandran, *Encyclopedia of the human brain*. (Academic Press, San Diego, Calif., 2002).
56. A. Sahay, D. A. Wilson, R. Hen, Pattern separation: a common function for new neurons in hippocampus and olfactory bulb. *Neuron* **70**, 582-588 (2011).
57. E. H. Holbrook, D. H. Coelho, Cranial Nerve Stimulation for Olfaction (Cranial Nerve 1). *Otolaryngol Clin North Am* **53**, 73-85 (2020).
58. F. Imamura, S. Hasegawa-Ishii, Environmental Toxicants-Induced Immune Responses in the Olfactory Mucosa. *Front Immunol* **7**, 475 (2016).
59. F. L. Heppner, R. M. Ransohoff, B. Becher, Immune attack: the role of inflammation in Alzheimer disease. *Nat Rev Neurosci* **16**, 358-372 (2015).
60. R. Steinfeld, J. T. Herb, R. Sprengel, A. T. Schaefer, I. Fukunaga, Divergent innervation of the olfactory bulb by distinct raphe nuclei. *J Comp Neurol* **523**, 805-813 (2015).
61. K. Sakurai *et al.*, Hyper BOLD Activation in Dorsal Raphe Nucleus of APP/PS1 Alzheimer's Disease Mouse during Reward-Oriented Drinking Test under Thirsty Conditions. *Sci Rep* **10**, 3915 (2020).
62. K. A. Michelsen, J. Prickaerts, H. W. Steinbusch, The dorsal raphe nucleus and serotonin: implications for neuroplasticity linked to major depression and Alzheimer's disease. *Prog Brain Res* **172**, 233-264 (2008).
63. N. L. Rey, D. W. Wesson, P. Brundin, The olfactory bulb as the entry site for prion-like

propagation in neurodegenerative diseases. *Neurobiol Dis* **109**, 226-248 (2018).
64. J. H. Brann, D. P. Ellis, B. S. Ku, E. F. Spinazzi, S. Firestein, Injury in aged animals robustly activates quiescent olfactory neural stem cells. *Front Neurosci* **9**, 367 (2015).
65. P. P. Graziadei, R. R. Levine, G. A. Graziadei, Regeneration of olfactory axons and synapse formation in the forebrain after bulbectomy in neonatal mice. *Proc Natl Acad Sci U S A* **75**, 5230-5234 (1978).
66. K. Miyamichi, S. Serizawa, H. M. Kimura, H. Sakano, Continuous and overlapping expression domains of odorant receptor genes in the olfactory epithelium determine the dorsal/ventral positioning of glomeruli in the olfactory bulb. *J Neurosci* **25**, 3586-3592 (2005).
67. Eerdunfu, N. Ihara, B. Ligao, Y. Ikegaya, H. Takeuchi, Differential timing of neurogenesis underlies dorsal-ventral topographic projection of olfactory sensory neurons. *Neural Dev* **12**, 2 (2017).
68. O. Levai, H. Breer, J. Strotmann, Subzonal organization of olfactory sensory neurons projecting to distinct glomeruli within the mouse olfactory bulb. *J Comp Neurol* **458**, 209-220 (2003).
69. H. Login, S. Haglin, A. Berghard, S. Bohm, The Stimulus-Dependent Gradient of Cyp26B1+ Olfactory Sensory Neurons Is Necessary for the Functional Integrity of the Olfactory Sensory Map. *J Neurosci* **35**, 13807-13818 (2015).
70. J. H. Coleman *et al.*, Spatial Determination of Neuronal Diversification in the Olfactory Epithelium. *J Neurosci* **39**, 814-832 (2019).
71. S. Hasegawa-Ishii, A. Shimada, F. Imamura, Lipopolysaccharide-initiated persistent rhinitis causes gliosis and synaptic loss in the olfactory bulb. *Sci Rep* **7**, 11605 (2017).
72. L. Calderon-Garciduenas *et al.*, DNA damage in nasal and brain tissues of canines exposed to air pollutants is associated with evidence of chronic brain inflammation and neurodegeneration. *Toxicol Pathol* **31**, 524-538 (2003).
73. K. Zhao, P. Dalton, G. C. Yang, P. W. Scherer, Numerical modeling of turbulent and laminar airflow and odorant transport during sniffing in the human and rat nose. *Chem Senses* **31**, 107-118 (2006).
74. Y. Oka, Y. Takai, K. Touhara, Nasal airflow rate affects the sensitivity and pattern of glomerular odorant responses in the mouse olfactory bulb. *J Neurosci* **29**, 12070-12078 (2009).
75. T. Imai, H. Sakano, L. B. Vosshall, Topographic mapping--the olfactory system. *Cold Spring Harb Perspect Biol* **2**, a001776 (2010).
76. O. R. Braubach *et al.*, Experience-dependent versus experience-independent postembryonic development of distinct groups of zebrafish olfactory glomeruli. *J Neurosci* **33**, 6905-6916 (2013).
77. B. Zapiec *et al.*, A ventral glomerular deficit in Parkinson's disease revealed by whole olfactory bulb reconstruction. *Brain* **140**, 2722-2736 (2017).
78. R. L. Doty, P. Shaman, M. Dann, Development of the University of Pennsylvania Smell Identification Test: a standardized microencapsulated test of olfactory function. *Physiol Behav* **32**, 489-502 (1984).

Chapter 3

Differential spatial expression of peripheral olfactory neuron-derived BACE1 induces olfactory impairment by region-specific accumulation of β-amyloid oligomer

Seung-Jun Yoo [1], Ji-Hye Lee [1], So Yeun Kim [1,2], **Gowoon Son** [1], Jae Yeon Kim [1], Bongki Cho [1,2], Seong-Woon Yu [1], Keun-A Chang [3], Yoo-Hun Suh [3], and Cheil Moon [1,2]

[Cell Death & Disease, 2017, doi: 10.1038/cddis.2017.349]

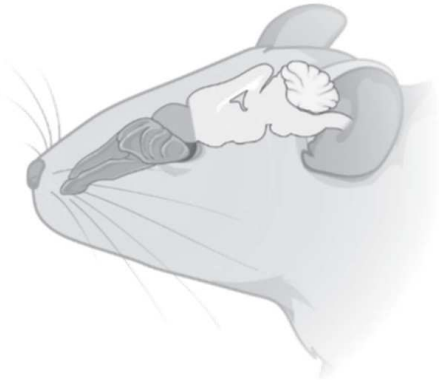

Abstract

Olfactory dysfunction is a common symptom associated with neurodegenerative diseases including Alzheimer's disease (AD). Although evidence exists to suggest that peripheral olfactory organs are involved in the olfactory dysfunction that accompanies AD pathology, the underlying mechanisms are not fully understood. As confirmed using behavioral tests, transgenic mice overexpressing a Swedish mutant form of human amyloid precursor proteins exhibited olfactory impairments prior to evidence of cognitive impairment. By measuring the expression of tyrosine hydroxylase, we observed that specific regions of the olfactory bulb (OB) in Tg2576 mice, specifically the ventral portion exhibited significant decreases in the number of dopaminergic neurons in the periglomerular regions from the early stage of AD. To confirm the direct linkage between these olfactory impairments and AD-related pathology, β-site amyloid precursor protein cleaving enzyme 1 (BACE1)—the initiating enzyme in Aβ genesis—and β-amyloid peptide (Aβ), hallmarks of AD were analyzed. We found that an increase in BACE1 expression coincided with an elevation of amyloid-β (Aβ) oligomers in the ventral region of OB. Moreover, olfactory epithelium (OE), in particular the ectoturbinate in which axons of olfactory sensory neurons (OSNs) have direct connections with the dendrites of mitral/tufted cells in the ventral part of OB, exhibited significant decreases in both thickness and cell number even at early stages. This result suggests that Aβ oligomer toxicity in the OE may have induced a decline in the number of OSNs and functional impairment of the olfactory system. We first demonstrated that disproportionate

levels of regional damage in the peripheral olfactory system may be a specific symptom of AD with Aβ oligomer accumulation occurring prior to damage within the CNS. This regional damage in the olfactory system early in the progression of AD may be closely related to AD-related pathological abnormality and olfactory dysfunction found in AD patients.

List of abbreviations

AD, Alzheimer's disease; Aβ, β-amyloid; APP, amyloid precursor protein; CNS, central nervous system; OSN, olfactory sensory neuron; OB, olfactory bulb; OE, olfactory epithelium; MOB, mouse olfactory bulb; GL, glomerular layer; PG, periglomerular cell; TH, tyrosine hydroxylase; BACE1, β-secretase protein 1; MAP2, microtubule protein 2; ADDL, $A\beta_{1-42}$ peptide-derived diffusible ligands.

1. Introduction

Alzheimer's disease (AD) is a neurodegenerative disorder characterized by memory decline and other functional cognitive impairments that result from the progressive degeneration of neurons in the brain (*1*). The AD brain has been histologically characterized by the presence of neuritic plaques and neurofibrillary tangles, which are composed of protein aggregates of amyloid β (Aβ) and tau, respectively (2). Specifically, soluble clusters of Aβ (Aβ oligomers) are involved in the early stage of AD prior to tau-mediated pathology (3, 4). The soluble monomeric forms, $A\beta_{1-40}$ and $A\beta_{1-42}$, are produced mainly in neurons from amyloid precursor protein (APP, ~120 kDa) via proteolytic process by β- and γ-secretases (5, 6). Although these monomeric forms of Aβ can drive formation of various oligomers in normal physiology, Aβ*56 (12-mer, ~56 kDa) and AβO (15-mer, ~80 kDa) have particularly high neurotoxicity (7, 8).

Declining sensory functions are also common in neurodegenerative disorders including AD (*9*). A number of recent reports have revealed pathological events in the sensory organs of patients with AD (*10, 11*). Symptoms of olfactory dysfunction in particular were believed to be the result of neurodegeneration occurring in olfaction-related limbic cortices of the central nervous system (CNS) until the late 1980s (*12*). Although the precise mechanisms remain unclear, recent reports suggest that olfactory dysfunction appears in the early symptomatic stages of AD pathology (*11, 13, 14*) and that sensory systems may be more vulnerable to AD pathology than

the CNS as a whole. Nevertheless, the peripheral olfactory system in AD models has been not sufficiently investigated.

AD-related olfactory dysfunction has been explored using transgenic mice, Tg2576, expressing a Swedish mutant form of human amyloid precursor protein (APP) (KM670/671NL) (*15-18*). Tg2576 mice exhibit progressive olfactory impairment in an age-dependent manner correlated to stages of disease progression. In addition, 6-month-old, early stage of AD progression, Tg2576 mice exhibited impairment of olfactory habituation and discrimination resulting from deposition of Aβ in OB (19), implying that impairment of the central olfactory circuit is involved in olfactory dysfunction. Additionally, recent studies have shown that impairment of the peripheral olfactory system may also contribute to AD-related olfactory dysfunction. Overexpression of human APP in olfactory sensory neurons (OSNs) induces abnormal axonal projections of OSNs residing in the olfactory epithelium (OE) to the olfactory bulb (OB) (*20*) and cell-autonomous cell death (*21*). Many previous studies have focused mainly on the OB and the central olfactory system rather than on OE and the peripheral olfactory organs, to explain the olfactory dysfunction observed in AD. Although some studies of olfactory behavior deficits and impaired OB functioning in this AD mouse model have been conducted (*22, 23*), there is little evidence to support the involvement of peripheral olfactory organs in olfactory dysfunction of the AD model.

In the current study, we first investigated the integrity of postsynaptic function and related structural changes between peripheral OE and OB for olfactory recognition using the Tg2576 mice at both early and late stages in order to understand the causes and mechanisms of the olfactory dysfunction related to AD. We also explored the feasibility of early AD diagnosis using the olfactory system.

2. Materials and methods

2.1. Transgenic mice

Tg2576 APP transgenic mice harboring the mutated human APP (695 amino acids) gene were obtained from Taconic (USA) and the production, genotyping, and background strain (C57BL/6 × SJL) have been described previously (*24*). All experiments were performed in accordance with 'the Guidelines for Animal Experiments from the Ethics Committee at Seoul National University' (IACUC No. SNU-091208-1).

2.2. Morris water maze

To test spatial memory formation, the Morris water maze was performed as previously described with some modification (*25*). More specifically, the sizes of the circular water tank (diameter, 140 cm; height, 45 cm) and the platform (width, 13 cm; length, 13 cm; height, 17 cm) for the mice were modified. A platform was submerged and placed 0.5 cm below water made opaque using milk (depth, 17.5 cm) at the midpoint of one quadrant. Three training trials per day were conducted for 7 days,

with a rotation order specified for each trial in a group. Mice were placed in the pool at one of the three possible quadrant starting positions (with the exception of the quadrant containing the platform). During each training trial, the time required to escape onto the hidden platform was recorded. Mice that found the platform were allowed to remain on it for 30 s, and were then returned to their home cages during the interval between trials. Mice that did not find the platform within 60 s were placed on the platform for 30 s at the end of each trial. The probe test was carried out for 48 h after the trials. For this test, the platform was removed from the pool and the trial was performed with a cutoff time of 60 s. The time spent in each quadrant was recorded.

2.3. Food-seeking test

All behavioral and histological analysis was conducted by personnel blind to group inclusion. Food-seeking tests were performed at 6 and 14 months of age for the Tg2576 and WT groups (n=8 per group). The food-seeking test was modified slightly but otherwise performed as described previously (*26, 27*). Additionally, the unburied food-seeking test was also performed and compared to the buried food-seeking test under the same conditions to confirm olfactory dysfunction without cognitive impairment. For the buried food-seeking test, the speed with which an animal fasted for over 35 h could find a food pellet, either hidden underneath a layer of bedding or not, was measured. Therefore, this test was used to assess latency in finding food as both the buried pellet-seeking test and the unburied pellet-seeking test. Prior to the food-seeking tests, food restriction was applied for over 35 h to

motivate animals to search for food. For the buried pellet-seeking test, mice were habituated in a clean home cage for 15 min prior to testing (*26*). A food pellet was buried ~2.5 cm under the bedding in a corner of the cage and a mouse was placed in the opposite corner. The time to first bite of the food pellet was measured using an installed digital camera (recording time: 15 min maximum based on the assumption that food-restricted mice which fail to use odor cues to locate the food within a 15-min period are likely to have deficits in olfactory abilities).

2.4. Aβ42 oligomers preparation

Aβ42 oligomers were prepared as previously described (*28*). Briefly, the Aβ42 peptide (GL Biochem, Shanghai, China) was initially dissolved to a concentration of 1 mM in hexafluoroisopropanol. For its aggregation, the peptide was resuspended in dry dimethyl sulfoxide at 5 mM, and then added to Hams F-12 cell culture medium (PromoCell, Labclinics, Spain) to a final concentration of 100 mM at 4 °C for 24 h.

2.5. Antibodies

The following commercially available antibodies were purchased: anti-Aβ oligomer (Millipore, Temecula, CA, #AB9234); anti-GAPDH (Millipore, #MAB374); anti-tyrosine hydroxylase (TH) (Millipore, # MAB318); anti-cleaved caspase-3 (Cell Signaling Technology, Beverly, MA, USA, #9661); anti-p38 (Cell Signaling Technology, #9212); anti-phosphorylated p38 (Cell Signaling Technology, #9211); GAPDH (Chemicon, Temecula, CA, USA, # MAB374).

2.6. Western blot

OE was harvested in a prechilled lysis buffer (Sigma, St. Louis, MO, USA) containing a protease inhibitor cocktail (Roche, Branchburg, NJ, USA). Extracts were thawed, homogenized by sonication, and centrifuged at 10 000 rpm to remove cellular debris. Protein (100 μg) from each sample was loaded for SDS-PAGE and transferred to 0.45 μm PVDF membranes (Millipore). The membranes were blocked with 5% non-fat dry milk in Tris-buffered saline buffer with 0.1% Tween 20 and then incubated with primary antibodies. The primary antibodies used were anti-cleaved caspase-3 (1:1000), anti-Aβ oligomer (1:500), anti-p38 (1:1000), anti-phosphorylated p38 (1:1000), and GAPDH (1:1000). Immunoblots were visualized using a commercial development kit (Pierce, Rockford, IL, USA) and quantification was performed using the ImageJ program (NIH, Bethesda, MD, USA).

2.7. Histology

Animals were anesthetized by intraperitoneal injection of 65 mg/kg ketamine with 5 mg/kg xylazine. The mice were then transcardially perfused with prechilled phosphate-buffered saline (PBS, pH 7.6). Heads were removed, skinned, and post-fixed overnight in 4% paraformaldehyde in PBS at 4 °C. The mandibles were discarded, and the trimmed heads were skinned and fixed by immersion in the same fixative for 1 week at 4 °C. The heads were decalcified in 10% EDTA (pH 7.0) for 1 week at 4 °C. After decalcification, the specimens were washed, dehydrated in increasing concentrations of ethanol, and transferred into xylene to clear the tissue. The specimens were infiltrated with paraplast and embedded. Frontal sections

(coronal, 6 μm) were cut serially from the tip of the nose to the posterior extension of the OE and OB, and each section was preserved on MAS-coated slides (Matsunami Glass Co., Tokyo, Japan).

We determined and measured the contents of the OE including thickness and cell number using hematoxylin-eosin (H&E) staining. For H&E staining, sections were deparaffinized and rehydrated in water. Samples were then stained with H&E, dehydrated again, mounted permanently with permount, and covered with coverslips.

2.8. TUNEL staining assay

For TUNEL staining, deparaffinized and rehydrated sections were washed in PBS for 5 min and treated with proteinase K (10 μg/ml) in PBS at room temperature for 30 min. After washing in distilled water for 5 min, the TUNEL incubation solution (Millipore) containing TdT buffer, cobalt chloride, TdT, and biotin-16 dUTP was prepared in accordance with the manufacturer's protocol. The sections were incubated in TdT buffer for 1 h at 37 °C and then exposed to a stop solution for 10 min. After washing twice in PBS (5 min each), the sections were incubated with anti-digoxigenin peroxidase conjugate at room temperature for 30 min. Finally, sections were incubated in the DAB solution for several minutes. The fragmented DNAs were visualized as a brownish color inside the nuclei. The sections were counter-stained with methyl green before being dehydrated and cleared through graded alcohols and xylenes.

2.9. Immunohistochemistry

For immunohistochemistry, the endogenous peroxidase in the samples was quenched using 3% hydrogen peroxide in 10% methanol for 30 min. In order to retrieve antigenicity, the samples were boiled in 0.1 M citrate-buffered saline (pH 6.0) for 5 min. The sections were allowed to cool for 30 min, and were then washed twice in PBS (5 min each). After washing in PBS-T (0.1% Triton X-100 in PBS) for 30 min, the sections were blocked for 1 h in blocking solution (5% normal donkey serum and 1% BSA in PBS-T) and incubated with primary antibodies overnight at 4 °C. Anti-A*β* oligomer (1:200), anti-A*β* (1:500), and anti-TH (1:200) antibodies were used. After washing in PBS-T, the sections were incubated with a biotinylated secondary antibody for 1 h at room temperature. Subsequently, sections were treated with the avidin-biotin-peroxidase complex (Vectastain Elite ABC kit) for 1 h at room temperature. The sections were developed for 5 min in a 0.05% DAB solution, and were counter-stained with hematoxylin. Images were captured with a Nikon digital camera (DS-Ri1) attached to a Nikon-Eclipse-90i microscope (Nikon Corp., Tokyo, Japan).

2.10. Imaging and data analysis

All images were captured using a Nikon ECLIPSE 90i microscope and a Nikon DS-Ri 1 digital camera (Nikon Inc). Digital images were processed using Adobe Photoshop, adjusting only brightness, contrast, and color balance. The numbers of immunoreactive cells were counted manually by two independent investigators

blinded to the experimental conditions. The stained OEs were divided into eight regions according to the same orientation. Three slides for each of the 10 regions were used for histological measurements or immunohistochemistry. The OB was divided into eight regions according to the same orientation. Three slides for each animal were analyzed and observed under a microscope (× 400). OE thickness was measured from the basal lamina to the apex by examining the structure of the hematoxylin-stained olfactory mucosa. Subsequently, the number of stained nuclei was counted in an area of 2500 μm^2 in the OE and for a glomerulus in the OB. In order to address this fixed area on the slide, the septum length in the OE and the OB length were measured. Immunoreactive cells were counted from the endoturbinate (2 × 2 regions), and the ectoturbinate (2 × 2 regions) in the OE and were counted from the glomerulus (2 × 2 regions) in the OB from three tissue sections per animal. To quantify the reciprocal intensity, by measuring the intensity per unit area, with ImageJ, using the color deconvolution plug-in (http://wiki.imagej.net/Colour_Deconvolution) (*29, 30*). The target unit area of images processed using the color deconvolution tool in imageJ to separate brown from other color in images. The area of brown staining was then quantified and divided by the total area to yield a percentage of staining area. Stereological analyses were conducted using Prism software (GraphPad Software, Inc., La Jolla, USA). Comparisons between WT and Tg2576 mice were conducted using two-way ANOVAs. Results are presented as mean±S.E.M. *P*-values of ≤0.05 were considered to be statistically significant.

2.11. Primary culture of OSNs

Cultures were prepared as previously described with some modifications (*31*). OSNs which were obtained from Sprague-Dawley rats were plated at a density of 2 × 106 cells/ml on tissue culture dishes (Falcon, Lincoln Park, NJ, USA) coated with 25 μg/ml laminin (BD Bioscience, San Diego, CA, USA) in modified Eagle's medium containing d-valine (MDV, Welgen Inc., Worcester, MA, USA). Cultures are placed in humidified 37 °C incubator receiving 5% CO_2. On 2 days *in vitro* every day thereafter, cells are fed with MDV containing 15% dialyzed fetal bovine serum (Gibco, Rockville, MD, USA), gentamicin, kanamycin, and 2.5 ng/ml nerve growth factor. Two days prior to use, the culture medium is changed to medium without nerve growth factor.

3. Results

3.1. Tg2576 mice exhibit olfactory dysfunction before the onset of observable AD pathology

Because olfactory dysfunction has been observed in the early phase of AD pathology, we postulated that olfactory dysfunction may occur before the CNS defects in the Tg2576 mouse. First, using the Morris water maze test (Figure 1a), we found that 6-month-old Tg2576 mice exhibited slightly delayed escape latency during the 6-days training compared with wild-type (WT), while 14-month-old Tg2576 mice showed severe defects (Figure 1b). In addition, spatial learning, further assessed using

the probe test, is impaired in the 14-month-old, but not the 6-month-old Tg2576 mice (Figure 1c). Next, we performed food-seeking tests to examine whether olfactory dysfunction appeared during the AD progression in Tg2576 mice. (Figure 1d). The olfactory dysfunction measured by the latency of seeking buried foods was aggravated between the 6 and 14 months in Tg2576 as well as WT mice. Interestingly, both 6- (Figures 1e and f) and 14- (Figures 1g and h) month-old Tg2576 mice exhibited a significant increase in the latency of seeking the buried food, but not the unburied food, compared with WT. These results demonstrate that olfactory dysfunction occurs even at the earliest stages of AD pathology. Collectively, we suggested that onset of olfactory dysfunction occurs early in AD pathology prior to the development of irretrievable impairments in the CNS of Tg2576 mice.

3.2. Tg2576 mice experience a loss of dopaminergic periglomerular neurons in the specific glomeruli of ventral MOB

The glomerular layer (GL) layer mainly consists of periglomerular (PG) neurons located around the distinct glomeruli (Figure 2a). These PG neurons are well-known dopaminergic neurons expressing tyrosine hydroxylase (TH) (*32*), and their survival is dependent on sensory input from OSNs (*33*). To examine whether the olfactory defect of Tg2576 mice could compromise the integrity of the OB, we measured the expression of TH in PG neurons (Figure 2a). The number of TH-positive PG neurons was significantly decreased in both 6- and 14-month-old Tg2576 mice (~20%) compared with age-matched WT mice (Figure 2b). Such declines in the number of TH-positive PG neurons were similarly observed in age-related decrements between

6- and 14-month-old WT mice (~20%), implying that Tg2576 mice may have a reduction of neural activity and integrity on the neuronal connection between the OE and OB (*34*) and appeared level of decrements similar to the influences of age on olfaction.

The glomeruli are spatially, especially ventrally and dorsally, organized in GL of OB (Figure 2c). Notably, TH-positive PG neurons in 6-month-old Tg2576 mice significantly decreased in the specific glomeruli of ventral MOB, but not dorsal MOB (Figures 2d and e). These results were also observed in 14-month-old mice (Figures 2f and g). These results suggested that region-specific impairment of neural integrity in OB, especially ventral MOB, would be involved in the AD-related olfactory dysfunction, and this symptom would be observed in the early phase when AD pathology in the CNS has not yet begun.

3.3. Tg2576 mice produce high levels of Aβ oligomer in the OB

From the previous results showing that soluble Aβ is able to disrupt network activity in neural circuits resulting in neural dysfunction, we confirmed Aβ oligomer immunoreactivity in the glomeruli of the OB of Tg2576 mice (35). Overall, we observed an overall increase in the Aβ oligomers expression in the OB of Tg2576 mice. Moreover, there were statistically significant differences between dorsal MOB and ventral MOB regardless of AD progression. Specifically, within the glomeruli of ventral MOB of 6-month-old Tg2567 mice, we observed increased levels of Aβ oligomer immunoreactivity compared with the dorsal MOB (ventral, ~53%; dorsal, ~15%) (Figures 3a and b). In 14-month-old Tg2576 mice, glomeruli of ventral MOB

also have highly accumulated immunoreactivity of Aβ oligomer and glomeruli of dorsal MOB also have significantly increased immunoreactivity (ventral, ~56%; dorsal, ~30%) (Figures 3c and d). Collectively, we suggested that the accumulation of Aβ oligomers in specific regions may result in impaired neural integrity in specific glomeruli of ventral MOB of Tg2576 mice during AD progression.

3.4. BACE1 is highly enriched in the axonal terminals of OSNs projecting to glomeruli and highly expressed in the ventral MOB in Tg2576 mice

The β-site amyloid precursor protein cleaving enzyme 1 (BACE1) is a membrane-bound aspartyl protease abundant in the brains of AD patients and may be involved in the initial stage of A*β* generation. First, to investigate BACE1 localization in the olfactory system, we co-labeled BACE1 protein with a presynaptic terminal marker protein, synaptophysin, or a somatodendritic marker protein, microtubule-associated protein 2 (MAP2), in OB glomerulus (Figure 4a). Consistent with a previous report (*36*), we found that BACE1 immunoreactivity mainly co-localizes with synaptophysin in the glomeruli of MOB (Figure 4c); very little co-localizes with MAP2 (Figure 4b). These data indicate that BACE1 protein is highly expressed within axonal terminals of OSNs and other OB neurons in OB glomerulus rather than other somatodendritic postsynaptic neurons.

Based on previous studies and our own finding of Aβ oligomer expression in the OB, we postulated that BACE1 is involved in the regional accumulation of Aβ oligomers in ventral MOB. Thus, the expression of BACE1 in the OB glomeruli was

assessed histologically. Expression of BACE1 was significantly enriched in the glomeruli of ventral MOB compared with the dorsal MOB both of 6- (ventral, ~39%; dorsal, ~15%) (Figures 4d and e) and 14-month-old mice regardless of AD progression (ventral, ~42%; dorsal, ~18%) (Figures 4f and g). It implies that the regional expression of BACE1 contributes to the accumulation of Aβ oligomers in the glomeruli of ventral MOB. Additionally, it significantly increased in all glomeruli of OB of both 6- (Figures 4a and b) and 14-month-old (Figures 4c and d) Tg2576 mice but still remains higher in the glomeruli of ventral MOB compared with the dorsal MOB (Figures 4e and g). These data indicate that increased expression of Aβ may reversibly enhance BACE1 expression in Tg2576 mice. Therefore, we suggest that region-specific expression of BACE1 leads to a vicious cycle of increased generation of Aβ oligomer and BACE1 expression in glomeruli of ventral MOB, finally contributing to the olfactory dysfunction. These data suggest that the BACE1 protein is enriched into presynaptic vesicles (36), thus we raised the possibility that peripheral OSNs are implicated with Aβ accumulation in the glomeruli of ventral regions of MOB leading to olfactory dysfunction in Tg2576 mice.

3.5. The OE is impaired by cell death in the earlier phase of AD onset in Tg2576 mice

The rodent nasal cavity comprises a few regions formed by the bony turbinate extensions (turbinates) and molecular properties, and the OE is divided into ectoturbinates (1, 2, and 3) and endoturbinates (I, II, and III) according to anatomical locations exposed to air flows and odorants (Figure 5a). Additionally, depending on

the OR expression, proliferation and relative maturation of the OSNs, OE is separated in four different 'zones', which correlate well with anatomical locations (*37*). OSNs in the OE have been shown to project their axons exclusively into predetermined glomeruli in the OB where their neural transmissions support the maintenance of neural circuits, which link the peripheral olfactory organ to the CNS (*38*). In addition, OSNs in the OE project to the MOB in a mutually exclusive pattern; the medial OE to the medial hemisphere of each MOB, the lateral OE to the lateral hemisphere, the central OE to the dorsal MOB, and the peripheral OE to the ventral MOB. Therefore, we analyzed histological characteristics in the regions of the OE including ectoturbinate and endoturbinate. The thickness of the OE was decreased in all regions to different extents (6 month: ecto ~10%, endo ~3%; 14 month: ecto ~12%, endo ~8%), most notably in ectoturbinate of 6-month-old Tg2576 mice, while all regions in the 14-month-old mice were decreased (Table 1a). The number of cells in the OE also decreased in the ectoturbinate and the endoturbinate of 6-month-old Tg2576 mice and in all regions in 14-month-old mice (6 month: ecto ~11%, endo ~5%; 14 month: ecto ~27%, endo ~14%) (Table 1b). Although Tg2576 mice displayed significant decreases in all regions tested (Tables 1a and b), both 6- and 14-month-old mice showed significant differences in both the thickness and the number of cells in a regional-dependent manner. These data indicate structural impairment of the OE in Tg2576 mice. In order to determine whether the impairment of the OE in

Tg2576 mice was due to cell death, TUNEL staining was conducted. The number of TUNEL-positive cells increased significantly in ectoturbinate-specific regions of the OE in both 6- (Figures 5b and c) and 14-month-old Tg2576 mice (Figures 5d and e) compared with the endoturbinates of WT and Tg2576 mice. The most significant increase was observed in the ectoturbinate of both 6- and 14-month-old Tg2576 mice compared with WT. However, slight but significant increases were also observed in the endoturbinate of 14-month-old Tg2576 mice. Notably, almost all TUNEL-positive cells were observed in a layer in which OSNs reside (Figures 5b and d), indicating cell death of OSNs in Tg2576 mice.

Table. 1 Thickness and cell numbers of the OE were decreased in Tg2576 mice compared with age-matched WT mice.

	OE thickness, um			
	6 month		14 month	
	WT	Tg	WT	Tg
Ecto	47.2 ± 3.2	43.4 ± 3.6 (**)	48.6 ± 8.3	42.8 ± 4.6 (***)
Endo	76.1 ± 6.7	73.9 ± 9.3 (*)	77.1 ± 8.1	70.2 ± 3.2 (***)

(A) Thickness in each region of the OE in 6-month-old WT (n=7) vs. Tg (n=7) and 14-month-old WT (n=9) vs. Tg (n=8). Two-way ANOVA, using Prism software (GraphPad software, USA), *P < 0.05, **P < 0.01 and ***P < 0.001 denote statistical significance.

	Total number of cells (2.5mm^2)			
	6 month		14 month	
	WT	Tg	WT	Tg
Ecto	42.7 ± 5.6	38.0 ± 5.7 (**)	41.4 ± 3.0	30.1 ± 2.9 (***)
Endo	83.1 ± 7.0	79.0 ± 8.8 (*)	61.0 ± 10.3	52.1 ± 9.9 (***)

(B) The number of cells in each region of the OE in 6-month-old WT (n=7) vs. Tg (n=7) and 14-month-old WT (n=9) vs. Tg (n=8). Two-way ANOVA, using Prism software (GraphPad software, USA), *P < 0.05, **P < 0.01 and ***P < 0.001 denote statistical significance.

3.6. Tg2576 mice produce high levels of Aβ oligomers and induce cell death in OSNs layer of the OE

To elucidate whether the cell death of OSNs is correlated with generation of Aβ oligomers, we examined the abundance of Aβ oligomers in the OE of Tg2576 mice. Immunohistochemistry data revealed that immunoreactivity of Aβ oligomer was considerably stronger in ectoturbinates of the OE of both 6- (Figures 6a and b) and 14-month-old WT and Tg2576 mice (Figures 6c and d). Compared to WT mice, however, Tg2576 mice exhibit an overall upregulation of Aβ oligomer expression in the OE, in particular within the ectoturbinate. To examine if Aβ oligomers showed toxic effects to OSNs, we investigated the neurotoxicity induced by the $A\beta_{1-42}$ peptide-derived diffusible ligands (ADDLs) in vitro using cultured OSNs (39). ADDLs induced OSN cell death with upregulated the cleavage of caspase-3, which is a final executor of apoptosis (40). In addition, phosphorylation of p38 MAPK, which is involved in the stress response (41) (Figure 6e), was also increased, comparable to a previous report describing increased p38 MAPK activity in the AD human brain (42) (Figure 6e). To elucidate whether the p38 signaling pathway was indeed involved in the ADDLs-mediated neurotoxicity, we co-treated OSNs with an inhibitor of p38 MAPK, SB 203580 at 20 μM, with ADDLs. SB 203580 efficiently abolished OSN cell death as well as p38 activation (Figures 6e and f), indicating that Aβ oligomers may induce OSN cell death via p38 activation. Taken together, we suggest that the cell-autonomous death of OSNs by Aβ oligomers in peripheral organs, especially

ectoturbinate of OE, of olfactory system, and it leads to impairment of integrity in glomeruli of OB, finally resulting in olfactory dysfunction in the earlier phase of AD pathology of Tg2576 mice.

Soluble monomeric forms, $A\beta_{1-40}$ and $A\beta_{1-42}$, are produced mainly in neurons from APP (~120 kDa) (6, 43), and these monomeric Aβs can drive the formation of various nonpathogenic oligomers as a part of normal physiological processes. Aβ*56 (12-mer, ~56 kDa) and AβO (15-mer, ~80 kDa) are highly neurotoxic without causing the formation of neuritic plaques or neurofibrillary tangles (39), and their high deposition have been found in the initial early stages of AD (44). By immunohistochemistry, we found that a toxic Aβ*56 was significantly increased in the OE of 6-month-old Tg2576 mice compared with WT, and was saturated in the OE of 14-month-old mice (Figure 6g). However, the other toxic Aβ oligomer, AβO (~80 kDa), was significantly increased in the OE of 14-month-old Tg2576 mice as compared with WT mice, but not in the OE of 6-month-old mice (Figures 6h and i). These data demonstrated that deregulated formation of Aβ oligomers, especially Aβ*56 rather than AβO, occurred in the ectoturbinate of Tg2576 mice and may be involved in cell death of OSNs resulting in olfactory dysfunction.

4. Discussion

In the current study, we found olfactory dysfunction in 6-month-old Tg2576 mice before severe and irreversible defects in the CNS, including failure of spatial learning and memory. Comparably, a previous report has described that olfactory habituation and discrimination were significantly reduced in 6-month-old Tg2576 mice (*19, 45*). Considering that olfactory habituation and discrimination have been known to be secondary or tertiary olfactory sensory pathways mediated by the central olfactory circuit including synapses between the OB and the piriform cortex in CNS (*19*), defects of olfactory habituation and discrimination in Tg2576 mice result from impairment in the CNS. In contrast, our current results from anatomical analyses using immunohistochemistry and behavior analysis (i.e., food-seeking tests) provide new evidence that Tg2576 mice have defects in the primary olfactory circuit, specifically peripheral OE and glomerular layer of OB where the first synapses are formed, for odor recognition rather than central olfactory circuit.

Dopaminergic PG neurons in the GL of the OB have been shown to influence olfactory processing including odor detection and memory (*46, 47*). The maturation of PG neurons is supported by glutamatergic input from OSNs (*48*) and is involved in the modulation of the excitability of mitral cells that form asymmetrical synapses with PG neurons (*49, 50*). Therefore, reduced activities between OSNs and mitral cells, or sensory deprivation may result in profound decreases in TH expression (*51, 52*). In the current study, glomerular regions in the ventral MOB were severely impaired in both 6-month-old and 14-month-old Tg2576 mice compared with the

dorsal region, and this region exhibited enriched accumulation of A*β* oligomer with increased expression of BACE1. Our additional immunohistochemistry data revealed region-specific expression of BACE1 protein in glomeruli of ventral MOB, but not dorsal MOB. Previously, it has been demonstrated that presynaptic dystrophy by Aβ oligomers disrupts lysosome-dependent degradation of BACE1 protein (36). Based on our data and previous reports, we demonstrated that reduced neural activity from OSNs in OE to glomeruli of ventral OB increases BACE1 expression leading to enhancing accumulation of Aβ oligomers and a subsequently viscous cycle.

One of our main question is, whether impairment of the PNS, but not the CNS, is involved in olfactory dysfunction in Tg2576 mice. Interestingly, our results showed that a specific group of OSNs, which are located in specific region of the OE, the ectoturbinate, and project their axons into glomeruli of ventral MOB, was severely degenerated in Tg2576 mice. Consistently, the region-specific deposition of Aβ oligomers in the ectoturbinate of Tg2576 (6- and 14-month old) mice was observed. This region-specific phenotype seems to result from region-specific expression of BACE1 (Figure 7). In addition, our biochemistry data revealed that Aβ*56 was upregulated in the OE during the early stage of AD in Tg2576 mice. It should be noted that Aβ*56 is one of the Aβ oligomer species correlated with cognitive deficits (39), and appears between the ages of 6 and 14 months in the Tg2576 mouse brain (44). Therefore, we suggest that evaluation of Aβ*56 deposition in the OE may be a

potential-inducing factor of neural toxicity in early stage of AD. By contrast, AβO, an oligomer that induces direct cytotoxicity, significantly mediates cell death in the late stage of AD (53, 54). Taken together, olfactory dysfunction in the early stage of AD may be associated with alterations in the network activity by upregulated Aβ*56 synaptic toxicity. In contrast, olfactory dysfunction in the late stage of AD may be associated with massive cell death resulting from increased AβO cytotoxicity. That is, different types of oligomers may cause distinct types of deleterious effects in the olfactory system during the progress of AD.

Neuronal death and functional abnormality due to Aβ oligomers have been considered to be the main cause of AD (1, 55). OSNs are also cell-autonomously degenerated by OSN-specific expression of the Swedish mutated form of the human APP gene (21). In the current study, TUNEL-positive cells appeared to be almost entirely located in the OSN layer in Tg2576 mice, and in vitro cultured OSNs were cell-autonomously degenerated after treatment with the Aβ oligomer. Moreover, OSN-specific expression of the Swedish mutated form of the human APP gene disrupted the precise projections of their axons to the OB during synapse formation in 3-month-old Tg2576 mice without OSN death (20). Therefore, it is possible that abnormal axonal projections of OSNs are involved in the earlier olfactory dysfunction and in turn induce the cell death of OSNs with aberrant projections, resulting in more severe dysfunction in the early stage of AD.

An interesting finding from this study was that uneven regional damage could be the specific symptom of AD in the olfactory system. Comparably, the CNS also has such vulnerable regions to the AD such as default mode network regions of the AD (56), thus the olfactory system may also have susceptible region to AD-specific pathological processes. It is apparent from the data herein that there is a difference in the proliferation and maturation depending on the location of the OE (57, 58), suggesting the olfactory epithelium in different zones are differentially regulated by activity. Ectoturbinate and endoturbinate of OE belong to completely different regions and renewal of OSNs is not uniform (59). Interestingly, our results proposed that an AD-related protein has possible spatioselectivity in the olfactory system. Moreover, AD-specific pathological processes are highly concentrated in the damaged region of the olfactory system. Taken together, the mechanism of AD-mediated damage we proposed may be caused by problems of odorant detection in the OE and suggest that the PNS is critically impacted in early AD, ahead of damage to the CNS.

In summary, using a mouse model of AD, we observed early accumulation of β-amyloid in specific regions of the olfactory system including the OE. Specifically, BACE1 expression and cell death was highly correlated with a defect of β-amyloid positive presynaptic terminals of OB. Therefore, partial impairment of olfactory function in the progress of AD may show strong differences to other type of anosmic models. Therefore, particular odorants may show low detection tendency in a specific stage of AD progression because of region-specific degradation in the OE.

Other reports showed the high sensitivity and specification of specific odorants in AD patients, for example, 'peanut butter' smell (60). Therefore, AD-specific symptoms in the olfactory system may present novel and feasible diagnostic targets for early diagnosis of AD.

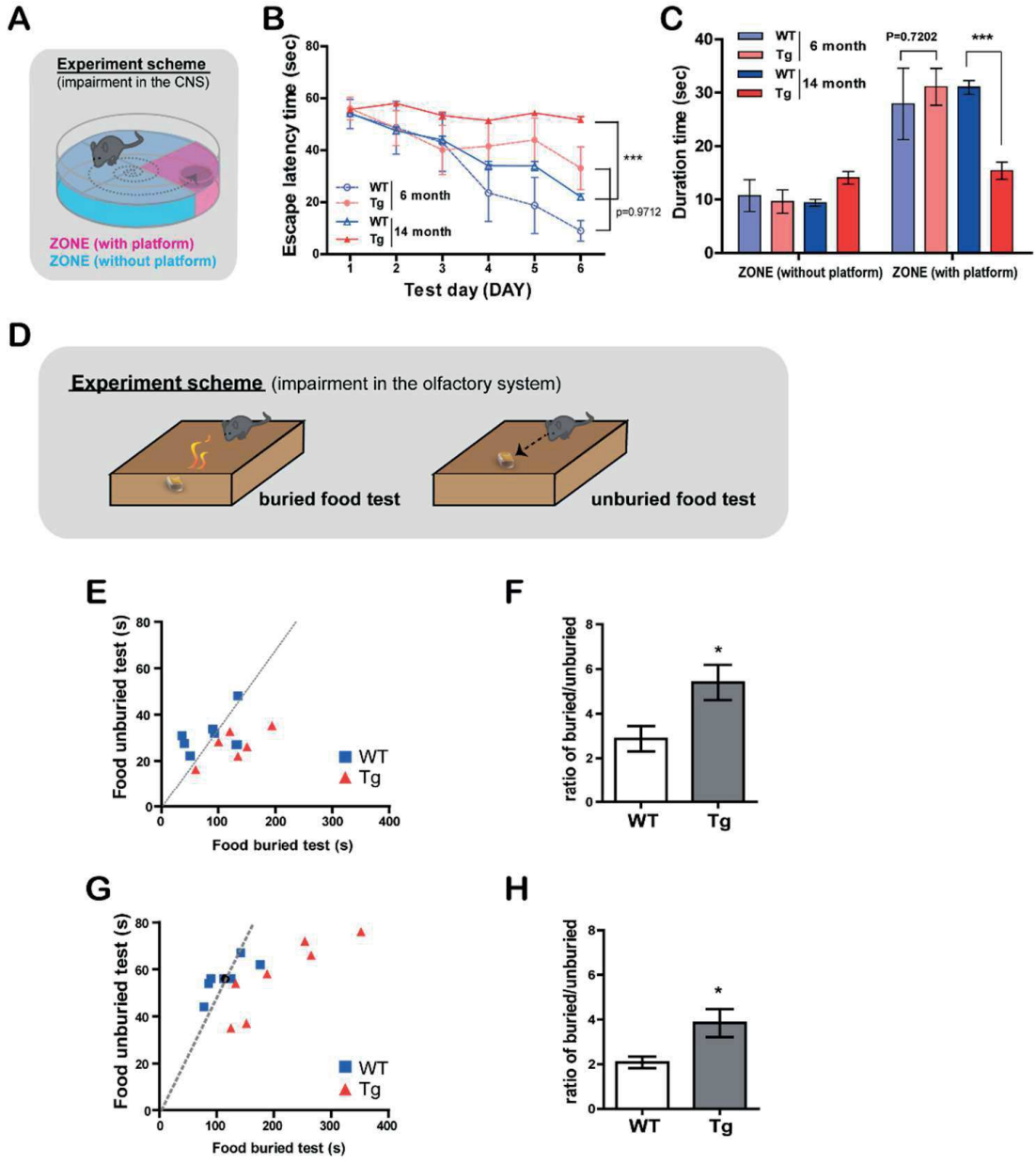
A
Experiment scheme
(impairment in the CNS)
ZONE (with platform)
ZONE (without platform)
B
Escape latency time (sec)
Test day (DAY)
WT
Tg
6 month
WT
Tg
14 month
***
p=0.9712
C
Duration time (sec)
WT
Tg
6 month
WT
Tg
14 month
P=0.7202
***
ZONE (without platform)
ZONE (with platform)
D
Experiment scheme (impairment in the olfactory system)
buried food test
unburied food test
E
Food unburied test (s)
Food buried test (s)
WT
Tg
F
ratio of buried/unburied
*
WT
Tg
G
Food unburied test (s)
Food buried test (s)
WT
Tg
H
ratio of buried/unburied
*
WT
Tg

Figure 1. Olfactory impairment appears in 6-month-old Tg2576 mice without failure of spatial learning and memory.

(A) The Morris water maze task was performed at 6-months (wild-type (WT), n=4; transgenic Tg2576 (Tg), n=6) or 14-months of age (WT, n=17; Tg, n=16). Training trials were conducted and the escape latency was measured for 6 days. ***P < 0.001 by Two-way ANOVA, using Prism software (GraphPad software, USA). (B) The probe test was conducted 48 hours after the final training session. A platform was located in zone with platform, and the durations that the mice of each group stayed in the zone without platform and the zone with platform were measured. ***P < 0.001 by Two-way ANOVA, using Prism software (GraphPad software, USA). (D) Illustration of scheme for buried/unburied food test. (E, F) Buried and unburied food tests in 6-month-old mice (WT, n=8; Tg, n=8). The latencies (E) to find buried or unburied food and their ratios (F) were measured (slope in the latencies graph [E] represents the average time to find buried or unburied food in WT mice) (G, H) Buried and unburied food tests in 14-month-old mice (WT, n=8; Tg, n=8). The latencies (G) to find buried or unburied food and their ratios (H) were measured (slope in the latencies graph (G) represents the average time to find buried or unburied food in WT mice) All data are presented as mean ± SEM. Two-way ANOVA, using Prism software (GraphPad software, USA), *P < 0.05 and ***P < 0.001 denote statistical significance.

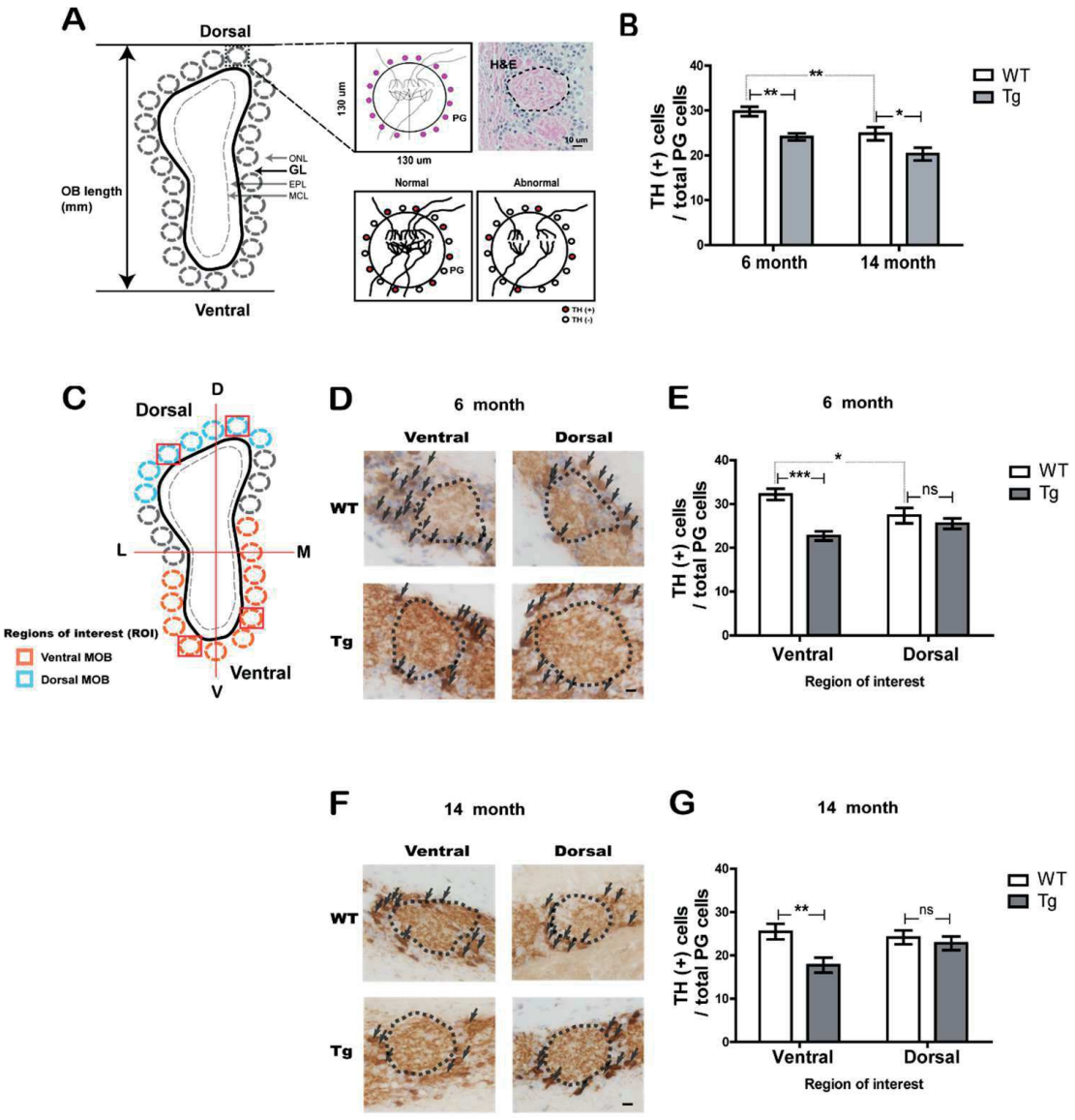
A
Dorsal
Ventral
OB length (mm)
ONL
GL
EPL
MCL
130 um
130 um
PG
H&E
10 um
Normal
Abnormal
PG
TH (+)
TH (-)
B
TH (+) cells / total PG cells
WT
Tg
**
**
*
6 month
14 month
C
D
Dorsal
L
M
Ventral
V
Regions of interest (ROI)
Ventral MOB
Dorsal MOB
D
6 month
Ventral
Dorsal
WT
Tg
E
6 month
TH (+) cells / total PG cells
***
*
ns
WT
Tg
Ventral
Dorsal
Region of interest
F
14 month
Ventral
Dorsal
WT
Tg
G
14 month
TH (+) cells / total PG cells
**
ns
WT
Tg
Ventral
Dorsal
Region of interest

Figure. 2 The number of dopaminergic periglomerular neurons (TH + PG cells) is decreased in Tg2576 mice compared with age-matched WT mice.

(A) Depictions of coronal sections through the OB. Single glomerulus and H&E staining depicting the glomerulus with dopaminergic periglomerular neurons (TH (+) PG cells) are represented. Reduced activity between ORNs and mitral cells, or sensory deprivation, may result in profound decreases in TH expression. (B) Stereological analysis of TH (+) PG cells / total PG cells in the OB of WT vs. Tg of 6 and 14-month-old. (C) Depictions of coronal sections through the OB with region of interest. Blue outline shading denotes the dorsal MOB. Orange outline shading denotes the ventral MOB. (D, F) Evolution of the TH (+) PG cells/total PG cells in WT vs. Tg in 6-month-old (WT, n=7; Tg, n=7) (D) and 14-month-old (WT, n=9; Tg, n=8) (F). (D, E) Stereological analysis of TH + periglomerular cells/total periglomerular cells (WT control in each group) in 6-month-old (E) and 14-month-old (F) mice. All data are presented as mean ± SEM. Scale bar = 10 μm. Two-way ANOVA, using Prism software (GraphPad software, USA), *P < 0.05, **P < 0.01 and ***P < 0.001 denote statistical significance.

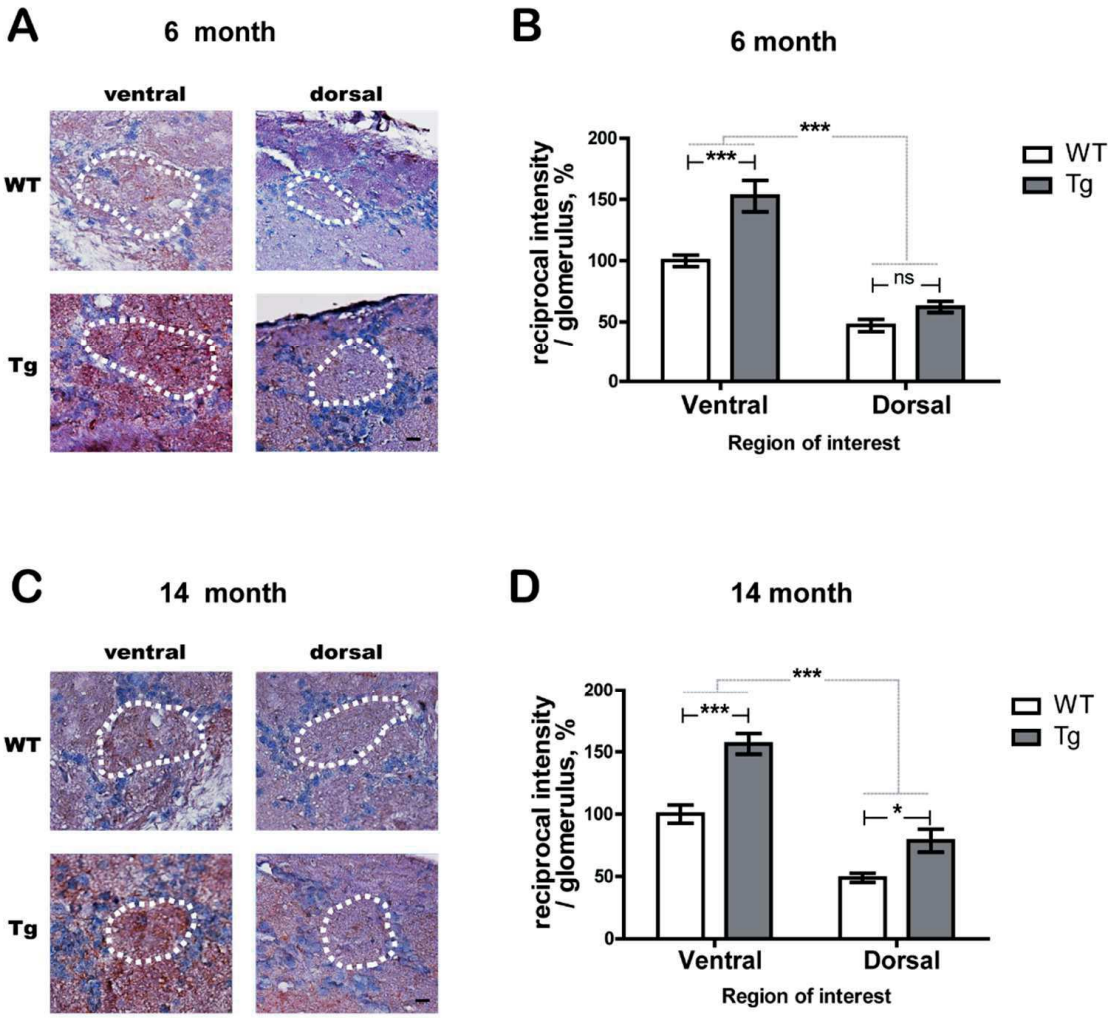
A
6 month
ventral
dorsal
WT
Tg
B
6 month
reciprocal intensity / glomerulus, %
200
150
100
50
0
***
***
ns
Ventral
Dorsal
Region of interest
WT
Tg
C
14 month
ventral
dorsal
WT
Tg
D
14 month
reciprocal intensity / glomerulus, %
200
150
100
50
0
***
***
*
Ventral
Dorsal
Region of interest
WT
Tg

Figure. 3 The intensity of the Aβ oligomer is increased in certain region OB of Tg2576 mice compared with age-matched WT mice.

(A, C) Evolution of the Aβ oligomer in WT vs. Tg in 6-month-old (WT, n=7; Tg, n=7) (A) and 14-month-old (WT, n=9; Tg, n=8) (C). (B, D) Stereological analysis of the Aβ oligomer intensity (WT control in each group) in 6-month-old (B) and 14-month-old (D) mice. All data are presented as mean ± SEM. Scale bar = 10 μm. Two-way ANOVA, using Prism software (GraphPad software, USA), *P < 0.05 and ***P < 0.001 denote statistical significance.

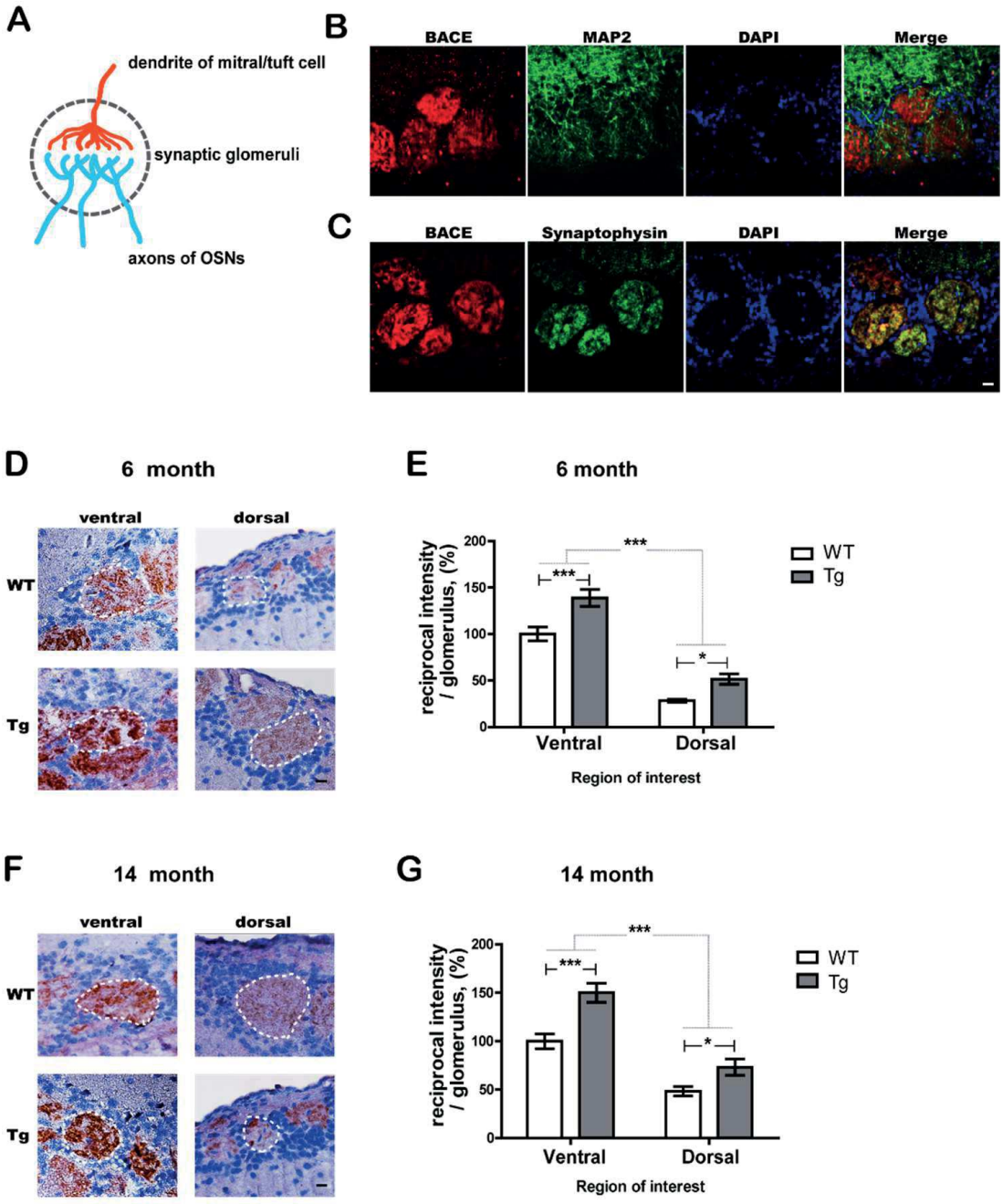
A
dendrite of mitral/tuft cell
synaptic glomeruli
axons of OSNs
B
BACE
MAP2
DAPI
Merge
C
BACE
Synaptophysin
DAPI
Merge
D
6 month
ventral
dorsal
WT
Tg
E
6 month
reciprocal intensity / glomerulus, (%)
200
150
100
50
0
***
***
*
WT
Tg
Ventral
Dorsal
Region of interest
F
14 month
ventral
dorsal
WT
Tg
G
14 month
reciprocal intensity / glomerulus, (%)
200
150
100
50
0
***
***
*
WT
Tg
Ventral
Dorsal
Region of interest

Figure. 4 BACE1 is localized within presynaptic terminals and the intensity of the BACE1 is increased in certain region OB of Tg2576 mice compared with age-matched WT mice.

(A) Illustration of coronal sections through the single glomerulus with presynaptic terminal of ORNs and postsynaptic region of mitral/tuft cells. (B, C) Representative images of coronal glomerulus sections from WT vs. Tg in 6-month-old (Tg, n=4). Co-stained with BACE1 (red) and MAP2 (B) or synaptophysin (C) (green) antibodies and imaged by confocal microscopy. BACE1 immunoreactivity and synaptophysin signals significantly co-localize within OSN terminals, but BACE1 expression does not overlap with that of the somatodendritic marker MAP2 (green) within the glomerulus across all the condition while different signal intensity. Scale bar = 10 μm. (D, F) Evolution of the BACE1 in WT vs. Tg in 6-month-old (WT, n=7; Tg, n=7) (D) and 14-month-old (WT, n=9; Tg, n=8) (F). (E, G) Stereological analysis of the BACE1 intensity (WT control in each group) in 6-month-old (E) and 14-month-old (G) mice. All data are presented as mean ± SEM. Scale bar = 10 μm. Two-way ANOVA, using Prism software (GraphPad software, USA), *P < 0.05 and ***P < 0.001 denote statistical significance.

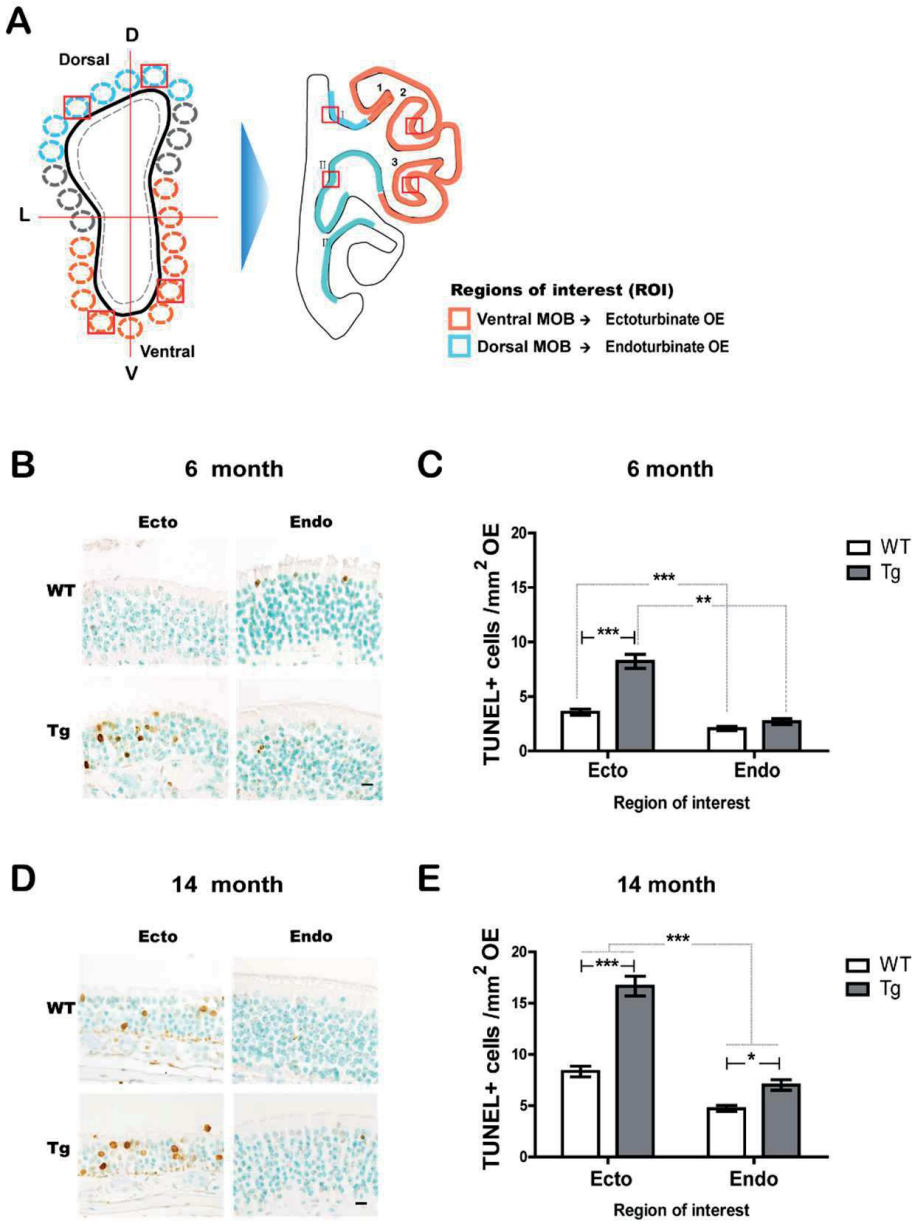
A
D
Dorsal
L
Ventral
V
Regions of interest (ROI)
Ventral MOB → Ectoturbinate OE
Dorsal MOB → Endoturbinate OE
B
6 month
Ecto
Endo
WT
Tg
C
6 month
TUNEL+ cells /mm2 OE
WT
Tg
Ecto
Endo
Region of interest
D
14 month
E
14 month

Figure 5. Specific region of OE shows massive cell death in Tg2576 mice.

(A) Illustration of coronal sections through the OB and OE with region of interest. Depictions represent predetermined glomeruli in the OB and corresponding OE with region of interest. Blue outline shading denotes the dorsal MOB and orange outline shading denotes the ventral MOB. Blue outline shading denotes the endoturbinate OE and orange outline shading denotes the ectoturbinate OE. (B, D) Images of TUNEL staining (brown signal) in the ectoturbinate, and endoturbinate of the OE in (B) 6-month-old and (D) 14-month-old WT vs. Tg mice. Methyl green was counterstained (sky blue signal). Scale bars represent 10 μm. (C, E) Stereological analysis of the incidence of TUNEL-positive cells (TUNEL-positive cells per mm2 OE in each group) in the OE of 6-month-old (C) (WT, n=7; Tg, n=7) and 14-month-old mice (E) (WT, n=9; Tg; n=8). All data are presented as mean ± SEM. Two-way ANOVA, using Prism software (GraphPad software, USA), *P < 0.05 and ***P < 0.001 denote statistical significance.

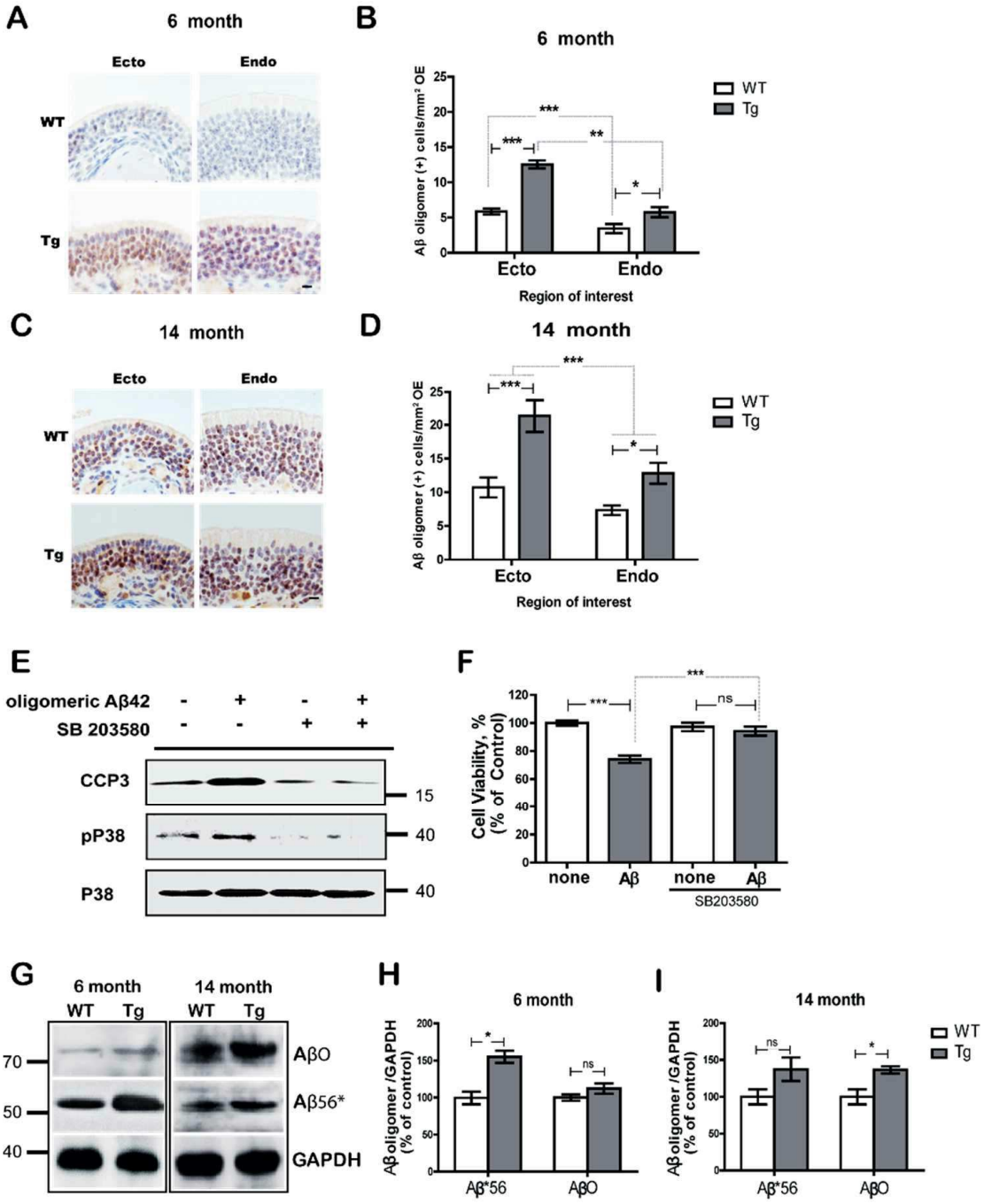
A
6 month
Ecto
Endo
WT
Tg
B
6 month
Aβ oligomer (+) cells/mm² OE
WT
Tg
Ecto
Endo
Region of interest
C
14 month
D
14 month
E
oligomeric Aβ42
SB 203580
CCP3
pP38
P38
15
40
40
F
Cell Viability, % (% of Control)
none
Aβ
SB203580
G
6 month
14 month
70
50
40
AβO
Aβ56*
GAPDH
H
6 month
Aβoligomer /GAPDH (% of control)
Aβ*56
AβO
I
14 month

Figure 6. Expression of Aβ-oligomer is significantly increased in the specific region OE of Tg2576 mice.

(A, C) Immunohistochemistry of Aβ-oligomers (brown signal) in the in the ectoturbinate, and endoturbinate of the OE of 6-month-old (A) and 14-month-old (C) WT vs. Tg mice. Sections were lightly counterstained with H&E (violet signal). Scale bars = 10 μm. (B, D) Stereological analysis of the incidence (Aβ oligomer-positive cells per mm2 OE in each group) of cells exhibiting high immunoreactivity of Aβ-oligomer in 6-month-old (B) (WT, n=7; Tg, n=7) and 14-month-old (D) (WT, n=9; Tg; n=8) mice. *P < 0.05 and ***P < 0.001 by one-way ANOVA, followed by Dunnett's post hoc test. (E) Cultured ORNs were incubated with Aβ-oligomer for 5 hours in the presence or absence of SB 203580, and Immunoblots of cleaved caspase-3 (CCP3), phosphorylated p38 (pP38), and p38 in ORNs treated with Aβ oligomers (25 μM). (F) ORN viability was increased upon Aβ-oligomer treatment. Inhibition of P38 significantly increased ORN survival under Aβ-oligomer treatment. (G) Immunoblots of AβO (~80 kDa) and Aβ*56 (~56 kDa) in the OE of 6- or 14-month-old WT vs. Tg mice. (H, I) Quantification of protein levels of AβO and Aβ*56 in 6-month-old (H) and 14-month-old (I) mice. Protein levels were normalized by reprobing the blots for GAPDH. The data were acquired from 3 independent experiments. All data are presented as mean ± SEM. Two-way ANOVA, using Prism software (GraphPad software, USA), *P < 0.05 denote statistical significance.

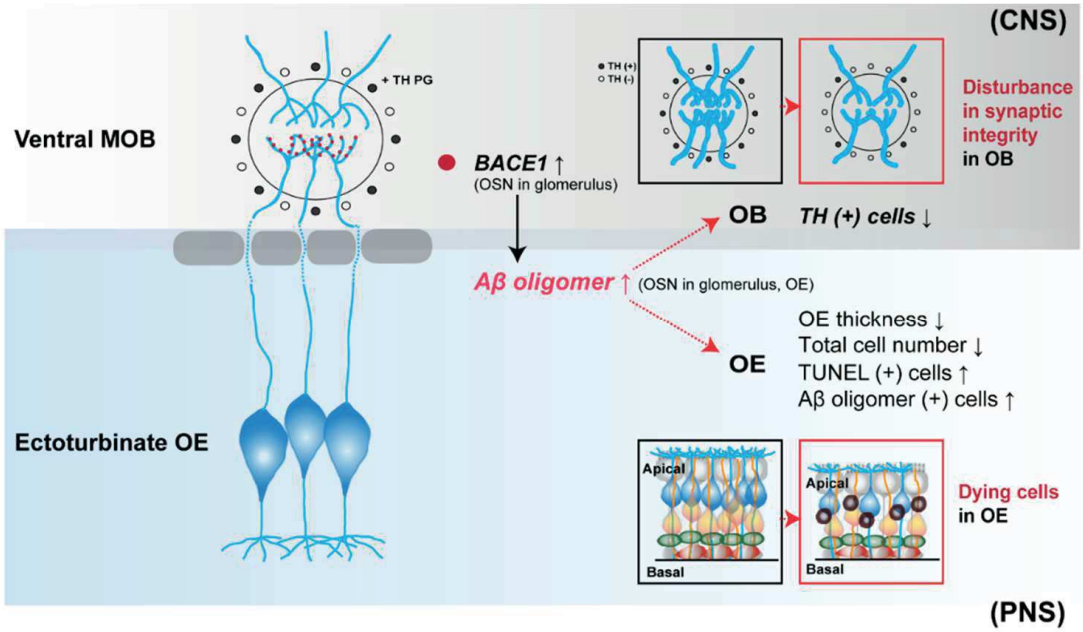

Figure. 7 A working hypothesis of olfactory dysfunction and impairment in an AD mouse model.

OE impairment and cell death occur in Tg2576 mice. In particular, the expression of Aβ-oligomers is increased in the OE of Tg2576 mice compared with WT mice. In addition, the integrity of the connection between axons from the OE and dendrites in the OB is disturbed in Tg2576 mice compared with WT mice. Furthermore, dopaminergic periglomerular cells (TH + PG cells) are reduced in the glomerulus. SC, mORN, iORN, GBC, and HC indicate sustentacular cells, mature olfactory receptor neuron, immature olfactory receptor neuron, globose basal cell, and horizontal cell, respectively.

Acknowledgments

This work was supported by the Ministry of Science, ICT and Future Planning & DGIST (16-BD-0402, DGIST Convergence Science Center) and the National Research Foundation of Korean (NRF-2015M3A9E2028884).

References

1. G. McKhann *et al.*, Clinical diagnosis of Alzheimer's disease: report of the NINCDS-ADRDA Work Group under the auspices of Department of Health and Human Services Task Force on Alzheimer's Disease. *Neurology* **34**, 939-944 (1984).
2. H. Braak, E. Braak, Demonstration of amyloid deposits and neurofibrillary changes in whole brain sections. *Brain Pathol* **1**, 213-216 (1991).
3. L. Mucke *et al.*, High-level neuronal expression of abeta 1-42 in wild-type human amyloid protein precursor transgenic mice: synaptotoxicity without plaque formation. *J Neurosci* **20**, 4050-4058 (2000).
4. A.Y. Hsia *et al.*, Plaque-independent disruption of neural circuits in Alzheimer's disease mouse models. *Proc Natl Acad Sci U S A* **96**, 3228-3233 (1999).
5. M. S. Wolfe, gamma-Secretase inhibitors as molecular probes of presenilin function. *J Mol Neurosci* **17**, 199-204 (2001).
6. M. S. Wolfe *et al.*, Two transmembrane aspartates in presenilin-1 required for presenilin endoproteolysis and gamma-secretase activity. *Nature* **398**, 513-517 (1999).
7. L. M. Ittner *et al.*, Dendritic function of tau mediates amyloid-beta toxicity in Alzheimer's disease mouse models. *Cell* **142**, 387-397 (2010).
8. J. P. Cleary *et al.*, Natural oligomers of the amyloid-beta protein specifically disrupt cognitive function. *Nat Neurosci* **8**, 79-84 (2005).
9. R. L. Doty, The olfactory system and its disorders. *Semin Neurol* **29**, 74-81 (2009).
10. K. A. Jellinger, J. Attems, Alzheimer pathology in the olfactory bulb. *Neuropathol Appl Neurobiol* **31**, 203 (2005).
11. S. Christen-Zaech *et al.*, Early olfactory involvement in Alzheimer's disease. *Can J Neurol Sci* **30**, 20-25 (2003).
12. H. Ferreyra-Moyano, E. Barragan, The olfactory system and Alzheimer's disease. *Int J Neurosci* **49**, 157-197 (1989).
13. D. B. FG, L. Pelland, D. G. Robertson, Kinetic analysis of forwards and backwards stair descent. *Gait Posture* **27**, 564-571 (2008).
14. J. Wang *et al.*, Olfactory deficit detected by fMRI in early Alzheimer's disease. *Brain Res* **1357**, 184-194 (2010).
15. D. W. Wesson, J. Morales-Corraliza, M. J. Mazzella, D. A. Wilson, P. M. Mathews, Chronic anti-murine Abeta immunization preserves odor guided behaviors in an Alzheimer's beta-amyloidosis model. *Behav Brain Res* **237**, 96-102 (2013).
16. J. Morales-Corraliza *et al.*, Immunization targeting a minor plaque constituent clears beta-amyloid and rescues behavioral deficits in an Alzheimer's disease mouse model. *Neurobiol Aging* **34**, 137-145 (2013).
17. M. Fusetti *et al.*, Smell and preclinical Alzheimer disease: study of 29 patients with amnesic mild cognitive impairment. *J Otolaryngol Head Neck Surg* **39**, 175-181 (2010).
18. J. Djordjevic, M. Jones-Gotman, K. De Sousa, H. Chertkow, Olfaction in patients with mild cognitive impairment and Alzheimer's disease. *Neurobiol Aging* **29**, 693-706 (2008).
19. D. W. Wesson, E. Levy, R. A. Nixon, D. A. Wilson, Olfactory dysfunction correlates with amyloid-beta burden in an Alzheimer's disease mouse model. *J Neurosci* **30**, 505-514 (2010).
20. L. Cao, G. T. Rickenbacher, S. Rodriguez, T. W. Moulia, M. W. Albers, The precision of axon targeting of mouse olfactory sensory neurons requires the BACE1 protease. *Sci Rep* **2**, 231 (2012).
21. N. Cheng, H. Cai, L. Belluscio, In vivo olfactory model of APP-induced

neurodegeneration reveals a reversible cell-autonomous function. *J Neurosci* **31**, 13699-13704 (2011).
22. D. Guerin, J. Sacquet, N. Mandairon, F. Jourdan, A. Didier, Early locus coeruleus degeneration and olfactory dysfunctions in Tg2576 mice. *Neurobiol Aging* **30**, 272-283 (2009).
23. A. Van Dijck, E. Vloeberghs, D. Van Dam, M. Staufenbiel, P. P. De Deyn, Evaluation of the APP23-model for Alzheimer's disease in the odour paired-associate test for hippocampus-dependent memory. *Behav Brain Res* **190**, 147-151 (2008).
24. K. Hsiao *et al.*, Correlative memory deficits, Abeta elevation, and amyloid plaques in transgenic mice. *Science* **274**, 99-102 (1996).
25. R. Morris, Developments of a water-maze procedure for studying spatial learning in the rat. *J Neurosci Methods* **11**, 47-60 (1984).
26. M. Yang, J. N. Crawley, Simple behavioral assessment of mouse olfaction. *Curr Protoc Neurosci* **Chapter 8**, Unit 8 24 (2009).
27. P. A. Dawson, S. E. Steane, D. Markovich, Impaired memory and olfactory performance in NaSi-1 sulphate transporter deficient mice. *Behav Brain Res* **159**, 15-20 (2005).
28. W. B. Stine, L. Jungbauer, C. Yu, M. J. LaDu, Preparing synthetic Abeta in different aggregation states. *Methods Mol Biol* **670**, 13-32 (2011).
29. A. C. Ruifrok, D. A. Johnston, Quantification of histochemical staining by color deconvolution. *Anal Quant Cytol Histol* **23**, 291-299 (2001).
30. A. M. Khan, N. Rajpoot, D. Treanor, D. Magee, A nonlinear mapping approach to stain normalization in digital histopathology images using image-specific color deconvolution. *IEEE Trans Biomed Eng* **61**, 1729-1738 (2014).
31. G. V. Ronnett, L. D. Hester, S. H. Snyder, Primary culture of neonatal rat olfactory neurons. *J Neurosci* **11**, 1243-1255 (1991).
32. H. Le Jeune, F. Jourdan, Acetylcholinesterase-containing intrinsic neurons in the rat main olfactory bulb: cytological and neurochemical features. *Eur J Neurosci* **6**, 1432-1444 (1994).
33. N. Mandairon, J. Sacquet, F. Jourdan, A. Didier, Long-term fate and distribution of newborn cells in the adult mouse olfactory bulb: Influences of olfactory deprivation. *Neuroscience* **141**, 443-451 (2006).
34. J. W. Cave, H. Baker, Dopamine systems in the forebrain. *Adv Exp Med Biol* **651**, 15-35 (2009).
35. Y. Levites *et al.*, Anti-Abeta42- and anti-Abeta40-specific mAbs attenuate amyloid deposition in an Alzheimer disease mouse model. *J Clin Invest* **116**, 193-201 (2006).
36. P. C. Kandalepas *et al.*, The Alzheimer's beta-secretase BACE1 localizes to normal presynaptic terminals and to dystrophic presynaptic terminals surrounding amyloid plaques. *Acta Neuropathol* **126**, 329-352 (2013).
37. T. Bozza, P. Feinstein, C. Zheng, P. Mombaerts, Odorant receptor expression defines functional units in the mouse olfactory system. *J Neurosci* **22**, 3033-3043 (2002).
38. P. Mombaerts *et al.*, Visualizing an olfactory sensory map. *Cell* **87**, 675-686 (1996).
39. I. Benilova, E. Karran, B. De Strooper, The toxic Abeta oligomer and Alzheimer's disease: an emperor in need of clothes. *Nat Neurosci* **15**, 349-357 (2012).
40. A. H. Wyllie, Apoptosis and carcinogenesis. *Eur J Cell Biol* **73**, 189-197 (1997).
41. A. Mikhailov, M. Shinohara, C. L. Rieder, The p38-mediated stress-activated checkpoint. A rapid response system for delaying progression through antephase and entry into mitosis. *Cell Cycle* **4**, 57-62 (2005).
42. K. Hensley *et al.*, p38 kinase is activated in the Alzheimer's disease brain. *J Neurochem* **72**, 2053-2058 (1999).

43. R. Vassar, M. Citron, Abeta-generating enzymes: recent advances in beta- and gamma-secretase research. *Neuron* **27**, 419-422 (2000).
44. S. Lesne *et al.*, A specific amyloid-beta protein assembly in the brain impairs memory. *Nature* **440**, 352-357 (2006).
45. L. Cao *et al.*, Abeta alters the connectivity of olfactory neurons in the absence of amyloid plaques in vivo. *Nat Commun* **3**, 1009 (2012).
46. G. Gheusi *et al.*, Importance of newly generated neurons in the adult olfactory bulb for odor discrimination. *Proc Natl Acad Sci U S A* **97**, 1823-1828 (2000).
47. B. D. Philpot, E. M. Lyders, P. C. Brunjes, The NMDA receptor participates in respiration-related mitral cell synchrony. *Exp Brain Res* **118**, 205-209 (1998).
48. D. A. Berkowicz, P. Q. Trombley, G. M. Shepherd, Evidence for glutamate as the olfactory receptor cell neurotransmitter. *J Neurophysiol* **71**, 2557-2561 (1994).
49. I. G. Davison, J. D. Boyd, K. R. Delaney, Dopamine inhibits mitral/tufted--> granule cell synapses in the frog olfactory bulb. *J Neurosci* **24**, 8057-8067 (2004).
50. K. Toida, K. Kosaka, Y. Aika, T. Kosaka, Chemically defined neuron groups and their subpopulations in the glomerular layer of the rat main olfactory bulb--IV. Intraglomerular synapses of tyrosine hydroxylase-immunoreactive neurons. *Neuroscience* **101**, 11-17 (2000).
51. D. M. Cummings, H. E. Henning, P. C. Brunjes, Olfactory bulb recovery after early sensory deprivation. *J Neurosci* **17**, 7433-7440 (1997).
52. N. S. Nadi *et al.*, Chemical deafferentation of the olfactory bulb: plasticity of the levels of tyrosine hydroxylase, dopamine and norepinephrine. *Brain Res* **213**, 365-377 (1981).
53. R. Kayed *et al.*, Common structure of soluble amyloid oligomers implies common mechanism of pathogenesis. *Science* **300**, 486-489 (2003).
54. A. Deshpande, E. Mina, C. Glabe, J. Busciglio, Different conformations of amyloid beta induce neurotoxicity by distinct mechanisms in human cortical neurons. *J Neurosci* **26**, 6011-6018 (2006).
55. J. C. Lambert *et al.*, Pronounced impact of Th1/E47cs mutation compared with -491 AT mutation on neural APOE gene expression and risk of developing Alzheimer's disease. *Hum Mol Genet* **7**, 1511-1516 (1998).
56. J. A. Harris *et al.*, Transsynaptic progression of amyloid-beta-induced neuronal dysfunction within the entorhinal-hippocampal network. *Neuron* **68**, 428-441 (2010).
57. J. W. Scott, D. E. Shannon, J. Charpentier, L. M. Davis, C. Kaplan, Spatially organized response zones in rat olfactory epithelium. *J Neurophysiol* **77**, 1950-1962 (1997).
58. Y. H. Liu, W. S. Lai, H. J. Tsay, T. W. Wang, J. Y. Yu, Effects of maternal immune activation on adult neurogenesis in the subventricular zone-olfactory bulb pathway and olfactory discrimination. *Schizophr Res* **151**, 1-11 (2013).
59. H. J. Kwon, J. H. Koo, F. Zufall, T. Leinders-Zufall, F. L. Margolis, Ca extrusion by NCX is compromised in olfactory sensory neurons of OMP mice. *PLoS One* **4**, e4260 (2009).
60. J. J. Stamps, L. M. Bartoshuk, K. M. Heilman, A brief olfactory test for Alzheimer's disease. *J Neurol Sci* **333**, 19-24 (2013).

Chapter 4

Region-specific amyloid-β accumulation in the olfactory system influences olfactory sensory neuronal dysfunction in 5xFAD mice

Gowoon Son[1,2]*, Seung-Jun Yoo[1,3,4]*, Shinwoo Kang[5], Ameer Rasheed[1], Da Hae Jung[1], Hyunjun Park[5], Bongki Cho[1,3], Harry W.M. Steinbusch[1,2], Keun-A Chang[5], Yoo-Hun Suh[5], and Cheil Moon[1,3,6]

[Alzheimer's Research & Therapy, 2021, doi: 10.1186/s13195-020-00730-2]

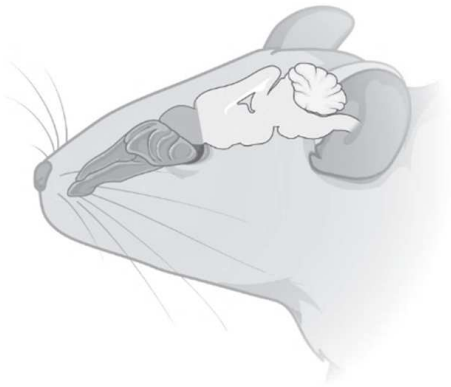

Abstract

Background: Hyposmia in Alzheimer's disease (AD) is a typical early symptom according to numerous previous clinical studies. Although amyloid-β (Aβ), which is one of the toxic factors upregulated early in AD, has been identified in many studies, even in the peripheral areas. The pathology involving olfactory sensory neurons (OSNs) remains poorly understood.

Methods: Here, we focused on peripheral olfactory sensory neurons (OSNs) and delved deeper into the direct relationship between pathophysiological and behavioral results using odorants. We also confirmed histologically the pathological changes in three-month-old 5xFAD mouse models, which recapitulates AD pathology. We introduced a numeric scale histologically to compare physiological phenomenon and local tissue lesions regardless of the anatomical plane.

Results: We observed the odorant group that the 5xFAD mice showed reduced responses to odorants. These also did not physiologically activate OSNs that propagate their axons to the ventral olfactory bulb. Interestingly, the amount of accumulated amyloid-β (Aβ) was high in the OSNs located in the olfactory epithelial ectoturbinate and the ventral olfactory bulb glomeruli. We also observed irreversible damage to the ectoturbinate of the olfactory epithelium by measuring the impaired neuronal turnover ratio from the basal cells to the matured OSNs.

Conclusions: Our results showed that partial and asymmetrical accumulation of Aβ coincided with physiologically and structurally damaged areas in the peripheral olfactory system, which evoked hyporeactivity to some odorants. Taken together, partial olfactory dysfunction closely-associated with peripheral OSN's loss could be a leading cause of AD-related hyposmia, a characteristic of early AD.

List of abbreviations

AD, Alzheimer's disease; OSN, olfactory sensory neuron; FAD, familial forms of AD; APP, amyloid precursor protein; PS1, presenilin 1; 5xFAD mouse, human APP and PS1 transgenic mouse with a total of five AD-linked mutations; Aβ, β-amyloid; OB, olfactory bulb; OE, olfactory epithelium; CNS, central nervous system; PNS, peripheral nervous system; WT, wild-type; L, lyral; A, acetophenone; E, eugenol; G, geraniol; AP, allyl phenylacetate; HA, heptanoic acid; H, heptanal; C57BL6, C57 black mouse; ROI, region of interest; TH, tyrosine hydroxylase; GL, glomerular layer; TUNEL, terminal deoxynucleotidyl transferase dUTP nick end labeling; OMP, olfactory marker protein; LTP, long-term potentiation; D, dorsal; V, ventral; A, anterior; P, posterior; IP, intraperitoneal; POI, point of interests; SEM, standard error of the mean; SD, standard deviation; IHC, immunohistochemistry; IF, immunofluorescence.

Keywords

Alzheimer's disease, Olfactory dysfunction, β-amyloid, 5xFAD, Olfactory sensory neuron, Zonal organization, Odor detection test, Ca^{2+} imaging, Topographic analysis, Neuronal turnover

1. Introduction

Olfactory dysfunction affects approximately 90% of patients with Alzheimer's disease (AD) (*1, 2*). Abnormal olfaction has been recognized as one of the earliest clinical manifestations of AD over the past few decades (*3, 4*). Numerous attempts have been made to comprehend early AD by using olfaction-based assessments (*5-7*). Recent research has shown that patients with AD who have difficulty with olfaction are not completely anosmic (*8*). According to the results of clinical studies, patients have difficulty identifying only a few odorants presented, and not all odorants (*9, 10*). Besides, the early-onset issues have sparked the mechanism study of hyposmia to understand AD progression. Interestingly, although amyloid-β (Aβ), which is one of the toxic factors upregulated early in AD, has been identified in many studies, even in the peripheral areas (*11-13*). The pathology involving olfactory sensory neurons (OSNs) remains poorly understood.

Odor detection via OSNs is the first step in smell processing. The signals converge in the glomerulus in the olfactory bulb (OB), where synapses form between the axon terminal of OSNs and the dendrites of mitral, periglomerular, and tufted cells (*14, 15*). Each OSN expresses one type of odorant receptor, and its axon propagates to the OB. The axons of OSNs that express the same odorant receptor form two or three glomeruli per each bulb, which follows a topological map or axis (*16, 17*). The OSNs targeted to ventral glomeruli are located in the ectoturbinate of the olfactory epithelium (OE), whereas the OSNs targeted to the dorsal glomeruli

are located in the endoturbinate of the OE (*18-21*). We also previously demonstrated a distinctive accumulation pattern of Aβ oligomers with specifically β-secretase 1 (BACE1) expression in the OSNs' terminal located in the OB. This suggested that the uneven partial spatial damage leads to abnormal AD hyposmic symptoms in the olfactory system (*11*). However, it has not been known how partial damage of the olfactory systems is causally related to distinct olfactory dysfunctions. Nor has a clear mechanism been proposed that induces damage to the olfactory epithelium by the accumulation of Aβ oligomers. In this study, we delve deeper into the functional impairment related to the spatial distribution of accumulated Aβ oligomers.

We observed a distinctive pattern of hyposmia using an olfactory detection test and electrophysiological changes in OSNs in the early stage of oligomerized Aβ accumulation. We also revealed the spatial correlation between the functional changes and immunohistological signals using a heat map analysis. Given the characterization of the olfactory topographical axis with intrinsic turnover, we identified an interrelation between Aβ oligomer deposits and the breakdown of OSNs-turnover. To explain the role of Aβ in hyposmia, we used transgenic mice with early-onset familial forms of AD (FAD). These mice have elevated Aβ levels caused by the coexpression of five FAD (5xFAD) mutations (three in amyloid precursor protein [APP] and two in presenilin 1 [PS1]) (*22*). This model develops a large $A\beta_{42}$ load (known to generate toxic oligomerized species of Aβs) starting at two months of age (*22*). It is also well known that these mice develop central nervous system

(CNS) deficits after five months (22). Thus, we used three-month-old 5xFAD mice as a means of identifying a potential causative role for Aβ-derived neurotoxicity in early AD (22). In particular, we here established a tool for monitoring the pathological features of the OSNs. We confirmed functional and anatomical damages and related mechanisms through Aβ-derived neurotoxicity by associating them with the characteristics of the olfactory system. Taken together, we show that region-specific damage of OSNs induces partial olfactory dysfunction, and this may be a feature of AD-specific olfactory dysfunction.

2. Materials and methods

2.1. Key Resources Table

Reagent or Resource	Source	Identifier
Antibodies		
anti-Aβ-oligomer (A11)	Invitrogen	#AHB0052
anti-6E10 ($A\beta_{1-16}$)	Covance	#SIG-39300
anti-D54D2 ($A\beta_{1-40}$, $A\beta_{1-42}$)	Cell signaling	#8243
anti-BrdU	Thermo	#MA3-071
anti-OMP	WAKO	#019-22291
anti-synaptophysin	Dako	#M0776
anti-TH	Santa Cruz	#sc-14007
anti-Ki67	Cell signaling	#12202
Chemicals		
Fura-2	Promo Cell	PK-CA707-50034
BrdU	Sigma-Aldrich	#59-14-3
Acetophenone	Sigma-Aldrich	#42163
Allyl phenylacetate	Sigma-Aldrich	#W203904
Eugenol	Sigma-Aldrich	#E51791
Geraniol	Sigma-Aldrich	#163333
Heptanal	Sigma-Aldrich	#W254002
Heptanoic acid	Sigma-Aldrich	#75190
Lyral	Sigma-Aldrich	#95594
Mineral oil	Sigma-Aldrich	#M5904
Experimental models: Organisms/Strains		
5xFAD (Tg6799)	K.A. Chang's Lab	
C57BL/6J	KOATECH	http://www.koatech.co.kr/
Software and Algorithms		
ImageJ	NIH	https://imagej.nih.gov/ij/
Fiji	NIH	https://imagej.nih.gov/ij/
Prism Software	GraphPad Software,Inc, La Jolla, USA	https://www.graphpad.com/scientific-software/prism/

2.2. *Animals*

All experimental protocols were approved by the Institutional Animal Care and Use Committees of DGIST(DGIST-IACUC_0104). All applicable guidelines for the care and use of laboratory animals from the National Institutes of Health Guide were followed. Only male animals were used in this study. Adult mice (C57/BL6, two-months-old) were obtained from KOATECH (Daegu, Korea). 5xFAD transgenic mice harboring the mutated human APP (695 amino acids) and human PS1 genes (Tg6799, 3–4 months old) were obtained from Prof. K.A. Chang (Gachon Medical School, Incheon, Korea). All behavioral, physiological and histological analyses using animals in this study were blind tested.

2.3. *Behaviors*

We conducted behavioral experiments with the isolated preparation.

2.3.1. *Y-maze test*

The test was performed to evaluate the ability of the mice to act in a sequence and to measure short-term memory. Each branch (A, B, and C) of the maze was 40 cm long, 5 cm wide, and 10 cm high at an angle of 120°. The maze was constructed of white polyvinyl plastic. The animal was placed in the maze for 8 min, and the frequency with which the tail entered each branch was counted for each branch. The number of times the animal entered the branches (in the A, B, C sequence) was also counted and awarded 1 point (real change, actual alternation). Ability to take

action to change (%) = Actual change (actual alternation)/maximum change (maximum alternation) × 100 (maximum change: the total entrance number − 2)

2.3.2. *Morris water maze (MWM) test*

The test was conducted in a circular pool (diameter 90 cm, height 45 cm, outer height [from the ground] 61.5 cm) using the EthoVision Maze task system (Noldus Information Technology, Wageningen, the Netherlands). The time required to find the platform and the latency to escape (escape latency) was measured. The animals underwent four training trials per day (one time per quadrant) over 4 consecutive days with a 30 min interval. If the animal could not find the platform within 60 s, they were placed on the platform for 20 s. The platform was removed on the last day, the animals were placed in the water to swim for 60 s, and memory was compared by measuring swimming around the area where the platform was installed. The C57/BL6 mouse was used for verifying the background feature of the adult olfactory system. The two months old mouse was considered as an adult. In our experimental condition, we compared all values from wild-type mice with age-matched.

2.3.3. *Food-seeking test*

The test was performed in three-month-old 5xFAD mice (WT, n=6; 5xFAD, n=6) and as described previously (*11*). Prior to the food-seeking tests, food restriction was applied for over 35 h to motivate animals to search for food, either hidden underneath a layer of bedding or not. Therefore, this test was used to assess latency in finding food as the buried pellet-seeking test. Mice were habituated in a

clean home cage for one day prior to testing. A food pellet was buried 5 cm under the bedding in a middle region of the edge of the cage and a mouse was placed at the opposite edge. The time to the first bite of the food pellet was measured using an installed digital camera (maximum recording time was 10 min based on the assumption that food-restricted mice that fail to use odor cues to locate the food within a 10-min period are likely to have deficits in olfactory abilities). In data analysis and figure, we normalized the data by an average of wildtype's time latency to evaluate effectively how time latency would be changed in a transgenic mouse.

2.3.4. Odor detection (nose poke) tests

The test was performed at three months of age for the Tg6799 and wild-type (WT) groups (n = 6 per group) and by modifying the odor-preference test described previously (*19, 23*). Instead of filter paper, a cotton tip scented with odorant was used to allow for the nose poke of mice to more accurately direct them to the odor (Fig. 1c). The following commonly used odor preference test odorants were used and presented for 2 min: acetophenone (8.6 M), allyl phenylacetate (5.9 M), eugenol (6.5 M), geraniol (5.7 M), heptanal (7.2 M), heptanoic acid (7.1 M), and lyral (4.7 M). Mineral oil (MO) was used as a control odorant. After 5 min habituation, mice were transferred to a new cage and the tip scented with a test odorant carefully set so that the mouse could not directly reach it. Investigation times were measured for 2 min. The performance index (PI) was determined based on a previously described method (*24*). PI is the percentage of time to detection of the experimental odorant

minus the percentage of time in the control. A PI close to 0 indicates difficulty in detecting an odor and a PI of 100 indicates that a mouse could definitively detect an odor. The mouse behavior was recorded with a digital video camera (rate of 30 frames/s). Four points of interest (POIs) that we tracked in each frame were the nose, ears, and tail (Movie S1). In each group, we first randomly selected 180 frames and manually labeled POIs in those frames and used them to train and test a neural network model implemented in DeepLabCut (*25*). Evaluation of labeling accuracy was achieved by comparing the labels acquired from the convolutional neural network on the test set with manual labels. The model was then used to evaluate all frames in each group of the 20 videos used for training. The resulting x and y coordinates corresponding to the middle position of four POIs within each frame were used to determine location. The test cage was divided into equally sized three compartments, and the duration that odorant part of mice stayed inside the third that contains a cotton tip was analyzed for odor attraction.

2.4. Calcium imaging

We conducted calcium imaging in the in vivo conditions with the isolated preparation of instrument.

2.4.1. Mice preparation

Imaging was performed at three months of age for the Tg6799, age matched WT, and C57BL6 mice (n = 5–6 per group). Prior to the operations and administration of a calcium indicator (Fura-dextran), mice were anaesthetized with

a mixture of ketamine (90 mg kg^{-1}) and xylazine (10 mg kg^{-1}). Calcium dye was administrated by nasal administration of a calcium indicator (using PE-90 tubes attached to a micropipette). A volume of 5–6 µl (8 µl mixture of 8 % / 0.2 % calcium dye/Triton-X) was administered to each nostril. Six hours after the operation, mice were anaesthetized again with a mixture of ketamine (90 mg kg^{-1}) and xylazine (10 mg kg^{-1}) and decapitated. The whole olfactory system (MOE and OB) was dissected and peeled off. The sample fixed on 4% low-melting agarose (Sigma A9414, St. Louis, MO, USA) and transferred into Ringer's solution (140 mM NaCl, 5 mM KCl, 1 mM $CaCl_2$, 1 mM $MgCl_2$, 10 mM HEPES, 10 mM glucose, 1 mM Na pyruvate, pH 7.4). The perfusion rate was 2 ml/min. The sample was flattened by trimming, transferred to a tissue slice chamber (Warner instruments) with the lateral side facing up.

2.4.2. Odor stimulation

Odorants were presented as dilutions from saturated vapor in cleaned air using a custom olfactometer which was designed to provide a constant flow of air blown. The olfactometer was built by using manually controlled valves, Teflon tubing, glass syringes (10 cc), scintillation vials, flowmeter, and air pump (600 ml/min). Odorant with specific concentration identified through behavioral experiments are made with saturated vapor, and they are adding on airflow through the odorant tube and delivered directly to the olfactory system. All the odorants diluted in mineral oil (0.0001%), or mineral oil only (control) were used to generate vapor saturation in the syringes. For the different odorant, different odorant tubes set (Teflon tubing,

glass syringes (10 cc), scintillation vials) were used to prevent contamination in the experiment (Fig. S2a).

2.4.3. Optical recording

A typical stimulation protocol was a 20 s duration including 2 s stimulation repeated 10 times separated by one min between stimulations. The bulb surface of wide-field optical signals was measured using a Nikon 10×, 0.5 NA (2.3 × 2.3 mm field of view), Nikon 16× 0.8 NA (1.4 × 1.4 mm field of view) with a 150 W Xenon arc lamp (Opti Quip), objectives with a 200 mm focal length lens for single bulb measurements. For fluctuation of calcium monitoring, we used 380/10 nm (Chroma, ET380x) excitation light and a 510/84 nm emission filter (Semrock FF01-510/84). Fluorescence emission was recorded with a NeuroCCD-SM256 camera with 2 × 2 binning between 25–125 Hz using NIS-Elements software (Nikon).

2.4.4. Data analysis

All target points for analysis were selected on the sagittal view of OB, aligned manually to each mouse, guided by skull features and overall outline connecting OE-OB-brain. In order to confirm the correlation with the IHC results to be followed, we analyzed the ($\Delta F/F_0$) change across OB to compare with the IHC analysis. Dorsal to the ventral line for our calcium analysis within OB were aligned to proceed correlation analysis with the coronal sectioned IHC analysis. The entire analysis area of OB is divided equally among 10 sections from the anterior to posterior and 180

sections from dorsal to ventral within a lateral olfactory bulb view, respectively (Fig. S2b).

Activity maps that could reflect the positional variability of glomeruli among individuals for the analysis of calcium activities are adopted. The activity map is defined by the selected target point which is automatically calculated using the LC Pro plugin for ImageJ and an outline with a distance of 200 μm from the selected target point using C57BL6 mice.

The 10 times recordings per each odorant with for the Tg6799, age matched WT were averaged per 1 s and processed for 20 s for further analysis. The individual trials were manually inspected, and occasional trials with obvious artifacts were discarded. Then resting-state (airflow without odorant) data (baseline fluorescence (F_0)) was intensity normalized with averaging frames over 3 s for 10 trials before stimulus onset. Activation data with odorant stimulation was calculated with fluorescence signal difference of every time point (ΔF) which was subsequently normalized ($\Delta F/F_0$). Calcium measurement ($\Delta F/F_0$) of specific activity maps were scaled with the averaged intensity value per each time point.

To perform the correlation, a heat map analysis was also performed on only the subsets of pixels overlaying the ROIs identified in each preparation's activity map using unfiltered activity maps. All experiments were performed and evaluated by five independent tests.

2.5. Tissue preparation

Animals were anesthetized by intraperitoneal injection of 65 mg/kg ketamine with 5 mg/kg xylazine. The mice were then transcardially perfused with prechilled phosphate-buffered saline (PBS, pH 7.6). Heads were removed, skinned, and post-fixed overnight in 4% paraformaldehyde in PBS at 4 °C. The mandibles were discarded, and the trimmed heads were skinned and fixed by immersion in the same fixative for one day at 4°C. The heads were decalcified in Calci-Clear Rapid solution (National diagnostics, GA, USA) for 20 min at room temperature. After decalcification, the specimens were washed, dehydrated in increasing concentrations of ethanol, and transferred into xylene to clear the tissue. The specimens were infiltrated with paraffin and embedded. For cryosectioning, tissue was soaked in sucrose and embedded in Tissue-Tek OCT compound (Sakura Finetek Europe BV, Zoeterwoude, the Netherlands) after post-fixation in 4% paraformaldehyde. Frontal sections (coronal, 5 μm) were cut serially from the tip of the nose to the posterior extension of the OE and OB, and each section was preserved on Matsunami coating slide glass (Matsunami Glass Co., Tokyo, Japan).

2.6. Immunohistochemistry (IHC)

For IHC, the tissue was permeabilized in PBS-T (0.1% Triton X-100 in PBS) for 15 min. The endogenous peroxidase in the samples was quenched using 3% hydrogen peroxide in 10% methanol for 30 min. To retrieve antigenicity, the samples were boiled in 0.1 M citrate buffered saline (pH 6.0) for 5 min. The sections were cooled for 30 min and then washed twice in PBS (5 min each). After washing in PBS-T for

30 min, the sections were blocked for 1 h in blocking solution (4% normal donkey serum in PBS-T) and incubated with primary antibodies overnight at 4 °C. Anti-Aβ oligomer (1:100) and anti-bromodeoxyuridine (BrdU; 1:250) antibodies were used. After washing in PBS-T, the sections were incubated with a biotinylated secondary antibody for 1 h at room temperature. Sections were subsequently treated with the avidin-biotin-peroxidase complex (Vectastain Elite ABC kit) for 1 h at room temperature. The sections were developed for 5 min in a 0.05% DAB solution, and counter-stained with hematoxylin. Images were captured with a Nikon digital camera (DS-Ri1) attached to a Nikon-Eclipse-90i microscope (Nikon Corp., Tokyo, Japan).

2.7. Immunofluorescence (IF)

For immunofluorescence, tissues were permeabilized in 0.1% PBS-T for 15 min. To retrieve antigens, the samples were boiled in 0.1 M citrate buffered saline (pH 6.0) for 5 min. The sections were cooled for 30 min and then washed twice in PBS (5 min each). After washing in PBS-T for 30 min, the sections were blocked for 1 h in blocking solution (4% normal donkey serum in PBS-T). The sections were incubated with primary antibody overnight at 4 °C. Anti-oligomer A11 (Invitrogen, CA, USA) (1:100), Anti-6E10 ($A\beta_{1-16}$) (Covance, NJ, USA) (1:500), Anti- D54D2 ($A\beta_{1-40}$, $A\beta_{1-42}$) (Cell Signaling, MA, USA) (1:500), anti-synaptophysin (Agilent Dako, CA, USA) (1:250), anti-TH (Santa Cruz Biotech, TX, USA) (1:250), and anti-Ki67 (Cell Signaling, MA, USA) (1:250) antibodies were used. Alexa 488 and Cy3-conjugated secondary antibodies (Jackson Laboratory, Bar Harbor, ME, USA) were used. The sections were counter-stained and mounted using VECTASHIELD

mounting medium with 4′,6-diamidino-2-phenylindole (DAPI; Vector Laboratories, CA, USA). The images were visualized and photographed by confocal fluorescence microscopy (Carl Zeiss, Thornwood, NY, USA).

2.8. TUNEL staining assay

For TUNEL staining, deparaffinized and rehydrated sections were washed in PBS for 5 min and treated with Proteinase K (10 μg/mL) in PBS at room temperature for 30 min. After they were washed with distilled water for 5 min, the TUNEL incubation solution (Promega, WI, USA), containing the TdT enzyme solution and label solution, was prepared following the manufacturer's protocol. The sections were incubated in the TdT enzyme and label mixture for 1 h at 37 °C and then washed three times with PBS (5 min each). Fragmented DNA was visualized as green fluorescence inside the nuclei.

2.9. BrdU assay

BrdU (Sigma, St. Louis, MO) was injected and detected with an antibody recognizing BrdU. For acute labeling experiments, 100 mg/kg BrdU was injected 1, 3, and 7 day(s) before sacrifice.

2.10. Image processing

All images were acquired using a Nikon ECLIPSE 90i microscope and a Nikon DS-Ri 1 digital camera (Nikon Inc., Japan) and LSM700 (+ Zeiss slide scanner). Digital images were processed adjusting only brightness, contrast, and color balance. The numbers of immunoreactive cells were counted manually by two independent

investigators blinded to the experimental conditions. Three slides were analyzed for each animal and observed under a microscope (×100–400). To quantify the reciprocal intensity, the intensity per unit area was measured using Image J and the color deconvolution plug-in (http://wiki.imagej.net/Colour_Deconvolution). The target unit area of images was processed using the color deconvolution tool in Image J to separate brown from other colors. The area of brown staining was then quantified and divided by the total area to yield a percentage of staining area. Stereological analyses were conducted using Prism software (GraphPad software, USA).

2.11. Spatial analysis

To rate olfactory synapse positions within the sectioned OB (sagittal view), we divided equally among 10 frames from the anterior to posterior within a sagittal olfactory view. The top of the glomeruli in each frame was considered as a "degree of zero" and used to set the relative angle from zero (dorsal to ventral of OB) (Fig. 2c). Spatial correlations of the calcium signal heat maps (Fig. 2d, Fig. S2e) were calculated using the function "cor" in the R software package (version 3.4.2; http://www.r-project.org/), and the correlation coefficient of each calcium signal map evoked by an odor was displayed as a heat map using the function "leverplot" in R (Fig. 2e, g). To rate olfactory synapse positions, the sectioned OB with coronal and rostral migratory stream (RMS) was used as the standard (center of the dorsal-ventral axis). The most pointed/top of the glomeruli are located along the upper RMS track and regarded as "degree of zero" (360° at the same time due to coronal

view), and the ROI was measured along with glomeruli; relative angles were then based on this zero point (Fig. 3a). Spatial heat maps (Fig. 3b) representing the Aβ oligomer expression were constructed using the function "leverplot" in R. A heat map matrix represents the intensity distribution of the deconvolution of the DAB signal by the protein expression along the angle. The intensity is presented as a scale bar (0–200 $\Delta F/F$) at the left side of the maps.

2.12. Statistical analysis

Statistical analyses for histological ROI evaluation were conducted using Prism software (GraphPad software, USA). Comparisons between WT and experimental mice were conducted using a t-test. Results are presented as mean ± standard error of the mean (SEM). Differences with P-values of ≤0.05 were considered to be statistically significant. Correlations were assessed with a non-parametric Spearman's rank correlation test. Graphs (Fig. 4) show regression lines with a 95% confidence interval.

3. Results

3.1. Atypical olfactory dysfunction is observed in 5xFAD mice overexpressing Aβ

We performed food-seeking tests to examine whether olfactory dysfunction was present (Fig. 1a). Our results show that three-month-old 5xFAD mice exhibited a significant increase in the latency time of seeking the buried food compared with wild-type (WT) mice (Fig. 1b) suggesting severe defects in olfactory function, as

opposed to learning and memory dysfunction. To better understand this abnormal odor detection in the early stages of AD progression, we conducted the odor detection test in three-month-old 5xFAD mice with several different odorants by modifying the odor preference test (Fig. 1c). We systematically compared seven different odorants for which odor detection has been associated within the main olfactory system; lyral [L], acetophenone [A], eugenol [E], geraniol [G], allyl phenylacetate [AP], heptanoic acid [HA], and heptanal [H] (0.001%). The WT mice detected all odors well and stayed near cotton tips scented with the odorants. The 5xFAD mice were able to detect lyral, acetophenone, and eugenol (odorant group A). However, geraniol, allyl phenylacetate, heptanoic acid, or heptanal (odorant group B) were not detected (Fig. 1d, e). The 5xFAD mice showed partial impairment of odor detection and not an entire loss of function. Based on this behavioral pattern, we concluded that the olfactory abnormality in 5xFAD mice has a particular uneven pattern.

In order to monitor olfactory dysfunction in the early stages of AD, we assessed cognitive and locomotor abilities that could be influenced by olfactory behavior. We performed the spontaneous alternation test and the Morris water maze task in two-, four-, and six-month-old mice (Fig. S1a). We noted that total arm entries were not significantly different between WT and 5xFAD mice in the Y-maze test (Fig. S1b). The results are shown as a ratio of the results from the two cognitive tests representing the number of new arm entries in the Y-maze test and the latency time to escape the platform in the Morris water maze test. Six-month-old mice had a decreased

ability to move to a new arm (Fig. S1c) and required more time to find the platform in the water maze (Fig. S1d). However, no statistically significant difference in memory impairment was found between two- and four-month-old mice (5xFAD as compared with WT; Fig. S1c, d). Based on these collective results, we confirmed that 5xFAD mice between the ages of two and four months display behaviors that mimic the early stages of AD progression (Fig. S1e).

3.2. OSNs-derived Ca^{2+} signals caused by odorants are decreased in the ventral glomeruli of 5xFAD mice

Because the previous results showing that olfactory dysfunction may appear in the peripheral nervous system (PNS) prior to defects in the CNS, we analyzed the sensory input signals by specific odorant stimulation in the OB (*11*). It is well known that OSNs expressing a specific odorant receptor project their axons to a specific set of glomeruli in the OB. We refer to the regional projection of OSNs as the endoturbinate-dorsal glomeruli axis and ectoturbinate-ventral glomeruli axis in the peripheral olfactory system (Fig. 2a).

Using these characteristics of the olfactory system, we have introduced a system that could isolate the detection function by introducing the calcium indicator (fura-2 AM) only in the OSNs (Fig. 2b). Specifically, we used a heat map model to represent the input activity from the OSNs terminal of the entire OB to digitize and visualize the local information. When the OB was sagittally sectioned, the highest point of olfactory synapses (anatomically glomeruli) was noted as a "degree of zero" (dorsal

side). On the contrary, the lowest point of olfactory synapses was noted as a "degree of 180" (ventral side) (Fig. 2c). To make a common odor map in the OB, we analyzed general OSNs-input patterns using C57 mice, a widely used inbred strain (Fig. S2c). The intensity of calcium signals by specific odorants was represented and compartmentalized with specific localization on the glomerulus layer by superimposing them over the repeated calcium image (Fig. S2d). Based on our results, the odor map grouping could be viewed from two different groups using the spatial correlation matrix: group A (lyral, acetophenone, and eugenol), or group B (geraniol, allyl phenylacetate, heptanoic acid, and heptanal) (Fig. S2e). Each odorant was classified according to a spatially correlated value. Interestingly, each of the two groups showed the same odor component in both the spatial matrix and odor detection pattern (Fig. 1e, 2d, S2e).

Similar to the results obtained in C57 mice, the intensity of calcium signals by specific odorants in WT/5xFAD mice localized to the glomerulus layer (Fig. S2f). Using the localized activity map, the intensity in WT/5xFAD mice was quantified as a heat map with the spatial information (Fig. 2e, g). It was clustered into two distinct groups, the dorsally located group (group A odorants) and the ventrally located group (group B odorants) (Fig. 2d). The group A odorants presented similar patterns of calcium intensity between WT and 5xFAD mice (Fig. 2e, f, Table 1). On the other hand, group B odors resulted in a significant decrease in the intensity of calcium on the glomerulus layer in the 5xFAD mice (Fig. 2g, h, Table 1). Through both behavioral and physiological tests using specific odorants, we suggest that the spatial abnormality

of OSNs calcium signaling is related to the pattern of olfactory dysfunction in the 5xFAD mice.

Table 1. Ca2+ activation in the peripheral olfactory glomeruli.

Unpaired *t-test*	L	A	E	G	AP	HA	H
P value (two-tailed)	**0.2271**	**0.8298**	**0.9171**	**< 0.0001**	**< 0.0001**	**< 0.0001**	**< 0.0001**
P value summary	ns	ns	ns	***	***	***	***
T	1.287	0.2207	0.1067	8.422	9.916	12.53	9.448
Df	10	10	10	10	10	10	10
Are means significantly different? (P < 0.05)	No	No	No	Yes	Yes	Yes	Yes

Data are represented as a numerical value representing the odor-derived Ca2+ activity between WT and 5xFAD mice (Fig. 2f, h). The experimental odorants included lyral [L], eugenol [E], acetophenone [A], geraniol [G], ally phenylacetate [AP], heptanoic acid [HA], and heptanal [H]. Alzheimer's disease (AD), five familial AD mutations (5xFAD). For the statistical analysis, a two-tailed unpaired t-test was performed. Statistical significances are denoted as follows: non-significant (ns); ***, P < 0.001.

3.3. OSNs accumulate Aδ oligomers with region specifically in 5xFAD mice

Next, we examined whether neurological pathology, including the olfactory defect of 5xFAD mice, is the result of Aβ oligomer formation. We examined the expression pattern of oligomeric Aβ by using A11-immunoreactivity in the OSNs. OSNs penetrate their axons into the glomerulus of the OB, which is considered as a first olfactory synapse. A11 can detect a marker of toxic soluble oligomeric Aβ (26).

By using coronal-sectioned 5xFAD olfactory tissue, A11-immunoreactivity was assessed histologically in both the OSNs layer and its synapses. We also double-checked the Aβ that has different isotope using 6E10 and D54D2 (Fig. S3b). The positive signals were higher in the ventral glomerular layer (180°±80°), rather than other inner layers such as an external plexiform layer, mitral cell layer, and granule cell layer (Fig. S3b). We introduced a novel stereological analysis on Aβ oligomers in the 5xFAD mice. First, a two-dimensional position of olfactory glomeruli was digitized as an angle (detailed criteria provided in the materials and methods section) (Fig. 3a). A heat map matrix represents the distribution of the A11-immunoreactivity in olfactory glomeruli along a specific angle (Fig. 3b, c).

The A11-positive region of interest (ROI) signal was significantly enriched in 5xFAD mice, especially the ventral layer of the glomeruli (WT dorsal: 5xFAD dorsal = 1.00: 1.13, WT ventral: 5xFAD ventral = 1.54:2.30) (Fig. 3d, e). The Aβ oligomers accumulated along the topographical axis. Specifically, they were within the OSN layer of the ectoturbinate as compared to the endoturbinate in 5xFAD mice (WT endo: 5xFAD endo = 1.00: 1.13, WT ecto: 5xFAD ecto = 1.13:2.10) (Fig. 3f, g). As shown above, the uneven Aβ distribution in 5xFAD mice implies that increasing Aβ oligomers correlates with the partial dysfunction of OSNs.

3.4. Ca^{2+} signals and Aβ accumulation are negatively correlated in the ventral glomeruli in 5xFAD mice

We conducted Spearman's correlation analysis to examine the relationship between A11-immunoreactivity and odorant-dependent calcium activity (Fig. 4). According to angle measurements, the ROI of A11-immunoreactivity displayed a strong correlation in the ventral glomeruli (180°±80°) and a weak correlation in the dorsal glomeruli (0°±80°) of the olfactory bulb (Fig. 3c). The changes in Ca^{2+} fluorescence in the glomeruli by group A odorants (lyral, acetophenone, and eugenol) were higher in the dorsal glomeruli, and group B odorants showed higher Ca^{2+} changes in the ventral glomeruli (Fig. 4a). Interestingly, the changes in Ca^{2+} fluorescence in the glomeruli by group B odorants (geraniol, allyl phenylacetate, heptanoic acid, and heptanal) reduced in line with the strong A11-immunoreactivity in the glomeruli of 5xFAD mice (Fig. 4b), and each group B odorant showed a negative correlation with A11 intensity, which was not seen for group A (Fig. S4). The most noticeable result is that the stronger the correlation to A11 intensity, the lower the odor detection and OSNs activation in 5xFAD mice (Table 2, Fig. 1d, 2h). The results indicate that decreased OSNs-derived activity and odor detection in 5xFAD mice are influenced by Aβ oligomers.

Table 2. Correlation analysis between levels of A11 immunoreactivity and odor-induced Ca2+ activity at the angle-matched olfactory synapse.

Parameter	group A	L	A	E	group B	G	AP	HA	H
Number of XY Pairs	180	180	180	180	180	180	180	180	180
Spearman's rho	**0.5951**	**0.3453**	**0.5132**	**0.4722**	**-0.4434**	**-0.1664**	**-0.2983**	**-0.4641**	**-0.5803**
95% confidence interval	-0.6849 to -0.4897	-0.4710 to -0.2058	-0.6159 to -0.3934	-0.5811 to -0.3466	0.3141 to 0.5565	0.01672 to 0.3809	0.1551 to 0.4292	0.3375 to 0.5743	0.4713 to 0.6719
P value (two-tailed)	< 0.0001	< 0.0001	< 0.0001	< 0.0001	< 0.0001	0.0251	< 0.0001	< 0.0001	< 0.0001
P-value summary	***	***	***	***	***	*	***	***	***
Exact or approximate P-value?	Gaussian Approximation	Gaussian Approximation	Gaussian Approximation	Gaussian Approximation	Gaussian Approximation	Gaussian Approximation	Gaussian Approximation	Gaussian Approximation	Gaussian Approximation
Is the correlation significant? (alpha=0.05)	Yes	Yes	Yes	Yes	Yes	Yes	Yes	Yes	Yes

Data represent the relationship between A11 immunoreactivity and odor-induced Ca2+ activity at the angle-matched olfactory synapse (Fig. S4). The experimental odorants included lyral [L], eugenol [E], acetophenone [A], geraniol [G], ally phenylacetate [AP], heptanoic acid [HA], and heptanal [H]. For the statistical analysis, a non-parametric Spearman's correlation was performed, followed by linear regression with a 95% confidence interval. Statistical significances are denoted as follows: non-significant (ns); *, $P < 0.05$; ***, $P < 0.001$.

3.5. Ventral periglomerular cells decrease the expression of tyrosine hydroxylase induced by input activity from ectoturbinate OSNs

We measured tyrosine hydroxylase (TH) immunoreactivity in glomeruli to identify the negative effect of Aβ oligomers on the synaptic function of OSNs. This represents a marker of active OSNs. The number of periglomerular neurons expressing TH was determined as a marker of sensory input in the OSNs. The number of TH-positive neurons was significantly decreased (on average twice as low as in 5xFAD mice than in WT mice) in the ventral glomeruli (WT dorsal: 5xFAD dorsal = 1.00:1.13, WT ventral: 5xFAD ventral = 1.67: 0.61) (Fig. 5a, b). These results show that the spatially one-sided accumulation of Aβ oligomers may topographically induce partial dysfunction of the OSNs in parallel.

3.6. Decreased maintenance of structure induced by OSNs turnover disruption in the ectoturbinate olfactory epithelium of 5xFAD mice

Neuronal synaptic dysfunction evokes interaction deficits of each neuron and leads to neural connection problems. The OB is the meeting place of the PNS and CNS, enabling a comparative study relative to an altered condition. Thus, we compared the proportion of each OB layer (Fig. 6a). The total volume of the OB did not differ between the WT and 5xFAD mice (Fig. 6b). The dorsal GL area was not significantly changed (Fig. 6c). However, the ventral glomerular layer (GL) area was decreased (WT:5xFAD = 0.17:0.14) in 5xFAD mice (Fig. 6d). We measured synaptophysin immunoreactivity in the glomeruli to monitor the populations of

presynaptic vesicles. The ROI of synaptophysin decreased in the ventral olfactory glomeruli of 5xFAD mice (WT dorsal: 5xFAD dorsal = 1.00:0.84, WT ventral: 5xFAD ventral = 0.99:0.63) (Fig. 6e, f).

Next, we examined the turnover cycle of OSNs that maintained the structure of the olfactory system. OSNs proliferation and death were considered as a "turn" and "over," respectively. The proliferating cells were evaluated by Ki67 positivity in basal cells. The number of Ki67-positive cells in the endoturbinate had a similar ratio between the WT and 5xFAD mice, but the ectoturbinate in the 5xFAD mice showed a significantly decreased number of Ki67-cells that was twice as low as in the WT mice (Fig. 6g, h). We further measured the ratio of apoptotic cell death using a TUNEL assay. The ratio of apoptotic cells was similar between the WT and 5xFAD mice. However, in the ectoturbinate, the TUNEL-positive cells increased two-fold in 5xFAD mice as compared to the WT mice (Fig. 6i, j). In addition to OE, the TUNEL-positive cells in the OB were monitored in the glomerulus layer rather than the granule cell layer. Besides, the OB could not be found the region differential distribution of TUNEL-positive cells (Fig. S5). Moreover, the mature OSNs marker, the olfactory marker protein (OMP) (+) OSNs numbers, were decreased in 5xFAD mice, especially in the ectoturbinate (Table 3), suggesting that these changes are caused by disruption of OSN turnover.

Table 3. OMP (+) OSNs in 5xFAD mice compared with age-matched WT mice.

	% of OMP (+) cells (mm^2)	
	WT	5xFAD
endo	65.29±5.10	62.70±4.04 (ns)
ecto	71.11±3.95	52.74±5.25 (***)

Data are represented as percentages of OMP (+) cells in the OE (mm2) (means ± SDs). For statistical analysis, a two-way ANOVA was performed, followed by the Bonferroni post hoc test. Olfactory marker protein (OMP), olfactory sensory neurons (OSNs), Alzheimer's disease (AD), five familial AD mutations (5xFAD), endo: endoturbinate; ecto: ectoturbinate. Statistical significances are denoted as follows: non-significant (ns); ***, $P < 0.001$.

4. Discussion

4.1. discussion

Previous studies have confirmed that olfactory abnormalities in AD may occur in its early stages (*11, 27*). In particular, AD-related olfactory abnormalities may be specific to the peripheral olfactory system and occur prior to the increased Aβ pathology in the CNS (*12, 13*). Based on the time frame we established, we confirmed the characteristics of potential AD-related olfactory problems using various odors. In order to exclude the CNS-derived effect on olfactory behavior, we examined functions that mainly involve the central nerves, including cognition, mood, and locomotion. We introduced the Y-maze test to evaluate not only cognitive tests by spontaneous arm alternation test (Fig. S1c) but also locomotor

ability including motivation to move (Fig. S1b). The locomotor ability can count the number of entries when they freely move in three-arm Y-maze. According to our results from the Y-maze test, the total arm entries were not significantly different between WT and 5xFAD mice (Fig 1b). Therefore, our Y-maze test could exclude the motor and motivational dysfunction issues influencing the observations in the food-seeking test. Additionally, these tests showed that 5xFAD mice were not affected by any abnormal behavior that can affect olfaction, such as anxiety and/or stress (Fig. S1). Although the mice were mutated so that every neuron (not specifically OSN) overexpresses Aβ, the olfactory behavior was significantly impaired before severe dysfunction of CNS behavior occurred. According to a previous study, a profound olfactory impairment has been demonstrated to precede severe memory decline and AD pathology in the brain (*11*). Concerning AD progression, our experimental time point suggests that hyposmia appears at an early stage of the disease.

Each odorant has a variety of chemical features, and it is well known that the mouse may show preference when detecting odors (*28, 29*). Olfactory signals are initiated in the periphery and propagate to the central olfactory system. This proceeds with three-step sequences. First, detection and identification of the odor occur via the peripheral olfactory system. Second, odor discrimination occurs, and third, odor cognition occurs via the central olfactory system. As the functional symptoms of AD are primarily related to the brain, studies of abnormal olfaction have pointed towards the dysfunction of the brain. Studies on the peripheral

pathology have been overlooked, and we are the first to thoroughly illustrate the relationship between disturbances of OSNs and AD hallmarks. Clinically patients with AD with olfactory dysfunction have been reported to have an atypical dysfunctional phenotype. They are not able to sense particular odors but are not completely anosmic. They recognize the presence of odor; however, this phenomenon does not mean that they can detect all odorant information correctly. In terms of the first step in the processing of odor information, a study of OSNs of the peripheral olfactory system is required to clarify mechanisms involved in hyposmia.

Odors could be divided into at least two groups according to the behavior and physiological response in this paper. One odor group was found to activate endoturbinate- OSNs targeting the dorsal glomeruli, and the other group activated ectoturbinate-OSNs targeting the ventral glomeruli. Considering the "zone organization" theory (*i.e.,* topographical axis), which suggests an important role for the projection from the OE to OB, it can be hypothesized that partial damage in the OE caused by AD may lead to differences in odor-specific responses. To better understand these mechanisms, we aimed to uncover the "region" involved by using various physiological analyses. It is thought that odor identity is determined by a combination of odorant receptors activated by an odorant. Activity maps are presented by each odorants' input, and the spatial patterns of input activity are created for glomeruli. Despite the OB receiving complex odor information, humans and other animals can identify a specific odorant owing to spatial patterns across

glomeruli. We attempted to quantify the relationship between the odor map by kinetics and the local information of the AD pathology of the glomerular layer in the olfactory system. The measurement applied to the degree of glomeruli suggests advanced topographical analysis in the peripheral olfactory system. This digitized measurement enables us to compare among various factors from anatomy to physiology and to confirm a correlation based on the virtual region-coordination. Our results show that odor grouping according to the odor map information (Fig. 2c), was consistent with odor grouping, in the behavioral study (Fig. 1e). Only odors from group B showed a larger difference in kinetics of 5xFAD than in the WT mice. Interestingly, the olfactory behavior corresponded with the level of calcium kinetics (Fig. 1e, Table 2). The results revealed a strong correlation between the partial behavioral defect and a pattern of low calcium kinetics. Additionally, the regional characteristics of the olfactory system in AD are associated with a topographical organization formed by the regeneration of OSNs. Further investigation on mapping OSNs-activity by various odorants needs to be conducted in the future to permit clearer visualization and quantification of global glomerular patterns. Although we focused only on the glomerular layer, the odor map data contains all the responses from the entire OB between WT/5xFAD mice. Thus, these methods can be easily applied to AD diagnosis by evaluating the patterns in distinct OB layers and correlating them with the glomerular patterns.

We identified the accumulation pattern of Aβ oligomers to define the relationship between abnormal behavior and AD pathology. Previous studies using transgenic mice suggested that both AD brain-derived and synthetically prepared Aβ oligomers could influence the neuronal network. The results imply that an increased threshold caused by Aβ oligomers may alter the behavioral and physiological thresholds for the detection of certain groups of odors, although more studies using various stimuli are necessary. Furthermore, Aβ could induce early synaptic toxicity (*30, 31*), long-term potentiation (LTP) deficits (*12*), and/or trigger cellular toxicity by involving tau phosphorylation and neurofibrillary tangles (*32*). Moreover, we previously pointed out that Aβ oligomer toxicity in the OE may induce direct impairment of the olfactory system in early AD as OSNs express an APP-cleavage enzyme and can generate Aβ autonomously (*11, 33*). Besides, oligomers are formed early in Aβ accumulation and can be harmful to the neural function and structure of olfaction in this paper. In addition to the widely-known pathological effect of Aβ, recent studies have noted an interesting feature of Aβ. Aβ species are suggested as being pathological seeds and a spreading process of deteriorating proteinopathy in neurodegenerative disease (*34*). Indeed, a protein pathology like α-synuclein could be associated with the toxic aggregation of proteins by being associated with endogenous Aβ expression in 5xFAD mice (*35*), an α-synuclein measured together with Aβ expression in the olfactory epithelium of human APP-overexpressing transgenic mice (N5 TgCRND8) (*36*). Hence, Aβ present in OSNs not only can generate and accumulate misfolding protein itself but also is enough to establish

systemic vulnerability in the early stage of AD. AD is a human disease, and extensive AD pathology has been shown in the human olfactory system. Not only amyloid pathology but also hyperphosphorylated tau (HP-τ) is present in the early and late stages of AD patients, and α-synuclein pathology may be seen in the OB. According to a review article by Attems *et al.* dealing with neuropathological findings in the OB (*37*), HP-τ and α-synuclein could be co-locally detected (*38*), and HP-τ pathology could be observed in the early stages of AD with low neuritic Braak stages before Aβ plaque occurrence. This suggests that cellular loss by HP-τ pathology may cause olfactory dysfunction in the early stages of AD (*39*). They reported Aβ deposits identified from pathologically verified AD patients in the late *Braak* stage, and they reported that Aβ deposits were higher than paired helical filament tau aggregates in AD patients' OE (*40*). In accordance with the aforementioned amyloid pathology, Aβ expression can seed subsequent pathological vulnerabilities such as promoting cellular damage by HP-τ, α-synuclein, or oxidative stress (*34*). Given those reports, our finding of the OSNs' pathology can be the last stage of Aβ pathogenesis inducing the synaptic inactivity and cellular loss by HP-τ and α-synuclein pathology rather than amyloid pathology alone. Moreover, clarifying whether other proteinopathies can exhibit region specific deposits in OSNs is a promising area for further study.

We confirmed the relationship between oligomerized Aβ proteins and odor dysfunction using 5xFAD mice. We determined the synaptic activity of our target glomeruli and confirmed the direct toxicity of Aβ. Sensory deprivation between OSNs and mitral cells induces decreasing TH expression. As dopaminergic

periglomerular neurons are maturated by the excitation of glutamatergic peripheral OSNs (*41*), the periglomerular neurons express TH and modulate the synaptic transmission of excitatory neurons (*42*). The maturated dopaminergic cells expressing TH secrete GABA in OSN axon terminals upon OSN stimulation, and which contributes to presynaptic inhibition (*41*). Given the physiological cascade, TH-immunoreactivity has been considered as a biochemical marker of OSNs activity (*11, 12, 43, 44*). In the current study, a significant loss of TH-positive neurons was observed in the ventral OB of 5xFAD mice. This indicates double-confirmed data of Ca^{2+} activity representing OSN-derived input signals. Most strikingly, damaged regions were found in the ventral region, our focused region, which matched well with the diminished amounts of OMP, mature olfactory sensory receptor neurons (*45*). This was also confirmed by the results of our TUNEL analyses and the reduced proliferation rate within this region. It is well known that a reduction in neurogenesis is induced by oligomerized Aβ proteins, but this is the first report showing that this event also occurs in the peripheral olfactory system.

Regarding the spatially different distributions of Aβ and partial olfactory dysfunction, we showed structural and functional deficits in the domain where OSNs regenerate greatly. The OE has topographical zones which have a distinct characteristic during their regeneration from both the external environment and intrinsic molecular mechanisms (*46, 47*). Given the cellular physiology in our results, this phenomenon was intrinsically faster in the ectoturbinate than in the endoturbinate (Fig. S6). Moreover, OSNs in the dorsal domain were maintained and

conserved neuronal turnover. However, the ventral domain showed higher plasticity in the normal state and deficits upon Aβ accumulation, suggesting the ventral domain has vulnerabilities such as Aβ pathogenesis. Since the OE maintains the number of OSNs by continuous proliferation and differentiation of basal cells, a reduction of this reconstitution may be a direct cause of the reduction in the number of OSNs. We can infer that the region could be the crossing point between regeneration and degeneration because APP and its cleavage enzyme, secretases give rise to not only Aβ generation but also neural development and axon guidance related to the synaptic formation and neural reconstitution (*48, 49*). Taken together, our result establishes that the ventral region may provide the pathogenic pool and initiate a vicious cycle of AD pathogenesis derived from Aβ, such as hyper inflammation as well as HP-τ and α-synuclein pathology.

4.2. Limitations

The main objective was to identify hyposmia accompanying in the early phase of AD using the 5xFAD mouse. This mouse line has a limitation in reflecting the complete human symptoms of AD. Nevertheless, the experiment using 5xFAD can recapitulate Aβ expression and accumulation in the neuron system, leading causes in AD. Furthermore, the experimental design was specifically employed to capture the pathological Aβ effect on the olfactory dysfunction, one of the cardinal AD symptoms. We have chosen the mouse model by rational hypothesis (Fig S1), but we also clarify the limitations in this selection.

We delved deeper into the pathophysiologic and anatomic effects in the peripheral olfactory sensory neurons by Aβ. The 5xFAD begins to exhibit a decline in cognition, neuronal loss, and changes in LTP/LTD in four to six months of age. Although the 5xFAD is a conventional transgenic line that has not been specifically mutated in the olfactory sensory neuron, our data showed a neuronal and functional loss in three-month-old mice. Also, we tested that the CNS-derived effects were excluded from the olfactory function, and therefore, we hypothesized that the stage mimics the early stage of AD. However, the study design that was hypothesized the early stages of AD progression should not be overlooked when interpreting the results because the early stage of AD may be relative and not always feasible for manifestation.

To test directly the function of olfactory sensory neuron, electroolfactogram (EOG) recording is one of the most reliable approaches to analyze the physiological functions of the olfactory sensory neurons. Instead, we chose calcium imaging in the glomerulus where axons of OSNs and dendrites of central olfactory neurons form synapses. Although we could not directly show the responses of OSNs in the OE, the results from the calcium imaging in the glomerulus may reflect the responses of OSNs. Therefore, it would be considered the EOG study whether the ecto-region responses in the OE are reduced or not upon specific odorants as a further study using more scents in addition to the scents used in this study.

Seven odorants were tested in the experiment based on the preference test in the previous research. Regarding the limited numbers of odorants, it could be argued

that these odorants cannot fully create categories for future therapeutic applications such as diagnosis and clinical trials. Hence, further experiments should classify odor types for AD-associated olfactory dysfunction.

The number of subjects can be a limitation of the behavioral tests for our current study, even though we consider the clear statistical significance and a small standard error of the mean. Therefore, an optimization and detailed set of conditions may be required, including an increase in the number of subjects to move on to the application as a clinical diagnosis.

5. Conclusion

The present study characterized hyposmia in 5xFAD mice. We found that the olfactory abnormality in 5xFAD mice was determined by the relationship between Aβ oligomers and the regions of the nervous system that are responsible for odor detection. We have also shown, through advanced topographical analysis, that the specific patterns of Aβ oligomer accumulation can attenuate the activity in our target synapses. We confirmed a negative correlation between aggregated Aβ and both OSN-derived Ca^{2+} signals and corrupted structural stability. Moreover, these effects were identified by focusing on the spatially ecto/ventral halves formed by OSNs turnover, representing a feature of the peripheral olfactory system. Thus, the collapse of the peripheral system could be the greatest feature of AD-related olfactory abnormalities.

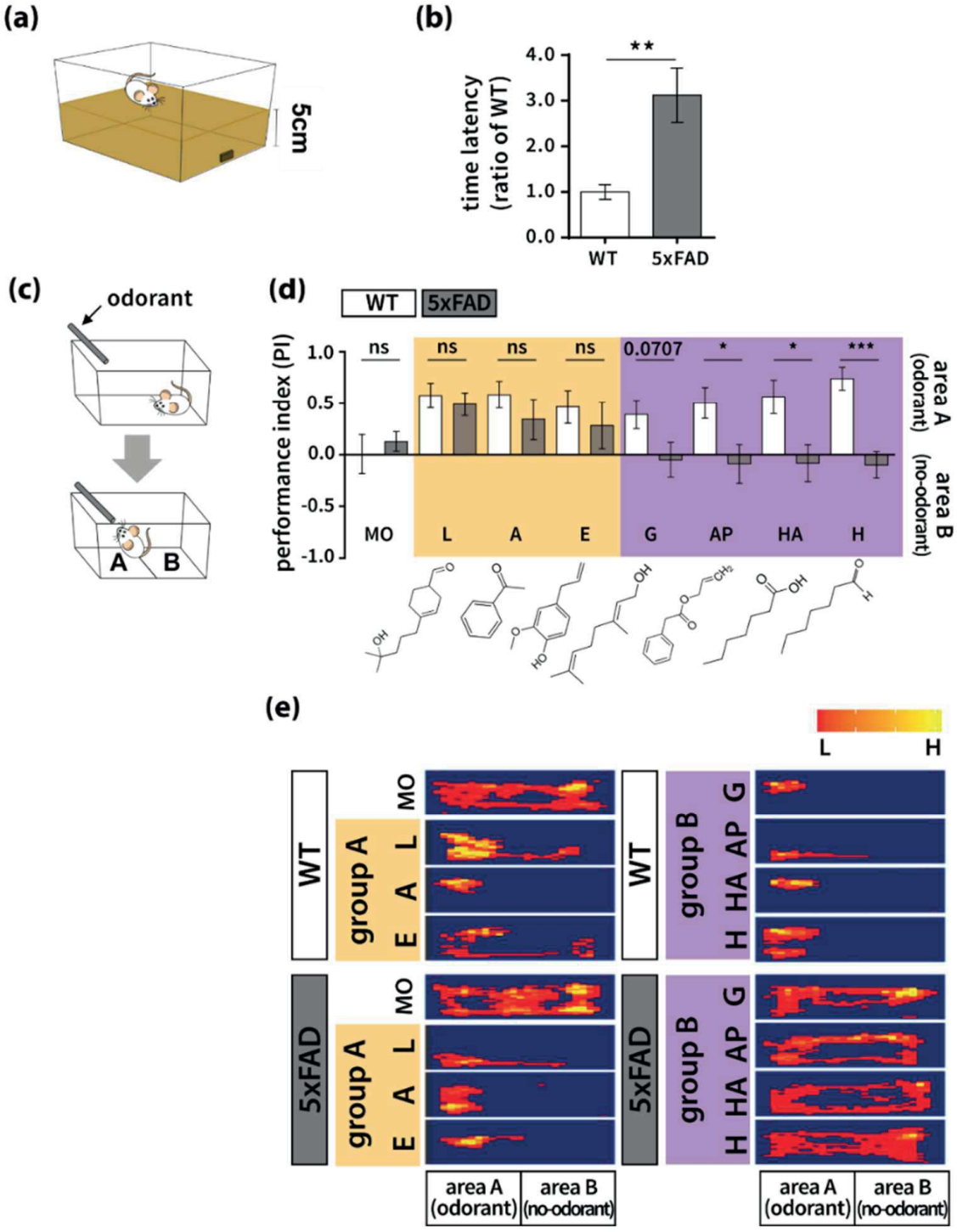
(a)
5cm
(b)
time latency (ratio of WT)
4.0
3.0
2.0
1.0
0.0
**
WT
5xFAD
(c)
odorant
A
B
(d)
WT
5xFAD
performance index (PI)
1.0
0.5
0.0
-0.5
-1.0
ns
ns
ns
ns
0.0707
*
*
***
MO
L
A
E
G
AP
HA
H
area A (odorant)
area B (no-odorant)
(e)
L
H
WT
group A
group B
5xFAD
MO
L
A
E
G
AP
HA
H
area A (odorant)
area B (no-odorant)

Figure 1. Atypical, AD-like olfactory behavior in 5xFAD transgenic mice.

Experimental subjects are three-month WT or 5xFAD mice unless otherwise noted. (a–b) Food seeking test (WT, n = 6; 5xFAD, n = 6). (a) Scheme illustration. (b) The latency was measured as mean ± SEM. For statistical analysis, an unpaired t-test was performed. (c–e) Odor detection test was performed (WT, n = 6; 5xFAD, n = 6). (c) Scheme illustration. For PI analysis, areas A and B were defined to distinguish the location of the experimental odorant in the cage. (d) The PI value is represented as mean ± SEM. The experimental odorants refer to lyral [L], eugenol [E], acetophenone [A], geraniol [G], ally phenylacetate [AP], heptanoic acid [HA], and heptanal [H]. For statistical analysis, an unpaired t-test was performed. (e) Representative heat map showing duration (H; high, L; low). Statistical significances are denoted as follows: ns, non-significant; *P < 0.05, **P < 0.01, ***P < 0.001). Wild-type (WT), five familial AD mutations (5xFAD), Alzheimer's disease (AD).

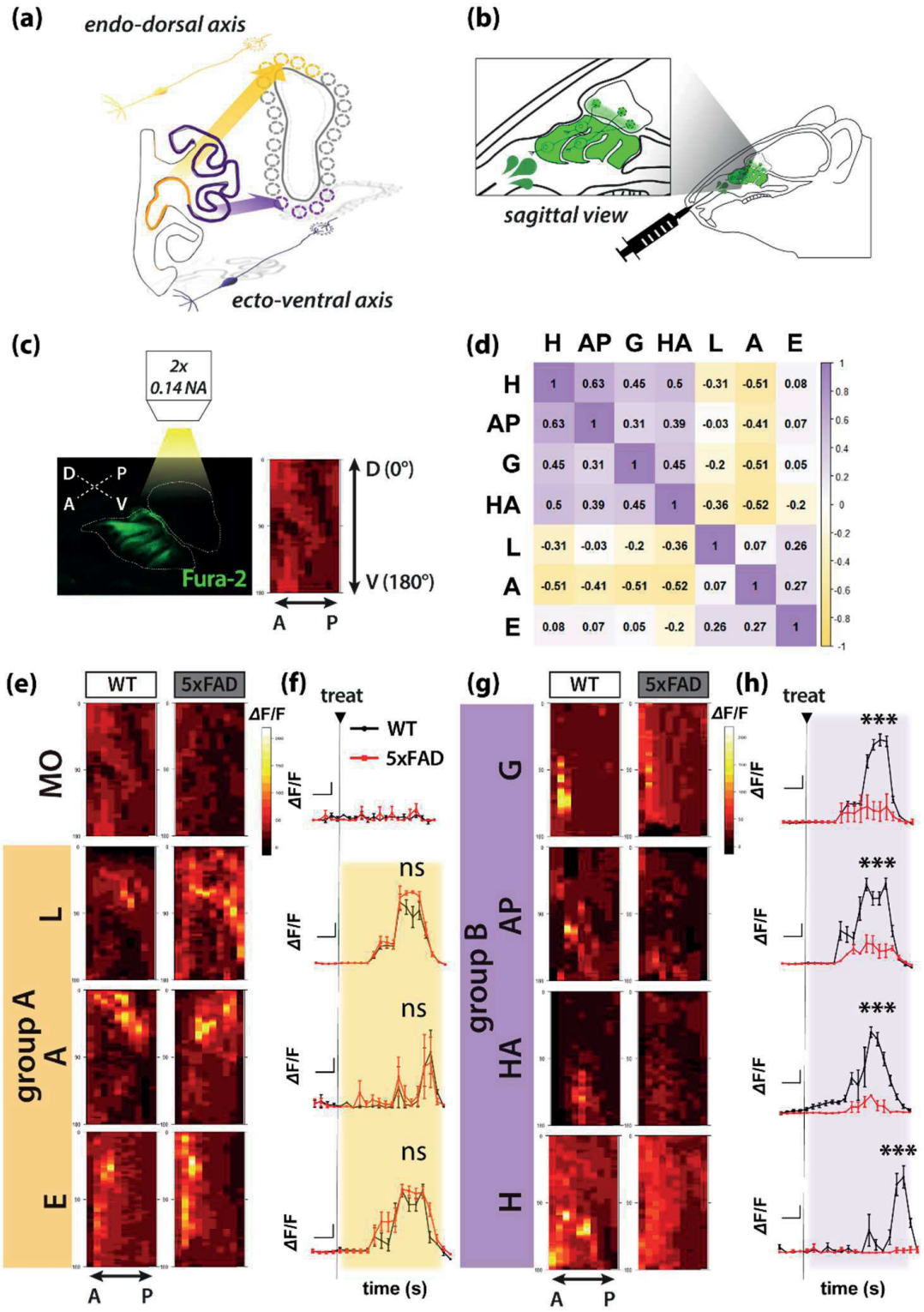
(a)
endo-dorsal axis
ecto-ventral axis
(b)
sagittal view
(c)
2x
0.14 NA
D
P
A
V
Fura-2
D (0°)
V (180°)
A
P
(d)
H AP G HA L A E
H 1 0.63 0.45 0.5 -0.31 -0.51 0.08
AP 0.63 1 0.31 0.39 -0.03 -0.41 0.07
G 0.45 0.31 1 0.45 -0.2 -0.51 0.05
HA 0.5 0.39 0.45 1 -0.36 -0.52 -0.2
L -0.31 -0.03 -0.2 -0.36 1 0.07 0.26
A -0.51 -0.41 -0.51 -0.52 0.07 1 0.27
E 0.08 0.07 0.05 -0.2 0.26 0.27 1
1 0.8 0.6 0.4 0.2 0 -0.2 -0.4 -0.6 -0.8 -1
(e)
WT
5xFAD
MO
group A
L
A
E
ΔF/F
A
P
(f)
treat
WT
5xFAD
ΔF/F
ns
ns
ns
time (s)
(g)
WT
5xFAD
group B
G
AP
HA
H
ΔF/F
A
P
(h)
treat
***
***
***
***
ΔF/F
time (s)

Figure 2. Odor-derived Ca2+ signal in peripheral olfactory glomeruli is divided into two groups.

(a) Illustration of the topographical axis. (b) Illustration of wide-field fluorescence imaging to measure OSNs-derived input signal. (c) The imaging location with high-resolution stereoscopic fluorescence image of fura-2 by OSNs calcium concentration (left) and averaged activity sample map along histologic angle (D; dorsal, V; ventral, A; anterior, P; posterior) (right). (d) Heat map clustering showing the Spearman's correlation coefficient between each active calcium signal pattern with the angle of glomeruli located. (WT, n = 5–6). Each odorant was divided into two groups; lyral [L], acetophenone [A], and eugenol [E] (group A), and geraniol [G], allyl phenylacetate [AP], heptanoic acid [HA], and heptanal [H] (group B). (e, g) The merged intensity (cumulated signal) (f, h) of olfactory synaptic activity ($\Delta F/F$) induced by each group odorant (WT, n = 5–6; 5xFAD, n = 5–6). (e–f) Odor-group A. (g–h) Odor-group B. $\Delta F/F$ represented as mean ± SEM from five independent experiments. For statistical analysis, an unpaired t-test was performed using Prism software (GraphPad software). Statistical significances are noted (***P < 0.001). Olfactory sensory neurons (OSNs), wild-type (WT), five familial AD mutations (5xFAD), Alzheimer's disease (AD).

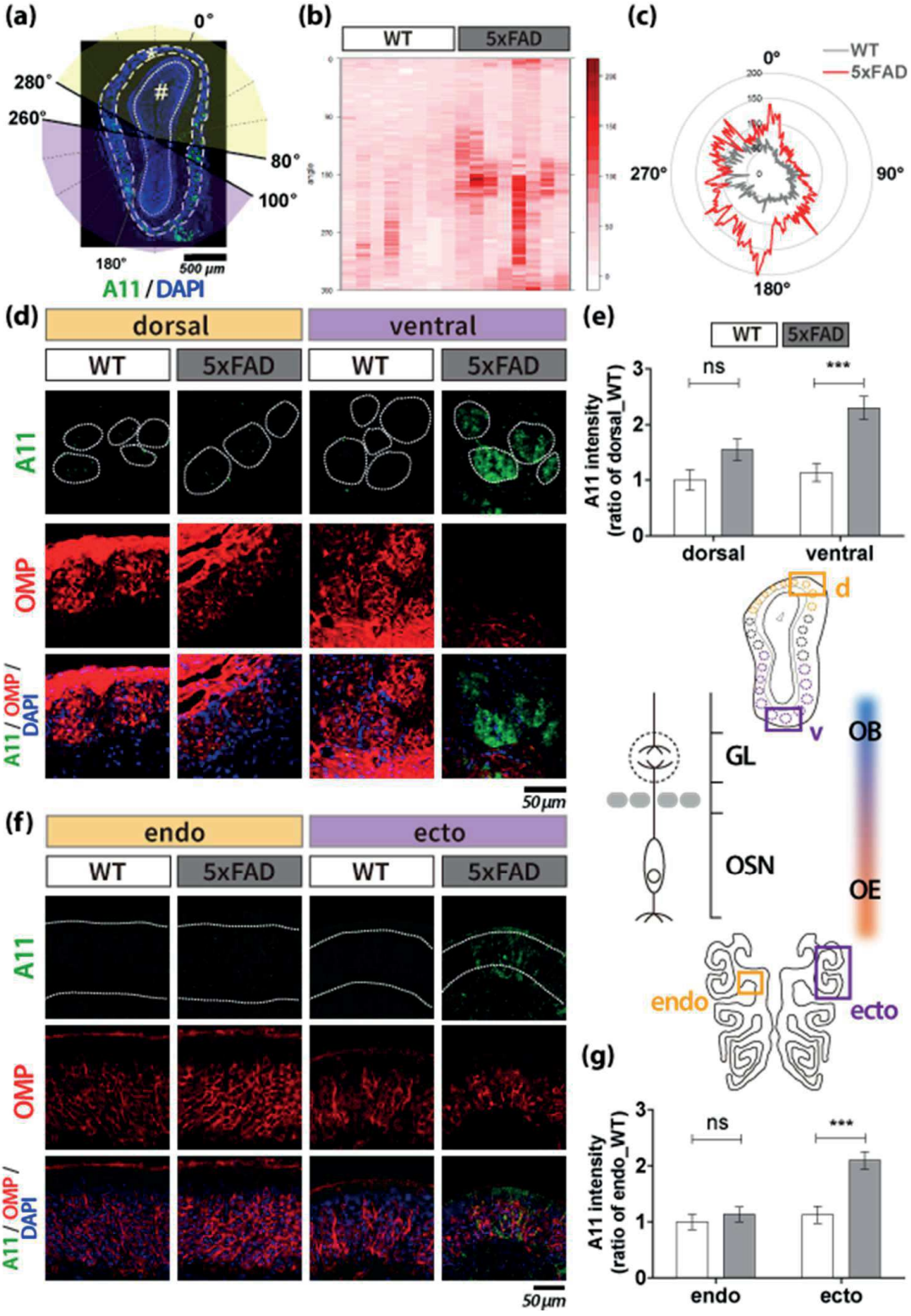
(a)
0°
280°
260°
80°
100°
180°
500 µm
A11 / DAPI
(b)
WT
5xFAD
(c)
0°
WT
5xFAD
270°
90°
180°
(d)
dorsal
ventral
WT
5xFAD
WT
5xFAD
A11
OMP
A11 / OMP / DAPI
50 µm
(e)
WT
5xFAD
ns
***
A11 intensity (ratio of dorsal_WT)
dorsal
ventral
d
v
OB
GL
OSN
OE
endo
ecto
(f)
endo
ecto
WT
5xFAD
WT
5xFAD
A11
OMP
A11 / OMP / DAPI
50 µm
(g)
ns
***
A11 intensity (ratio of endo_WT)
endo
ecto

Figure 3. Aβ oligomer accumulation in the ecto/ventral halves of the peripheral olfactory system of 5xFAD mice.

(a) Illustration of criteria to indicate the relative angular position of olfactory synapses. (b) Representative A11-positive ROI heatmap in WT (left) and 5xFAD (right) mice. (c) The radial chart represents A11-positive ROI along the angle of olfactory synapses. (d-e) A11 immunoreactivity was determined in the olfactory glomeruli of WT versus 5xFAD mice (WT, n = 7; 5xFAD, n = 9). (d) The local intensity of A11 (+) (green), OMP (+) (red), and DAPI (blue). (e) A11 immunoreactivity in the glomerulus (top) and topographical illustration (bottom). (f–g) A11 immunoreactivity was determined in the OSNs-layers of WT versus 5xFAD mice (WT, n = 7; 5xFAD, n = 9). (f) The local intensity of A11 (+), OMP (+), and DAPI (blue). (g) A11 immunoreactivity in OSNs-layers (top) and topographical illustration (bottom). All data are presented as mean ± SEM from three independent experiments. For statistical analysis, a two-way ANOVA was performed, followed by the Bonferroni post hoc test. Statistical significances are noted (ns, non-significant; ***P < 0.001). Olfactory marker protein (OMP), Olfactory sensory neurons (OSNs), wild-type (WT), five familial AD mutations (5xFAD), Alzheimer's disease (AD).

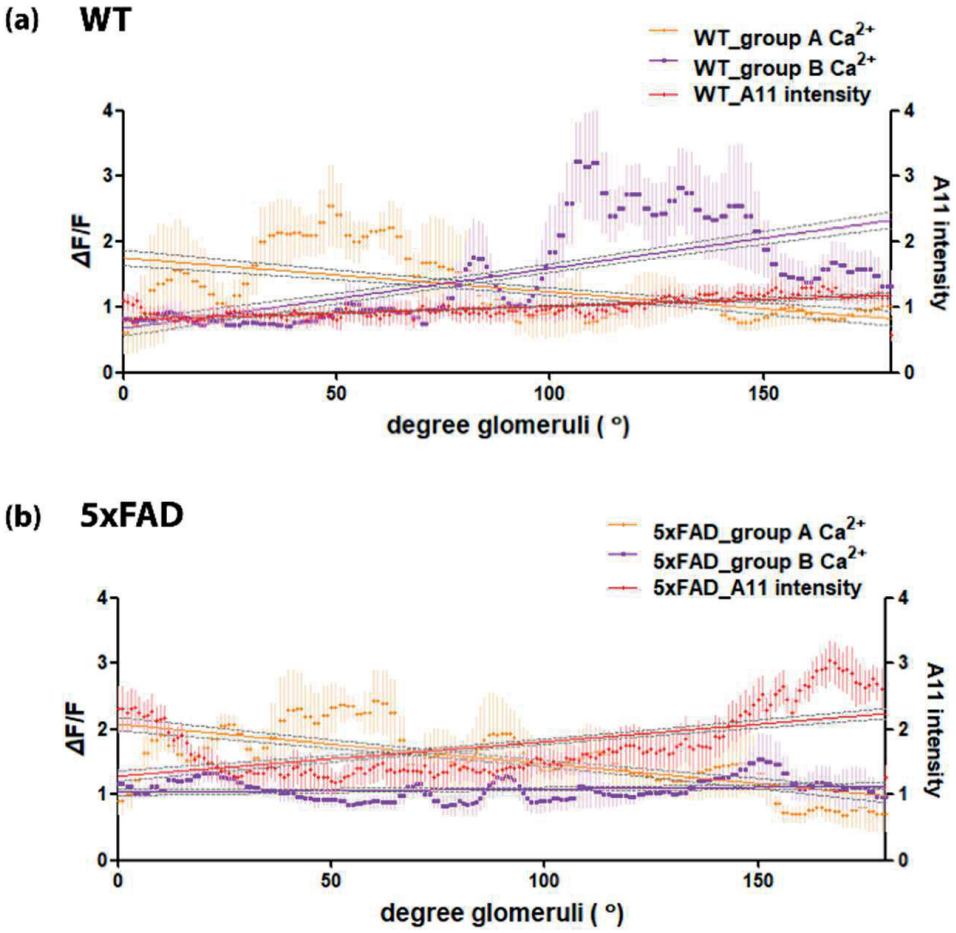

Figure 4. Increased A11 immunoreactivity and decreased odor Ca2+ activity in the ventral glomeruli of 5xFAD.

(a–b) Scatter plots with Spearman's correlations among the degree of glomeruli (°), A11 immunoreactivity (intensity), and odor Ca2+ activity in the olfactory glomeruli in WT (a) compared with 5xFAD (b) mice. Scatter diagrams displaying correlations between each variation, linear regression analysis with 95% confidence intervals was used (gray dashed line). Dot and line showing odor Ca2+ activity indicated in orange (group A) and purple (group B), and A11 immunoreactivity data indicated in red dots and line. Wild-type (WT), five familial AD mutations (5xFAD), Alzheimer's disease (AD).

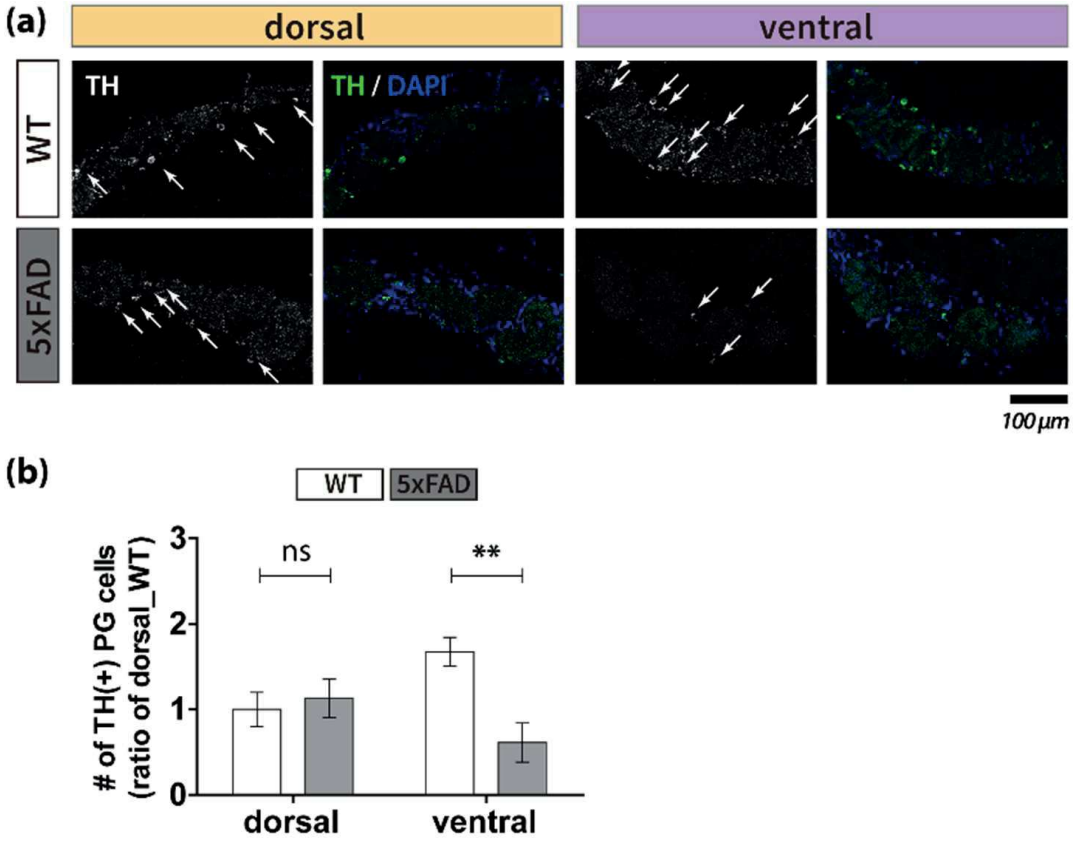

Figure 5. Reduction of TH expression in the ventral olfactory periglomerular cells of 5xFAD mice.

(a–b) TH (+) (green) PG cells were identified in the olfactory glomeruli of WT versus 5xFAD mice (WT, n = 4; 5xFAD, n = 3). (a) The local intensity of TH (+) PG cells. (b) Quantitative analysis of TH (+) PG cells/5 GL cells. Data are represented as means ± SEMs from three independent experiments. For statistical analysis, a two-way ANOVA was performed, followed by the Bonferroni post hoc test. Statistical significances are denoted (ns, non-significant; **P < 0.01). Wild-type (WT), five familial AD mutations (5xFAD), Alzheimer's disease (AD).

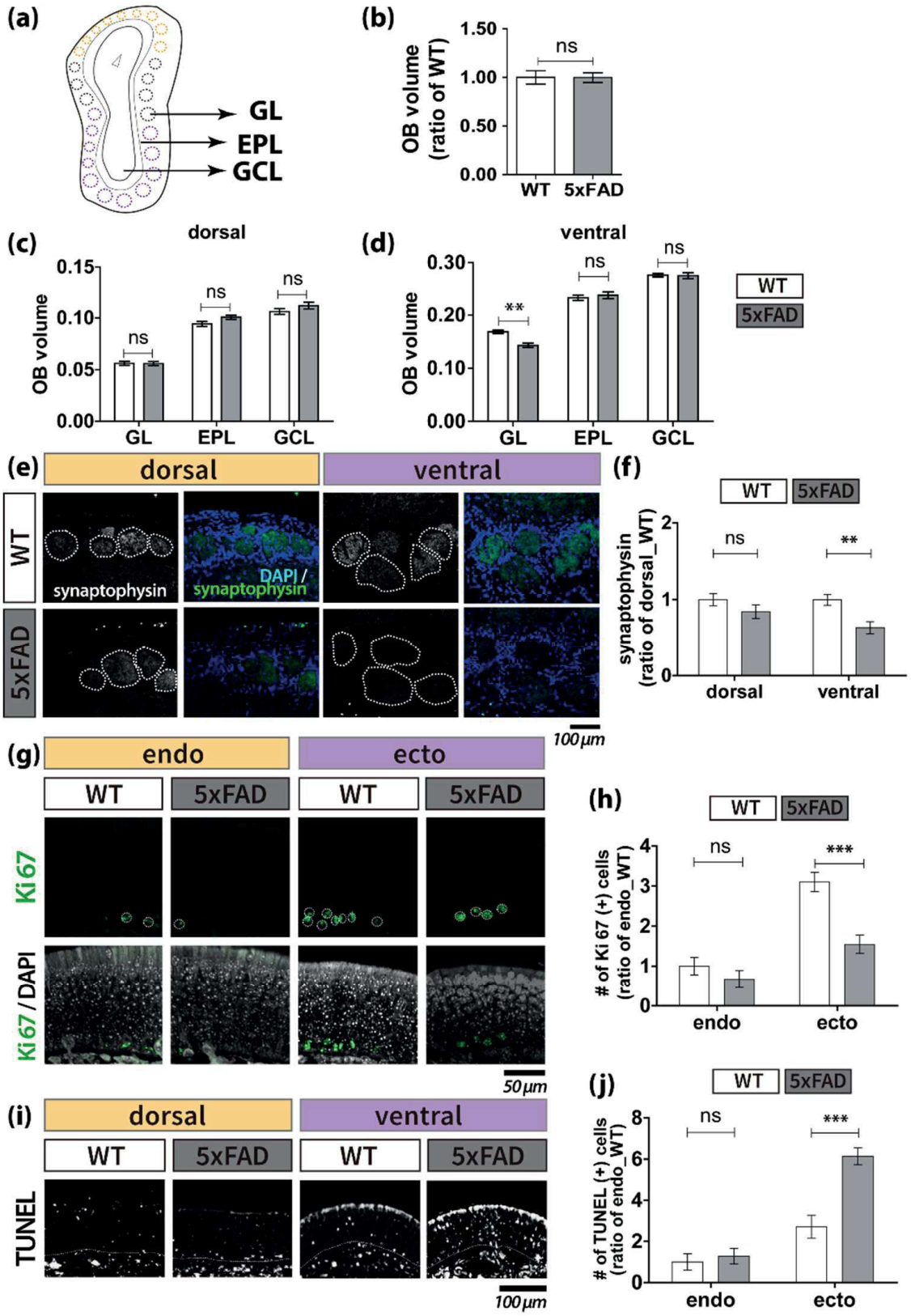
(a)
GL
EPL
GCL
(b)
OB volume (ratio of WT)
1.50
1.00
0.50
0.00
ns
WT
5xFAD
(c)
dorsal
OB volume
0.15
0.10
0.05
0.00
ns
ns
ns
GL
EPL
GCL
(d)
ventral
OB volume
0.30
0.20
0.10
0.00
**
ns
ns
GL
EPL
GCL
WT
5xFAD
(e)
dorsal
ventral
WT
5xFAD
synaptophysin
DAPI / synaptophysin
100 µm
(f)
WT
5xFAD
synaptophysin (ratio of dorsal_WT)
2
1
0
ns
**
dorsal
ventral
(g)
endo
ecto
WT
5xFAD
WT
5xFAD
Ki 67
Ki 67 / DAPI
50 µm
(h)
WT
5xFAD
# of Ki 67 (+) cells (ratio of endo_WT)
4
3
2
1
0
ns
***
endo
ecto
(i)
dorsal
ventral
WT
5xFAD
WT
5xFAD
TUNEL
100 µm
(j)
WT
5xFAD
# of TUNEL (+) cells (ratio of endo_WT)
8
6
4
2
0
ns
***
endo
ecto

Figure 6. Disrupted OSNs structure in the ecto/ventral region of the peripheral olfactory system.

(a–d) Analysis of the volume of the olfactory glomerular layer (WT, n = 3; 5xFAD, n = 3). (a) Depiction of coronal sections of the olfactory bulb with laminar structure. glomerular layer (GL), external plexiform layer (EPL), granule cell layer (GCL). (b) Total OB volume. GL, EPL, and GCL volume was measured in the dorsal olfactory synapses (c) and ventral olfactory synapses (d). (e–f) Synaptophysin (+) (green) glomeruli in WT versus 5xFAD mice (WT, n = 4; 5xFAD, n = 3). (e) The local immunoreactivity of synaptophysin (+) glomeruli. (f) Synaptophysin immunoreactivity. (g) Representative Ki67 (+) data in the local OSNs layer (WT, n = 3; 5xFAD, n = 3). (h) Quantitative analysis of Ki67 (+) cells. (i) Representative TUNEL-positive data in local OSNs layers and (j) comparative quantification (WT, n = 3; 5xFAD, n = 3). Data are represented as mean ± SEM from three independent experiments. For statistical analysis, a two-way ANOVA was performed, followed by the Bonferroni post hoc test. Statistical significances are noted (ns, non-significant; **P < 0.01, ***P < 0.001). Olfactory sensory neurons (OSNs), wild-type (WT), five familial AD mutations (5xFAD).

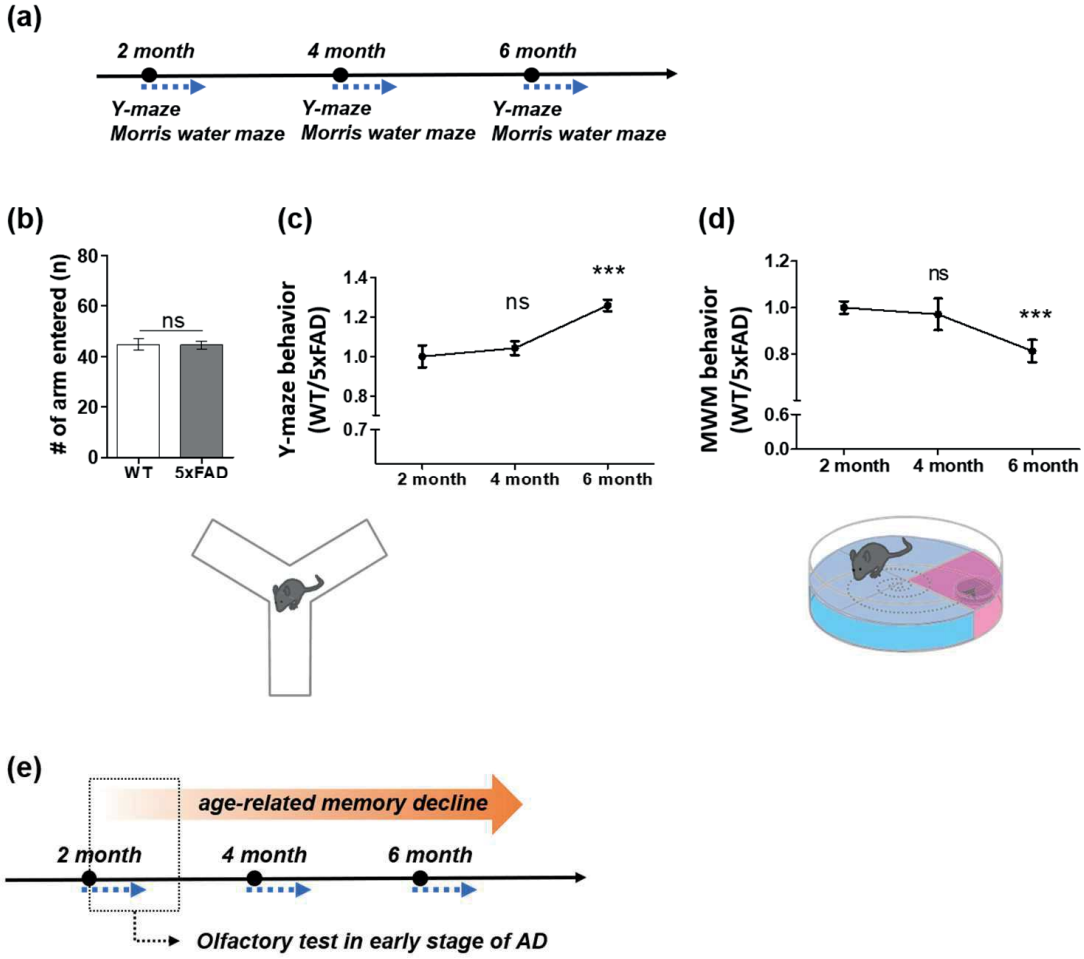
(a)
2 month
4 month
6 month
Y-maze
Morris water maze
Y-maze
Morris water maze
Y-maze
Morris water maze
(b)
# of arm entered (n)
80
60
40
20
0
ns
WT
5xFAD
(c)
Y-maze behavior
(WT/5xFAD)
1.4
1.2
1.0
0.8
0.7
ns
***
2 month
4 month
6 month
(d)
MWM behavior
(WT/5xFAD)
1.2
1.0
0.8
0.6
0.0
ns
***
2 month
4 month
6 month
(e)
age-related memory decline
2 month
4 month
6 month
Olfactory test in early stage of AD

Figure S1. Verification of early-stage AD phenotype in 5xFAD transgenic mice.

(a) Illustration of the time course for Y-maze and Morris water maze test. (b) Basic mobility tests using Y-maze showed the total number of arm entries (WT, n = 23; 5xFAD, n = 16). (c–d) Spontaneous alternation test using the Y-maze and Morris water maze test was performed to evaluate working memory (two-month: WT, n = 23; 5xFAD, n = 16, four-month: WT, n = 6; 5xFAD, n = 6, six-month: WT, n = 10; 5xFAD, n = 10). (c) A spontaneous alternation test using Y-maze was performed and the number of entries to another arm was measured (top). Scheme illustration (bottom). (d) The Morris water maze task was performed and the ratio of escape latency (WT/5xFAD) was measured (top). Scheme illustration (bottom). (e) Illustration of experimental timepoints identified in this research based on the result interpretation. One-way ANOVA was performed for statistical analysis. All data presented as mean ± SEMs. Statistical significances are noted [ns, non-significant; ***P < 0.001]. Alzheimer's disease (AD), wild-type (WT), five familial AD mutations (5xFAD).

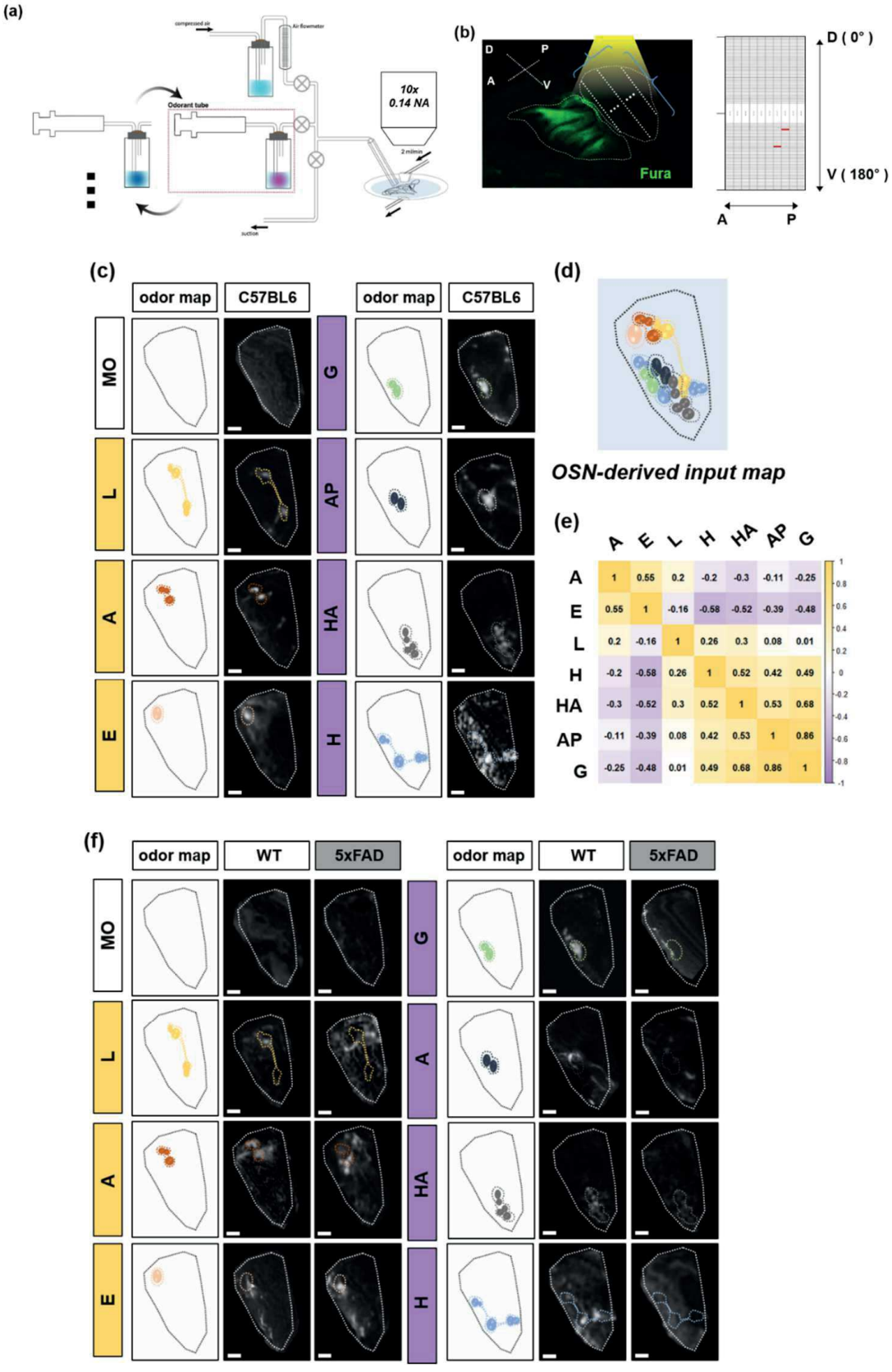
(a)
Odorant tube
10x
0.14 NA
(b)
D
P
A
V
Fura
D (0°)
V (180°)
A
P
(c)
odor map
C57BL6
odor map
C57BL6
MO
L
A
E
G
AP
HA
H
(d)
OSN-derived input map
(e)
A E L H HA AP G
A 1 0.55 0.2 -0.2 -0.3 -0.11 -0.25
E 0.55 1 -0.16 -0.58 -0.52 -0.39 -0.48
L 0.2 -0.16 1 0.26 0.3 0.08 0.01
H -0.2 -0.58 0.26 1 0.52 0.42 0.49
HA -0.3 -0.52 0.3 0.52 1 0.53 0.68
AP -0.11 -0.39 0.08 0.42 0.53 1 0.86
G -0.25 -0.48 0.01 0.49 0.68 0.86 1
1
0.8
0.6
0.4
0.2
0
-0.2
-0.4
-0.6
-0.8
-1
(f)
odor map
WT
5xFAD
odor map
WT
5xFAD
MO
L
A
E
G
A
HA
H

Figure S2. Clustering based on spatial information of the activity maps and signal size in olfactory synapses.

(a) A schematic diagram of the olfactometer. Compressed air was used as the carrier gas. olfactometer delivered mixed air and saturated with odorant vapor in the odor applicator. The flow rates of the air and the odorant vapor were controlled by a flow meter and a syringe pump, respectively. Turning-off of the suction to the outer barrel releases odorant from the end of the applicator. (b) In order to confirm the correlation with the IHC results to be followed, we analyzed the (*ΔF/F0*) change across the whole OB. The entire analysis area of OB is divided equally among 10 sections from the anterior to posterior and 180 section from dorsal to ventral within a lateral olfactory bulb view, respectively. (c–e) The spatial information of a widely used inbred strain of mouse (C57BL/6). (c) Illustration of OSNs-derived input signal map based on calcium activity of individual odorants. (d) Clustering based on the spatial correlation between each calcium activity pattern with angle glomeruli located in Fig. 2. (e) Each odorant was divided into two groups; lyral [L], acetophenone [A], and eugenol [E] (group A); geraniol [G], allyl phenylacetate [AP], heptanoic acid [HA], and heptanal [H] (group B). (f) Representative spatial information from WT and 5xFAD mice. Olfactory sensory neurons (OSNs), wild-type (WT), five familial AD mutations (5xFAD).

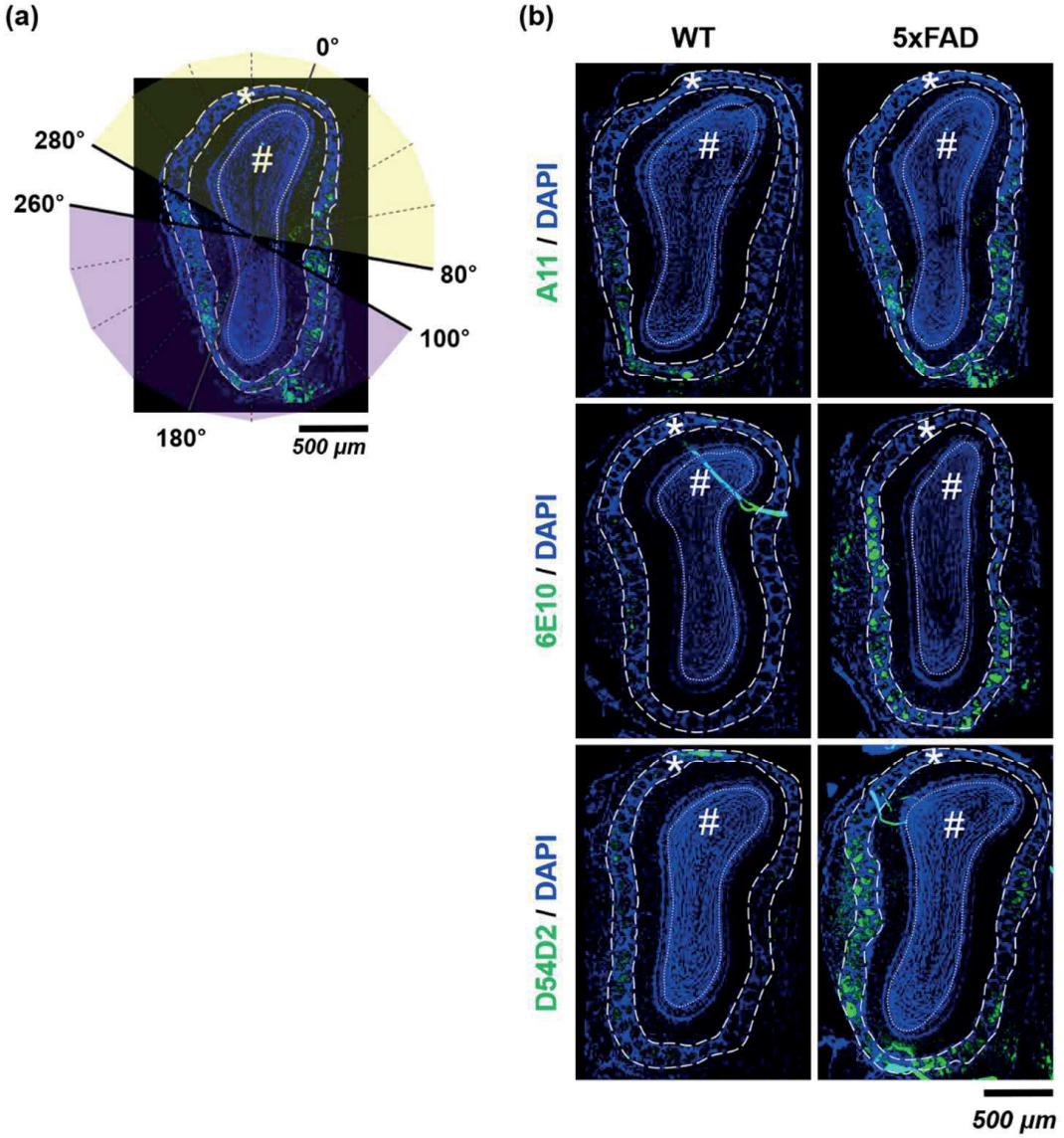

Figure S3. The immunoreactivity of Aβ isoforms in the coronal section of the olfactory bulb.

(a) Illustration of criteria to indicate the relative angular position of olfactory synapses. (b) The immunoreactivity of Aβ isoforms in the coronal section of the olfactory bulb (green); (Top) anti-A11 (oligomeric), (Middle) anti-6E10 (Aβ1-16), (Bottom) anti-D54D2 (Aβ1-40, Aβ1-42), and DAPI (blue). Asterisk (*): glomerular layer, Hash (#): granule cell layer. Scale bar: 500 μm. Wild-type (WT), five familial AD mutations (5xFAD).

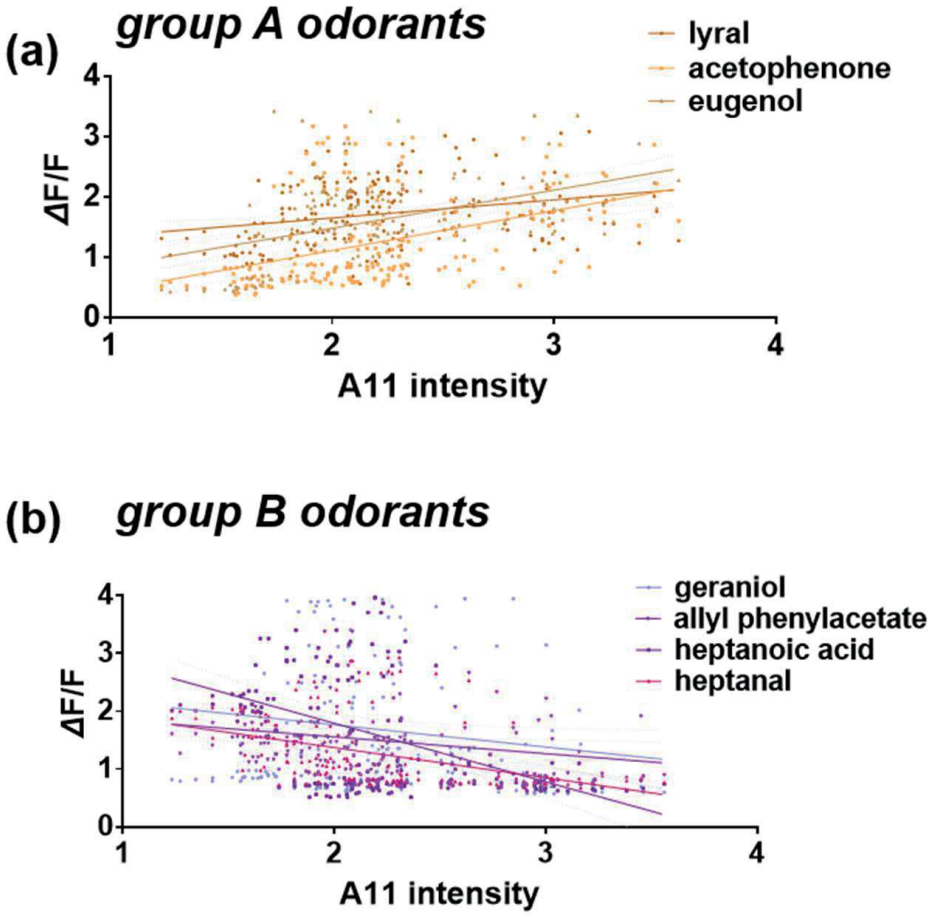

Figure S4. The angle-matched spatial correlation between A11 level in 5xFAD and calcium activity in WT.

Scatter diagrams displaying correlations between each variable and linear regression analysis with 95% confidence intervals were used (gray dashed line). (a) Correlation with lyral, acetophenone, and eugenol. (b) Correlation with geraniol, allyl phenylacetate, heptanoic acid, and heptanal. Wild-type (WT), five familial AD mutations (5xFAD), Alzheimer's disease (AD).

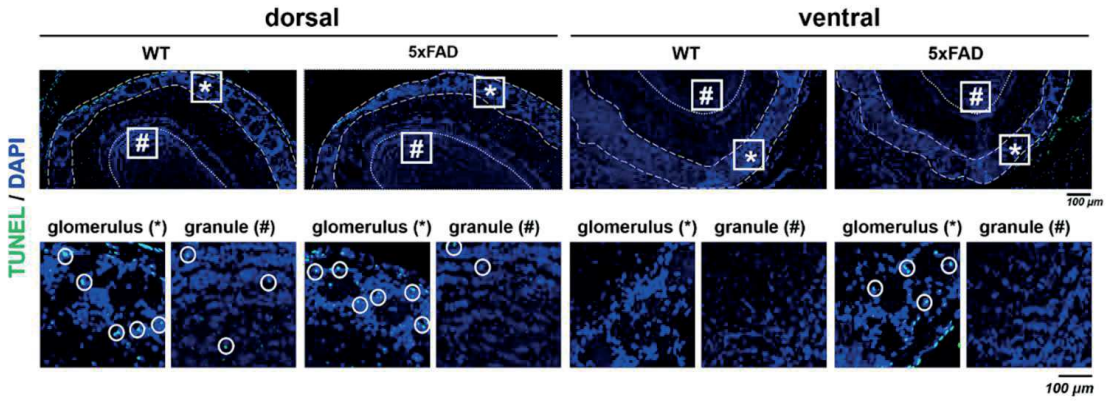

Figure S5. Cell death of the OB. The TUNEL-positive signal in the coronal section of olfactory bulb (green).

(Top) Domain section image, (bottom) magnified cropped image from upper domain section image, and DAPI (blue). Asterisk (*): glomerular layer, Hash (#): granule cell layer, circle (O): TUNEL positive cell. Scale bar: 100 μm. Wild-type (WT), five familial AD mutations (5xFAD).

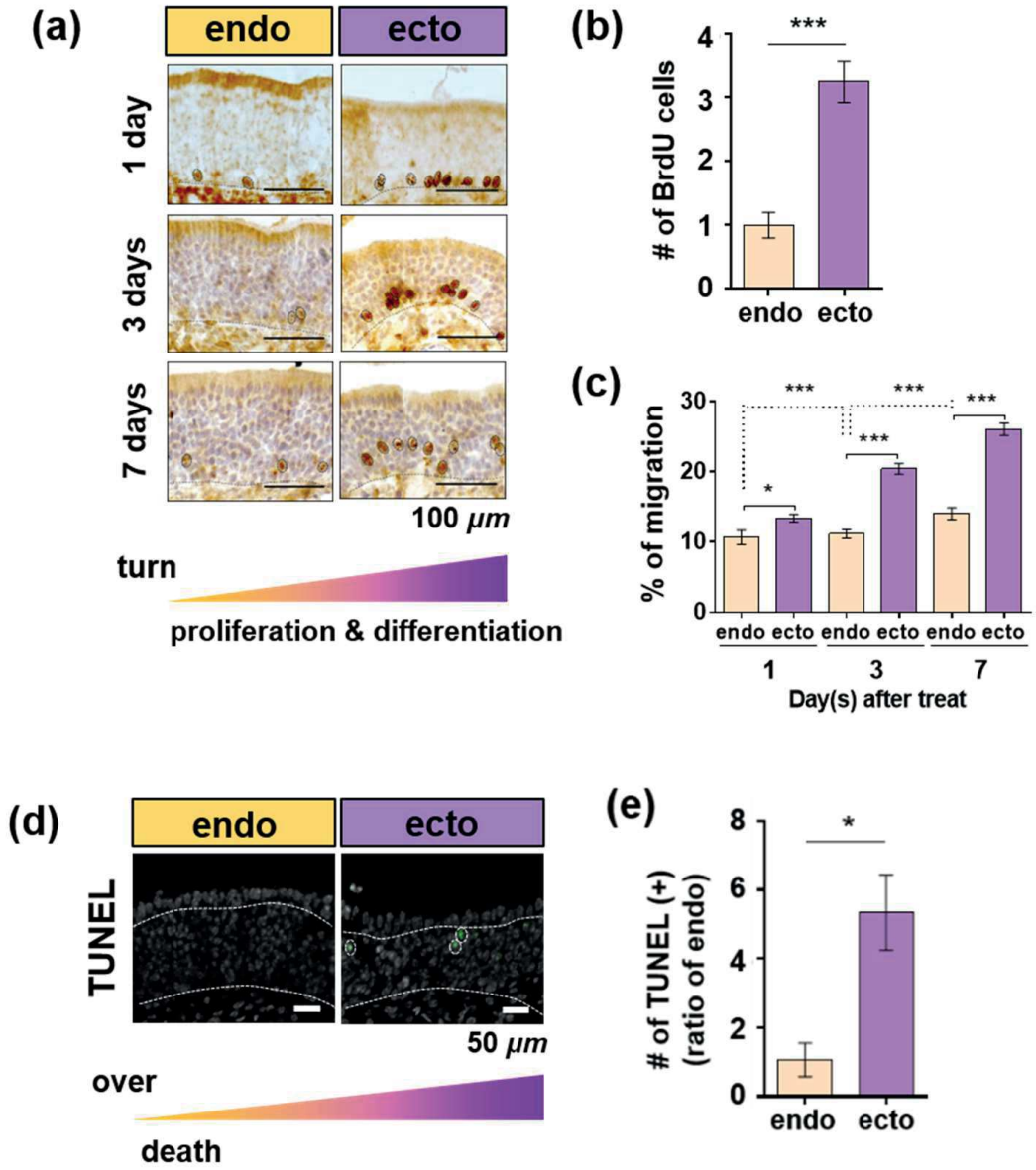

Figure S6. Intrinsic turnover characteristics of OSNs.

All experimental subjects in this figure were two-month C57BL/6 mice, a widely used inbred strain. (a–c) Analysis of OSNs proliferation and differentiation ("turn"). (a) Representative IHC data quantifying BrdU (+) cells by time after BrdU intraperitoneal (IP) injection between turbinate ecto and endo. (b) Comparative quantification one day after injection between ecto and endoturbinate. (c) Differentiation ratio through quantification by migration degree by time after injection between the ecto and endoturbinate. (d–e) Analysis of the death of OSNs ("over"). (d) TUNEL (+) cells indicated as IF data in each turbinate and (e) comparative quantification. Data are represented as mean ± SEM from three independent experiments. For statistical analysis, a two-tailed unpaired t-test was performed using Prism software (GraphPad software, USA). Statistical significances are noted (*P < 0.05, ***P < 0.001). Olfactory sensory neurons (OSNs), wild-type (WT), five familial AD mutations (5xFAD), Alzheimer's disease (AD).

Acknowledgments

This work was supported by the Korea Health Industry Development Institute (HI18C0154) and Basic Science Research Program through the National Research Foundation of Korea (NRF) funded by the Ministry of Education (2020R1A6A1A03040516).

References

1. R. I. Mesholam, P. J. Moberg, R. N. Mahr, R. L. Doty, Olfaction in neurodegenerative disease: a meta-analysis of olfactory functioning in Alzheimer's and Parkinson's diseases. *Arch Neurol* **55**, 84-90 (1998).
2. Y. Ruan, X. Y. Zheng, H. L. Zhang, W. Zhu, J. Zhu, Olfactory dysfunctions in neurodegenerative disorders. *J Neurosci Res* **90**, 1693-1700 (2012).
3. S. Waldton, Clinical observations of impaired cranial nerve function in senile dementia. *Acta Psychiatr Scand* **50**, 539-547 (1974).
4. M. Serby, P. Larson, D. Kalkstein, The nature and course of olfactory deficits in Alzheimer's disease. *Am J Psychiatry* **148**, 357-360 (1991).
5. L. Velayudhan, Smell identification function and Alzheimer's disease: a selective review. *Curr Opin Psychiatry* **28**, 173-179 (2015).
6. K. Duff, R. J. McCaffrey, G. S. Solomon, The Pocket Smell Test: successfully discriminating probable Alzheimer's dementia from vascular dementia and major depression. *J Neuropsychiatry Clin Neurosci* **14**, 197-201 (2002).
7. R. O. Roberts *et al.*, Association Between Olfactory Dysfunction and Amnestic Mild Cognitive Impairment and Alzheimer Disease Dementia. *JAMA Neurol* **73**, 93-101 (2016).
8. Y. M. Zou, D. Lu, L. P. Liu, H. H. Zhang, Y. Y. Zhou, Olfactory dysfunction in Alzheimer's disease. *Neuropsychiatr Dis Treat* **12**, 869-875 (2016).
9. D. Jimbo, M. Inoue, M. Taniguchi, K. Urakami, Specific feature of olfactory dysfunction with Alzheimer's disease inspected by the Odor Stick Identification Test. *Psychogeriatrics* **11**, 196-204 (2011).
10. S. Parola, P. Liberini, Assessing olfaction in the Italian population: methodology and clinical application. *Ital J Neurol Sci* **20**, 287-296 (1999).
11. S. J. Yoo *et al.*, Differential spatial expression of peripheral olfactory neuron-derived BACE1 induces olfactory impairment by region-specific accumulation of beta-amyloid oligomer. *Cell Death Dis* **8**, e2977 (2017).
12. L. Cao *et al.*, Abeta alters the connectivity of olfactory neurons in the absence of amyloid plaques in vivo. *Nat Commun* **3**, 1009 (2012).
13. D. W. Wesson *et al.*, Sensory network dysfunction, behavioral impairments, and their reversibility in an Alzheimer's beta-amyloidosis mouse model. *J Neurosci* **31**, 15962-15971 (2011).

14. M. Wachowiak, L. B. Cohen, Representation of odorants by receptor neuron input to the mouse olfactory bulb. *Neuron* **32**, 723-735 (2001).
15. H. U. Fried, S. H. Fuss, S. I. Korsching, Selective imaging of presynaptic activity in the mouse olfactory bulb shows concentration and structure dependence of odor responses in identified glomeruli. *Proc Natl Acad Sci U S A* **99**, 3222-3227 (2002).
16. P. Mombaerts *et al.*, Visualizing an olfactory sensory map. *Cell* **87**, 675-686 (1996).
17. R. Vassar *et al.*, Topographic organization of sensory projections to the olfactory bulb. *Cell* **79**, 981-991 (1994).
18. K. Miyamichi, S. Serizawa, H. M. Kimura, H. Sakano, Continuous and overlapping expression domains of odorant receptor genes in the olfactory epithelium determine the dorsal/ventral positioning of glomeruli in the olfactory bulb. *J Neurosci* **25**, 3586-3592 (2005).
19. K. Kobayakawa *et al.*, Innate versus learned odour processing in the mouse olfactory bulb. *Nature* **450**, 503-508 (2007).
20. K. Mori, Y. K. Takahashi, K. M. Igarashi, M. Yamaguchi, Maps of odorant molecular features in the Mammalian olfactory bulb. *Physiol Rev* **86**, 409-433 (2006).
21. S. L. Sullivan, M. C. Adamson, K. J. Ressler, C. A. Kozak, L. B. Buck, The chromosomal distribution of mouse odorant receptor genes. *Proc Natl Acad Sci U S A* **93**, 884-888 (1996).
22. H. Oakley *et al.*, Intraneuronal beta-amyloid aggregates, neurodegeneration, and neuron loss in transgenic mice with five familial Alzheimer's disease mutations: potential factors in amyloid plaque formation. *J Neurosci* **26**, 10129-10140 (2006).
23. M. Shirasu *et al.*, Olfactory receptor and neural pathway responsible for highly selective sensing of musk odors. *Neuron* **81**, 165-178 (2014).
24. G. S. Suh *et al.*, A single population of olfactory sensory neurons mediates an innate avoidance behaviour in Drosophila. *Nature* **431**, 854-859 (2004).
25. T. Nath *et al.*, Using DeepLabCut for 3D markerless pose estimation across species and behaviors. *Nat Protoc* **14**, 2152-2176 (2019).
26. S. H. Yang *et al.*, Nec-1 alleviates cognitive impairment with reduction of Abeta and tau abnormalities in APP/PS1 mice. *EMBO Mol Med* **9**, 61-77 (2017).
27. D. W. Wesson, E. Levy, R. A. Nixon, D. A. Wilson, Olfactory dysfunction correlates with amyloid-beta burden in an Alzheimer's disease mouse model. *J Neurosci* **30**, 505-514 (2010).
28. L. R. Saraiva *et al.*, Combinatorial effects of odorants on mouse behavior. *Proc Natl Acad Sci U S A* **113**, E3300-3306 (2016).
29. H. Kida *et al.*, Vapor detection and discrimination with a panel of odorant receptors. *Nat Commun* **9**, 4556 (2018).
30. I. Benilova, E. Karran, B. De Strooper, The toxic Abeta oligomer and Alzheimer's disease: an emperor in need of clothes. *Nat Neurosci* **15**, 349-357 (2012).
31. A. Demuro, M. Smith, I. Parker, Single-channel Ca(2+) imaging implicates Abeta1-42 amyloid pores in Alzheimer's disease pathology. *J Cell Biol* **195**, 515-524 (2011).
32. S. Forner, D. Baglietto-Vargas, A. C. Martini, L. Trujillo-Estrada, F. M. LaFerla, Synaptic Impairment in Alzheimer's Disease: A Dysregulated Symphony. *Trends Neurosci* **40**, 347-357 (2017).
33. J. Y. Kim *et al.*, Distinct amyloid precursor protein processing machineries of the olfactory system. *Biochem Biophys Res Commun* **495**, 533-538 (2018).
34. C. Peng, J. Q. Trojanowski, V. M. Lee, Protein transmission in neurodegenerative disease. *Nat Rev Neurol* **16**, 199-212 (2020).
35. F. Bassil *et al.*, Amyloid-Beta (Abeta) Plaques Promote Seeding and Spreading of

Alpha-Synuclein and Tau in a Mouse Model of Lewy Body Disorders with Abeta Pathology. *Neuron* **105**, 260-275 e266 (2020).
36. J. J. Tomlinson *et al.*, Holocranohistochemistry enables the visualization of alpha-synuclein expression in the murine olfactory system and discovery of its systemic anti-microbial effects. *J Neural Transm (Vienna)* **124**, 721-738 (2017).
37. J. Attems, L. Walker, K. A. Jellinger, Olfactory bulb involvement in neurodegenerative diseases. *Acta Neuropathol* **127**, 459-475 (2014).
38. H. Fujishiro, Y. Tsuboi, W. L. Lin, H. Uchikado, D. W. Dickson, Co-localization of tau and alpha-synuclein in the olfactory bulb in Alzheimer's disease with amygdala Lewy bodies. *Acta Neuropathol* **116**, 17-24 (2008).
39. S. Christen-Zaech *et al.*, Early olfactory involvement in Alzheimer's disease. *Can J Neurol Sci* **30**, 20-25 (2003).
40. S. E. Arnold *et al.*, Olfactory epithelium amyloid-beta and paired helical filament-tau pathology in Alzheimer disease. *Ann Neurol* **67**, 462-469 (2010).
41. S. Bonzano, S. Bovetti, C. Gendusa, P. Peretto, S. De Marchis, Adult Born Olfactory Bulb Dopaminergic Interneurons: Molecular Determinants and Experience-Dependent Plasticity. *Front Neurosci* **10**, 189 (2016).
42. S. Nagayama, R. Homma, F. Imamura, Neuronal organization of olfactory bulb circuits. *Front Neural Circuits* **8**, 98 (2014).
43. B. Zapiec *et al.*, A ventral glomerular deficit in Parkinson's disease revealed by whole olfactory bulb reconstruction. *Brain* **140**, 2722-2736 (2017).
44. H. Baker, Unilateral, neonatal olfactory deprivation alters tyrosine hydroxylase expression but not aromatic amino acid decarboxylase or GABA immunoreactivity. *Neuroscience* **36**, 761-771 (1990).
45. A. Keller, F. L. Margolis, Immunological studies of the rat olfactory marker protein. *J Neurochem* **24**, 1101-1106 (1975).
46. S. Hasegawa-Ishii, A. Shimada, F. Imamura, Lipopolysaccharide-initiated persistent rhinitis causes gliosis and synaptic loss in the olfactory bulb. *Sci Rep* **7**, 11605 (2017).
47. H. Sakano, Neural map formation in the mouse olfactory system. *Neuron* **67**, 530-542 (2010).
48. R. Vassar *et al.*, Beta-secretase cleavage of Alzheimer's amyloid precursor protein by the transmembrane aspartic protease BACE. *Science* **286**, 735-741 (1999).
49. H. Yu *et al.*, APP processing and synaptic plasticity in presenilin-1 conditional knockout mice. *Neuron* **31**, 713-726 (2001).

Chapter 5

Severe histomorphological alterations in post-mortem olfactory glomeruli in Alzheimer's disease

Gowoon Son[1,2,3], Harry W.M. Steinbusch[1,3], Carmen López-Iglesias[4], Cheil Moon[1,5,6*] and Ali Jahanshahi[2,3*]

[Submitted]

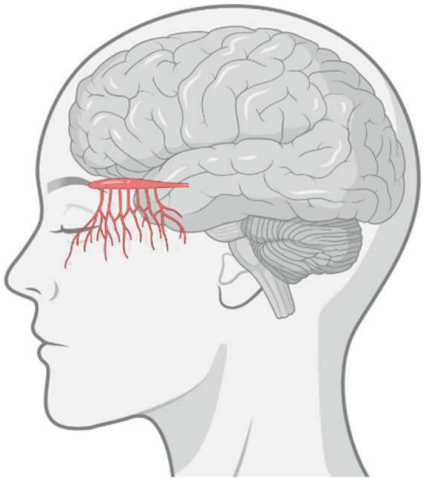

Abstract

Alzheimer's disease (AD) is the most prevalent form of dementia. Key AD symptoms include memory and cognitive decline; however, comorbid symptoms such as depression and sensory-perceptual dysfunction are often reported. Among these, a deterioration of olfactory sensation is observed in approximately 90% of AD patients. However, the precise pathophysiological basis underlying olfactory deficits remains elusive. The olfactory glomeruli in the olfactory bulb (OB) that first receive sensory information from the olfactory processing pathway. Maintaining the structural and functional integrity of the olfactory glomerulus is critical to olfactory signaling. Herein, we conducted an in-depth histopathological assessment to reveal detailed structural alterations in the olfactory glomeruli in AD patients. Fresh frozen post-mortem OB specimens obtained from six AD patients and seven healthy age-matched individuals were examined. We used combined immunohistochemistry and stereology to assess the gross morphology and histological alterations, such as those in the expression of Aβ protein, microglia, and neurotransmitters, in the OB. Electron microscopy was employed to study the ultrastructural features in the glomeruli. Significant accumulation of Aβ, morphologic damage, altered neurotransmitter levels, and microgliosis in the olfactory glomeruli of AD patients suggests that glomerular damage could affect olfactory function. Moreover, greater neurodegeneration was observed in the ventral olfactory glomeruli of AD patients. The synaptic ultrastructure revealed distorted postsynaptic densities and a decline in presynaptic vesicles in AD specimens. This provides that primary olfactory pathway is affected by the pathogenesis of AD and may represent clues to identifying the mechanism involved in olfactory dysfunction in AD.

List of abbreviations

AD, Alzheimer's disease; OB, olfactory bulb; Aβ, β-amyloid; OE, olfactory epithelium; OSN, olfactory sensory neuron; PCA, principle component analysis; MAP2, microtubule-associated protein 2; VGLUT2, vesicular glutamate transporter 2; CTL, control; D, dorsal; V, ventral; A11, oligomeric Aβ; TH, tyrosine hydroxylase; EM, electron microscopy; IBA1, ionized calcium binding adaptor molecule 1.

Keywords

Alzheimer's disease, morphology, olfactory bulb, post-mortem histology, ultras tructure

1. Introduction

Alzheimer's disease (AD) is a neurodegenerative disease that accounts for 60–80% of all dementia cases (*1*). Primary AD symptoms include memory and cognitive decline, depression, and sensory-perceptual dysfunction (*2, 3*). Deterioration in smelling function is a common symptom that affects approximately 90% of AD patients (*4*). Since olfactory dysfunction occurs in the early stages of the disease, studying its underlying pathophysiological processes could help understand the mechanisms and develop tools for early diagnosis. So far, neuropathological alterations in cortical olfactory areas have been considered as the main cause of smelling deficits in AD (*5*). Nevertheless, non-cortical areas, especially the olfactory bulbs (OB), have recently gained a considerable deal of attention.

The human olfactory system comprises the primary olfactory pathway and the secondary olfactory pathway. In the primary olfactory pathway, the olfactory sensory neurons (OSNs) in the OE encounter odorants and project their axons to the OB. Thus, the OB hosts the first synapse in the primary olfactory processing pathway (*6*). OSN synapses, namely as the olfactory glomeruli, which are spherical neuropil structures that wire both peripheral and central neurons (*7*). Olfactory glomeruli act as the site for encoding olfactory signals, a gateway to the secondary olfactory pathway. In turn, OSNs expressing a specific odorant receptor gene project their sensory information along their axons to specific glomeruli with highly precise stereotypy, where they form synapses with mitral/tufted cells and sharpen olfactory signals via lateral inhibition (*8*). Ample evidence suggests that these topographical

characteristics play a crucial role in sense of smell (*9*). Therefore, maintaining the structural integrity of the olfactory glomerulus is essential for olfactory signaling (*10*). In vivo studies on rodents have indicated that damaged olfactory glomeruli could contribute to olfactory dysfunction in mice (*11*).

The expression of β-amyloid (Aβ) plaques is the cardinal pathological hallmark in the brains of patients with AD. Aggregated Aβ proteins are positively associated with impaired synaptic transmission and neural network malfunction (*12*). Animal studies have shown that amyloidosis of amyloid precursor proteins in presynaptic terminals reduces excitatory transmitter release and results in Aβ-induced synaptic deficits (*13*). Moreover, these synaptic deficits induce postsynaptic depression by suppressing long-term potentiation or promoting long-term depression (*14*). Moreover, the accumulation of Aβ proteins can trigger sequential pathogenic cascades such as microglial reactivation and infiltration around damaged neurons by driving disrupting neurotransmitter release and accelerating amyloidopathy (*15, 16*). In AD, the accumulation of Aβ proteins and abnormal neuroinflammatory processes can cause structural deficits and functional instability in the neural networks. Aβ protein expression has already been reported in the primary olfactory pathway of pathologically verified AD patients (*17*). Gliosis have also been shown to impair cell signaling in the OB of AD patients (*18*). However, it is not clear how and to what extent these aggregates play a role in the pathophysiology of olfactory impairment.

Herein, we assessed the morphological and histochemical alterations in the

olfactory glomeruli of the OB obtained from clinically-confirmed AD patients and age-matched controls (CTLs). We addressed whether the structural integrity of the olfactory glomeruli could be affected by Aβ protein expression and microgliosis in individuals with AD. To this end, we used designed-based stereology and immunohistochemical analysis as tools to assess pathological and morphological changes in the olfactory glomeruli. We measured Aβ proteins and microglial morphological change. To predict the functional consequences of this pathogenesis in the OB, we examined the dopaminergic neurotransmitter system, a key factor in OSN signaling for the detection of olfactory stimuli (*19*). Furthermore, we evaluated ultrastructural changes in the axonal, dendritic, and synaptic structures.

2. Materials and methods

2.1. Tissue collection

Post-mortem freshly-frozen OBs were obtained from the Netherlands Brain Bank (NBB) (www.brainbank.nl) in Amsterdam, The Netherlands. The NBB received permission to perform autopsies and use tissue and medical records from the Ethical Committee of the Vrij Universiteit (VU) Medical Center (Registration number NHB Project 1147). All donors provided informed consent for autopsies and use of their brain tissue for research purposes. The post-mortem tissues were stored as non-paraformaldehyde (PFA) fixed fresh frozen tissue.

2.2. Specimens

A total of 13 subjects were selected based on the Braak stages (*20*) and ApoE/Aβ levels, including seven healthy CTLs and six AD patients (Table 1). All AD patients were classified into *Braak* stage six, of which half harbored two ε4 alleles of *apoE*. One subject was excluded from subregional analysis due to distorted OB tissue. Age and sex were not statistically different between the two groups (healthy CTLs: four women + three men; AD patients: four women + two men; mean ± SD of age: healthy CTLs vs AD patients: 77 ± 12.1 vs 76 ± 7.3 years; P = 0.91). For unbiased protein immunostaining results, the post-mortem delay (PMD) time was also similar in the two groups (healthy CTLs: 7.3 ± 2.1 [hours]; AD: 5.4 ± 0.9; P = 0.1) (Table 2).

The specimens were stored at -80°C upon arrival at Maastricht University. Tissues for immunohistochemistry were embedded in cryo-embedding medium, optimal cutting temperature (OCT) compound and were cut into 40 μm sections in 10 series and mounted on Superfrost® Plus slides (VWR, Leuven, Belgium) at a working temperature of -20°C. Given the anterior-posterior orientation of the OBs, coronal sections were prepared for optimal stereological analysis (Supplementary Fig. 1). Each series was processed immunohistochemically and subjected to stereological quantification.

Table 1. Subject information

Description	Case #	Gender	Age	PMD	*Braak*	Amyloid level	APOE	Diagnosis
CTL								
CTL 1	S01/016	F	64	8.5	0	B	42	CTL
CTL 2	S12/002	M	55	7	0	B	43	CTL
CTL 3	S11/111	M	93	5	I	O	33	CTL
CTL 4	S03/035	F	82	11.5	I	O	33	CTL
CTL 5	S09/134	F	84	7	I	O	33	CTL with infarct
CTL 6	S14/029	F	78	7	I	A	33	CTL
CTL 7	S13/016	M	83	5	I	A	33	CTL
AD								
AD 1	S15/013	F	73	7.5	6	C	33	AD with CAA and neurofibrillary tangles
AD 2	S12/125	M	71	6.5	6	C	33	AD
AD 3	S14/049	F	78	5	6	C	44	AD with CAA and cotton wool plaques
AD 4	S13/040	F	70	4.5	6	C	44	AD
AD 5	S15/040	M	76	5	6	C	44	AD with CAA, amygdala alpha-synucleinopathy and hippocampal sclerosis
AD 6	S13/036	F	90	4	6	C	32	AD with, small infarction in CA1 and in putamen left

PMD: Post mortem delay (h) / CTL: non-demented control / AD: Alzheimer's Disease / CAA: cerebral amyloid angiopathy / CA: Cornu Ammonis

Table 2. Demographics and descriptive statistics of subjects

Parameters	CTL		AD		
	Mean	SD (±)	Mean	SD (±)	P
Subject	7		6		-
Gender	Female: 4 / Male: 3		Female: 4 / Male: 2		> 0.05
Age (years)	77	12.1	76	7.3	0.91
PMD (h)	7.3	2.1	5.4	0.9	0.10

PMD: Post mortem delay (h) / CTL: non-demented control / AD: Alzheimer's Disease / SD: Standard deviation. Gender was compared using two-way ANOVA. Age and PMD was compared using two-tailed unpaired Welch's t-test.

2.3. Immunohistochemistry

Slides were air-dried for 30 min at 37°C and post-fixed with 4% PFA buffer for 20 min at 4°C. After washing in Tris-buffered saline (TBS) (pH=7.5) for 10 min three times, slides were incubated with TBS-Triton (TBS-T) (0.3%) containing 3% normal donkey serum (NDS) for 30 min. Each series of sections was incubated with one of the following primary antibodies (diluted 1:100~500 in accordance with the manufacturer's instruction in TBS-T with 3% NDS): mouse anti-6E10, a marker for Aβ (Covance); rabbit anti-A11, a marker for oligomeric Aβ (Thermo); mouse anti-VGLUT2 (Novus Biologicals); rabbit anti-tyrosine hydroxylase (TH) (Santa Cruz); chicken anti-MAP2 (Abcam); and rabbit anti-IBA1 (Wako) for 48 h at 4°C in a humidified chamber. On the third day, the sections were washed with TBS-T, TBS, and TBS-T (in this order) for 10 min each and then incubated with secondary antibodies (Invitrogen; diluted 1:200~500 in TBS-T with 3% NDS), including donkey anti-rabbit

Alexa Fluor 488 (against A11, IBA1), Alexa Fluor 647 (against TH), anti-mouse Alexa Fluor 488 (against 6E10, VGLUT2), and anti-chicken Alexa Fluor 647 (against MAP2), for 2 h at room temperature (RT) in a humidified chamber. After washing in TBS for 10 min three times, the sections were incubated with Hoechst 33342 (diluted 1:10,000) for 10 min at RT. After washing in TBS for 10 min three times, slides were submerged for 10 min in 0.3% Sudan black solution to avoid autofluorescence. After washing rapidly eight times in TBS, slides were mounted using 80% glycerol in PBS.

2.4. Fluorescence density measurement

The expression of 6E10 and A11 was measured using fluorescence density measurement. Images were taken with a stereology microscope connected to an Olympus BX51WI using 10× or 20× objectives. ImageJ (ver. 1.51j8, NIH, USA) was used for fluorescence intensity measurement, which was quantified using the region of interest (ROI) using the function 'Measure' in ImageJ. For data-color coherence, the fluorescence of VGLUT2 and MAP2 of adjusted to pseudo-color using a function of 'Look Up Table' in ImageJ (Fig 1g, h). The threshold was calculated based on negative control sections both in the CTL and AD sections.

2.5. Cell counting and area/volume measurement

Images were taken with a stereology microscope coupled to an Olympus BX51WI using 10× or 20× objectives. Stereo Investigator (ver. 11, MBF Bioscience, USA) and ImageJ (ver. 1.51j8, NIH, USA) software were used for cell counting and calculating the cross-sectional area, as previously reported (*21*). TH-positive

periglomerular cells co-labelled with Hoechst-nuclei were counted using 'Optical Fractionator' in Stereo Investigator. For unbiased quantification, the number and area of individual glomeruli were measured from the same 'ROI' using the function 'Measure' in ImageJ. We used the images taken after Hoechst counterstaining. The volume of every part was calculated by multiplying the surface with the section thickness and the number of slices per series. Finally, all these parts were summed, and the total volume of the OBs was calculated.

2.6. Evaluation of microglial morphology

We assessed the microglial reactivation in the glomeruli by quantifying the number and morphology of IBA1-positive microglial cells. Images were taken with a stereology microscope connected to an Olympus BX51WI using a 20× objective and analyzed with ImageJ software. The number, size, and morphology of IBA-1 positive microglial cells were quantified based on previously published criteria (*22, 23*). Based on their morphology, IBA-1-positive microglial cells were divided into four types, including ramified, hyper-ramified, bushy, and amoeboid, and were further subjected to quantification. For unbiased quantification, the IBA-1 positive microglial cells were assessed in the same 'ROI' using the 'Measure' function in ImageJ.

2.7. Three-dimensional reconstruction of the olfactory bulb

Three-dimensional reconstruction from serial sections of the OB was conducted to assess the structure, volume, and distribution of different markers across the OB (Supplementary Movie 1). For this reconstruction, the images were taken using stereology microscopes connected to an Olympus BX51WI camera. We

used images taken after immunostaining for VGLUT2 and MAP2 and Hoechst counterstaining. The images were stacked using the 'Stitching' tool in ImageJ (ver. 1.51j8). Immunofluorescence images were fed into a virtual structure using a Stereo Investigator software. Contoured Images were aligned according to the reference point and fiducial point. Reconstruction was completed using the 'Reconstruction' function (https://www.mbfbioscience.com/help/si11/Content/SSR/SSR_imageMulti1.htm) (*24*).

2.8. Electron microscopy

Tissue preparation and fixation were performed based on a published protocol (*25*). In brief, the ventral part of the freshly-frozen OB was carefully punched to extract approximately 1 mm^3 of a glomerular layer. Then, tissue was immediately immersed in freshly prepared ice-cold 1.5% PFA in PBS, followed by overnight incubation in the same solution at 4°C. Thereafter, the tissue was post-fixed in 3% glutaraldehyde, post-fixed in osmium tetroxide, dehydrated in ethanol, and embedded in Epon (EMS, Hatfield, USA). Sections were cut into 70-nm ultra-thin sections. Ultra-thin sections were prepared for transmission electron microscopy according to a routine procedure for sample processing. Transmission electron microscopy was conducted using a Tecnai G2 Spirit BioTWIN electron microscope (Thermo Fisher Scientific, Eindhoven, The Netherlands) coupled with an Eagle 4kx4k digital camera (Thermo Fisher Scientific, Eindhoven, The Netherlands). Several tissue overview images were captured and evaluated for possible damage induced by the freezing procedure. From the overview, higher magnification images were selected in areas not presenting any visible freezing damage, and areas within the captured images of

the electron micrographs were observed. When interpreting images, we took into account the criteria that had been described in an earlier study on AD brains (*26*).

2.9. *Subregional analysis of the olfactory bulb*

The OB was assessed based on arbitrarily defined dorsal and ventral subregions. In the frontal anatomical plane, the part of the OB that faced the ventral surface of the frontal lobe was defined as the dorsal half, and the opposite half was named the ventral OB (Fig. 1a).

Principal component analysis (PCA) was used for multivariate analysis of distinct pathological factors to construct a predictive model for neurodegeneration in the above-mentioned subregions of the OB. Eleven parameters were used for PCA analysis, including age; Braak stage; *apoE4*; the number and size of glomeruli; expression of Aβ and TH; and the number of ramified, hyper-ramified, bushy, and amoeboid microglia in 13 subjects in each dorsal/ventral region of the olfactory glomeruli. PCA was conducted using the 'prcomp ()' function in R (ver. 3.6.3). PCA plots were clustered using the 'ggplot ()' and 'fviz_pca_ind ()' functions in R.

2.10. Statistical analysis

General statistics were calculated using GraphPad Prism software (ver. 7.0). Values are presented either as the mean and standard error of the mean or as the mean and coefficient of error. Normal distribution of the data was proved using two-tailed unpaired Welch's t-test and two-way ANOVA. Age and sex were used as confounding factors in the analyses. During experiments, the experimenter was blinded to the experimental condition to prevent biased assessment.

3. Results

3.1. Gross morphology analysis of the olfactory glomerulus

Figure 1a showed schematic representation of the human OB (Fig. 1a). The gross images indicated human OB specimen, CTL (Fig. 1b) and AD (Fig. 1c). Figure 1d exhibited a snapshot of three-dimensional reconstruction of human OB (Fig. 1d). In Nissl/Hoechst staining, the CTL OB exhibited a laminar organization (Fig. 1e, g). The olfactory glomerular layer had discrete spherical assemblies located at the outer layer of the OB (Fig. 1f). Detailed inspection of the section stained with antibodies against MAP2 and VGLUT2 revealed the neuropil structure of the olfactory glomeruli containing presynaptic vesicles markers and dendritic fibers in the outermost layer of the OB (Fig. 1h).

We then quantified the number and size of the glomeruli in the AD samples and CTLs samples (Fig. 2). Quantitative volumetry revealed a significant reduction in the volume of the glomerular layer in AD samples compared to that in CTL samples (CTL = 1.00, AD = 0.73, P = 0.0477) (Fig. 2a). However, the total number of glomeruli did not differ between the AD and CTL samples (CTL = 1.00, AD = 1.04, P = 0.8005) (Fig. 2b). In contrast, the quantitative analysis revealed a significant reduction in average glomerular cross-sectional area in the AD samples compared to that in CTL samples (CTL = 1.00, AD = 0.58, P = 0.0011) (Fig. 2c). Similar changes were observed in the dorsal and ventral subregions of the OB; the total number of glomeruli (CTL-D = 1.00, AD -D = 1.58, CTL-V = 2.11, AD -V = 2.09, P > 0.05) (Fig. 2d); and the average glomerular cross-sectional area (CTL-D = 1.00, AD -D = 0.58, CTL-V = 1.06, AD -V = 0.65, P < 0.05] (Fig. 2e).

3.2. β-amyloid immunohistochemistry

Qualitative inspection revealed a robust expression of Aβ in the glomerular layer and to a lesser extent in areas adjacent to the mitral cell layer (Fig. 3a). Aβ was mostly expressed inside the olfactory glomeruli (Fig. 3b). In addition, the 6E10 was co-localized with A11 immunoreactivity (Supplementary Fig. 2a). Quantitative analysis showed that A11 immunoreactivity was also higher in the glomeruli of AD patients than in the glomeruli of CTLs (Supplementary Fig. 2b).

Quantitative analysis showed a significant difference in Aβ expression (6E10-immunoreactivity) in olfactory glomeruli in AD samples compared to that in CTL samples (CTL = 1.00, AD = 3.09 arbitrary unit [au]), P = 0.0062) (Fig. 3g).

The distribution of Aβ protein was significantly higher in the ventral glomeruli than in dorsal glomeruli (CTL-D = 1.00, AD-D = 4.62, P > 0.05, CTL-V = 1.48, AD-V = 11.74, P < 0.01) (Fig. 3h). The ratio of Aβ protein expression in the ventral glomeruli varied across AD patients, ranging from a fold increase of 1.24 (AD 2) to that of 28.14 (AD 6) (Fig. 3i, j).

3.3. Microglia immunohistochemistry

We compared the microglia in the glomerulus between CTL subjects (Fig. 4a, c) and AD patients and observed that there was more robust infiltration of reactive microglia in the olfactory glomeruli of AD patients (Fig. 4b, d).

The number of the IBA-1-positive microglial cells was increased in the ventral glomeruli and increased to a lesser extent in the dorsal glomeruli. Quantitative

analysis revealed a more than two-fold increase in the number of IBA-1-positive microglial cells in the glomeruli of AD patients than in the glomeruli of CTLs (CTL = 1.00, AD = 2.35, P = 0.0048) (Fig. 4e). Both dorsal and ventral glomeruli showed increased immunoreactivity, although the number of IBA-1 positive cells was higher in ventral olfactory glomeruli (CTL-D = 1.00, AD-D = 2.21, P < 0.01, CTL-V = 1.40, AD-V = 3.44, P < 0.001) (Fig. 4f). The size of the IBA1-positive microglial cell bodies was significantly larger in AD patients than in CTLs (CTL = 1.00, AD = 1.76, P = 0.0011) (Fig. 4g). The cell size values were greater in the ventral OB glomeruli than in the dorsal OB glomeruli (CTL-D = 1.00, AD-D = 1.38, P > 0.05, CTL-V = 0.90, AD-V = 1.96, P < 0.001) (Fig. 4h).

Moreover, the microglial cell body size increased, and their morphology shifted toward reactive states in the olfactory glomeruli of AD patients. Quantification of microglial morphology demonstrated that the microglia in the normal glomeruli were in ramified, hyper-ramified, bushy, or amoeboid form (Fig. 4j-q) with the following ratio: 0.38:0.21:0.37:0.04 (Fig. 4i). In AD-glomeruli, this ratio was 0.17:0.13:0.33:0.36 (Fig. 4i). There was a sharp decline in the number of ramified forms (CTL = 1.00, AD = 0.45, P < 0.001) (Fig. 4r) and a rise in the number of amoeboid forms (CTL = 1.00, AD = 0.45, P < 0.001) (Fig. 4u) but not in the number of hyper-ramified and bush forms in AD samples compared to that in CTL samples (Fig. 4s, t). The number of ramified microglia decreased significantly in the ventral part (CTL-D = 1.00, AD-D = 0.61, P > 0.05, CTL-V = 0.88, AD-V = 0.33, P < 0.05) (Fig. 4v), and the proportion of the amoeboid form increased on both sides, although the increase on the ventral

side was more significant (CTL-D = 1.00, AD-D = 3.27, P < 0.01, CTL-V = 0.14, AD-V = 6.06, P < 0.001) (Fig. 4y).

3.4. Tyrosine hydroxylase immunohistochemistry

Qualitative inspection revealed that TH-positive periglomerular cells were co-labelled with Hoechst-nuclei, and the fibers were intertwined within the neuropil structure (Fig. 5a, c). However, in AD-OB, the TH-positive neurites were rarely visible (Fig. 5b, d).

We quantified the number of TH-positive periglomerular cells, which were co-labelled with Hoechst. The quantitative cell count showed that AD-glomeruli had fewer TH-periglomerular cells than CTL-glomeruli (CTL = 1.00, AD = 0.43, P = 0.0011) (Fig. 5e). The lack of TH-positive periglomerular cells was more prominent in the ventral side of the olfactory glomeruli than in the dorsal side in AD patients (CTL-D = 1.00, AD-D = 0.63, P > 0.05, CTL-V = 1.43, AD-V = 0.42, P < 0.001) (Fig. 5f).

3.5. Subregional clustering of the variables

We reassessed the investigated variables based on the regional distribution of changes in the OB region. Using PCA, 'dimensionality reduction' data processing was conducted on input variables to create a predictive model based on the anatomical and pathological changes observed in this study. PCA analysis indicated an overlapping pattern of the alterations between CTL and AD samples in the dorsal OB region (Fig. 6a), whereas it showed distinctively clustered alterations between CTL and AD in the ventral OB region (Fig. 6b).

3.6. Ultrastructure analysis of the olfactory glomerulus

The ventral glomerular layer of the OB was assessed for ultrastructural changes using electron microscopy. Detailed inspection of the images obtained from AD specimens revealed neuropil threads containing constricted filaments (Fig. 7a–c). However, in the dendrites, those constricted filaments were present to a lesser extent (Fig. 7a, b). These highly constricted filaments had the appearance of dense inclusions (Fig. 7c). In CTL specimens, the synapses contained dense postsynaptic areas and abundant synaptic vesicles (Fig. 7d, e). In contrast, the synaptic clefts in AD were lost, the synaptic structure was distorted, and greater distances between synapses were observed (Fig. 7f, g).

4. Discussion

Herein, we assessed the morphologic and histologic alterations in the OB obtained from patients with advanced AD and compared them with those in matched CTLs (Fig. 8). We found robust expression of the pathological hallmarks of AD, such as Aβ accumulation, in the OB of AD patients, especially in the olfactory glomerular layer, where the first synapse is formed with the OSN. Aβ accumulation co-existed with additional histological alterations such as infiltration of reactivated microglia and severe atrophy, mainly caused by loss of periglomerular cells. Advanced PCA indicated a predominantly ventral deficit in the glomeruli (Fig. 6, Table 3).

The OB constitutes a layered structure with specific cell types and functions in each layer. The functional characteristics and structural integrity of each layer and the OB are critical for its activity (*27*). Our results showed a severe shrinkage of the olfactory glomerular layer that could affect signal transduction between OE and OB neurons and could lead to significant disruption in olfactory detection (Fig. 2). Electron microscopy of the glomeruli revealed detectible damage in this area, in accordance with our histological findings (Fig. 7). In the electron microscopy images, neuropil threads containing constricted filaments were observed, which affected dendrites that also shared similar features, as revealed in an earlier study on AD brains (*26*). When inspecting the synaptic ultrastructure, we observed distorted postsynaptic densities and fewer presynaptic vesicles in AD image, which could be a contributing factor to synaptic failure in the glomeruli and the eventual olfactory dysfunction, which is known to be a common symptom in AD patients. Impaired

synaptic transmission between the OSNs and mitral/tufted cells may explain compromised processing of odor stimuli in general (*28*). It could lead to degeneration of periglomerular cells, which disrupts the lateral inhibition processes critical for sharpening sensory inputs and eventually discriminating odorants (*19*).

Our PCA analysis showed apparent dissimilarities in the distribution of degeneration along the dorsal-ventral axis of the OB (Fig. 6). This was in line with the findings from our previous rodent studies suggesting that region-specific degeneration and pathogenesis might be associated with the topographical organization of the OB (*29*). In the murine OE, spatial cues within the tissue can direct the spatially-restricted differentiation of the OSN, critical for normal olfactory function (*30*). OSNs, in turn, play a prominent role in defining the structural organization and cellular composition of the glomeruli (*31*). According to our findings, it is plausible that a toxic event caused by spatial Aβ accumulation and inflammation leads to ventrally oriented dysregulation of the OSNs' axon convergence toward the glomerulus and abnormal effects on the structural integrity of the OB. We propose that the ventrally oriented OB deficit observed in this study was predominantly caused by an impaired interaction between the OSNs and olfactory neurons (mitral and tufted cells) in the glomeruli. Interestingly, volumetric analysis showed that OB shrinkage was mainly caused by atrophy of the glomeruli rather than a change in their numbers (Fig. 2). This provides additional evidence that impaired convergence of OSNs' axons toward the glomerulus could be the cause of tissue loss. Although some deficits were evenly distributed across the dorsal-ventral

axis of the OB, such as increased microglia reactivity, these changes could be a consequence of systemic deficits beyond the OSNs' convergence to the OB. Intriguingly, predominantly ventral deficits in the OB have also been reported along the dorsal-ventral dimension in patients with advanced Parkinson's disease who also exhibit olfactory dysfunction (*32*). The study suggested that their finding is consistent with the 'olfactory vector hypothesis' for the pathogenesis of this neurodegenerative disease (*33*). Based on their hypothesis, the olfactory system may provide a potential route, which can trigger neurodegenerative diseases (*34*).

Microglia monitor the neural system in the resting state (*35*). They can sense an inflammatory response and become reactive following infiltration into the site of injury (*35*). Reactive microglia undergo several morphological changes based on their activity level (*36*). In AD, excessive Aβ accumulation promotes microgliosis (*37*). Furthermore, gliosis is a driving force for Aβ pathology by sustaining increased Aβ levels and accelerating the pathological vicious cycle (*16*). Although the causal relationship between microglial activation and Aβ accumulation in olfactory deficits remains elusive, the olfactory glomeruli of AD patients undergo intense pathological alterations following neuroinflammation, which could likely cause olfactory dysfunction.

We observed significant co-labelling of Aβ-immunoreactivity with oligomeric Aβ-immunoreactivity primarily in the glomerular layer (Fig. 3b, f). Most deposits of Aβ aggregates co-existed with oligomeric forms in the glomerulus layer (Supplementary Fig. 2). Typically, soluble Aβs are cleaved and oligomerized in presynaptic vesicles and released into the extracellular space (*13*). These oligomeric Aβs accumulate in the

extracellular space and induce toxicity (*38*). Since 2010, several studies have reported signs of Aβ amyloidosis and tau pathology in the olfactory areas, including OE and OB (*17, 18*). However, those findings have not identified a mechanism by which those neurodegenerative processes would lead to olfactory dysfunction in AD. It remains to be determined whether the misfolded Aβ protein originates from the upstream areas in the brain or from OSNs. Altogether, these data indicate that concomitant inflammatory processes and proteopathy occur in the OB of AD patients, similar to that reported in AD brains (*39*). This inflammation could further exacerbate the neurodegeneration in the OB, resulting in olfactory malfunction (*40*).

Despite the limitations of our post-mortem approach, we addressed the potential effects of Aβ-associated pathology on signal processes in the glomeruli. In periglomerular cells, dopamine plays a key role in the neurotransmission of olfactory signals. The fate of dopaminergic periglomerular cells depends on excitatory input from the OSNs (*19*). After receiving this input from the OSNs, they mature and release dopamine, which is critical for the lateral inhibition that sharpens the odor signals (*27*). Therefore, TH expression indicates increased functional inputs from the OSNs (*11, 19*). We observed that TH-immunoreactivity was drastically reduced in the glomeruli of AD patients (Fig. 5), suggesting the loss of sensory input from the OSNs. This loss of input could be caused by a disrupted synaptic structure and function in the glomeruli, as shown in the electron microscopy assessment (Fig. 7). Notably, most studies to date suggest that olfactory abnormalities in AD are due to impaired central information processing rather than sensory dysfunction namely 'conductive'

dysfunction (reviewed in (*41*)). Nevertheless, our data suggest that next to the neurodegeneration present in the cortical areas, local pathological alterations in the olfactory glomeruli (i.e., structural disintegration) could lead to an olfactory dysfunction in patients with AD. Nonetheless, it remains to be determined whether the pathologies in the olfactory glomerulus precede the cortical deficits or occur simultaneously. Given the fact that olfactory dysfunction occurs prior to the onset of clinical cognitive symptoms, one may suggest that at least distinct neurodegenerative processes may involve cortical and OB degeneration in AD.

We observed Aβ pathology and concomitant Aβ-associated pathologic alterations in the olfactory glomerulus in AD patients. The olfactory glomeruli showed plausible degeneration with Aβ accumulation and microgliosis. These alterations, together with the ultrastructural changes at the level of periglomerular cells that regulate neurotransmission by OSNs, indicate that altered glomerular structural integrity may affect OB function in AD. Remarkably, olfactory glomeruli in AD patients were affected to a greater extent on the ventral side (Fig. 6, Table 3), suggesting that impaired neuronal interactions could initiate OB degeneration in AD. Taken together, damage to the human olfactory glomerulus with a high Aβ burden in AD illustrates the potential phenotypic features for explaining the olfactory dysfunction in AD. These findings may convey a better understanding of the loss of olfactory sensation in AD patient which has received limited attention and propose that a better understanding of the underlying mechanisms of AD.

Table 3. Subregional analysis between AD and normal

Type	Quantifying factors	dorsal OB			ventral OB		
		CTL	AD	CTL vs AD	CTL	AD	CTL vs AD
Anatomy I	glomerular #	1.00	1.58	ns	2.21	2.09	ns
Anatomy II	glomerular area	1.00	0.58	↓ (*)	1.06	0.65	↓ (*)
Pathology I	β-amyloid	1.00	4.62	ns	1.48	11.74	↑ (**)
Pathology II	activated microglia	1.00	1.38	ns	0.90	1.96	↑ (***)
Physiology	tyrosine hydroxylase	1.00	0.62	ns	1.43	0.42	↓ (***)

For the statistical analysis, a two-way ANOVA was performed. Statistical significances are denoted as follows: non-significant (ns); *, $P < 0.05$; **, $P < 0.01$; ***, $P < 0.001$.

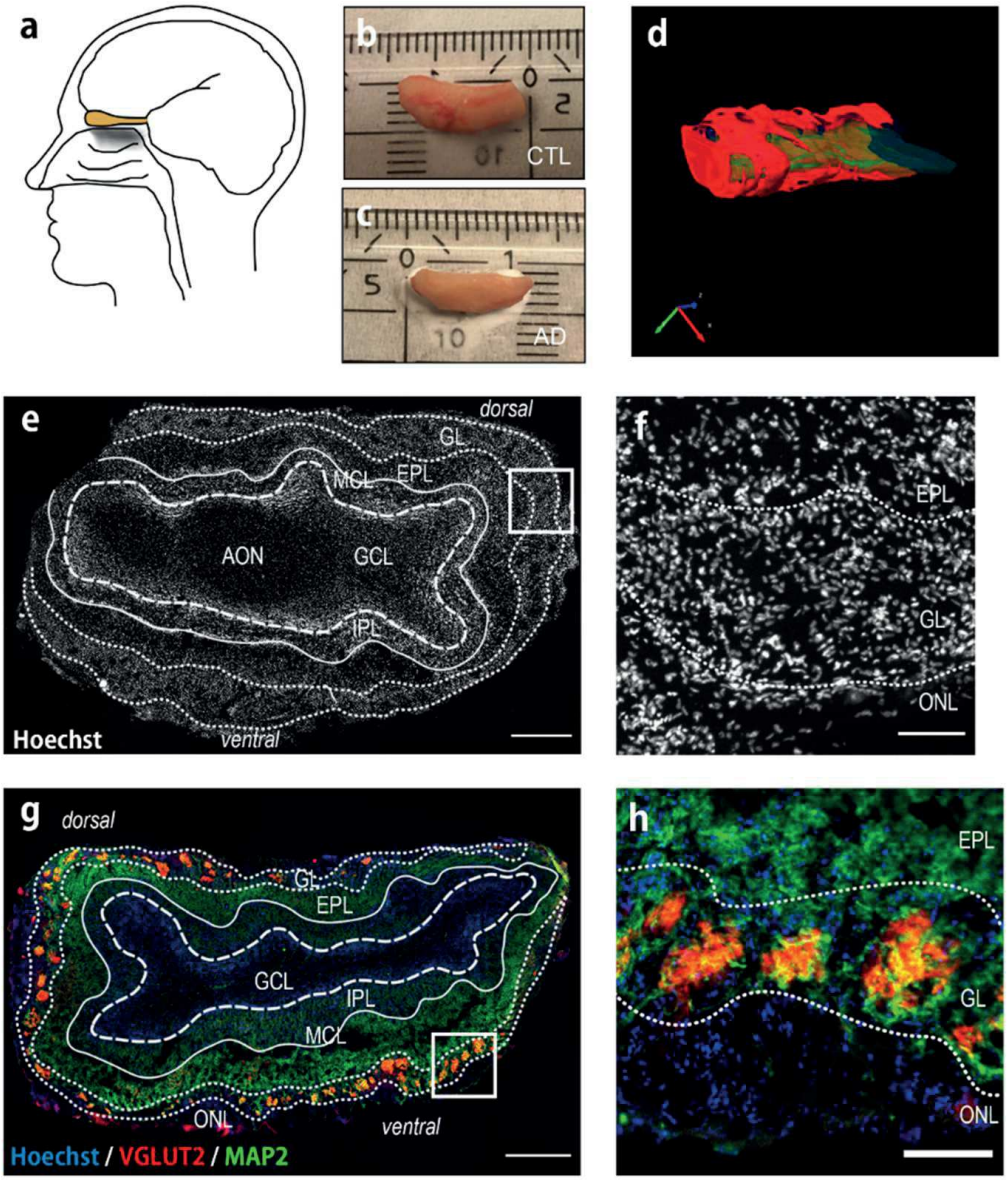

Figure 1. Gross morphology of the human olfactory bulb. Schematic representation of human OB (**a**). An OB specimen obtained from an 80-year-old healthy CTL (**b**), and a specimen obtained from a 73-year-old Alzheimer's disease patient (**c**). Screen shot showing the three-dimensional reconstruction of the human OB (blue: outer boundaries of the OB; red: glomerular layer; green: granule cell layer (**d**). A coronal OB section, stained with Hoechst, showing the laminar organisation of the OB (**e**), scale bar 500 µm. The olfactory glomeruli are shown in a coronal OB section (**f**), scale bar 100 µm. A coronal OB section immunohistochemically stained for MAP2 (green) and VGLUT2 (red) and counterstained with Hoechst stain (blue) showing the distribution of the glomeruli across the OB (**g**), scale bar 500 µm. The neuropil structure of the olfactory glomeruli is shown in a coronal OB section (**h**), scale bar 100 µm. Abbreviations: olfactory bulb (OB), age-matched control (CTL), Alzheimer's Disease (AD), dorsal (D), ventral (V), Anterior (A), Posterior (P), Lateral (L), Median (M), Microtubule associated protein 2 (MAP2), Vesicular glutamatergic protein 2 (VGLUT2).

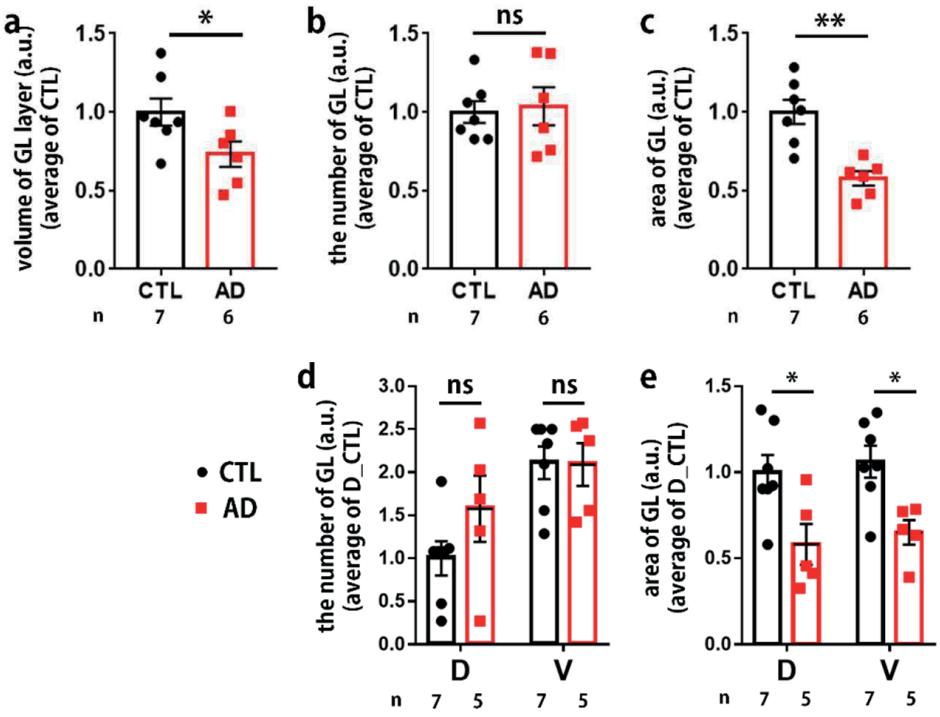

Figure 2. Quantification of structural alterations in the olfactory bulb. Graphs showing the quantification of the structural alterations in the olfactory glomeruli of CTLs and Alzheimer's disease patients (**a-c**). The volume of the glomerular layer (**a**). The num ber of glomeruli (**b**). The cross-sectional area of glomeruli (**c**). The number of glome ruli in the dorsal and ventral OB subregions (**d**). The cross-sectional area of the glo meruli in the dorsal and ventral OB subregions (**e**). In (**a-c**), two-tailed unpaired We lch's t-test was performed; in (**d, e**), two-way ANOVA was performed. Statistical sig nificance: non-significant, (ns); *, $P < 0.05$; **, $P < 0.01$. Abbreviations: olfactory glom erulus (GL), dorsal (D), ventral (V), age-matched control (CTL), Alzheimer's disease (AD), arbitrary unit (au), the number of subjects (n).

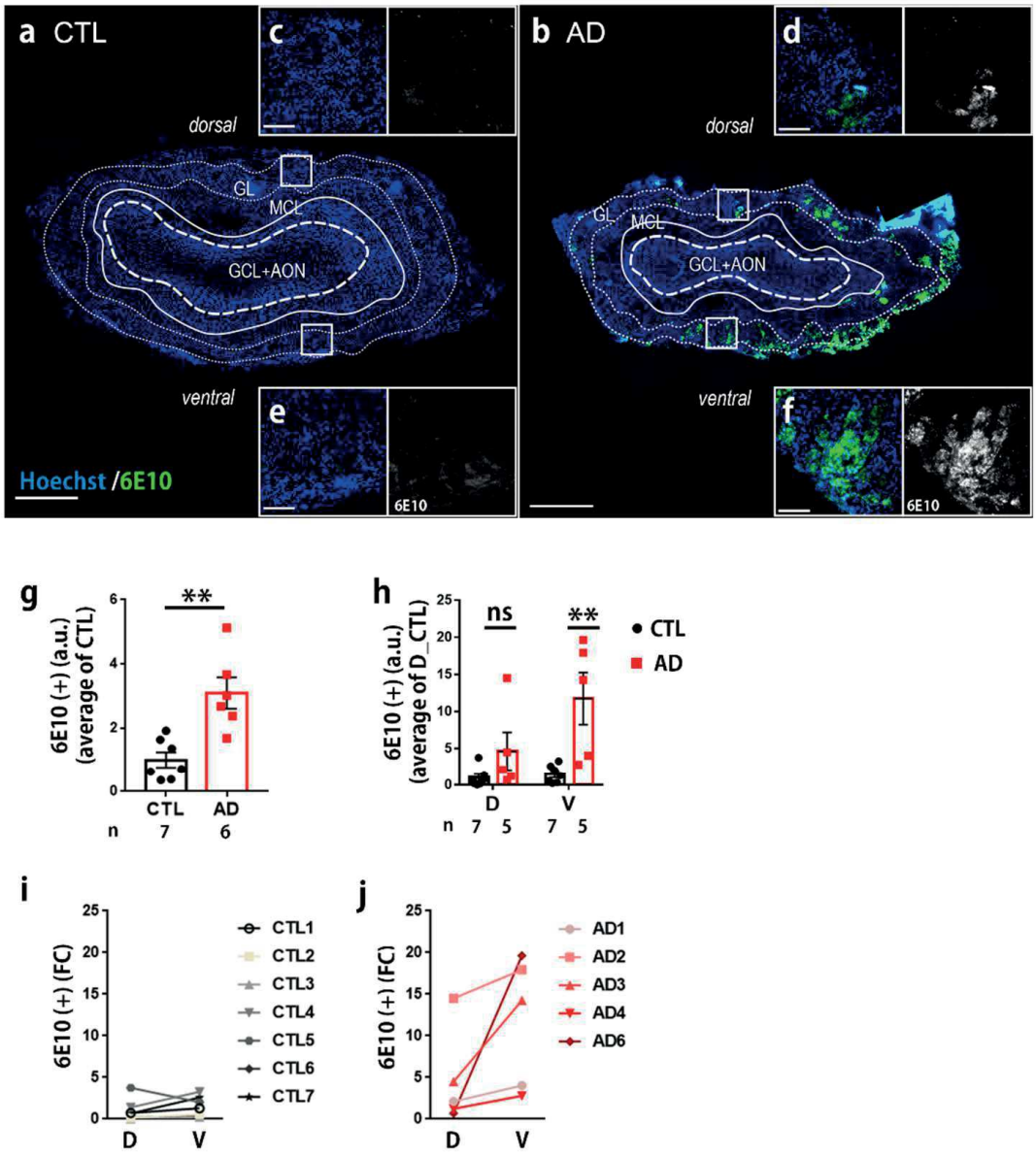

Figure 3. Representative images of coronal olfactory bulb sections immunohistochemically stained for 6E10. Images show Aβ expression in the healthy CTLs (**a**) and Alzheimer's disease patients (**b**). Magnified 6E10 signals in the dorsal olfactory glomeruli (**c-d**) and ventral olfactory glomeruli (**e, f**). Graph showing the quantification of 6E10 expression in the olfactory glomeruli of healthy CTLs and AD patients (**g**). Quantification of the subregional distribution of 6E10 in the dorsal and ventral olfactory glomeruli (**h**). Domain distribution of fold changes in healthy CTLs (**i**) and AD patients (**j**). In graphs (**k**) and (**l**), two-tailed unpaired Welch's t-test and two-way ANOVA were performed, respectively. Scale bar: 500 μm (**a, b**), 250 μm (**c, d, e, f**). Statistical significances: non-significant (ns); *, $P < 0.05$; **, $P < 0.01$. Abbreviations: glomerular layer (GL), mitral cell layer (MCL), granule cell layer (GCL), anterior olfactory nucleus (AON), dorsal (D), ventral (V), age-matched control (CTL), Alzheimer's disease (AD), positive signal (+), arbitrary unit (au), fold change (FC), the number of subjects (n).

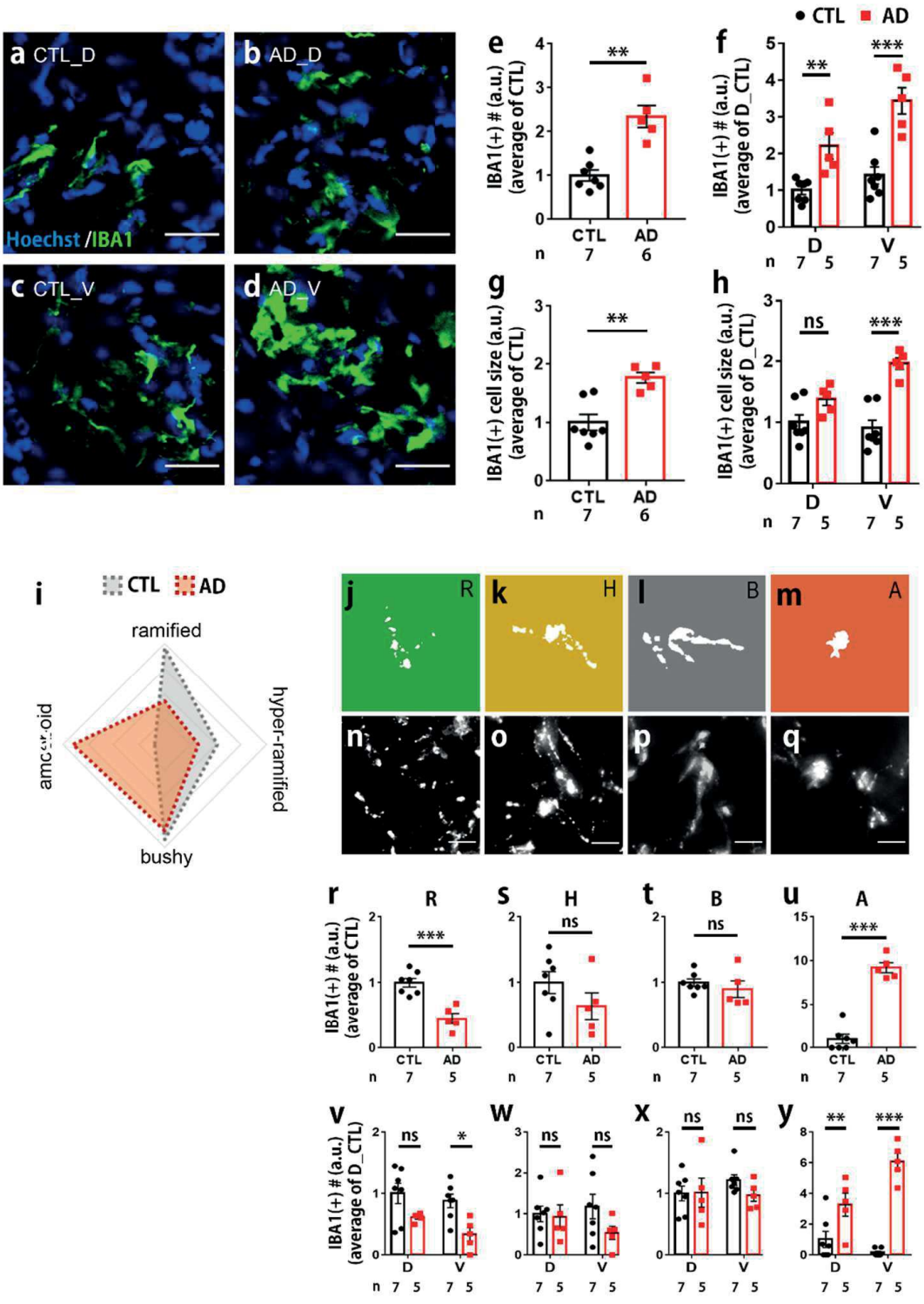
a CTL_D
b AD_D
c CTL_V
d AD_V
Hoechst /IBA1
e
IBA1(+) # (a.u.) (average of CTL)
CTL
AD
n 7 6
f
CTL
AD
IBA1(+) # (a.u.) (average of D_CTL)
D
V
n 7 5 7 5
g
IBA1(+) cell size (a.u.) (average of CTL)
h
IBA1(+) cell size (a.u.) (average of D_CTL)
ns
i
ramified
hyper-ramified
bushy
j R
k H
l B
m A
n
o
p
q
r R
s H
t B
u A
v
w
x
y

Figure 4. Photomicrographs taken from olfactory bulb (OB) sections immunohistochemically stained for IBA1. Images show microglia cells in the OB glomeruli of healthy CTLs and Alzheimer's disease patients (**a-d**). Graphs showing quantitative data pertaining to the number (**e**), dorsal vs ventral distribution (**f**), and size (**g**) of the IBA-1 positive microglial cells in the OB of healthy CTLs vs AD patients. The size of the IBA1-positive microglial cells in the dorsal vs ventral OB (**h**). Distribution of microglial with different morphology in olfactory glomeruli of healthy CTLs and AD patients (**i**). Different types of microglial morphology in the human olfactory glomerulus (**j-q**). Quantitative data pertaining to the number of microglia with ramified (**r**), hyper-ramified microglia (**s**) bushy (**t**), and amoeboid (**u**) morphology in the OB of healthy CTLs vs AD patients. Graphs "**v-y**" show quantitative distributing of the ramified (**v**), hyper-ramified (**w**), bushy (**x**), and amoeboid (**y**) microglia in the dorsal vs ventral glomeruli in the OB of healthy CTLs and AD patients. Scale bar 25 μm (**a-d**), 10 μm (**n-q**). In (**e**), (**g**), and (**r-u**), two-tailed unpaired Welch's t-test was performed; and in (**f**), (**h**), and (**v-y**), two-way ANOVA was performed. Statistical significances: non-significant (ns); *, $P < 0.05$; **, $P < 0.01$; ***, $P < 0.001$. Abbreviations: dorsal (D), ventral (V), age-matched control (CTL), Alzheimer's disease (AD), ramified (R), hyper-ramified (H), bushy (B), amoeboid (A), the number of subjects (n).

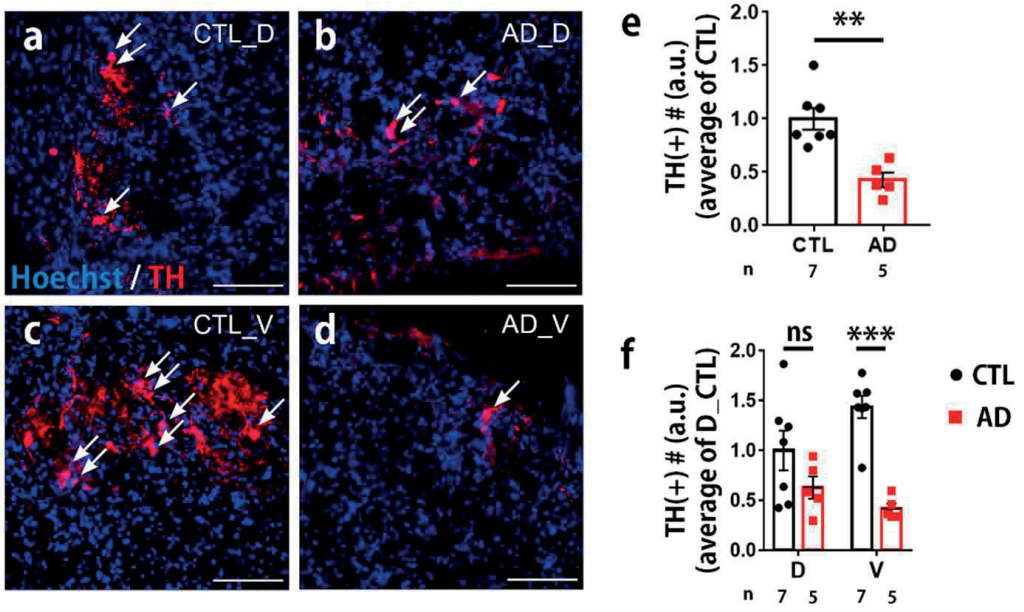

Figure 5. Photomicrographs of olfactory bulb (OB) sections immunohistochemically stained for tyrosine hydroxylase (TH). Photomicrographs taken of the olfactory bulb (OB) sections immunohistochemically stained for TH. Images show the TH-positive cells in the OB glomeruli of healthy CTLs and AD patients (**a-d**). The graph shows the quantification of TH expression in the olfactory glomeruli of healthy CTLs and AD patients (**e**). Graphs show the quantitative data pertaining to the number and dorsal/ventral distribution of TH-positive periglomerular cells in the OB of healthy CTLs and AD patients (**f**). Scale bar 100 μm. Graphs "**e, f**" two-tailed unpaired Welch's t-test and two-way ANOVA were performed, respectively. Statistical significances: non-significant (ns); **, $P < 0.01$; ***, $P < 0.001$. Abbreviations: dorsal (D), ventral (V), age-matched control (CTL), Alzheimer's disease (AD), the number of subjects (n).

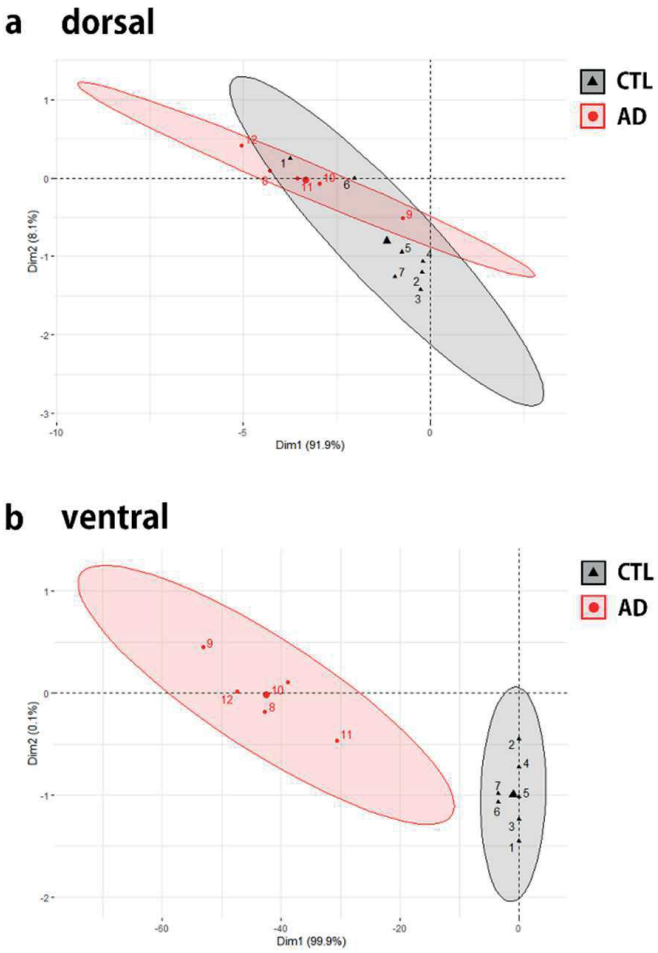

Figure 6. Principal component analysis (PCA) plot of distinct pathological factors in the dorsal and ventral glomeruli of the olfactory bulb (OB). PCA plot of distinct pathological factors in the dorsal (**a**) and ventral (**b**) glomeruli of the olfactory bulb (OB) in healthy CTLs and Alzheimer's disease patients. Unit variance scaling was applied to rows, and singular value decomposition (SVD) with imputation was used to calculate principal components. X and Y axis show principal component 1 and 2 which explain (a) 91.9%, (b) 8.1% and (a) 99.9%, (b) 0.1% of the total variance, respectively. Prediction ellipses exhibit 0.95 probability. n = 7 (CTL), 5 (AD) data points. Abbreviations: age-matched control (CTL), Alzheimer's disease (AD).

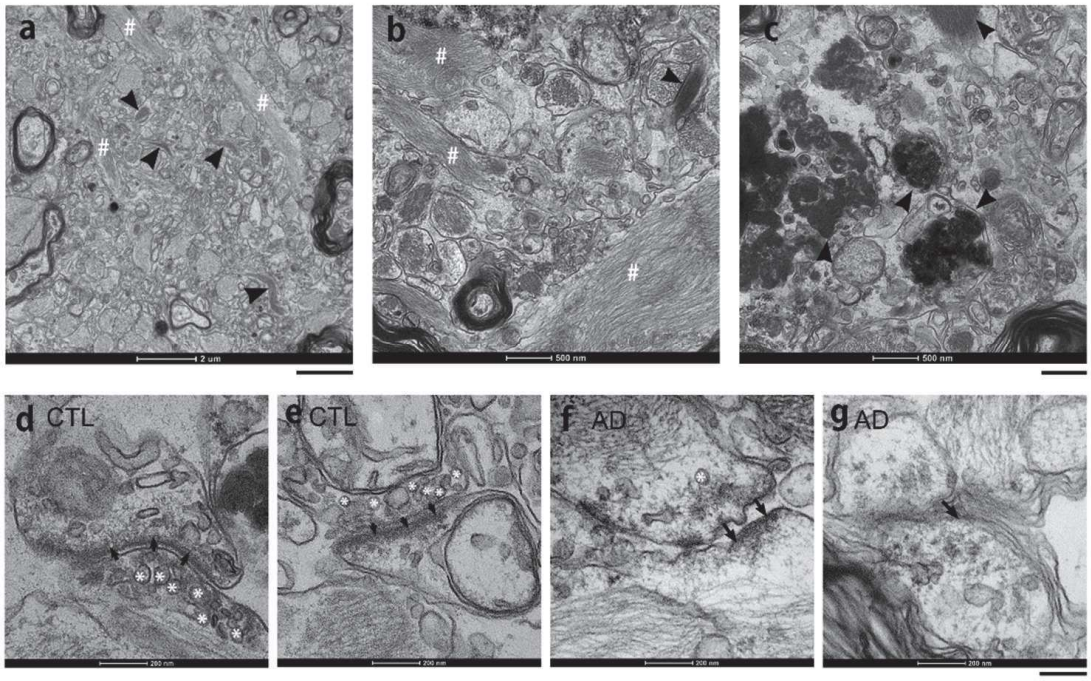

Figure 7. The ultrastructure of the olfactory glomerulus. The ultrastructure of the olfactory glomerulus in Alzheimer's disease (a-c). Arrowheads indicate neuropil threads typical in Alzheimer's dendrites showing constricted filaments (a-c). Sharp lines appear as slightly constricted filaments in neuropil threads in AD dendrites (a, b). Arrowheads in (c) indicate highly constricted filaments giving the appearance of dense bodies. The ultrastructure of synapse in the olfactory glomerulus in CTLs (d, e) and AD (f, g). White asterisks indicate synaptic vesicles and black arrows indicate postsynaptic density (d, e). Scale bar 2 μm (a), 500 nm (b, c), 200 nm (d-g). Abbreviations: age-matched control (CTL), Alzheimer's disease (AD).

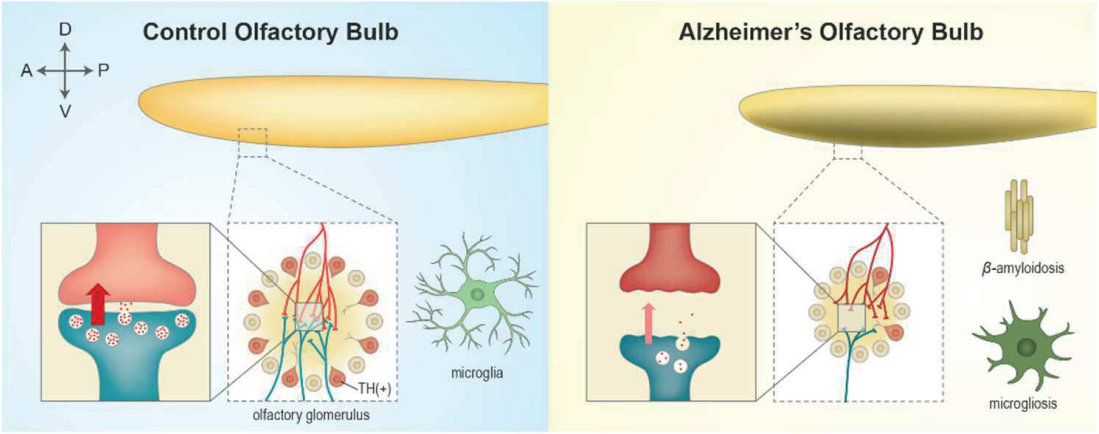

Figure 8. Alterations in human olfactory glomeruli with high β-amyloid burden in Alzh eimer's disease. Abbreviations: dorsal (D), ventral (V), anterior (A), posterior (P), olf actory bulb (OB), tyrosine hydroxylase (TH), Alzheimer's disease (AD).

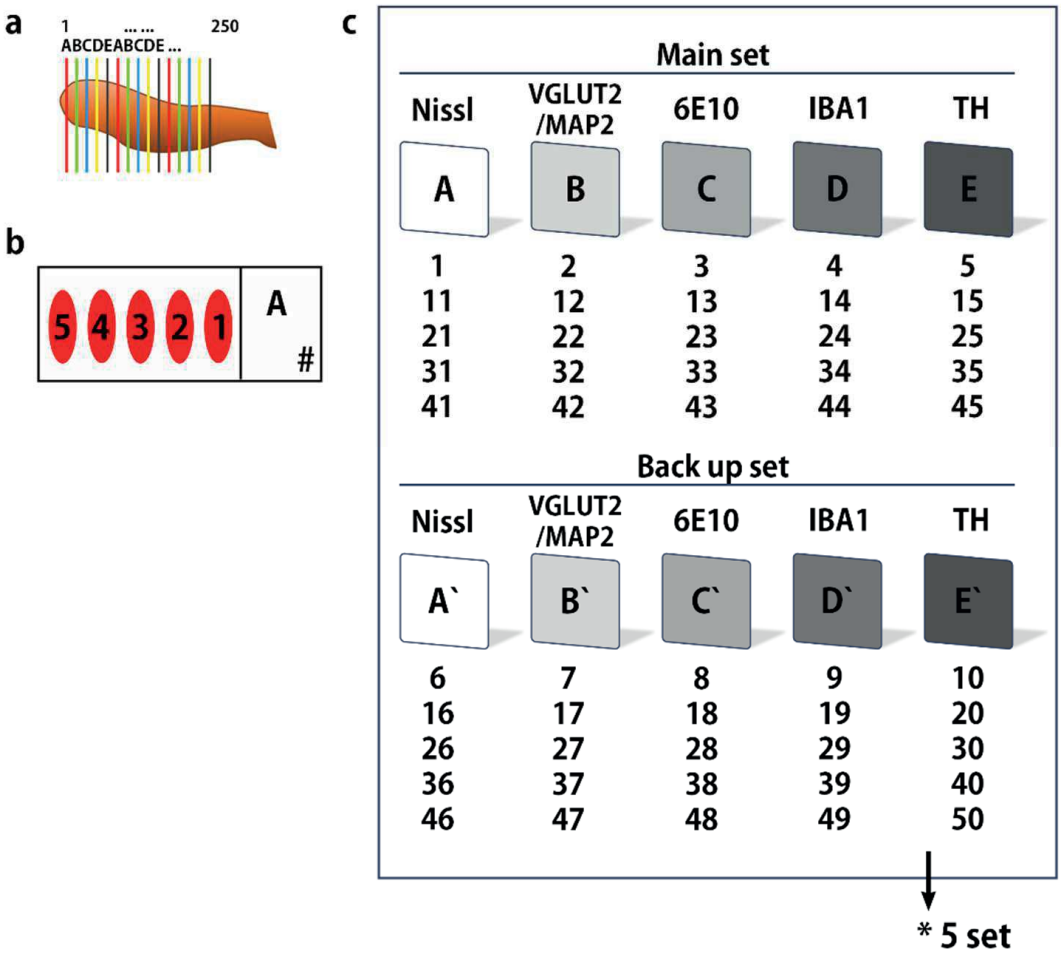

Figure S1. Stereological histology experimental scheme. (a) Section scheme of human olfactory bulb. (b) Example of specimen section slide glass. Every 10th section was aligned by serial. A set number and a caption mark were labelled. (c) Summary of stereological histology experimental scheme. A normal postmortem olfactory bulb had approximately five sets of slide glass, a set composed 10 slide glasses. First five glasses were considered as a group of main slides and other five slides were a group of back-up slides. A slide glass had five olfactory bulb specimen sections. Captions (A-E) are corresponded to immune and/or chemical markers.

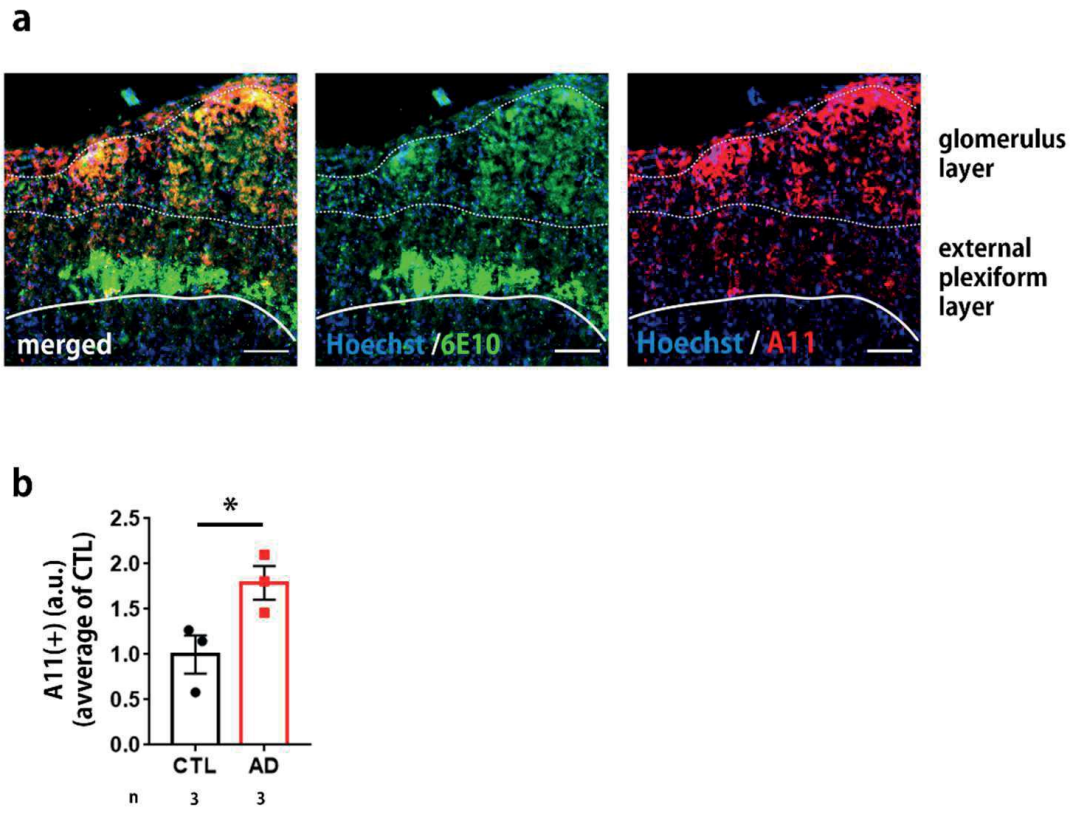

Figure S2. Distribution of oligomeric Aβ immunohistochemistry in the human olfactory bulb. (a) Immunofluorescence for localization of 6E10 and A11, (green) 6E10, (red) A11, (blue) Hoechst. (b) Ratio of A11 immunoreactivity in olfactory glomerulus. Scale bar 100 μm. In (b), two-tailed unpaired t-test was performed. Statistical significances are denoted as follows: *, $P < 0.05$. Abbreviations: age-matched control (CTL), Alzheimer's disease (AD).

Acknowledgments

The authors are grateful to Mrs. Hellen Steinbusch for her support for immunohistology and microscopy and to the members of the Microscopy CORE Lab of the Faculty of Health, Medicine and Life Sciences of Maastricht University for their support with electron microscopy. This work was supported by research grant from the KBRI basic research program through Korea Brain Research Institute funded by the Ministry of Science and ICT (18-BR-04-01) and Basic Science Research Program through the National Research Foundation of Korea (NRF) funded by the Ministry of Education (2020R1A6A1A03040516). The funding sources had no such involvement in study design; in the collection, analysis and interpretation of data; in the writing of the report; and in the decision to submit the article for publication.

References

1. Alzheimer's-Association, 2021 Alzheimer's disease facts and figures. *Alzheimers Dement*, (2021).
2. C. Murphy, Olfactory and other sensory impairments in Alzheimer disease. *Nat Rev Neurol* **15**, 11-24 (2019).
3. D. A. Espiritu *et al.*, Depression, cognitive impairment and function in Alzheimer's disease. *Int J Geriatr Psychiatry* **16**, 1098-1103 (2001).
4. K. Duff, R. J. McCaffrey, G. S. Solomon, The Pocket Smell Test: successfully discriminating probable Alzheimer's dementia from vascular dementia and major depression. *J Neuropsychiatry Clin Neurosci* **14**, 197-201 (2002).
5. R. S. Wilson, S. E. Arnold, J. A. Schneider, Y. Tang, D. A. Bennett, The relationship between cerebral Alzheimer's disease pathology and odour identification in old age. *J Neurol Neurosurg Psychiatry* **78**, 30-35 (2007).
6. H. B. Treloar, P. Feinstein, P. Mombaerts, C. A. Greer, Specificity of glomerular targeting by olfactory sensory axons. *J Neurosci* **22**, 2469-2477 (2002).
7. E. E. Morrison, R. M. Costanzo, Morphology of the human olfactory epithelium. *J Comp Neurol* **297**, 1-13 (1990).
8. J. Tan, A. Savigner, M. Ma, M. Luo, Odor information processing by the olfactory bulb analyzed in gene-targeted mice. *Neuron* **65**, 912-926 (2010).
9. R. Vassar *et al.*, Topographic organization of sensory projections to the olfactory bulb. *Cell* **79**, 981-991 (1994).
10. D. A. Storace, L. B. Cohen, Measuring the olfactory bulb input-output transformation reveals a contribution to the perception of odorant concentration invariance. *Nat Commun* **8**, 81 (2017).
11. L. Cao *et al.*, Abeta alters the connectivity of olfactory neurons in the absence of amyloid plaques in vivo. *Nat Commun* **3**, 1009 (2012).
12. J. J. Palop, L. Mucke, Amyloid-beta-induced neuronal dysfunction in Alzheimer's disease: from synapses toward neural networks. *Nat Neurosci* **13**, 812-818 (2010).
13. F. Kamenetz *et al.*, APP processing and synaptic function. *Neuron* **37**, 925-937 (2003).
14. H. Hsieh *et al.*, AMPAR removal underlies Abeta-induced synaptic depression and dendritic spine loss. *Neuron* **52**, 831-843 (2006).
15. H. Sarlus, M. T. Heneka, Microglia in Alzheimer's disease. *J Clin Invest* **127**, 3240-3249 (2017).
16. T. Wyss-Coray, L. Mucke, Inflammation in neurodegenerative disease--a double-edged sword. *Neuron* **35**, 419-432 (2002).
17. S. E. Arnold *et al.*, Olfactory epithelium amyloid-beta and paired helical filament-tau pathology in Alzheimer disease. *Ann Neurol* **67**, 462-469 (2010).
18. P. Bathini, A. Mottas, M. Jaquet, E. Brai, L. Alberi, Progressive signaling changes in the olfactory nerve of patients with Alzheimer's disease. *Neurobiol Aging* **76**, 80-95 (2019).
19. H. Baker, T. Kawano, F. L. Margolis, T. H. Joh, Transneuronal regulation of tyrosine hydroxylase expression in olfactory bulb of mouse and rat. *J Neurosci* **3**, 69-78 (1983).
20. D. R. Thal, U. Rub, M. Orantes, H. Braak, Phases of A beta-deposition in the human brain and its relevance for the development of AD. *Neurology* **58**, 1791-1800 (2002).
21. V. M. Golub *et al.*, Neurostereology protocol for unbiased quantification of neuronal injury and neurodegeneration. *Front Aging Neurosci* **7**, 196 (2015).
22. F. T. Crews, C. J. Lawrimore, T. J. Walter, L. G. Coleman, Jr., The role of neuroimmune signaling in alcoholism. *Neuropharmacology* **122**, 56-73 (2017).
23. X. Zhao *et al.*, Noninflammatory Changes of Microglia Are Sufficient to Cause

Epilepsy. *Cell Rep* **22**, 2080-2093 (2018).
24. W. Shi *et al.*, Ontogenetic establishment of order-specific nuclear organization in the mammalian thalamus. *Nat Neurosci* **20**, 516-528 (2017).
25. F. Fortunato, T. Hackert, M. W. Buchler, G. Kroemer, Retrospective electron microscopy: Preservation of fine structure by freezing and aldehyde fixation. *Mol Cell Oncol* **3**, e1251382 (2016).
26. H. Yamaguchi, Y. Nakazato, M. Shoji, Y. Ihara, S. Hirai, Ultrastructure of the neuropil threads in the Alzheimer brain: their dendritic origin and accumulation in the senile plaques. *Acta Neuropathol* **80**, 368-374 (1990).
27. S. Nagayama, R. Homma, F. Imamura, Neuronal organization of olfactory bulb circuits. *Front Neural Circuits* **8**, 98 (2014).
28. M. Wachowiak *et al.*, Inhibition [corrected] of olfactory receptor neuron input to olfactory bulb glomeruli mediated by suppression of presynaptic calcium influx. *J Neurophysiol* **94**, 2700-2712 (2005).
29. G. Son *et al.*, Region-specific amyloid-beta accumulation in the olfactory system influences olfactory sensory neuronal dysfunction in 5xFAD mice. *Alzheimers Res Ther* **13**, 4 (2021).
30. J. H. Coleman *et al.*, Spatial Determination of Neuronal Diversification in the Olfactory Epithelium. *J Neurosci* **39**, 814-832 (2019).
31. F. G. Morrison, B. G. Dias, K. J. Ressler, Extinction reverses olfactory fear-conditioned increases in neuron number and glomerular size. *Proc Natl Acad Sci U S A* **112**, 12846-12851 (2015).
32. B. Zapiec *et al.*, A ventral glomerular deficit in Parkinson's disease revealed by whole olfactory bulb reconstruction. *Brain* **140**, 2722-2736 (2017).
33. R. L. Doty, The olfactory vector hypothesis of neurodegenerative disease: is it viable? *Ann Neurol* **63**, 7-15 (2008).
34. G. Son *et al.*, Olfactory neuropathology in Alzheimer's disease: a sign of ongoing neurodegeneration. *BMB Rep* **54**, 295-304 (2021).
35. A. Nimmerjahn, F. Kirchhoff, F. Helmchen, Resting microglial cells are highly dynamic surveillants of brain parenchyma in vivo. *Science* **308**, 1314-1318 (2005).
36. K. Young, H. Morrison, Quantifying Microglia Morphology from Photomicrographs of Immunohistochemistry Prepared Tissue Using ImageJ. *J Vis Exp*, (2018).
37. J. Frackowiak *et al.*, Ultrastructure of the microglia that phagocytose amyloid and the microglia that produce beta-amyloid fibrils. *Acta Neuropathol* **84**, 225-233 (1992).
38. I. Benilova, E. Karran, B. De Strooper, The toxic Abeta oligomer and Alzheimer's disease: an emperor in need of clothes. *Nat Neurosci* **15**, 349-357 (2012).
39. I. Ubeda-Banon *et al.*, The human olfactory system in two proteinopathies: Alzheimer's and Parkinson's diseases. *Transl Neurodegener* **9**, 22 (2020).
40. T. Bartels, S. De Schepper, S. Hong, Microglia modulate neurodegeneration in Alzheimer's and Parkinson's diseases. *Science* **370**, 66-69 (2020).
41. N. L. Rey, D. W. Wesson, P. Brundin, The olfactory bulb as the entry site for prion-like propagation in neurodegenerative diseases. *Neurobiol Dis* **109**, 226-248 (2018).

Chapter 6

Longitudinal profiling of oligomeric Aβ in human nasal discharge reflecting cognitive decline in probable Alzheimer's disease

Seung-Jun Yoo[1,2,*], **Gowoon Son**[1,*], Jisub Bae[1],
So Yeun Kim[1,2] Yong Kyoung Yoo[3], Dongsung Park[3],
Seung Yeop Baek[4], Keun-A Chang[5], Yoo-Hun Suh[5], Yeong-Bae Lee[6],
Kyo Seon Hwang[3], YoungSoo Kim[4], Cheil Moon[1,2,*.]

[Scientific Reports, 2020, doi: 10.1038/s41598-020-68148-2]

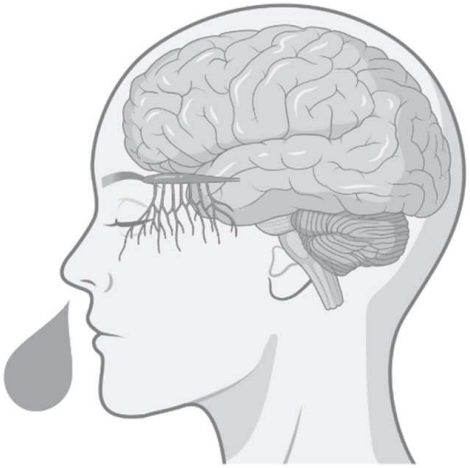

Abstract

Despite clinical evidence indicating a close relationship between olfactory dysfunction and Alzheimer's disease (AD), further investigations are warranted to determine the diagnostic potential of nasal surrogate biomarkers for AD. In this study, we first identified soluble amyloid-β (Aβ), the key biomarker of AD, in patient nasal discharge using proteomic analysis. Then, we profiled the significant differences in Aβ oligomers level between patient groups with mild or moderate cognitive decline (n = 39) and an age-matched normal control group (n = 21) by immunoblot analysis and comparing the levels of Aβ by a self-standard method with interdigitated microelectrode sensor systems. All subjects received the Mini-Mental State Examination (MMSE), Clinical Dementia Rating (CDR), and the Global Deterioration Scale (GDS) for grouping. We observed higher levels of Aβ oligomers in probable AD subjects with lower MMSE, higher CDR, and higher GDS compared to the normal control group. Moreover, mild and moderate subject groups could be distinguished based on the increased composition of two oligomers, 12-mer Aβ*56 and 15-mer AβO, respectively. The longitudinal cohort study confirmed that the cognitive decline of mild AD patients with high nasal discharge Aβ*56 levels advanced to the moderate stage within three years. Our clinical evidence strongly supports the view that the presence of oligomeric Aβ proteins in nasal discharge is a potential surrogate biomarker of AD and an indicator of cognitive decline progression.

List of abbreviations

AD, Alzheimer's disease; CDR, clinical dementia rating; Aβ, amyloid-β; $A\beta_{42}$, amyloid-β 1–42 peptide; CSF, cerebrospinal fluid; ELISA, enzyme-linked immunosorbent assay; GDS, global deterioration scale; HRP, horseradish peroxidase; MDS, multimer detection system; MMSE, mini mental state examination; MRI, magnetic resonance imaging; PBS, Phosphate-buffered saline; RLU, relative light/luminescence units; TBST, Tris-buffered saline with Tween 20.

Keywords

amyloid-β oligomer; Alzheimer's disease; biomarker; cognitive decline; dementia; nasal discharges

1. Introduction

Alzheimer's disease (AD) is the most common type of dementia characterized by progressive cognitive decline and the accumulation of the both amyloid-β (Aβ) plaques and tau neurofibrillary tangles in the brain. The diagnosis of AD requires pathological observations in the central nervous systems (*1-7*). However, current diagnostic methods are not for routine measurements to consider the reliability of diagnosis. In addition, accessing brain tissues and cerebrospinal fluid is invasive and positron emission tomography exposes subjects to radioactive tracers. Although blood is considered one of the most promising fluid biomarker candidates for AD, this approach still has to overcome critical issues, such as low concentrations (e.g. p-tau: ~ pg/ml) (*8*), plasma stability, blood-brain barrier penetration of key protein biomarkers to be used for primary diagnosis and prognosis.

Fluid biomarkers within the peripheral nervous systems could be an excellent solution to avoid limitations utilizing cerebrospinal fluid and blood. The olfactory system, in particular the olfactory epithelium, has unique amyloid precursor protein (APP) - processing mechanisms. The olfactory epithelium (OE) has unusual secretases expression compare to CNS, and distinct increased expression of presenilin 1 and 2 (γ-secretase) under pathological conditions (*9*). Olfactory dysfunction is often observed concurrently with or prior to cognitive impairment in AD and other dementia based on epidemiological evidence (~90%)(*10-12*). In particular, the high prevalence of olfactory dysfunction among AD patients indicates

a possible correlation between olfactory deficits and AD pathogenesis (i.e., the expression of Aβ in the olfactory tissue)(*13-16*).

Based on this clinical and experimental evidence, we hypothesized that nasal discharge could be a candidate to monitor pathophysiological changes in the olfactory system during neurodegeneration that may result in AD. Our previous animal study supports the hypothesis by reporting that specific oligomeric Aβ (Aβ*56 and AβO) was existed in the olfactory epithelium at different progression stages of AD with evident cognitive impairment in AD transgenic mice; Tg2576, a Swedish mutant form of human amyloid precursor protein (APP) (KM670 / 671NL) (promoter: hamster prion protein (PrP)))(*16*). In addition, there are previous studies that prove that there is a direct linkage pathway between CSF and olfactory systems that directly reflect alterations occurring in the CNS, and there are also previous studies in which biomarkers of CSF are found in olfactory mucosa. Taking all possibilities together, nasal discharge may contain a wide assortment of proteins released from damaged olfactory sensory neurons or outflow of CSF through the cribriform plate under pathological condition (*17-19*).

In this study, we obtained nasal discharge samples from both the probable AD group and the age-matched normal control group and examined the presence of Aβ in the nasal discharge and determined the type of Aβ oligomers specific to the patient group. Then, we demonstrated that Aβ was expressed in the nasal discharge from AD patients by liquid chromatography-mass spectrometry (LC-MS) and that changes

in the oligomeric Aβ composition in the nasal discharge were correlated with cognitive decline among the patient groups by immunoblot analysis. We also identified the expression patterns of oligomeric Aβ species in patients with different stages of cognitive dysfunction by immunoassays and comparing the levels of Aβ by a self-standard (CLASS) method to measure the self-standard ratio defined the value of the impedance change in the monomerized sample divided by intact sample with interdigitated microelectrode (IME) sensor systems (*20*). Lastly, we assessed alterations in two specific types of oligomeric Aβ levels in nasal discharges in three-year longitudinal cohorts.

2. Materials and methods

2.1. Group selection criteria

Patient criteria in this study followed the NINCDS/ADRDA of the American Psychiatric Association criteria for the diagnosis of probable AD (*1, 21-23*).

Briefly, samples from the patients were divided into three groups based on the following criteria. Patients with probable AD was selected according to the following criteria: (1) predominant and progressive episodic memory impairment characterized by low free recall, not normalized to cueing and not associated with other cognitive deficits; and (2) scores of the MMSE, the CDR, and the GDS tests that are commonly applied to measure the severity of dementia from various causes (*1, 2, 21*). All tests of cognitive ability were analyzed as previously described (*24*). Briefly, the Korean version of the MMSE is comprised of tests of orientation (10

points), short-term memory registration and recall (6 points), attention (5 points), naming (2 points), following verbal commands (4 points), judgment (2 points), and copying a double pentagon (1 point). The CDR scale is a structured interview of the subject and informant in which the subjects are rated by scores of 0 (asymptomatic), 0.5 (equivocal or mild impairment), 1, 2 or 3 (mild, moderate, or severe dementia, respectively). The normal group had MMSE scores greater than 27 and normal scores in the memory section of the MMSE. The probable AD patient group had scores of 24 or less on the MMSE and CDR scores (1) greater than 1 or (2) 0.5 with box score sums greater than 2.5. The GDS scale is one of the most popular scales for the evaluation of depression symptoms in older adults. In the long form, a score is considered normal if it is between 0 and 0.9. An indicator of mild depression is between 1.0 and 1.9 and a positive score for severe depression is between 2.0 and 3.0. Patients with other neurodegenerative diseases, such as Parkinson's disease; cerebral vascular disease (which may affect cognitive function); metabolic derangement, including thyroid disease, a history of alcohol or medication poisoning; or a history of trauma or neuropsychiatric disease were excluded from the current study.

2.2. Measurement of Aβ levels in nasal discharge using an IME sensor (an impedimetric biosensor with an interdigitated microelectrode structure)

An IME biosensor with 30 pairs of interdigitated microelectrodes with 5 μm-wide gaps was utilized for this analysis (*25, 26*). The gap surface was functionalized with 6E10 antibodies to capture the Aβ protein from nasal discharge samples. The

fabrication, antibody immobilization, and detection procedures are described in our previous study [27]. When a specific interaction occurred between 6E10 on the sensor surface and an Aβ peptide, the impedance value between the interdigitated microelectrodes was altered because the Aβ protein occupied the space instead of the fluid. To perform the CLASS method, the nasal discharge samples were aliquoted into two samples. For measuring the EPPS-treated sample and PBS-added sample, 40μL of each sample was used. One sample was incubated for 30 min with 500 mM EPPS [4-(2-hydroxyethyl)-1-piperazinepropanesulfonic acid] dissolved in phosphate-buffered saline (PBS) (nasal discharge sample: EPPS, 4:1) and the other sample was treated the same with the exclusion of EPPS. The prepared nasal discharge sample was injected onto individual IME devices, incubated for 20 min, and washed with PBS buffer. Then, the impedance of 6E10-immobilized IME before (Z_{before}) and after (Z_{after}) the reaction of nasal discharge containing Aβ proteins was measured. The impedance of the impedimetric biosensors was measured using commercial equipment (PGSTAT302N, Metrohm Autolab, Utrecht, The Netherlands; & IME Sensor, Cantis Corporation, Ansan, Korea). The impedance change was used to quantify the Aβ levels in nasal discharge which was defined by the equation below.

$$Impedance\ change\ (\%) = \left|\frac{Z_{after} - Z_{before}}{Z_{before}}\right| * 100$$

The self-standard ratio defined the value of the impedance change in the EPPS-treated sample (monomerized) divided by the impedance change in the PBS buffer-added sample.

2.3. Statistical analysis

The results were presented as mean ± SEM. Value of samples were identified as outliers through Grubbs' test, also called the ESD method. The Kolmogorov-Smirnov test, paired t-test, one-way analysis, and two-way RMANOVA of variance were used to assess the normality of the data. The nonparametric Spearman's rank correlation test was used to assess correlations between the data. The graphs revealed regression lines with a 95% confidence interval. P-values of < 0.05 were considered significant. Cognitive function changes were measured by MMSE and GDS scores over three years in AD subjects, defined by the equation below. (h = MMSE score or GDS score, L = year)

$$Slope = \frac{h_3 - h_1}{L_3 - L_1}$$

2.4. Study approval

The Institutional Review Boards (IRB) of Gachon University Gil Medical Center [GAIRB2013-264] approved the study protocol. All subjects provided written informed consent before participating via self-referral or referral from their family.

2.5. Nasal discharge collection and processing

Nasal discharge samples from 60 donors were analyzed. Twenty additional samples were collected but excluded from the analysis due to insufficient protein concentration (n = 8) or insufficient sample for three independent WB and IME sensor analyses (n = 12). Age-matched normal subjects (n = 21) and patients with probable AD (n = 39) were also assessed. The details of each group are presented in Table 1.

The whole nasal discharges were pooled (> 1.5 ml) in a microtube and immediately sonicated for 10 – 15 s, followed by centrifugation (10,000xg for 10 min at 4°C) to remove cells and cellular debris. A Protease Inhibitor Cocktail was added to the supernatants (Roche, Mannheim, Germany), which were immediately stored at -80 °C until analysis. Nasal discharge aliquots were thawed on the day of the experiment.

2.6. Liquid chromatography-mass spectrometry/mass spectrometry (LC-MS/MS) analysis

The immunoprecipitation and immunoblots was modified and performed as described previously (27). For immunoprecipitation, aliquots of human nasal discharge samples (300 µl) were pre-cleared with 30 µl of Protein-G Fast Flow Sepharose (GE Healthcare Life Sciences, Uppsala, Sweden) for 1 h at 4 °C, then centrifuged at 9300g for 5 min. Subsequently, 250 µl of immunoglobulin-depleted nasal discharge was incubated with 1 µg of 6E10 antibodies (6E10, Covance, Princeton, NJ, USA) and 50 µl of Protein-G coated magnetic beads (Life Technologies, CA, USA) overnight at 4 °C. The beads were washed sequentially with immunoprecipitation buffer A [50 mM Tris-HCl, 300 mM NaCl, 0.1% Triton X-100 (v/v), 1 mM EDTA, pH 7.4] and immunoprecipitation buffer B [50 mM Tris-HCl, 150 mM NaCl, 0.1% Triton X-100 (v/v), 1 mM EDTA, pH 7.4] for 20 min under gentle agitation at 4 °C. Next, the captured proteins were eluted and digested with trypsin. Initially, sample reduction was conducted using 20 mM dithiothreitol for 1 hour and alkylated with 55 mM iodoacetamide for 45 min. Trypsin digestion was carried out

overnight using mass spectrometry-grade TPCK-treated small trypsin (ABSciex, Framingham, MA, USA). The stabilized, digested peptides were extracted and lyophilized. Before LC-MS / MS analysis, the peptide samples were resuspended in 10 µl of 1% formic acid.

Prior to mass spectrometry, the peptides were separated using EasynLCII (Bruker Daltonics, Bremen, Germany) nano high-performance liquid chromatography (HPLC) for intervals of at least 60 minutes after using water/acetonitrile gradient with increases in acetonitrile concentrations from 0 to 100% for 90 minutes. The peptide mixture was desorbed on a Zorbax 300SB-C18 analytical column (150 mm x 75 µm 3.5 µm pore size, Agilent, Santa Clara, CA, USA) after desalination on a Zorbax 300SB-C18 inline trap column (5 x 0.3 mm, 5 µm pore size, Agilent). Solvent A was 0.1% formic acid in LC/MS Grade water, solvent B was LC/MS Grade acetonitrile containing 0.1% formic acid, and the flow rate was 300 nl/min.

The obtained LC-MS/MS data were used to search for matches in the SwissProt database (release: 2015.07, 548872 sequence item) using the ProteinPilot 4.0 (AB SCIEX, Framingham, MA) search engine and to identify proteins using the biological variation tables included in the ProteinPilot 4.0 software (Fig. S1A).

2.7. Immunoprecipitation and immunoblots

The immunoprecipitation and immunoblots was modified and performed as described previously (*28*). For immunoprecipitation with 6E10 and immunoblotting with the A11 antibody, aliquots of the samples (100 µl) were pre-cleared with 30 µl of a 1:1 slurry with Protein-G Fast Flow Sepharose (GE Healthcare Life Sciences, Uppsala, Sweden) for 1 h at 4 °C, then centrifuged at 9300g for 5 min. Subsequently, 250 µl of immunoglobulin-depleted nasal discharge was incubated with 0.1 µg of 6E10 antibodies and 50 µl of Protein-G coated magnetic beads (Life Technologies, CA, USA) overnight at 4 °C. The beads were washed sequentially with immunoprecipitation buffer A [50 mM Tris-HCl, 300 mM NaCl, 0.1% Triton X-100 (v/v), 1 mM EDTA, pH 7.4] and immunoprecipitation buffer B [50 mM Tris-HCl, 150 mM NaCl, 0.1% Triton X-100 (v/v), 1 mM EDTA, pH 7.4] for 20 min under gentle agitation at 4 °C. The captured proteins were eluted with SDS-sample buffer. The proteins were separated by sodium dodecyl sulfate-polyacrylamide gel electrophoresis and transferred to a 0.45-µm polyvinylidene difluoride membrane (Millipore, Temecula, CA, USA). The membranes were blocked with 5% non-fat dry milk in Tris-buffered saline with 0.1% Tween 20 and then incubated with primary A11 (Invitrogen, Carlsbad, CA, USA) antibodies for oligomerized Aβ proteins and 6E10 (Covance, Princeton, NJ, USA) for total Aβ proteins.

For immunoblotting with the A11, D54D2 and 6E10 antibody, the nasal discharge was thawed and the proteins were quantified by BCA assay. Then 5 µg of protein were separated by sodium dodecyl sulfate-polyacrylamide gel electrophoresis and transferred to a 0.45-µm polyvinylidene difluoride membrane (Millipore, Temecula,

CA, USA). The membranes were blocked with 5% non-fat dry milk in Tris-buffered saline with 0.1% Tween 20 and then incubated with primary antibodies, A11 (Invitrogen, Carlsbad, CA, USA) and 6E10 (Covance, Princeton, NJ, USA). The immunoblots were visualized using a commercial development kit (Pierce, Dallas, TX, USA). Quantification of the immunoblots was performed using the ImageJ program (NIH, USA). The normalization of the data was performed by dividing the quantified value of protein by the total protein amount.

3. Results

3.1. Cohorts

We recruited participants and grouped them into clinically confirmed cohorts. Subjects were categorized according to the National Institute of Neurological and Communicative Disorders and Stroke and the Alzheimer's Disease and Related Disorders Association (NINCDS/ADRDA) of the American Psychiatric Association criteria for the diagnosis of probable AD (*1, 21, 22*) (*29*). A total of 60 participants were enrolled, 21 in the normal control group and 39 in the probable AD group (Table 1) (*29*). Statistically significant differences between the groups were detected in the Mini-Mental State Examination (MMSE) (dementia: 20.47 ± 3.73; normal: 27.61 ± 0.85, $P < 0.001$) and the Clinical Dementia Rating (CDR) scores (dementia: 0.65 ± 0.23; normal: 0.47 ± 0.12, $P < 0.001$) (Table 1). Moreover, the Global Deterioration Scale (GDS) scores of the dementia group was significantly higher than the normal group (dementia: 3.29 ± 0.37; normal: 1.94 ± 0.24, $P < 0.001$) (Table 1).

Table 1. Summary of cognitive assessments and age by disease status and gender

Conditions	**Normal**		**Dementia (probable AD)**	
Gender	**Male**	**Female**	**Male**	**Female**
Number of subjects	21		39	
	10	11	24	15
Age (years; mean ± SE)	71.92 ± 5.27		76.30 ± 6.18 (ns)	
	73.72 ± 6.92	70.29 ± 3.77	76.92 ± 6.84	75.32 ± 5.12
MMSE (mean ± SE)	27.61 ± 0.85		20.47 ± 3.73 (***)	
	27.55 ± 0.82	27.71 ± 0.95	21.62 ± 3.43	19.88 ± 0.63
CDR (mean ± SE)	0.47 ± 0.12		0.65 ± 0.23 (***)	
	0.45 ± 0.15	0.50 ± 0.00	0.61 ± 0.22	0.66 ± 0.24
GDS (mean ± SE)	1.94 ± 0.24		3.29 ± 0.37 (***)	
	2.00 ± 0.00	1.85 ± 0.38	3.31 ± 0.63	3.36 ± 0.57

The data are presented as means ± SEs. For the statistical analysis, one-way ANOVA was performed, followed by Dunnett's post-hoc test. Statistical significance is denoted as ns: $P > 0.05$, ***: $P < 0.001$. MMSE, CDR, and GDS refer to the Mini-Mental State Examination, the Clinical Dementia Fate, and the Global Deterioration Scale, respectively.

3.2. Identification of oligomeric Aβ in nasal discharge

We first examined the presence of Aβ monomers and oligomers in the nasal discharge samples of two probable AD subjects. We performed LC-MS/MS analysis using samples immunoprecipitated with an antibody against an Aβ peptide (6E10, Covance, Princeton, NJ, USA). A 12-residue internal tryptic peptide sequence of LVFFAEDVGSNK, identical to human Aβ (17-28), was detected. Because various forms of distinct Aβ are deposited in spatially and temporally distinct manners during AD progression, we examined the specific soluble oligomerized Aβ species in nasal discharges using immunoblot analysis. We performed an immunoblot assay of nasal

discharges from the possible AD group using an antibody against various Aβ oligomers (A11, Invitrogen, Carlsbad, CA, USA) after immunoprecipitation with 6E10. We identified assemblies of Aβs, Aβ*56, 12-mer peptide (~56 kDa), and AβO, 15-mer peptide (~80 kDa), in the nasal discharge from the probable AD group (Fig. 1A). Next, we measured levels of Aβ*56 and AβO in the nasal discharge samples of normal controls and probable AD subjects by an immunoblot assay with an anti-oligomeric A11 antibody and an anti- Aβ D54D2. Compared to the normal control group, the probable AD group exhibited the increased expression of both sizes of oligomeric Aβ in their nasal discharges (Fig. 1B).

3.3. Increased oligomeric Aβ in the nasal discharge of the probable AD group

To verify the presence of upregulated soluble Aβ oligomers in the probable AD group, we used our previously verified CLASS method with IME sensor systems(*20*). In our previous research, the CLASS method demonstrated high accuracy in discerning the normal group from the AD group in human plasma. The CLASS method dissociates aggregated Aβ into monomers by a chemical, EPPS ([4-(2-hydroxyelthyl)-1-piperazinepropanesulfonic acid]), and allows quantitative measurements of oligomeric Aβ in proportion to the total Aβ pool in nasal discharge samples. The IME sensor system is a highly sensitive electrical detection tool to identify the presence of protein biomarkers at sub pg/mL scales. The integration of the CLASS method along with a highly sensitive IME sensor system enabled us to avoid the individual fluctuations that can occur from the conventional analysis of

amyloid aggregates under heterogeneous conditions. Conventional methods measuring Aβ levels under the presence of various Aβ conformations were not successful, which led to the misinterpretation of Aβ as an unreliable biomarker(*30-32*). The self-standard ratio obtained from both the normal control group and the probable AD group was used to assess the levels of oligomeric Aβ in the nasal discharge. The levels of oligomeric Aβ species in the nasal discharge of the probable AD group (n = 39) were significantly higher than those of the normal control group (n = 21) (Fig. 1C).

The levels of Aβ*56 and AβO in the nasal discharge samples were also measured by immunoblot analysis and we found higher expression of both oligomeric Aβs in the probable AD group compared to the normal control group (Fig. 1D, E). When we examined the correlations between the Aβ oligomer levels and other non-AD factors (e.g., age and sex), there was no correlation between Aβ oligomer levels and age and sex (Fig. S2). Taken together, our results suggest that the detection of soluble Aβ oligomers in the nasal discharge could be a specific feature of probable AD patients.

*3.4. Different profiles of Aβ*56 and AβO in AD stages*

The probable AD group was further categorized based on their MMSE, CDR, and GDS scores into mild (n = 26) and moderate stages (n = 13) as summarized in Table 2 (*1, 21*). Compared to the normal group, the sum of the Aβ*56 and AβO levels was significantly higher in both groups and different between the two stages (Fig. 2A, B). The mean Aβ*56 levels were significantly higher in both the mild and moderate

probable AD groups than the normal group, whereas we detected no significant difference between the mild and moderate AD groups (Fig. 2C). In contrast, the mean AβO levels were significantly higher in the moderate stage probable AD group than in the other two groups, whereas no significant difference was found between the normal and mild AD groups (Fig. 2D). Taken together, the Aβ oligomerization profiles in nasal discharge may vary depending on the AD progression, shown by the higher expression of Aβ*56 in the mild stage and higher expressions of both Aβ*56 and AβO in the moderate stage compared to the normal group.

Table 2. Summary of cognitive assessments and age by disease progression status.

Conditions	Normal	Dementia (probable AD)	
		Mild stage	Moderate stage
Number of subjects	21	26	13
Age (mean ± SE) (years)	72.39 ± 6.01	75.17 ± 5.61 (ns)	76.93 ± 5.92 (ns)
MMSE (mean ± SE)	27.61 ± 0.85	23.17 ± 1.11 (***)	16.33 ± 2.12 (***)
CDR (mean ± SE)	0.47 ± 0.12	0.52 ± 0.10 (ns)	0.83 ± 0.24 (***)
GDS (mean ± SE)	1.94 ± 0.24	3.04 ± 0.21 (***)	3.80 ± 0.68 (***)

The data are presented as means ± SEs. For the statistical analysis, one-way ANOVA was performed, followed by Dunnett's post-hoc test. Statistical significance is denoted as ns: $P > 0.05$, ***: $P < 0.001$. MMSE, CDR, and GDS refer to the Mini-Mental State Examination, the Clinical Dementia Fate, and the Global Deterioration Scale, respectively. (continue to the next page)

These results suggest that profiling alterations of Aβ*56 and AβO levels in nasal discharge may distinguish the stages of AD-associated cognitive decline. We compared the oligomer proportion of total Aβ (Fig. S3A), the levels of Aβ*56 (Fig. S3B), and the levels of AβO (Fig. S3C) with MMSE scores (Table 3). Our results revealed that the self-standard ratio (a.u.) for the levels of oligomeric Aβ species moderately (0.6 > R > 0.4) correlated across the full range of MMSE scores (R = 0.5293; black line; Fig. S3A Fig. S3A and Table 3). However, when stratified by MMSE scores, the levels of Aβ*56 better (R > 0.6) correlated (R = 0.6069; red line) with the mild AD and normal groups compared to the moderate AD group (R = 0.6815; pink line; Fig. S3B and Table 3). According to our results, the expression level of Aβ*56 in the nasal discharge was most correlated with cognitive function in the mild AD stage. In contrast, AβO levels strongly correlated (R = 0.6061; pink line) with moderate AD stage, and correlated (R = 0.4010; red line) slightly with the mild AD and normal stages (Fig. S3C). The expression level of AβO in the nasal discharge was most correlated with cognitive function in the moderate AD stage. Our results statistically confirmed that the level of specific oligomerized Aβs in the nasal discharge correlated with changes in cognitive function in different AD stages, which was probably due to AD-related dementia progression.

Table 3. Correlation analysis between levels of soluble Aβ oligomers and cognitive function

	Normal - mild	Normal - Moderate	Normal - Mild + Moderate
Self-standard ratio (a.u)	R = 0.5603 (***)	R = 0.3087 (***)	R = 0.5239 (***)
Aβ *56 level (a.u) (ratio of normal)	R = 0.6815 (***)	R = 0.6909 (***)	R = 0.5246 (***)
AβO level (a.u) (ratio of normal)	R = 0.6061 (***)	R = 0.4010 (***)	R = 0.5173 (***)

Correlation analysis between the total levels of soluble Aβ species (Self-standard ratio, Aβ *56 and AβO) in nasal discharges and MMSE scores was conducted. Linear regression analyses of the total oligomeric soluble Aβ showed significant correlation with the MMSE score. We calculated the correlation between soluble Aβ oligomer levels and cognitive function with the line shows the regression line with 95% confidence interval. Statistical significances are denoted (***P < 0.001)

Table 4. Summary of divided groups by Aß*56 level

Group	Low (Aß*56 level <2.65)			High (Aß*56 level≥2.65)		
Age	76.82±4.88			74.45±5.77		
Sex	M	F		M	F	
	4	7		3	8	
Aß*56 level	2.01±0.48			3.58±0.58		
Test year	1st year	2nd year	3rd year	1st year	2nd year	3rd year
MMSE	21.09±3.34	21.82±3.19	21.55±2.97	18.82±3.21	18.45±4.36	17.45±4.98
GDS	3.27±0.45	3.36±0.48	3.18±0.39	3.55±0.66	3.55±0.66	3.82±0.72

The data are represented as means ± SDs. Each group was divided to include the same number of subjects based on the Aß*56 level. Low group: Aß*56 levels below 2.65, High group: Aß*56 levels above 2.65. MMSE and GDS refer to the Mini-Mental State Examination and the Global Deterioration Scale, respectively.

*3.5. Longitudinal measurements of cognitive function with high Aβ * 56 expression levels in their nasal discharges*

We performed the longitudinal cohort study of mild AD patients with distinct Aβ*56 expression levels in their nasal discharges over three years. We divided the mild AD group (n = 22) within the total AD subjects into two groups based on their Aβ*56 levels in nasal discharges. We determined the baseline for dividing the groups using the average of Aβ*56 levels in the total AD subjects (n = 38). Since the average Aβ*56 level was 2.65, we set 2.65 as the baseline for dividing the mild AD group (n = 22). The subjects with Aβ*56 levels below 2.65 were grouped as into a Low group (n = 11), whereas participants with Aβ*56 levels above 2.65 were grouped into a High group (n = 11) (Table 4). Then, the changes in the MMES and GDS scores in both groups were monitored annually for three years (46 ± 7 months) (Table 4). We found that the High group experienced a declining trend in MMSE scores (Fig. 3A) and a significant increase in the GDS scores (Fig. 3B) within three years. We also found that the expression level of Aβ*56 in nasal discharge correlated with changes in cognitive function in the AD subjects. When stratified by MMSE score changes in the AD subjects over three years (1st to 3rd-year data), the levels of Aβ*56 were moderately correlated with MMSE scores (R = 0.4226; red line) (Fig. 3C). Similarly, the expression levels of Aβ*56 were also moderately correlated (R = 0.4103; red line) with changes in the GDS scores in AD subjects over three years (1st to 3rd year data) (Fig. 3D). This finding suggests that high Aβ * 56 expression levels in their nasal discharges are associated with cognitive decline in AD patients.

4. Discussion

Declining sensory function is common in neurodegenerative disorders, including AD (*33, 34*). In particular, olfactory dysfunction is an indisputable characteristic of patients with AD (*35, 36*). Meta-analysis studies on olfactory function and cognitive dysfunction reported significant problems in an odor processing pathway in presumed and confirmed cases of AD (*37*). Therefore, it is highly intriguing to test whether a particular state of olfaction represents AD pathology. The symptoms of olfactory dysfunction have been attributed to neurodegeneration occurring in the olfactory central pathway in the central nervous system (*4, 38*). However, the findings of the present study that soluble Aβ oligomers were easily detectable in the nasal discharge of the probable AD group may suggest an alternative explanation. Moreover, the finding that the expression profile of soluble Aβ oligomers closely correlated with a decline in the cognitive performance of patients with probable AD pathology may provide an opportunity for the early screening of AD by nasal discharge samples.

The peripheral olfactory system contributes to AD-related olfactory dysfunction via its processing of the amyloid precursor protein (*9*), although the precise mechanisms remain unclear. Moreover, another study on the peripheral olfactory system in an AD mouse model also showed that the expression of soluble Aβ oligomers, Aβ*56 and AβO in the olfactory system was toxic to olfactory sensory neurons and consequently led to olfactory impairments (*16*). Direct links to studies using an AD model mouse of human AD dementia should be made cautiously, however, the results using an AD model mouse were highly comparable to the results using human nasal discharge presented here. The

unregulated oligomerization of Aβ in the nasal secretion of patients with AD dementia was also recently reported (*39*), although the direct identification of Aβ in nasal discharge, as well as the relative expression of Aβ oligomer isoforms in the nasal discharge, were not shown. Here, we first identified Aβ proteins in human nasal discharge in patients with serious cognitive decline (probably with AD dementia) and the total amount of Aβ proteins increased in the nasal discharge of patients with possible AD dementia. From our qualitative analysis of Aβ in nasal discharge, we revealed two specific types of Aβ oligomers, which were well validated by previous studies in either mice or humans. Through the results, we confirmed that a certain amount of amyloid β can be detected in both the normal and patient groups. However, a specific amyloid beta (Aβ * 56, AβO) that can clearly distinguish the normal group from the patient group was tested. In previous study, it has been demonstrated that an oligomerized form of Aβ, Aβ*56, correlated with cognitive deficits and that AβO, a more oligomerized form, induced direct cytotoxicity and significantly mediated cell death during AD progression in a mouse model (*40, 41*). Taken together, we propose that Aβ*56 is dramatically upregulated in the peripheral olfactory system during the early stages of dementia, followed by an increase in AβO expression during the later stages of AD dementia. Furthermore, we suggest that these observations imply that increases in soluble Aβ aggregates in the peripheral olfactory system may be closely related to AD progression and then, that Aβ aggregation in the peripheral olfactory system may precede diminished cognitive function in the CNS. In fact, our 3-year longitudinal cohort study showed that high levels of Aβ*56 in the nasal discharge in the mild AD group could be a premonitory symptom of the further

catastrophic progression of dementia. It is still difficult to claim a direct link between Aβ oligomers in nasal discharge and AD pathogenesis in the brain since such a claim requires an explanation of how the soluble Aβ oligomers in the olfactory system are associated with AD-related cognitive impairment. Despite many reservations, we propose a novel and convenient approach for monitoring cognitive decline with possible AD progression (Fig. 4).

To date, a number of clinical trials have been conducted to overcome progressive neural dysfunction in patients with AD dementia. However, only minor delays in disease progression have been achieved (*42-44*). Therefore, treatment effectiveness may be maximized by timely intervention. To this end, a great deal of effort is currently being exerted to optimize the monitoring or either AD initiation or progression. Here, we showed that the levels of soluble Aβ oligomers in nasal discharge were significantly higher in patients with probable AD. Furthermore, routine nasal discharge screenings can be a better option in AD screening due to additional advantages, such as relatively low cost, non-invasive sampling and so on. A few issues still need to be clarified, such as retrospective cross-sectional verification studies of Aβ in the nasal discharge and identification of other biomarker candidates in the nasal discharge. In addition, Relationships with other neurodegenerative diseases by associations in underlying pathological, physiological, and possibly genetic linkages also need to be considered in the selection of other biomarker candidates (*45*). In particular, when considering limitations in the accuracy of AD diagnosis known to date (*46*), additional experiments considering other neurodegenerative disease patient groups, such as PDs, may be necessary in future

plan. However, our results from patients with probable AD reveal the feasibility of using nasal discharge to screen for AD biomarkers, as well as biomarkers to monitor AD progression. Taken together, the results of this study introduce a novel and simple approach to assessing AD progression by monitoring the expression profile of soluble Aβ oligomers in nasal discharge.

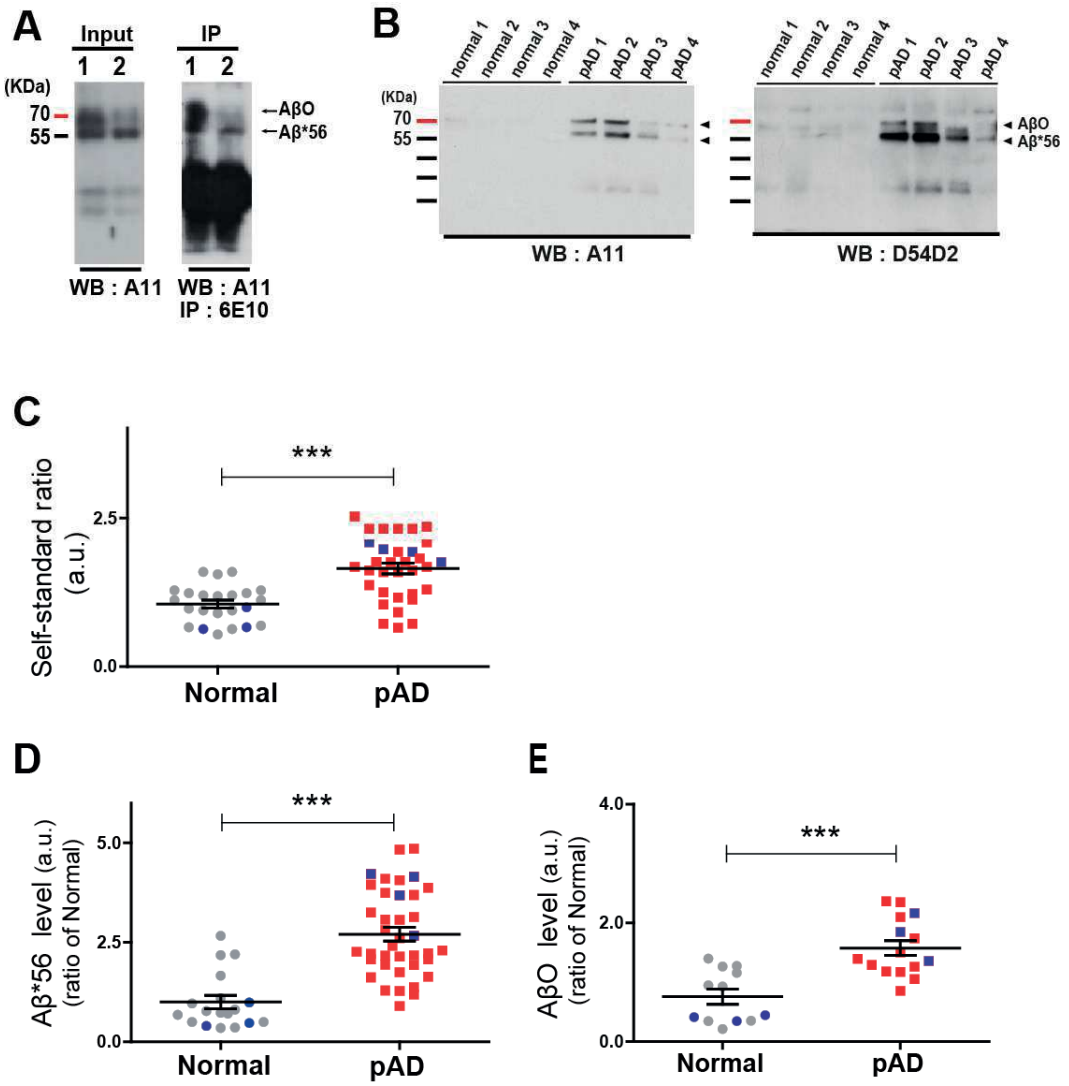

Figure 1. Soluble Aβ oligomers are detected in the nasal discharges from probable AD group (pAD). Immunoblotting verification; soluble Aβ oligomers were detected in the nasal discharges of pAD group. (A) Identification of Aβ oligomer, assessed by western blot (WB; A11) with or without immunoprecipitation (IP: 6E10) using samples (1; pAD1 and 2; pAD2) from pAD group. (B) Representative data for A11-immunoreaactive (left) and D54D2-immunoreaactive (right) soluble Aβ oligomers are detected in nasal discharges of pAD group (4; pAD1, pAD2, pAD3 and pAD4) and normal group (4; normal 1, normal 2, normal 3 and normal 4). (C) The total levels of soluble Aβ species in nasal discharges were measured between the normal and pAD groups using CLASS method (self-standard ratio (a.u.)). (D) Quantification of soluble Aβ*56 protein. Expression levels of proteins were quantified using stereological analysis (ImageJ program). (E) Quantification of soluble AβO protein. Expression levels of proteins were quantified using stereological analysis (ImageJ program). Data are represented as means ± SEMs from three independent experiments. Value of samples were identified as outliers through Grubbs' test, also called the ESD method. For statistical analysis, paired t-test was performed. Statistical significances are denoted (***P < 0.001).

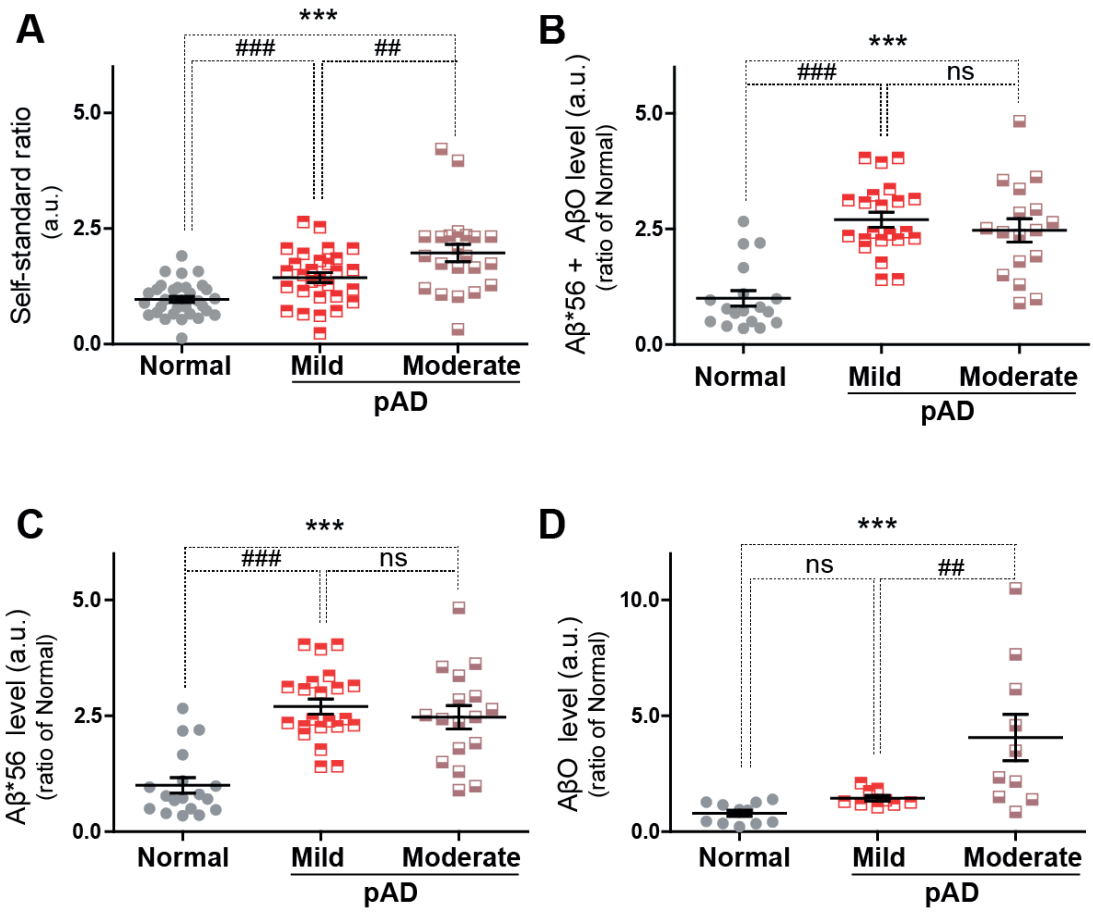

Figure 2. The specific composition of soluble Aβ in nasal discharges from different stages of probable AD group (pAD). (A) The total levels of soluble Aβ species using CLASS method (self-standard ratio (a.u.)) in nasal discharges were measured in (Normal (22), mild stage (25) and moderate stage (13) of pAD groups. (B) Quantification of soluble Aβ *56 + AβO protein levels. Expression levels of proteins were quantified using stereological analysis (ImageJ program) in Normal (18), mild stage (22) and moderate stage (17) of pAD groups. (C) Quantification of soluble Aβ *56 protein. Expression levels of proteins were quantified using stereological analysis (ImageJ program) in Normal (18), mild stage (22) and moderate stage (17) of pAD groups. (D) Quantification of soluble AβO protein. Expression levels of proteins were quantified using stereological analysis (ImageJ program) in Normal (12), mild stage (9) and moderate stage (10) of pAD groups. Data are represented as means ± SEMs from three independent experiments. Value of samples were identified as outliers through Grubbs' test, also called the ESD method. For the statistical analysis, one-way ANOVA was performed, followed by Dunnett's post hoc test. Statistical significance is denoted (ns > 0.05, ***P < 0.001). In addition, paired t-test was performed. Statistical significances are denoted (ns > 0.05, # P < 0.05, ## P < 0.01, ### P < 0.001).

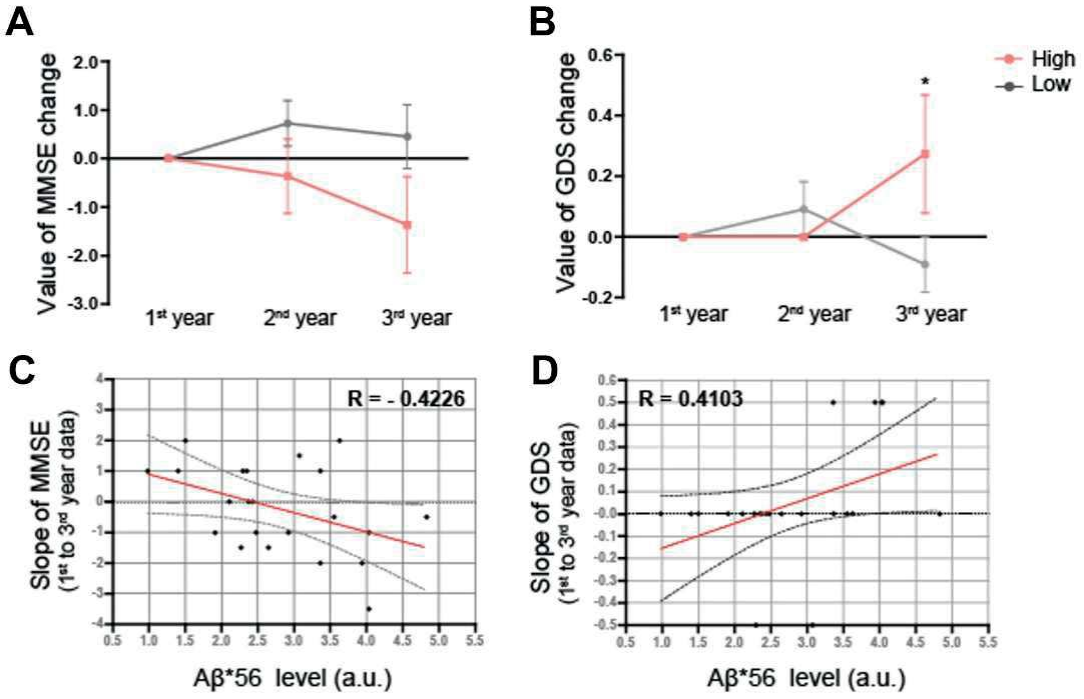

Figure 3. The association between soluble Aβ oligomer levels and cognitive performance over time (for 3 years). (A) MMSE change pattern over 3 years (baseline is 1st year). (B) GDS change pattern over 3 years (baseline is 1st year). Marginally significance on interaction by two-way RMANOVA (p=0.050). High group show higher change of GDS compare to Low group on 3rd year. Statistical significance is denoted (ns>0.05 and *P < 0.05) followed by Bonferroni post hoc test. (C-D) Correlation analysis between soluble Aβ oligomer levels and slope of cognitive performance. Increased levels of soluble Aβ oligomers in nasal discharge are associated with declining cognitive status over time. This effect is constant over time; levels of soluble Aβ oligomers in nasal discharge are significantly associated with declining cognitive status after 3 years.

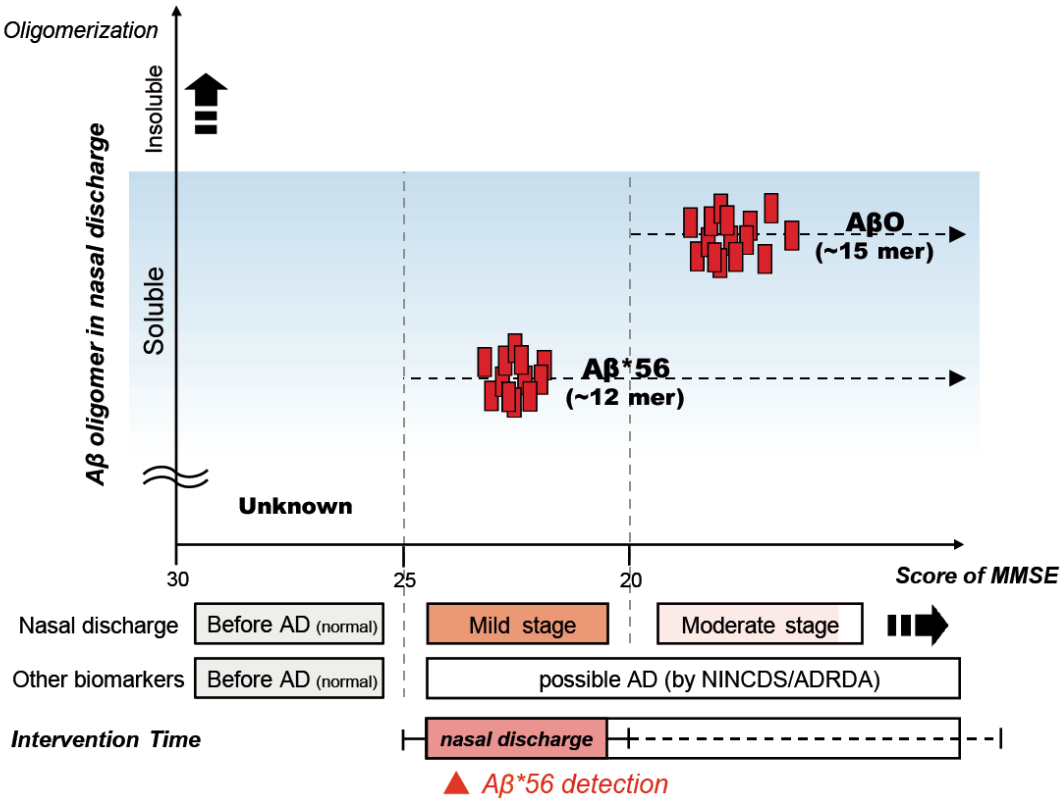

Figure 4. Schematic diagram which laid advantage out of AD diagnosis using nasal discharge.

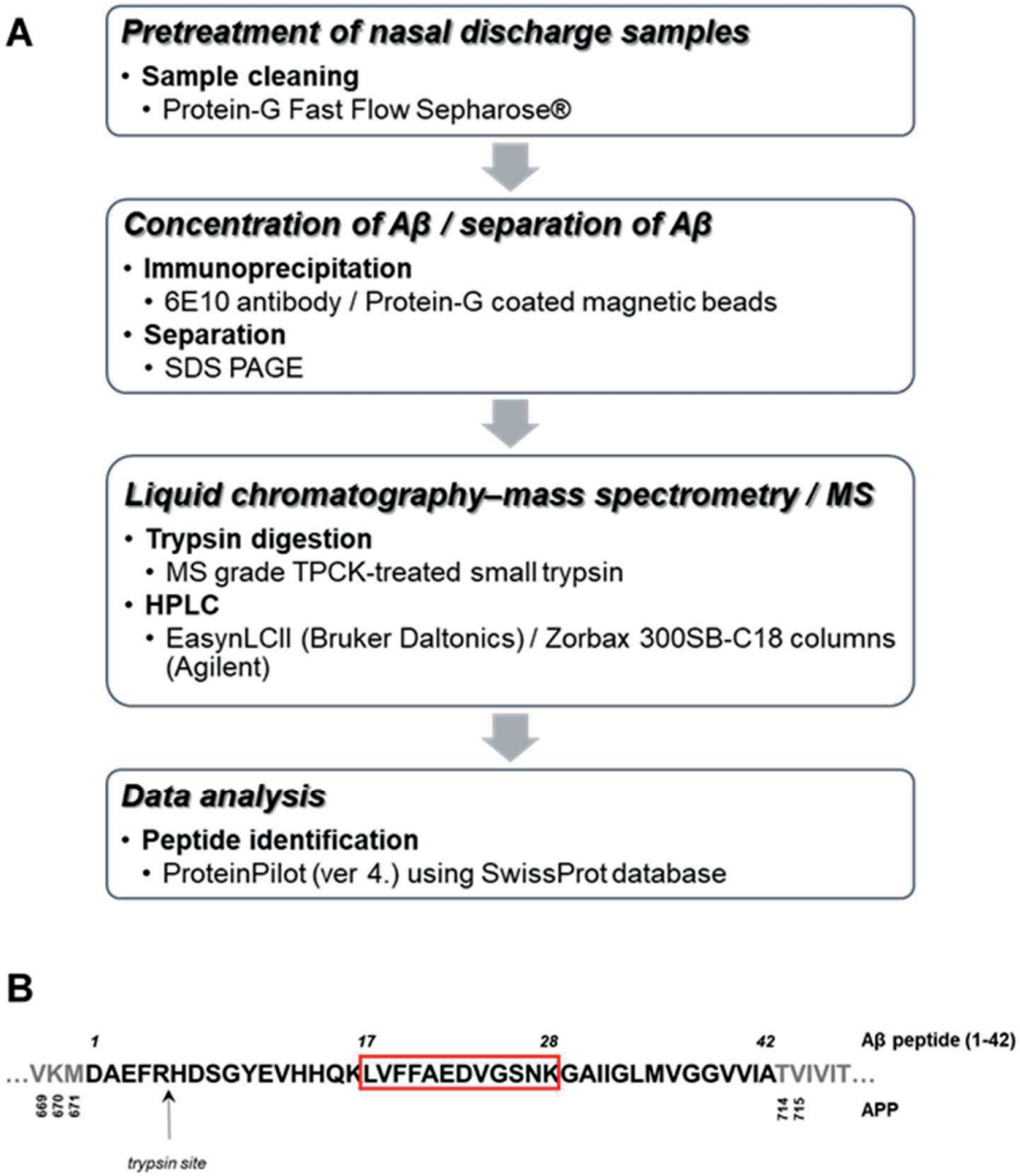

Figure S1. Identification and quantification; soluble Aβ oligomers were detected in the nasal discharge of patients with AD. (A) Proteomic identification of soluble Aβ oligomers by immunoprecipitation (IP). Schematic of the workflow of profiling of soluble Aβ oligomers by IP combined with LC-MS/MS. (B) Sequence of Aβ1−42, with the cleavage sites for trypsin (arrows at the bottom of the sequence). Identified sequence is belonged to Aβ sequence.

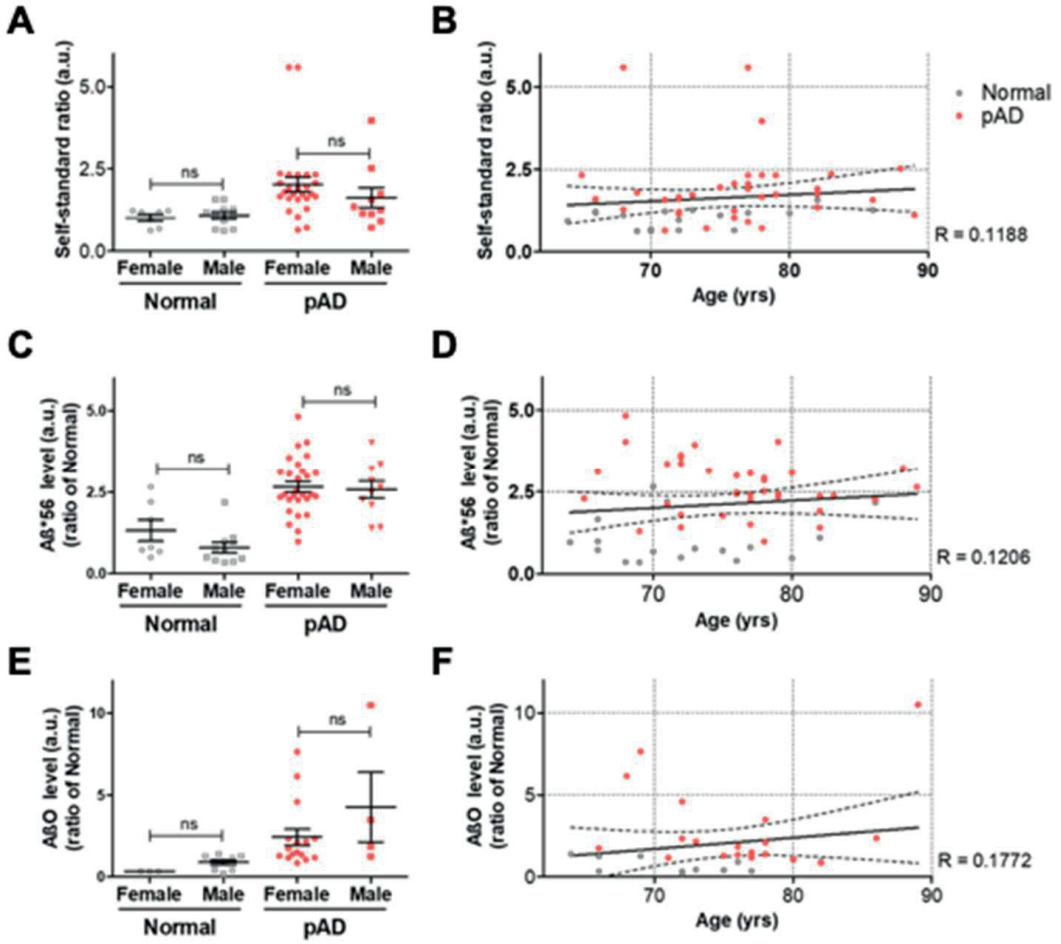

Figure S2. Non-significant correlation between soluble Aβ oligomer and age/gender. The total levels of soluble Aβ species using CLASS method (self-standard ratio (a.u.)) were analyzed by gender (A) and age (B). (B) Linear regression analyses showed no significant effects of storage time on biomarker concentrations. (R = 0.1188). Quantification of soluble Aβ *56 protein was analyzed by gender (C) and age (D). (D) Linear regression analyses showed no significant effects of age on biomarker concentrations. (R = 0.1206). Quantification of soluble AβO protein was analyzed by gender (E) and age (F). (F) Linear regression analyses showed no significant effects of age on biomarker concentrations. (R = 0.1772). (A), (C), (E) Data are represented as means ± SEMs from three independent experiments. For statistical analysis, paired t-test was performed. Statistical significances are denoted. (ns; $P > 0.05$) (B), (D), (F) Linear regression analyses shows significant correlation between levels of the total levels of soluble Aβ species using CLASS method (self-standard ratio (a.u.)) (B), Aβ *56 protein (D) and AβO protein (F) with the age(yrs). The line shows the regression line with 95% confidence interval (dashed line).

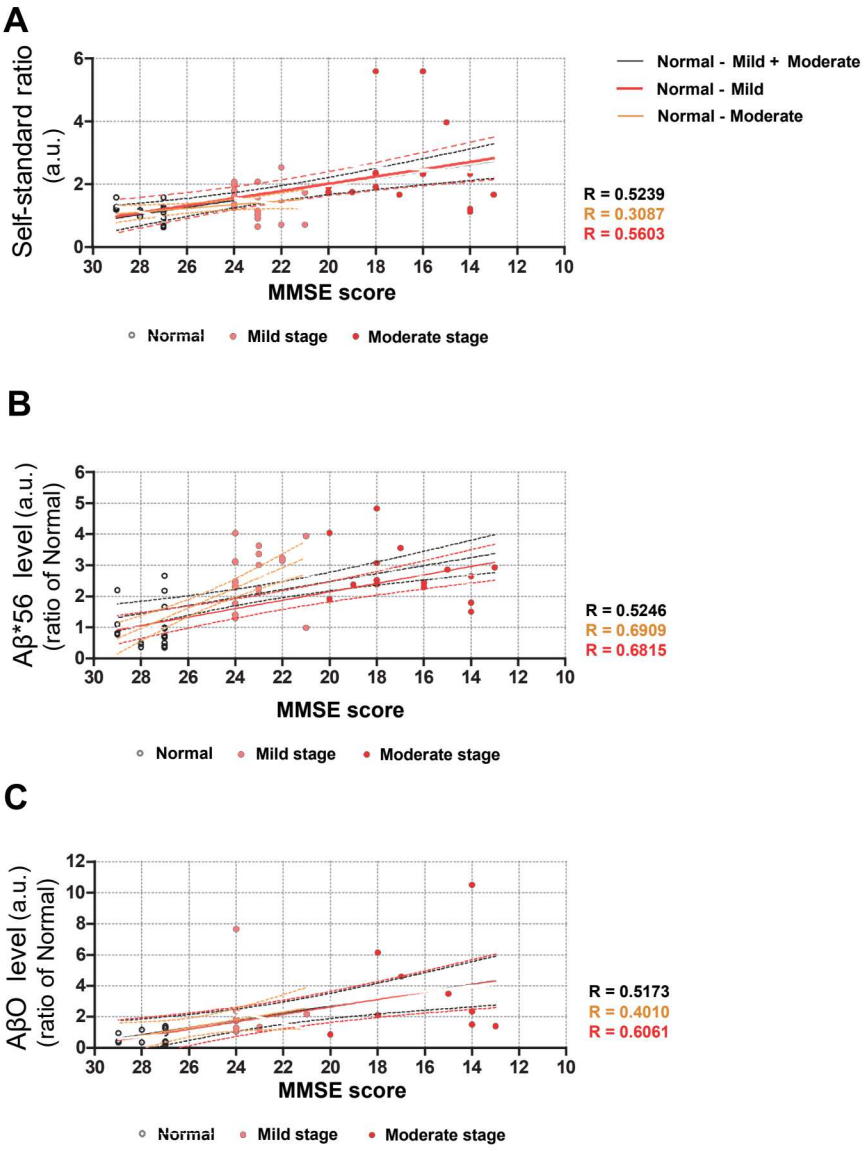

Figure S3. Correlation analysis between levels of soluble Aβ oligomers and cognitive function. (A) Correlation analysis between the total levels of soluble Aβ species in nasal discharges and MMSE scores was conducted. Linear regression analyses of the total oligomeric soluble Aβ showed significant correlation with the MMSE score. (B) Correlation analysis between Ratio of Aβ *56 protein and MMSE scores was conducted. Linear regression analyses of Aβ *56 protein showed significant correlation with the MMSE score. (C) Correlation analysis between Ratio of AβO protein and MMSE scores was conducted. Linear regression analyses of AβO protein showed significant correlation with the MMSE score. Scatter diagrams displaying correlation between soluble Aβ oligomer levels and cognitive function. The line shows the regression line with 95% confidence interval (dashed line).

Acknowledgments

This work was supported by the National Research Foundation of Korean (NRF-2015M3A9E2028884). Authors are grateful to Dr. Sohyun Ahn for her critical reading.

References

1. M. F. Folstein, S. E. Folstein, P. R. McHugh, "Mini-mental state". A practical method for grading the cognitive state of patients for the clinician. *Journal of psychiatric research* **12**, 189-198 (1975).
2. B. Reisberg, S. H. Ferris, M. J. de Leon, T. Crook, The Global Deterioration Scale for assessment of primary degenerative dementia. *The American journal of psychiatry* **139**, 1136-1139 (1982).
3. R. A. Sperling *et al.*, Toward defining the preclinical stages of Alzheimer's disease: recommendations from the National Institute on Aging-Alzheimer's Association workgroups on diagnostic guidelines for Alzheimer's disease. *Alzheimers Dement* **7**, 280-292 (2011).
4. T. Hummel *et al.*, Olfactory FMRI in patients with Parkinson's disease. *Frontiers in integrative neuroscience* **4**, 125 (2010).
5. A. Nakamura *et al.*, High performance plasma amyloid-beta biomarkers for Alzheimer's disease. *Nature* **554**, 249-254 (2018).
6. R. M. Nitsch *et al.*, Cerebrospinal fluid levels of amyloid beta-protein in Alzheimer's disease: inverse correlation with severity of dementia and effect of apolipoprotein E genotype. *Ann Neurol* **37**, 512-518 (1995).
7. B. Olsson *et al.*, CSF and blood biomarkers for the diagnosis of Alzheimer's disease: a systematic review and meta-analysis. *The Lancet. Neurology* **15**, 673-684 (2016).
8. S. Janelidze *et al.*, Plasma P-tau181 in Alzheimer's disease: relationship to other biomarkers, differential diagnosis, neuropathology and longitudinal progression to Alzheimer's dementia. *Nat Med* **26**, 379-386 (2020).
9. J. Y. Kim *et al.*, Distinct amyloid precursor protein processing machineries of the olfactory system. *Biochemical and biophysical research communications* **495**, 533-538 (2018).
10. J. Alves, A. Petrosyan, R. Magalhaes, Olfactory dysfunction in dementia. *World J Clin Cases* **2**, 661-667 (2014).
11. J. J. Stamps, L. M. Bartoshuk, K. M. Heilman, A brief olfactory test for Alzheimer's disease. *J Neurol Sci* **333**, 19-24 (2013).
12. Y. M. Zou, D. Lu, L. P. Liu, H. H. Zhang, Y. Y. Zhou, Olfactory dysfunction in Alzheimer's disease. *Neuropsychiatr Dis Treat* **12**, 869-875 (2016).
13. S. E. Arnold *et al.*, Olfactory epithelium amyloid-beta and paired helical filament-tau pathology in Alzheimer disease. *Ann Neurol* **67**, 462-469 (2010).
14. R. O. Roberts *et al.*, Association Between Olfactory Dysfunction and Amnestic Mild

Cognitive Impairment and Alzheimer Disease Dementia. *JAMA Neurol* **73**, 93-101 (2016).
15. N. Wu, X. Rao, Y. Gao, J. Wang, F. Xu, Amyloid-beta deposition and olfactory dysfunction in an Alzheimer's disease model. *J Alzheimers Dis* **37**, 699-712 (2013).
16. S. J. Yoo *et al.*, Differential spatial expression of peripheral olfactory neuron-derived BACE1 induces olfactory impairment by region-specific accumulation of beta-amyloid oligomer. *Cell Death Dis* **8**, e2977 (2017).
17. D. Pagelow *et al.*, The olfactory epithelium as a port of entry in neonatal neurolisteriosis. *Nat Commun* **9**, 4269 (2018).
18. R. D. Strous, Y. Shoenfeld, To smell the immune system: olfaction, autoimmunity and brain involvement. *Autoimmunity reviews* **6**, 54-60 (2006).
19. J. N. Norwood *et al.*, Anatomical basis and physiological role of cerebrospinal fluid transport through the murine cribriform plate. *Elife* **8**, (2019).
20. Y. Kim *et al.*, Comparative analyses of plasma amyloid-beta levels in heterogeneous and monomerized states by interdigitated microelectrode sensor system. *Sci Adv* **5**, eaav1388 (2019).
21. K. Juva *et al.*, Staging the severity of dementia: comparison of clinical (CDR, DSM-III-R), functional (ADL, IADL) and cognitive (MMSE) scales. *Acta neurologica Scandinavica* **90**, 293-298 (1994).
22. G. W. Small *et al.*, Diagnosis and treatment of Alzheimer disease and related disorders. Consensus statement of the American Association for Geriatric Psychiatry, the Alzheimer's Association, and the American Geriatrics Society. *JAMA* **278**, 1363-1371 (1997).
23. G. McKhann *et al.*, Clinical diagnosis of Alzheimer's disease: report of the NINCDS-ADRDA Work Group under the auspices of Department of Health and Human Services Task Force on Alzheimer's Disease. *Neurology* **34**, 939-944 (1984).
24. K. A. Chang *et al.*, Plasma soluble neuregulin-1 as a diagnostic biomarker for Alzheimer's disease. *Neurochem Int* **97**, 1-7 (2016).
25. J. Kim *et al.*, Wafer-scale high-resolution patterning of reduced graphene oxide films for detection of low concentration biomarkers in plasma. *Scientific reports* **6**, 31276 (2016).
26. Y. K. Yoo *et al.*, A highly sensitive plasma-based amyloid-beta detection system through medium-changing and noise cancellation system for early diagnosis of the Alzheimer's disease. *Scientific reports* **7**, 8882 (2017).
27. M. Berna, B. Ackermann, Increased throughput for low-abundance protein biomarker verification by liquid chromatography/tandem mass spectrometry. *Analytical chemistry* **81**, 3950-3956 (2009).
28. S. Lesne *et al.*, A specific amyloid-beta protein assembly in the brain impairs memory. *Nature* **440**, 352-357 (2006).
29. G. M. McKhann *et al.*, The diagnosis of dementia due to Alzheimer's disease: recommendations from the National Institute on Aging-Alzheimer's Association workgroups on diagnostic guidelines for Alzheimer's disease. *Alzheimers Dement* **7**, 263-269 (2011).
30. R. Mayeux *et al.*, Plasma A[beta]40 and A[beta]42 and Alzheimer's disease: relation to age, mortality, and risk. *Neurology* **61**, 1185-1190 (2003).
31. J. Sundelof *et al.*, Plasma beta amyloid and the risk of Alzheimer disease and dementia in elderly men: a prospective, population-based cohort study. *Arch Neurol* **65**, 256-263 (2008).
32. M. van Oijen, A. Hofman, H. D. Soares, P. J. Koudstaal, M. M. Breteler, Plasma Abeta(1-

40) and Abeta(1-42) and the risk of dementia: a prospective case-cohort study. *The Lancet. Neurology* **5**, 655-660 (2006).
33. M. Smitka *et al.*, Is there a correlation between hippocampus and amygdala volume and olfactory function in healthy subjects? *NeuroImage* **59**, 1052-1057 (2012).
34. C. Sorg *et al.*, Selective changes of resting-state networks in individuals at risk for Alzheimer's disease. *Proceedings of the National Academy of Sciences of the United States of America* **104**, 18760-18765 (2007).
35. Z. Huihong *et al.*, Olfactory and Imaging Features in Atypical Alzheimer's Disease. *Translational neuroscience* **9**, 1-6 (2018).
36. P. A. Thomann *et al.*, MRI-derived atrophy of the olfactory bulb and tract in mild cognitive impairment and Alzheimer's disease. *J Alzheimers Dis* **17**, 213-221 (2009).
37. R. I. Mesholam, P. J. Moberg, R. N. Mahr, R. L. Doty, Olfaction in neurodegenerative disease: a meta-analysis of olfactory functioning in Alzheimer's and Parkinson's diseases. *Arch Neurol* **55**, 84-90 (1998).
38. Y. M. Kuo *et al.*, Extensive enteric nervous system abnormalities in mice transgenic for artificial chromosomes containing Parkinson disease-associated alpha-synuclein gene mutations precede central nervous system changes. *Human molecular genetics* **19**, 1633-1650 (2010).
39. Y. H. Kim *et al.*, Amyloid beta in nasal secretions may be a potential biomarker of Alzheimer's disease. *Sci Rep* **9**, 4966 (2019).
40. E. N. Cline, M. A. Bicca, K. L. Viola, W. L. Klein, The Amyloid-beta Oligomer Hypothesis: Beginning of the Third Decade. *J Alzheimers Dis* **64**, S567-S610 (2018).
41. I. Benilova, E. Karran, B. De Strooper, The toxic Abeta oligomer and Alzheimer's disease: an emperor in need of clothes. *Nature neuroscience* **15**, 349-357 (2012).
42. R. M. Anderson, C. Hadjichrysanthou, S. Evans, M. M. Wong, Why do so many clinical trials of therapies for Alzheimer's disease fail? *Lancet* **390**, 2327-2329 (2017).
43. T. E. Golde, S. T. DeKosky, D. Galasko, Alzheimer's disease: The right drug, the right time. *Science* **362**, 1250-1251 (2018).
44. J. Vina, J. Sanz-Ros, Alzheimer's disease: Only prevention makes sense. *European journal of clinical investigation* **48**, e13005 (2018).
45. T. G. Beach, S. E. Monsell, L. E. Phillips, W. Kukull, Accuracy of the clinical diagnosis of Alzheimer disease at National Institute on Aging Alzheimer Disease Centers, 2005-2010. *J Neuropathol Exp Neurol* **71**, 266-273 (2012).
46. A. C. Costa Sa, H. Madsen, J. R. Brown, Shared Molecular Signatures Across Neurodegenerative Diseases and Herpes Virus Infections Highlights Potential Mechanisms for Maladaptive Innate Immune Responses. *Scientific reports* **9**, 8795 (2019).

Chapter 7

General discussion and conclusion

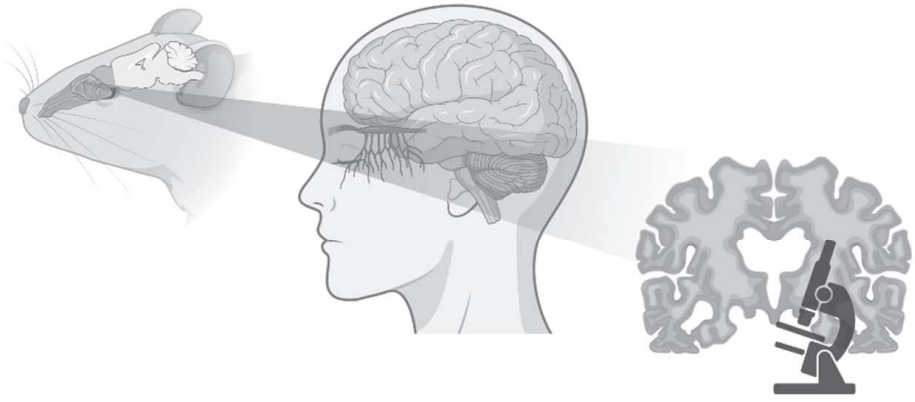

1. Summary

Although Alzheimer's disease (AD) is an irreversible and incurable neurodegenerative disease, olfactory dysfunction as an early AD indicator provides clues towards diagnostic methods and gives insight into onset mechanisms in AD pathogenesis. This thesis describes the relationship between olfactory pathology and olfactory dysfunction in AD. First, the olfactory sensory neuron has independent enzyme expression that can produce β-amyloid (Aβ). Second, AD pathology, including Aβ accumulation and microgliosis, is associated with structural damage of the olfactory system. Third, the olfactory pathologies are related to the olfactory sensory neuronal deficits that are, in turn, correlated with cognitive decline in AD. Therefore, these findings examining olfactory pathology are essential to unraveling the mechanism of olfactory dysfunction related to the development of AD. These findings support the need for further investigations towards potential diagnostic methods and understanding the basis of early pathogenesis in the olfactory system.

2. General discussion

2.1. Early onset of olfactory dysfunction in AD

The most notable feature of olfactory dysfunction is an early onset in AD pathogenesis. Aβ aggregation and accumulation are typical early pathological symptoms in AD progression (*1*). The well-characterized and widely used AD-related pathology model mouse, overexpressing human amyloid precursor protein (hAPP), Tg2576, exhibited olfactory dysfunction as an early phenotype among pathologic progression (*2*). The APP/PS1 mouse mutated with hAPP and presenilin1 (PS1; γ-secretase) displaying Aβ pathogenesis showed early Aβ deposition in the olfactory epithelium (*3*). Although the transgenic mouse expresses mutant genes ubiquitously in the whole-cell-genome, smell dysfunction and olfactory pathology were significantly observed in early AD pathogenesis regardless of olfactory neuron-specific mutation. In line with early pathology, understanding the pathophysiological relationship between Aβ pathogenesis and the olfactory system is a valid and reasonable approach (Chapter 2).

To induce Aβ-enriched conditions, synthetic Aβ was injected into the olfactory system in previous research (*4*). Additionally, the olfactory sensory neuron-specific hAPP expression model was designed to probe the role of human Aβ in the peripheral olfactory neural circuit (*5, 6*). Compared to these artificial conditions, this thesis pinpoints the presence and nature of the olfactory impairment simultaneously with concomitant pathology in Aβ pathogenesis. Specifically, β-secretase and Aβ were

enriched in the first synaptic interface of the olfactory sensory neurons in AD model mice with smell dysfunction (Chapter 3), illustrating that olfactory sensory neuronal β-amyloidosis is involved in the dysfunction. Oligomerization of soluble Aβ species proceeded in the olfactory epithelium, therefore, Aβ with the higher molecular weight was measured as a mouse is aged (Chapter 3), indicating that β-amyloidosis progresses in the epithelium. Notably, high Aβ accumulation in the olfactory system spatially coincided with low sensory neuronal calcium activity (Chapter 4). Neuronal calcium activity represents active synaptic transmission (7). The finding indicates Aβ influenced olfactory sensory neuronal impairment because the accumulation of soluble Aβ affects synaptic depression.

In addition, active pathogenesis and damage in the olfactory system coexisted with the region of high sensory neuronal turnover (Chapter 4). In other words, high Aβ overload drives reduced sensory neuronal number by increasing olfactory neurodegeneration and decreasing neuroregeneration. Investigation of mouse pathology revealed that Aβ genesis occurs in the olfactory sensory neurons and affects the olfactory sensory neuronal deficits. The pathogenesis is associated with activity-dependent neuronal turnover.

In this regard, this thesis explains the early onset of olfactory dysfunction in AD and that the olfactory sensory neuron has autonomous neurodegenerative mechanisms in AD progression associated with the Aβ accumulation.

2.2. Olfactory neurodegeneration: outcome of neuroinflammation and synaptic impairment by Aβ accumulation

The mouse model can recapitulate the conditions of pathogenesis, but it is limited because, in contrast, most sufferers of AD are sporadic, and the genetically modified mouse encompasses intensive and extensive pathological conditions. Therefore, profiling the postmortem olfactory system gives "as is" outcomes and evidence about the causes of olfactory neural damage and related pathological mechanism that mirror olfactory neurodegeneration in AD.

The immunoreactivity of Aβ proteins and tau inclusions were identified in the extended human olfactory system, including the epithelium (*8*), olfactory bulb (*9*), and cortex (*10*). Existing human histopathology research was restricted to demonstrating the pathology-positive domain and distribution in the tissue. However, this thesis shows both morphological damage and physiological disturbances linked with Aβ deposition. The altered structure of the olfactory synapse was concomitant with Aβ accumulation and microgliosis (Chapter 5). Reactive microglia coincided with the Aβ abundant region in the olfactory glomerulus in AD (Chapter 5). In AD, microglia promote neuroinflammation and induce reactive oxygen species such as nitric oxide, superoxide radical, and its derivatives (*11*). The oxidative stress exacerbate a vicious cycle that could further cellular instability triggering persistent neuroinflammation, such as DNA damage (*12*), mitochondrial dysregulation (*13*), and abnormal hAPP proteolysis, increasing amyloidosis (*14*). Evidence supported that the

olfactory dysfunction in AD induced by the neurotoxicity occurred in the olfactory system because a marker protein of cellular oxidative damage was localized in olfactory sensory neuron of AD patients with impaired odor sensitivity (*15*). Given the early onset of olfactory impairment, this thesis supports the mechanism of "The olfactory vector hypothesis" (*16*).

Tyrosine hydroxylase, expressed by olfactory sensory neuronal-synaptic activity in the periglomerular cell (*17*), was reduced (Chapter 5), consistent with the finding that amyloid accumulation and microglia influence the loss of sensory input from the olfactory epithelium. A severe shrinkage of the olfactory glomerular layer (Chapter 5), confirming that the impaired signal transduction between the olfactory epithelium and olfactory bulb neurons, explains the cause of smell deficits in AD. Additionally, ultrastructural analysis of the glomeruli underpins detailed evidence showing synaptic damage (Chapter 5). Therefore, the olfactory pathologies in AD patients account for the synaptic impairment and dysfunction of the olfactory system, which is the principal cause of hyposmia in AD.

2.3. Identification of AD progression using olfactory biomarkers: from bench to bedside

Olfactory pathology allows us to speculate that impaired olfactory epithelium includes altered cellular and molecular components. In this regard, nasal fluid from the olfactory epithelium is feasible material containing high-throughput biological information that mirrors pathological changes in the olfactory system. Although

cerebrospinal fluid and blood have been notified as a primary material detecting AD biomarkers, significant concerns remain regarding application of using olfactory biomarkers. A review of fluid biomarkers in AD summarized that CSF-Aβ is less-sensitive due to a decrease in the severe-AD stage (*18*). Another standard body fluid, plasma-Aβ, is less-specific due to difficulties finding "true-negative" controls or because of influence by heterogeneity of a patient's disease (*19*).

This thesis revealed that soluble Aβ could be detected in nasal discharge. Moreover, higher soluble Aβ detection is correlated with cognitive decline along with AD progression (Chapter 6). Thus, a strategy monitoring olfactory pathogenesis can trace or reflect cerebral degeneration. In comparison to CSF and plasma, nasal fluid collection is non-invasive and user-friendly. Therefore, the nasal fluid is specific and accessible material for detecting biomarkers. In a recent AD biomarker study using a large-scale proteomic analysis of body fluid has profiled the pathological alteration at a systemic level associated with the progress of AD beyond identifying a single biomarker (*20*). The olfactory pathology in AD could extend to a versatile approach in the clinic and also characterize the mechanism of olfactory neurodegeneration in AD (*21*).

3. Conclusion

This thesis highlights the role of olfactory pathophysiology and olfactory dysfunction in AD progression. The olfactory system is affected by a component of AD pathogenesis, such as APP processing and microgliosis. The olfactory sensory neuronal dysfunction causes smell abnormality, which correlates with Aβ accumulation. The pathogenesis is associated with high neuronal activity. Soluble Aβ is detected in the nasal discharge derived from the olfactory system, which can correlate with cognitive decline in AD. Therefore, olfactory pathology is a sign of olfactory neurodegeneration itself, which induces olfactory dysfunction in AD, and is a promising diagnostic tool for AD progression.

References

1. C. R. Jack, Jr. *et al.*, Hypothetical model of dynamic biomarkers of the Alzheimer's pathological cascade. *Lancet Neurol* **9**, 119-128 (2010).
2. D. W. Wesson, E. Levy, R. A. Nixon, D. A. Wilson, Olfactory dysfunction correlates with amyloid-beta burden in an Alzheimer's disease mouse model. *J Neurosci* **30**, 505-514 (2010).
3. N. Wu, X. Rao, Y. Gao, J. Wang, F. Xu, Amyloid-beta deposition and olfactory dysfunction in an Alzheimer's disease model. *J Alzheimers Dis* **37**, 699-712 (2013).
4. R. Alvarado-Martinez, K. Salgado-Puga, F. Pena-Ortega, Amyloid beta inhibits olfactory bulb activity and the ability to smell. *PLoS One* **8**, e75745 (2013).
5. L. Cao *et al.*, Abeta alters the connectivity of olfactory neurons in the absence of amyloid plaques in vivo. *Nat Commun* **3**, 1009 (2012).
6. N. Cheng, H. Cai, L. Belluscio, In vivo olfactory model of APP-induced neurodegeneration reveals a reversible cell-autonomous function. *J Neurosci* **31**, 13699-13704 (2011).
7. M. J. Berridge, Neuronal calcium signaling. *Neuron* **21**, 13-26 (1998).
8. S. E. Arnold *et al.*, Olfactory epithelium amyloid-beta and paired helical filament-tau pathology in Alzheimer disease. *Ann Neurol* **67**, 462-469 (2010).
9. I. Ubeda-Banon *et al.*, The human olfactory system in two proteinopathies: Alzheimer's and Parkinson's diseases. *Transl Neurodegener* **9**, 22 (2020).
10. D. Saiz-Sanchez, C. De la Rosa-Prieto, I. Ubeda-Banon, A. Martinez-Marcos, Interneurons, tau and amyloid-beta in the piriform cortex in Alzheimer's disease. *Brain Struct Funct* **220**, 2011-2025 (2015).
11. T. Wyss-Coray, L. Mucke, Inflammation in neurodegenerative disease--a double-edged sword. *Neuron* **35**, 419-432 (2002).
12. M. Dizdaroglu, P. Jaruga, M. Birincioglu, H. Rodriguez, Free radical-induced damage to DNA: mechanisms and measurement. *Free Radic Biol Med* **32**, 1102-1115 (2002).
13. K. Hirai *et al.*, Mitochondrial abnormalities in Alzheimer's disease. *J Neurosci* **21**, 3017-3023 (2001).
14. E. Tamagno *et al.*, Oxidative stress activates a positive feedback between the gamma- and beta-secretase cleavages of the beta-amyloid precursor protein. *J Neurochem* **104**, 683-695 (2008).
15. M. L. Getchell, D. S. Shah, S. K. Buch, D. G. Davis, T. V. Getchell, 3-Nitrotyrosine immunoreactivity in olfactory receptor neurons of patients with Alzheimer's disease: implications for impaired odor sensitivity. *Neurobiol Aging* **24**, 663-673 (2003).
16. R. L. Doty, The olfactory vector hypothesis of neurodegenerative disease: is it viable? *Ann Neurol* **63**, 7-15 (2008).
17. H. Baker, Unilateral, neonatal olfactory deprivation alters tyrosine hydroxylase expression but not aromatic amino acid decarboxylase or GABA immunoreactivity. *Neuroscience* **36**, 761-771 (1990).
18. C. Rosen, O. Hansson, K. Blennow, H. Zetterberg, Fluid biomarkers in Alzheimer's disease - current concepts. *Mol Neurodegener* **8**, 20 (2013).
19. K. Henriksen *et al.*, The future of blood-based biomarkers for Alzheimer's disease. *Alzheimers Dement* **10**, 115-131 (2014).
20. E. C. B. Johnson *et al.*, Large-scale proteomic analysis of Alzheimer's disease brain and cerebrospinal fluid reveals early changes in energy metabolism associated with microglia and astrocyte activation. *Nat Med* **26**, 769-780 (2020).
21. G. Son *et al.*, Olfactory neuropathology in Alzheimer's disease: a sign of ongoing neurodegeneration. *BMB Rep* **54**, 295-304 (2021).

Appendix

Valorization

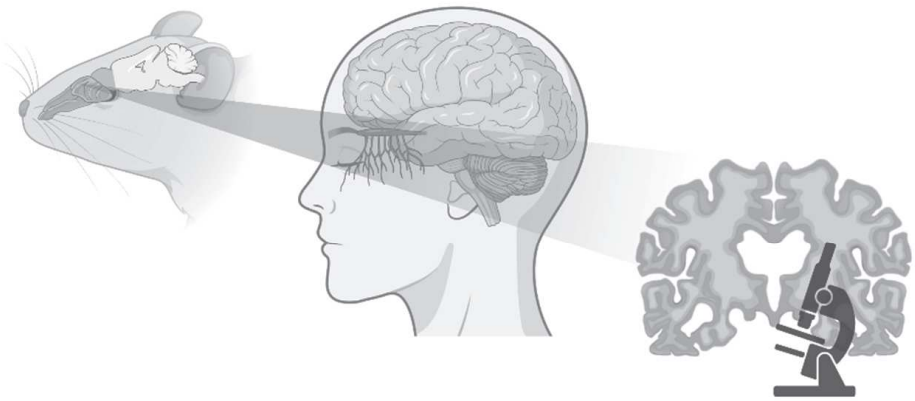

Given that Alzheimer's disease (AD) is progressive and incurable, the current principal application against AD progression is an early identification for appropriate clinical intervention. Although researchers in universities, pharmaceutical industries, and medical centers have endeavored to discover effective monitoring and diagnostic method of AD, it remains incomplete.

As an early symptom of AD, olfactory dysfunction has important implications. The olfactory system has generated a great deal of interest in recent years as a novel tool for diagnosis. In specific, an olfactory test for AD has been proposed for clinical research over the last 30 years. The findings in this thesis provide scientific evidence about partial hyposmia or specific anosmia in AD and imply the significance of development measuring AD-specific olfactory dysfunction. Notably, partial hyposmia is a significant discovery because it can develop diagnostic methods that can easily monitor a mild cognitive impairment group. Even it might be applied to cognitively asymptomatic groups in AD progression. Moreover, the mechanism between the olfactory dysfunction in AD progression and the misfolded protein (e.g., amyloid-beta) accumulated in the olfactory system can lead to a new concept in AD therapeutic strategies.

Furthermore, olfactory pathology allows us to speculate that the impaired olfactory epithelium includes altered cellular and molecular components. In this regard, nasal discharge from the olfactory epithelium may feasibly contain high-throughput biological material information that mirrors AD pathological changes in the olfactory system that could be linked to the olfactory epithelium. The results of

this thesis indicated a positive correlation between the biomarkers' level in nasal discharge and AD progression. Nasal discharge biomarker would be a better option to screen for AD because of the advantages; AD-specific early detection, economic accessibility, and non-invasive sample collection. This new diagnostic resource will aid much convenient and more accessible detection of AD before the laborious and expensive diagnosis in the clinic, thus bringing much relief to millions suffering from AD.

Correspondingly, these findings about olfactory neuropathology may provide a new platform for conducting preclinical and clinical studies to improve diagnostics in AD and better understand the mechanisms behind neurodegeneration in AD.

Appendix

Acknowledgement

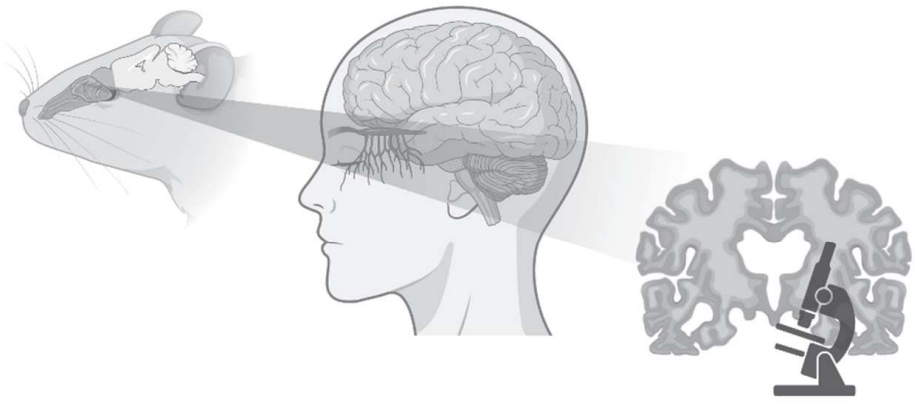

I would like to express my deepest gratitude to my parents, two younger brothers, Grandparents who believe in me and pray for me all the time. Because of your love, I could raise myself up when challenges were encountered.

This thesis would never be initiated, processed, and successfully completed without the unlimited support of my promotion team, my advisor, and supervisors. Dear Harry, I appreciate you for allowing me the opportunity to work in this department and for all your support and trust. Your motivation to investigate various research topics based on your expertise showed me continuous curiosity that is important to be a good scientist. You shared and opened up your scientific network. I learned from you how to communicate in the research field and how to think positively for making a successful outcome. Dear Jerry, thank you very much for your advice and many great opportunities to study and work with various coworkers during phD scholar. You told me "be an honest and diligent scientist," and I have kept in my mind your lesson since I have joined your lab and tried to leave your legacy everywhere I worked. It was great to start a long journey to be a scientist as your student. Dear Ali, you are my role model. You showed me responsibilities for the research project with your expertise and the way to cooperate within and beyond the team. You showed your experience, wisdom, and practical support that it needs to survive in real life. Dear Han, a special thank you for all your efforts and time to settle a dual degree program between two universities.

I would like to thank all the members of the reading committee. Dear Professor Linden, Professor Mariman, Professor Moroni, Dr. Grinberg, and Dr. Choe, I am honor to hear your opinion and thank you for your acceptance as a reading committee. I look forward to your thoughtful considerations and advice.

Dear Hellen, I could not have successfully done my work in UM without your practical advice. I respect all your technical expertise and wisdom. Also, the tech-team members, Denise, Wouter, and Sandra, many thank you for the perfect experimental solutions, well-organized laboratory rules, logistics, and your kind feedback, although I bothered you many times to get sample box, slide glasses, and solutions ;). Thank you, Rachelle and Ankie. I got helped with the administrative work. Additionally, I appreciate Ron your IT expertise. I was pleased to communicate the histologic and microscopic knowledge through Expert-division 3-microscopy. I felt that this is a helpful system to share novel scientific ideas and produce advanced common values.

I appreciate my coworkers and mentor. Dear Dr. Geun-A Chang, for your thoughtful support and kind advice about the project and use of transgenic mouse, Dr. Shin woo Kang, for your wonderful work, validation, and care transgenic mouse, Dr. Hyunjun Park, for your great effort, nasal discharge sample management. Dear Dr. Young Hye Kim, I remember your thoughtful advice, and I was motivated by your professional attitude. Dear M4I microscopy core lab members, Dr. Lopez-Iglesias, Hans, Helma, Kevin, and Willine, I got great results thanks to your great advice. I learned a lot in all processes, from the post-fixation of postmortem specimens to imaging analysis.

I have been pleased to study and work together with my colleagues. Thanks

for the Fundamental Neuromodulation lab member in UM; Jackson, Sarah, Stijn, Faisal, Faris, Sylvana, and Liu. I was motivated by your collaborative teamwork and happy to join you during the stay in UM. Especially, thanks, Jackson, for your thoughtful English editing for chapter 2. Thank you, the Chemical Senses lab members in DGIST; Oh-Hoon, Jisub, Tammy, Kwangsu, Jiyun, Da Hae, Won-Cheol, Do-Kyeong, and Kyung-Hee, and alumni; Seung-Jun, Sang Eun, SeungYeong, Samhwan, JaeYeon, Sunae, Juyeon, Seonghwan, Sun Joo, Jeewon, and other previous members who have been created and developed our identity. I learned countless experiences and lessons during phD scholar from you. Thanks for your kindness, Martin, Renzo, and Phillippos; my office-mate at room F1.156. Especially, Dear Martin, I was pleased to meet and have a time with you in UM, and thank you for your advice for some moments during my stay in UM. Thank you, Qian and Catarina, for sharing your analytic idea and your consideration about a microscope. Dear Takashi, it was nice to meet you. I hope you are well since you have been back to Japan.

Dear friends have been shared invaluable memory during phD scholar; Hyun-Kyu, Inah, Kyeongho, Jae Hyun, Tammy, Yong-Seok, Jihoon, Kyung Lim. I adore you and the time we have been together. Dear Chris and Hailey (Kyonghwan and Hyun Young) (and Choco), I cannot forget your hospitality and kindness. Thank your thoughtful advice during living in Maastricht. I miss the time we go grocery shopping together and share our free time with amazing weather. Dear Gony, I remember your warm hospitality. It was a great time with you. Dear Kimberly, I was pleased to meet you and talk with you about my and your experience in each university. Thank you,

Su and Minna; I can grow up and build confidence because of your trust. You are my first and best mentee. Dear my friends for my whole life, Bohye, Seip, Hyeonmin, Jaejoon, Seryong, and Yeji, I appreciate your endless love and encouragement.

Dear my cousin; Hyung-Hoon, thanks to your advice, I decided to apply to DGIST, and I would not have been here without your support. Dear Simon, my best friend of life, you truly have encouraged me to overcome challenges.

From the bottom of my heart, I would like to thank Seung-Jun's insight and your every consideration for our long-time discussion. As a team leader, you showed me what science is, how researcher works together, and how to enjoy a journey to be a scientist.

"Truly great partners are hard to find, harder to leave, and impossible to forget"

Appendix

Curriculum vitae

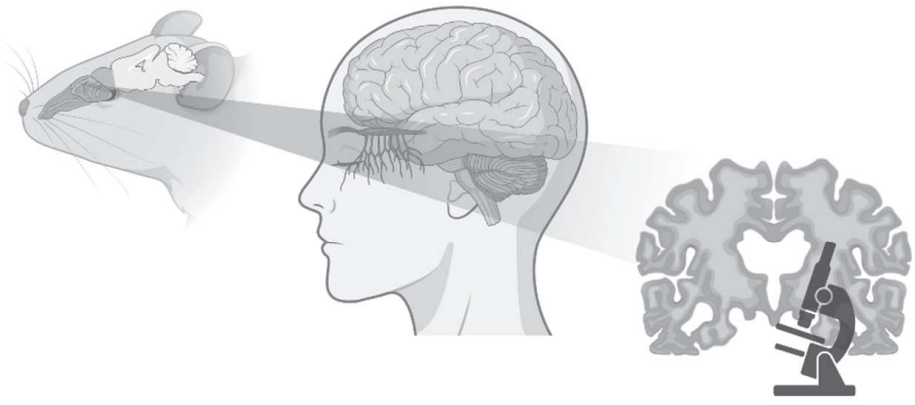

Gowoon Son was born on September 12th 1992 in Anyang, Republic of Korea. She grew up in Daegu where she graduated from Seungseo high school in 2011. The following year she started studies with major in Applied Microbiology and graduated from Yeungnam University (2011-2015). During that period, she got academic honors and was awarded scholarships. After receiving her a Bachelor of Science degree, she started her Ph.D. studies in March 2015 at the department of Brain & Cognitive Sciences, DGIST, Republic of Korea, under the supervision of Prof. Dr. Cheil Moon. She qualified to join double doctoral degree in February 2019 at the School for Mental Health and Neuroscience of the Faculty of Health, Medicine and Life Sciences, Maastricht University, the Netherlands, under the supervision of Prof. Dr. Harry W.M. Steinbusch and Dr. Ali Jahanshahi. During the five and a half-year-period she investigated the feature of olfactory pathology inducing olfactory dysfunction in Alzheimer's disease. In 2016, she was awarded an International Conferences Scholarship in DGIST which gave her the opportunity to present her research in Society for Neuroscience, San Diego, USA. In 2018, she got honors a Best poster presentation award in the Korean Society for Brain and Neural Sciences, Republic of Korea. In same year, her research was selected to oral presentation in Society for Neuroscience, San Diego, USA. During Ph.D. candidate period, she had three oral and eight poster presentations, registered four patents and published six papers. The results of her Ph.D. project are described in this thesis.

Appendix

Publications